

Development of Biopolymeric Nanoparticles for Controlled Drug Delivery

**A thesis submitted in partial fulfillment of
the requirements for the degree of
Doctor of Philosophy**

By
Nibedita Banik
Registration No. 033 of 2010



**Department of Chemical Sciences
School of Sciences
Tezpur University
Tezpur -784028, Assam
India**

Dedicated
to
my Papa and Maa
with
love and gratitude



तेजपुर विश्वविद्यालय

(केंद्रीय विश्वविद्यालय)

नपाम, तेजपुर - 784 028, असम, भारत

TEZPUR UNIVERSITY

(A Central University)

Napaam, Tezpur - 784 028, Assam, India

CERTIFICATE OF THE SUPERVISOR

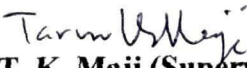
This is to certify that the thesis entitled “*Development of biopolymeric nanoparticles for controlled drug delivery*” submitted to the School of Sciences, Tezpur University for the partial fulfillment for the award of the degree of Doctor of Philosophy in the Department of Chemical Sciences is a record of research work carried out by **Ms. Nibedita Banik** under my supervision and guidance.

All helps received by her from various sources have been duly acknowledged.

No part of this thesis has been submitted elsewhere for award of any other degree.

Date: 22/10/14

Place: Tezpur


T. K. Maji (Supervisor)

Department of Chemical Sciences
School of Sciences
Tezpur University
Assam, India

DECLARATION BY THE CANDIDATE

The thesis entitled “*Development of biopolymeric nanoparticles for controlled drug delivery*” is being submitted to Tezpur University in partial fulfillment for the award of the degree of Doctor of Philosophy in Chemical Sciences is a record of bonafide research work accomplished by me under the supervision of *Prof. T. K. Maji*.

All helps from various sources have been duly acknowledged.

No part of this thesis has been submitted elsewhere for award of any other degree.

Date: 22.10.2014

Place: Tezpur

Nibedita Banik
Nibedita Banik

Department of Chemical Sciences
Tezpur University
Assam, India

Acknowledgement

I express my deep sense of profound gratitude and respect to my respected teacher and guide, Prof. T. K. Maji for his inspiring guidance, strong motivation, constant encouragement and freedom for work during the course of the work. It would have not been possible for me to bring out this thesis without his help and fatherly care.

I express heartiest thanks to Honorable Vice Chancellor, Tezpur University, Prof. M.K. Chaudhuri, for allowing me to utilize the facilities of this institution for carrying out my research work.

I am grateful to Prof. N. Karak, Dr. A. J. Thakur and Prof. R. C. Deha, Tezpur University for their suggestion and discussion. I am grateful to all the faculty members of Department of Chemical Sciences for their help and suggestions.

I wish my sincere thanks to my entire lab colleague Rashmiba, Murshid, Chinmayee, Pankaj, Prasanta and Mandip and wish to thank all my friends Rasna, Monalisha, Sweety, Rekha, Chandramika, Chandrama, Anisha, for their cooperation during entire work of period.

My special thanks to all well wisher specially, Minakshiba, Jayashriba and Dr. Amarjyoti Kalita for their constant encouragement, hospitality and warmth.

My heartfelt thank goes to the technical staff, Department of Chemical Sciences for instrumentation facilities throughout the study. I would like to thank Dr. A. Ramteke, Department of Molecular Biology & Biotechnology, Tezpur University and Mr. H.K. Sharma, Department of Pharmaceutical Sciences, Dibrugarh University for analysis.

I am grateful to Council of Scientific and industrial Research (CSIR) for funding the project (Sanction No: 01/2502/11-EMR-II) to complete this research.

Finally, I thank the authorities of Tezpur University for granting me the permission to carry out this work.

Last but not least, I would like to thank my Papa, Maa and my brother Niloy Banik for their blessing, love, inspiration and support throughout my studies to fulfill my dream.

Nibedita Banik.
Nibedita Banik

ABSTRACT

Control over drug delivery is important when situations requiring the slow release of water-soluble drugs, the fast release of low-solubility drugs, drug delivery to specific sites, drug delivery using nanoparticulate systems, delivery of two or more agents with the same formulation, and systems based on carriers that can dissolve or degrade and be readily eliminated. The ideal drug delivery system should be inert, biocompatible, mechanically strong, comfortable for the patient, capable of achieving high drug loading, safe from accidental release, simple to administer and remove, and easy to fabricate and sterilize.

A drug delivery system may be a matrix of polymer incorporating a drug. Polymeric drug carrier systems have several advantages in optimizing patient treatment regimes. In particular, swelling-controlled release systems are capable of delivering drugs at constant rates over an extended period of time. In these systems, the rate of drug delivery is controlled by the balance between drug (solute) diffusion across a concentration gradient, the polymer relaxation occurring as the crosslinked polymer imbibes water, and the osmotic pressure occurring during the swelling process.

Polysaccharides are widely distributed in nature. These materials are important in different fields since they possess unique structures and characteristics that are different from those of typical synthetic polymers. Although the experience with synthetic polymers is extensive and encouraging the recent trend has been to shift toward natural polymers. The major advantage of natural polymers includes their availability and compatibility with the encapsulation of wide range of drugs. Furthermore, bioadhesion, stability, safety, and their approval for human use are additional advantages.

Among the many kinds of polysaccharides, cellulose and chitin are the most important biomass resources. Cellulose is synthesized in plants, whereas chitin is obtained from lower animals. They are the most abundant organic compounds on Earth.

Chitosan is a technologically important polysaccharide polymer. Chemically, it is a heteropolysaccharide composed of β -(1-4)-2-deoxy-2-amino-D-glucopyranose units and β -(1,4)-2-deoxy-2-acetamino-D-glucopyranose units. Chitosan occurs in nature, particularly in the cell wall of some fungi such as *Mucor rouxii* and is mainly produced by the N-deacetylation of chitin, which is a major component of the exoskeleton of insects, the cuticles of annelids and mollusks, and the shell of crustaceans such as shrimp, crab and lobster. The physicochemical and biological properties of chitosan led to the recognition of this polymer as a promising material for drug delivery. Chitosan has been extensively examined in the pharmaceutical industry for its potential in the development of controlled release of drug delivery due to its excellent biocompatibility, biodegradability, bioactivity and non-toxicity. Chitosan's unique characteristics make it potentially useful in a variety of applications such as a drug carrier; for wound healing, implantation, and gene therapy because of the following advantages :

- Chitosan is obtained from the second most abundant natural polymer chitin
- Chitosan is nontoxic, biocompatible and biodegradable.
- Chitosan possesses more bioactivities: it has antacid and antiulcer activities that prevent or weaken drug irritation in the stomach
- Organic solvents are not required in solubilization of chitosan.
- It is simple and easy to prepare chitosan microspheres of the desired size.

The greatest advantage of the degradable polymers is that they are broken down into biologically acceptable molecules that are metabolized and removed from the body via normal metabolic pathways.

The typical commercial chitosan has approximately 85% deacetylation. The main problem of chitosan lies in their solubility. Pure, native chitosan is insoluble in water, in alkaline medium and even in organic solvents. However, water soluble salts of chitosan may be formed by neutralization with organic acids (aqueous acetic, formic, succinic, lactic, glutamic and malic acids or inorganic acids such as HCl).

The pH- dependent solubility of chitosan is attributed to its amino group ($-\text{NH}_2$), which become protonated upon dissolution at pH 6 or below to form cationic amine

groups (-NH₃), increasing intermolecular electric repulsion and resulting in a polycationic soluble polysaccharide, with a large number of charged groups on a weight basis. On the other hand, chitosan tends to lose its charge at a higher pH and may therefore precipitate from solution due to deprotonation of the amine groups.

The amino group in chitosan has a pKa value of ~6.5, thus, chitosan is positively charged. This makes chitosan a bioadhesive which readily binds to negatively charged surfaces such as mucosal membranes. Chitosan enhances the transport of polar drugs across epithelial surfaces, and is biocompatible and biodegradable.¹⁰ Purified qualities of chitosans are available for biomedical applications.

Hence, to solve the problem of solubility, chitosan derivatives, like carboxymethyl chitosan, trimethyl chitosan, thiolated chitosan etc. are synthesized. These derivatives of chitosan are soluble in water at all pH. Furthermore, these derivatives increase the drug loading efficiency and also the mucoadhesion with the cell membranes.

Nanofillers like clay, cellulose whiskers etc. can be used in nanoparticle synthesis. The nanofillers can give mechanical stability to the nanoparticles. Crosslinkers, such as, glutaraldehyde, genipin, etc. can be used to give dimensional stability to the nanoparticles. Both hydrophilic (e.g. Isoniazid) and hydrophobic drug (e.g. Curcumin) can be used as model drug. Curcumin is insoluble in water. So, its bioavailability in the system decreases. But, when nanoparticles are made, the bioavailability of Curcumin increases.

Keeping all these points in mind, in the present study, chitosan and its derivatives are used to develop nanoparticles which can be used in drug delivery applications.

Objectives of the present investigation

The main objectives of the present investigation were:

- i) To develop nanoparticles employing, different natural biodegradable polymers like, soy flour, chitosan and its water soluble derivatives, either alone or in combination with filler (MMT, cellulose whisker), cross linking agents and other additives.

- ii) To study the effect of various parameters like amount of filler, polymer, percentage of cross linking agents, etc. on drug loading capacity, release characteristics, water absorption, etc.
- iii) To characterize the composite using FTIR, X-ray diffractometer, scanning electron microscope, transmission electron microscope, etc.
- iv) To study the cytotoxicity effect of the nanoparticles on the living system.

Chapter 1 includes the introduction part. This covers the concept of controlled delivery, advantages and limitations of controlled delivery, component of controlled delivery systems, natural polymers, mainly chitosan and soy flour used for controlled delivery, surfactant, crosslinkers – their properties and effect on crosslinking of polymers, nanoparticles – their fabrication techniques, properties and application in drug delivery. This chapter also includes general literature related to properties of chitosan, soy flour, montmorillonite, cellulose whiskers, glutaraldehyde, genipin, isoniazid and curcumin.

Chapter 2 includes the available literatures involving controlled release applications of chitosan, soy flour, montmorillonite, cellulose whiskers, glutaraldehyde, genipin, isoniazid and curcumin. Besides this, literatures related to analysis of controlled systems like Fourier transform infrared spectroscopy (FTIR), X-Ray diffraction (XRD), Scanning electron microscopy (SEM), Transmission electron microscopy (TEM), Swelling study, cumulative release study, encapsulation efficiency, drug loading efficiency, surface properties, cell viability study, etc. are covered. This chapter also focuses the objectives along with the plan of work and methodologies for the present investigation.

Chapter 3 describes the experimental part i.e., the materials and methods, which includes the raw materials used and techniques for sample preparation. This chapter also contains different techniques used for characterization of nanoparticles.

Chapter 4 includes results and discussion part of isoniazid encapsulated biopolymer nanoparticles containing montmorillonite or cellulose whiskers as reinforcing agents and glutaraldehyde as the crosslinking agent. This chapter has been subdivided into the following five sections.

Section A-Preparation and characterization of isoniazid loaded chitosan/cellulose whisker microspheres for controlled drug delivery applications.

This section embodies the preparation process of cellulose whisker (CW) from filter paper by acid hydrolysis. Drug encapsulated chitosan –CW particles were prepared by microemulsion technique using isoniazid as the model drug and glutaraldehyde as the crosslinker. The microparticles were characterized by Fourier Transmission Infra-red Spectroscopy (FTIR), X-ray diffractometry (XRD), Scanning electron microscopy (SEM), Transmission emission microscopy (TEM). The effect of cellulose whisker and glutaraldehyde on the microparticles were assessed with regard to swelling, encapsulation efficiency and consequently on the release of isoniazid in different mediums. The drug release mechanism was studied for different time periods by UV-visible spectrophotometer. Cytotoxicity test was performed by MTT assay analysis. The results entailed that the microparticles can be exploited as potential drug carrier for controlled release applications.

This work demonstrated the successful preparation of CW and isoniazid loaded chitosan-CW microparticles by microencapsulation method. FTIR study indicated the successful preparation of CW and successful incorporation of CW and isoniazid in the microparticles. XRD results illustrated the increase in the crystallinity of CW compared to untreated ground filter paper. XRD results also showed the molecular level dispersion of isoniazid in the chitosan-CW microparticles. XRD and TEM showed successful incorporation of CW in chitosan microparticles. SEM study demonstrated that both isoniazid loaded CW incorporated chitosan microparticles and only isoniazid loaded chitosan microparticles had spherical shape. The surface of isoniazid loaded chitosan-CW microparticles was more rough compared to isoniazid loaded chitosan microparticles suggesting good adhesion between CW and chitosan matrix. Both the swelling and release of isoniazid from the microparticles were found to enhance with the decrease in the MMT and GA content. The percentage swelling degree and cumulative release increased in gastric pH compared to intestinal pH. Cytotoxicity study revealed that the synthesized CW was not cytotoxic and the microparticles containing CW was less cytotoxic than those of CW free nanoparticles.

Section B-Preparation and characterization of isoniazid loaded chitosan /montmorillonite nanoparticles for controlled drug delivery applications.

This section reports the development of isoniazid loaded chitosan-montmorillonite nanoparticles by ionic gelation of chitosan with pentasodium tripolyphosphate. The nanoparticles have been characterized by FTIR, XRD, SEM and TEM. The effect of surfactant, Montmorillonite and glutaraldehyde on chitosan nanoparticles have been assessed with regard to swelling, encapsulation efficiency and consequently to the release of isoniazid in different mediums (pH 1.2 and 7.4). Swelling experiment provides important information on drug diffusion properties, which indicates that the chitosan nanoparticles are highly sensitive to the pH environment. The drug release mechanism has been studied in different time periods by UV-visible spectrophotometer. Cytotoxicity has been assessed by MTT assay analysis. Mucoadhesion properties have been appraised by *in vitro* wash off test and *ex vivo* mucoadhesion test.

Both the swelling and release of isoniazid from the nanoparticles were found to enhance with the decrease in the pH of the medium and size of the nanoparticles. FTIR study indicated the interaction of clay with chitosan polymer. The exfoliation of MMT layers was examined by XRD and TEM study. XRD results also showed the molecular level dispersion of isoniazid in the chitosan-MMT nanoparticles. SEM study showed that the surface of the chitosan-MMT nanoparticles was less smoother compared to those of isoniazid loaded nanoparticles. Nanoparticles containing clay was less cytotoxic than those of clay free nanoparticles. The lower the particle size of the nanoparticles, the higher was the cytotoxicity. The mucoadhesivity of the nanoparticles was better in gastric pH and increased with the decrease in particle size.

Section C-Preparation and characterization of isoniazid loaded carboxymethyl chitosan /montmorillonite nanoparticles for controlled drug delivery applications.

This section studies the preparation of carboxymethyl chitosan (CMC), a water soluble derivative of chitosan and evaluates the prospective of crosslinked CMC-Montmorillonite (MMT) nanoparticles for controlled delivery of isoniazid. CMC/ MMT nanoparticles were synthesized by ionic gelation method by using CaCl_2 . The nanoparticles were

characterized by FTIR, NMR, XRD, SEM, and TEM. The effects of MMT and glutaraldehyde on nanoparticles were assessed with regard to encapsulation efficiency, percentage swelling degree and cumulative release. Percentage swelling degree and cumulative release were studied in pH medium 1.2 and 7.4 for 6 h. The cumulative release was studied by UV-visible spectrophotometer. Cell viability study was performed by MTT assay analysis.

FTIR and NMR study indicated the successful preparation of CMC. FTIR study confirmed the interaction of MMT with CMC. The exfoliation of MMT layers and molecular level dispersion of isoniazid in CMC was examined by XRD and TEM. SEM study showed that the surface of the CMC-MMT nanoparticles was smooth compared to those of CMC nanoparticles. Swelling and release of isoniazid from the nanoparticles increased with the decrease in the MMT and glutaraldehyde content. The percentage swelling degree and cumulative release was more in pH 1.2. Cell viability study revealed that CMC was not cytotoxic and the nanoparticles containing MMT was less cytotoxic than those of MMT free nanoparticles. CMC-MMT nanoparticles can be exploited as potential drug carrier for controlled release applications.

Section D-Preparation and characterization of isoniazid loaded phosphorylated chitosan /montmorillonite nanoparticles for controlled drug delivery applications.

This part of the chapter reports the preparation of phosphorylated chitosan (PCTS), a water soluble derivative of chitosan and evaluates the prospective of crosslinked PCTS-Montmorillonite (MMT) nanoparticles for controlled delivery of isoniazid. The nanoparticles were prepared by ionic gelation process using pentasodium tripolyphosphate. The nanoparticles were characterized by FTIR, NMR, XRD, SEM, and TEM. The effects of MMT and glutaraldehyde on nanoparticles were assessed with regard to encapsulation efficiency, percentage swelling degree and cumulative release. Percentage swelling degree and cumulative release were studied in pH medium 1.2 and 7.4 for 6 h. The cumulative release was studied by UV-visible spectrophotometer

FTIR and NMR study indicated the successful preparation of PCTS. FTIR study confirmed the interaction of MMT with PCTS. The exfoliation of MMT layers and

molecular level dispersion of isoniazid in PCTS was examined by XRD and TEM. SEM study showed that the surface of the PCTS-MMT nanoparticles was smooth compared to those of PCTS nanoparticles. Swelling and release of isoniazid from the nanoparticles increased with the decrease in the MMT and glutaraldehyde content. The percentage swelling degree and cumulative release was more in pH 1.2. Cell viability study revealed that PCTS was not cytotoxic and the nanoparticles containing MMT was less cytotoxic than those of MMT free nanoparticles. PCTS-MMT nanoparticles can be exploited as potential drug carrier for controlled release applications.

Section E-Preparation and characterization of isoniazid loaded soy flour /montmorillonite nanoparticles for controlled drug delivery applications.

This section reports the preparation of glutaraldehyde crosslinked soy flour (SF)-Montmorillonite (MMT) nanoparticles loaded with isoniazid. The nanoparticles have been characterized by FTIR, XRD, SEM and TEM. The effect of MMT and glutaraldehyde on the nanoparticles has been assessed in terms of swelling, encapsulation efficiency and consequently to the release of isoniazid in different mediums. The drug release mechanism has been assessed in different time periods by UV-visible spectrophotometer. Cytotoxicity test has been performed by MTT assay analysis. Both the swelling and release of isoniazid from the nanoparticles have been found to enhance with the decrease in the MMT and GA content. The % swelling degree and cumulative release increased in alkaline pH compared to acidic pH. FTIR study indicated the interaction of MMT with SF polymer. The exfoliation of MMT layers was examined by XRD and TEM study. XRD results also showed the molecular level dispersion of isoniazid in the SF-MMT nanoparticles. SEM study showed that the surface of the SF-MMT nanoparticles was less smoother compared to those of only SF nanoparticles. Nanoparticles containing MMT was less cytotoxic than those of clay free nanoparticles and cytotoxicity decreased with increase in the MMT content.

Chapter 5 embodies the results and discussion part of curcumin encapsulated biopolymeric nanoparticles where montmorillonite and genipin have been used as the

Section A-Preparation and characterization of curcumin loaded chitosan/MMT nanoparticles for controlled drug delivery applications.

This section reports the development of curcumin loaded chitosan-montmorillonite nanoparticles by ionic gelation of chitosan with pentasodium tripolyphosphate. The nanoparticles have been characterized by FTIR, XRD, SEM and TEM. The effect of montmorillonite and genipin on carboxymethylchitosan nanoparticles have been assessed with regard to swelling, encapsulation efficiency and consequently to the release of curcumin in different mediums (pH 1.2 and 7.4). The drug release mechanism has been studied in different time periods by UV-visible spectrophotometer. Cytotoxicity has been assessed by MTT assay analysis. Mucoadhesion properties have been conducted by *in vitro wash off* test and *ex vivo* mucoadhesion test.

Both the swelling and release of curcumin from the nanoparticles were found to enhance with the decrease in the pH of the medium, decrease in MMT content and decrease in genipin content. FTIR study indicated the interaction of clay with carboxymethylchitosan polymer. The exfoliation of MMT layers was examined by XRD and TEM study. XRD results also showed the molecular level dispersion of curcumin in the chitosan-MMT nanoparticles. SEM study showed that the surface of the carboxymethylchitosan-MMT nanoparticles was less smoother compared to those of curcumin loaded nanoparticles. Nanoparticles containing clay was not cytotoxic to lymphocyte. The lymphocyte toxicity profile of chitosan, MMT, curcumin and different formulations were studied by measuring the lipid peroxidation and lactate dehydrogenase (LDH) activity. Treatment of lymphocytes with chitosan, MMT, curcumin and the different formulation decreases the malondialdehyde (MDA) formation. The level of MDA formation in different formulations was slightly higher than that of Curcumin alone. Similar pattern was also observed in case of LDH activity measured in the cell free medium. The decrease in the LDH activity suggested that there was no membrane damage in the cells and the MDA level suggested the lacking of cellular damage. Reduced glutathione (GSH), the non-enzymatic component of antioxidant system measured as acid soluble sulfahydryl group (-SH) was elevated by only chitosan, MMT, curcumin treatment. Curcumin loaded nanoparticle increased the GSH level compared to curcumin alone. Superoxide dismutase

(SOD) and catalase, the two major enzymatic component of antioxidant system also enhanced by the different treatments. The increased activity was found more compared to curcumin alone. The elevated level of antioxidants in the lymphocytes confers protective function against cellular damage.

The MTT assay was also done on two cancer cell lines, namely MCF-7 (which is a breast cancer cell line) and HePG2 (cell lines derived from hepatocellular carcinoma). It was found that the nanoparticles were cytotoxic to the cancer cells and the toxicity level increased with the increase in the MMT content.

The mucoadhesivity of the nanoparticles was better in gastric pH.

Section B-Preparation and characterization of curcumin loaded carboxymethyl chitosan/MMT nanoparticles for controlled drug delivery applications.

This section reports the development of curcumin loaded carboxymethyl chitosan-montmorillonite nanoparticles by ionic gelation of chitosan with CaCl₂. The nanoparticles have been characterized by FTIR, XRD, SEM and TEM. The effect of montmorillonite and genipin on carboxymethylchitosan nanoparticles have been assessed with regard to swelling, encapsulation efficiency and consequently to the release of curcumin in different mediums (pH 1.2 and 7.4). The drug release mechanism has been studied in different time periods by UV-visible spectrophotometer. Cytotoxicity has been assessed by MTT assay analysis. Mucoadhesion properties have been conducted by *in vitro wash off* test and *ex vivo* mucoadhesion test.

Both the swelling and release of curcumin from the nanoparticles were found to enhance with the decrease in the pH of the medium and size of the nanoparticles. FTIR study indicated the interaction of clay with carboxymethyl chitosan polymer. The exfoliation of MMT layers was examined by XRD and TEM study. XRD results also showed the molecular level dispersion of curcumin in the carboxymethyl chitosan-MMT nanoparticles. SEM study showed that the surface of the carboxymethyl chitosan-MMT

nanoparticles was less smoother compared to those of only curcumin loaded nanoparticles. MTT assay to determine cytotoxicity was done in normal human lymphocyte, cancer cell lines MCF-7 and HePG2. It was found that the nanoparticles were not cytotoxic to normal lymphocytes but they were highly toxic to the cancer cell lines. The mucoadhesivity study showed that the nanoparticles were more mucoadhesive in gastric pH.

Section C-Preparation and characterization of curcumin loaded phosphorylated chitosan/MMT nanoparticles for controlled drug delivery applications.

This part of the chapter reports the development of curcumin loaded phosphorylated chitosan-montmorillonite nanoparticles by ionic gelation of chitosan with pentasodium tripolyphosphate. The nanoparticles have been characterized by FTIR, XRD, SEM and TEM. The effect of montmorillonite and genipin on phosphorylated chitosan nanoparticles were assessed with regard to swelling, encapsulation efficiency and consequently to the release of curcumin in different mediums (pH 1.2 and 7.4). The drug release mechanism has been studied in different time periods by UV-visible spectrophotometer. Cytotoxicity has been assessed by MTT assay analysis. Mucoadhesion properties have been conducted by *in vitro* wash off test and *ex vivo* mucoadhesion test.

Both the swelling and release of curcumin from the nanoparticles were found to enhance with the decrease in the pH of the medium and size of the nanoparticles. FTIR study indicated the interaction of clay with phosphorylated chitosan polymer. The exfoliation of MMT layers was examined by XRD and TEM study. XRD results also showed the molecular level dispersion of curcumin in the phosphorylated chitosan-MMT nanoparticles. SEM study showed that the surface of the phosphorylated chitosan-MMT nanoparticles was less smoother compared to those of only curcumin loaded nanoparticle.

The MTT assay to determine cytotoxicity was done in normal human lymphocyte, cancer cell lines MCF-7 and HePG2. It was found that the nanoparticles were not cytotoxic to normal lymphocytes but they were highly toxic to the cancer cell lines. The

mucoadhesivity study showed that the nanoparticles were more mucoadhesive in gastric pH.

Chapter 6, the last chapter of the thesis includes the highlights of the findings, concluding remarks, and future scopes of the present investigation. The salient features that come out from the present study could be summarized as follows:

1. In this present experimental study, isoniazid loaded biopolymer/MMT(or cellulose whisker) nanoparticles and Curcumin loaded biopolymer/MMT nanoparticles were successfully prepared using glutaraldehyde and genipin as the crosslinkers and Tween 80 as the surfactant.
2. NMR studies confirmed the synthesis of carboxymethyl chitosan and phosphorylated chitosan. FTIR and XRD studies established the successful synthesis of the nanoparticles. TEM studies showed the delamination/dispersion of MMT layers and cellulose whiskers inside the polymer matrix.
3. Swelling and cumulative release study showed that the nanoparticles were pH dependent. All the systems , such as, Isoniazid loaded chitosan/cellulose whisker microparticles, isoniazid loaded chitosan/MMT nanoparticles, isoniazid loaded carboxymethyl chitosan/MMT nanoparticles, isoniazid loaded phosphorylated chitosan/MMT nanoparticles, Curcumin loaded chitosan/MMT nanoparticles, Curcumin loaded carboxymethyl chitosan/MMT nanoparticles and Curcumin loaded phosphorylated chitosan/MMT nanoparticles showed higher swelling and cumulative release in gastric pH compared to intestinal pH. Whereas in the case of isoniazid loaded soy flour/MMT nanoparticles, both percentage swelling degree and cumulative release were more in intestinal pH compared to gastric pH.
4. Cytotoxicity study indicated that isoniazid loaded biopolymer/ MMT nanoparticles were less toxic to lymphocytes compared to either MMT free isoniazid loaded biopolymeric nanoparticles or isoniazid alone. Cytotoxicity study of Curcumin loaded biopolymer/ MMT nanoparticles showed that the nanoparticles were not at all harmful to the human lymphocytes; in fact they helped in cell proliferation. But when the cytotoxicity was studied in cancer cell line, like, MCF-7 and HePG2, it was found that the nanoparticles were quite cytotoxic to the cancer cell lines and the toxicity increased with the increase in MMT content. A substantial amount of (40%) destruction of cancer

cell lines was observed on treatment with nanoparticles containing 5% (w/w) MMT of polymer. This suggested that Curcumin loaded biopolymer/ MMT nanoparticles can be exploited as potential anticancer agents.

5. Mucoadhesivity study showed that the isoniazid loaded chitosan/MMT nanoparticles, Curcumin loaded chitosan/MMT nanoparticles, Curcumin loaded carboxymethyl chitosan/MMT nanoparticles and Curcumin loaded phosphorylated chitosan/MMT nanoparticles-all were more mucoadhesive in gastric pH compared to intestinal pH.

6. All the above systems can be used for the purpose of drug delivery.

Future scopes

Isoniazid and curcumin loaded biopolymer nanoparticles reinforced with MMT and cellulose whiskers were successfully prepared. It was also found that MMT, cellulose whiskers and pH of the medium can control the degree of swelling and cumulative release of drug from the nanoparticles. However, the present study is restricted to laboratory scale only. Further trial of the nanoparticles on animal models are needed for better understanding and use of the nanoparticles.

Contents

Abstract	i-xiii
Tables of Contents	xiv-xxi
List of Tables	xxii-xxiii
List of Figures	xxiv-xxxii
Abbreviations	xxxiii-xxxiv
Chapter 1: Introduction	1-42
1.1. Concept of Controlled Release Drug Delivery	1-2
1.1.1. Need for Controlled Delivery Systems	2-3
1.1.2. Demerits of Controlled Release Systems	3
1.2. Fundamental components of controlled delivery formulations	3-20
1.2.1. Polymers	4-12
1.2.1.1. Chitosan	5-7
1.2.1.2. Carboxymethyl chitosan	7-8
1.2.1.3. Phosphorylated chitosan (PCTS)	8-9
1.2.1.4. Soy flour	9-12
1.2.2. Active Agents	12-15
1.2.2.1. Isoniazid	12-13
1.2.2.2. Curcumin	13-15
1.2.3. Reinforcing agents	15-19
1.2.3.1. Montmorillonite (MMT)	16-17
1.2.3.2. Cellulose whiskers (CW)	17-19
1.2.4. Crosslinking agents	19-20
1.3. Role of micro- and nanoparticles in controlled release drug delivery	20-22
1.4. Fabrication techniques of nanoparticles for controlled delivery formulations	22-30
1.4.1. Evaporation or Extraction of Solvent Based Process	23-25
1.4.1.1. Coacervation phase separation method	23-25
1.4.1.1.1. Simple Coacervation Method	23-24
1.4.1.1.2. Complex Coacervation Method	24-25
1.4.2. Emulsion Based Process	25-27
1.4.2.1. Single emulsion	25-26
1.4.2.2. Double emulsion technique	27
1.4.3. Ionotropic Gelation Technique	28

1.4.4. Desolvation method	29
1.4.5. Spray Drying	29-30
1.4.6. Other fabrication techniques	30
References	31-42
Chapter 2: Literature Search	43-60
2.1. Isoniazid: An antituberculosis drug	43-44
2.2. Curcumin: An anticancer drug	44-46
2.3. Natural polymers for controlled drug delivery formulations	46-50
2.4. Montmorillonite (MMT) and Cellulose whisker (CW) in Biomedical Applications	50-52
2.5. Glutaraldehyde and Genipin as Crosslinkers	52-53
2.6. Objectives and plan of work	53-55
References	56-60
Chapter 3: Experimental	61-85
3.1. Material used	61-62
3.2. Methods	63-85
3.2.1. Section A: Preparation of Nanoparticles/microparticles loaded with hydrophilic drug, Isoniazid	63-73
3.2.1.1. Preparation of cellulose whisker (CW)	63-64
3.2.1.2. Preparation of Isoniazid loaded Chitosan–CW microparticles by microencapsulation method	64-65
3.2.1.3. Preparation of Isoniazid loaded Chitosan Montmorillonite nanoparticles using ionic gelation method	65-67
3.2.1.4. Synthesis of carboxymethyl chitosan	67
3.2.1.5. Preparation of Isoniazid loaded CMC-MMT nanoparticles by ionic gelation method	68-69
3.2.1.6. Synthesis of phosphorylated chitosan (PCTS)	69
3.2.1.7. Preparation of Isoniazid loaded PCTS-MMT nanoparticles by ionic gelation method	70-71
3.2.1.8. Preparation of isoniazid-loaded SF nanoparticles by desolvation method	72-73

3.2.2. Section B: Preparation of nanoparticles loaded with hydrophobic drug, Curcumin.	73-77
3.2.2.1. Preparation and characterization of curcumin loaded chitosan/MMT nanoparticles for controlled drug delivery applications	73-74
3.2.2.2. Preparation and characterization of curcumin loaded carboxymethyl chitosan/MMT nanoparticles for controlled drug delivery applications.	74-75
3.2.2.3. Preparation and characterization of curcumin loaded phosphorylated chitosan/MMT nanoparticles for controlled drug delivery applications	76-77
3.2.3. Preparation of calibration curve	77
3.2.3.1. Calibration curve of Isoniazid	77
3.2.3.2. Calibration curve of Curcumin	77
3.2.4. Calculation of Process Yield	78
3.2.5. Calculation of Drug loading efficiency and Encapsulation efficiency of the nanoparticles	78
3.2.6. Fourier Transmission Infra-red Spectroscopy (FTIR) study	73
3.2.7. X-ray diffraction (XRD) study	78
3.2.8. Particle size determination	78
3.2.9. Scanning electron microscopy (SEM) study	79
3.2.10. Transmission emission microscopy (TEM) study	79
3.2.11. Water Uptake Studies	79
3.2.12. <i>In vitro</i> drug release studies	79-80
3.2.13. Isolation of Lymphocytes, culture and treatment	80
3.2.14. Cytotoxicity experiments	80
3.2.15. Statistical analysis	81
3.2.16. Cell culture	81
3.2.16.1. Preparation of the cell lysate	81
3.2.16.2. Preparation of samples for LDH activity assay	81
3.2.16.3. LDH assay	81-82
3.2.16.4. Lipid Peroxidation Assay	82
3.2.16.5. Reduced glutathione assay	82
3.2.16.6. Catalase assay	82-83
3.2.16.7. Superoxide dismutase	83

3.2.17. Mucoadhesion study	83-84
3.2.17.1. In vitro wash-off test	83
3.2.17.2. <i>Ex vivo</i> mucoadhesive test	83-84
References	85
Chapter 4: Results and Discussion (Part 1)	86-136
<i>4.1. Section A-Preparation and characterization of isoniazid loaded chitosan/cellulose whisker microspheres for controlled drug delivery applications.</i>	86-96
4.1.1. Effect of variation of CW and GA concentration on the different properties of isoniazid loaded chitosan CW microparticles	86-88
4.1.2. Fourier Transmission Infra-red Spectroscopy (FTIR) study	88-89
4.1.3. X-ray diffraction (XRD) study	90-91
4.1.4. Scanning electron microscopy (SEM) study	91
4.1.5. Transmission electron microscopy (TEM) study	92
4.1.6. Swelling Study	92-93
4.1.7. <i>In vitro</i> Release Studies	93-94
4.1.8. Cell Viability Study	95-96
<i>4.2. Section B-Preparation and characterization of isoniazid loaded chitosan /montmorillonite nanoparticles for controlled drug delivery applications</i>	96-106
4.2.1. Effect of variation of surfactant concentration on the different properties of chitosan nanoparticles	96-98
4.2.2. Fourier Transmission Infra-red Spectroscopy (FTIR) study	98-99
4.2.3. X-ray diffraction (XRD) study	99
4.2.4. Scanning electron microscopy (SEM) study	100
4.2.5. Transmission electron microscopy (TEM) study	100
4.2.6. Swelling Study	101

4 2 7 <i>In vitro</i> Release Studies	101-102
4 2 8 Cell Viability Study	102-104
4 2 9 <i>In vitro</i> wash-off test for evaluation of mucoadhesive property	104-105
4 2 10 <i>Ex vivo</i> mucoadhesive test	105-106
4 3 Section C-Preparation and characterization of isoniazid loaded carboxymethyl chitosan /montmorillonite nanoparticles for controlled drug delivery applications	106-117
4 3 1 Nuclear Magnetic Resonance (NMR) study	106-107
4 3 2 Effect of variation of MMT and GA concentration on the different properties of isoniazid loaded CMC-MMT nanoparticles	107-109
4 3 3 Fourier Transmission Infra-red Spectroscopy (FTIR) study	109-110
4 3 4 X-ray diffraction (XRD) study	110-111
4 3 5 Scanning electron microscopy (SEM) study	112
4 3 5 Transmission electron microscopy (TEM) study	113
4 3 6 Swelling Study	113-114
4 3 7 <i>In vitro</i> Release Studies	114-116
4 3 8 Cell Viability Study	116-117
4 4 Section D-Preparation and characterization of isoniazid loaded phosphorylated chitosan /montmorillonite nanoparticles for controlled drug delivery applications	117-126
4 4 1 Nuclear Magnetic Resonance (NMR) study	117-118
4 4 2 Effect of variation of MMT and GA concentration on the different properties of isoniazid loaded CMC-MMT nanoparticles	118-119
4 4 3 Fourier Transmission Infra-red Spectroscopy (FTIR) study	119-120
4 4 4 X-ray diffraction (XRD) study	120-121
4 4 5 Scanning electron microscopy (SEM) study	121-122
4 4 6 Transmission electron microscopy (TEM) study	122

4.4.7. Swelling Study	122-123
4.4.8. In vitro Release Studies	124-125
4.4.9. Cell Viability Study	125-126
<i>4.5. Section E-Preparation and characterization of isoniazid loaded soy flour /montmorillonite nanoparticles for controlled drug delivery applications.</i>	126-134
4.5.1. Effect of variation of MMT and GA concentration on the different properties of SF nanoparticles	126-128
4.5.2. Fourier Transmission Infra-red Spectroscopy (FTIR) study	128-129
4.5.3. X-ray diffraction (XRD) study	129-130
4.5.4. Scanning electron microscopy (SEM) study	130-131
4.5.5. Transmission electron microscopy (TEM) study	131
4.5.6. Swelling Study	131-132
4.5.7. In vitro Release Studies	132-133
4.5.8. Cell Viability Study	130-131
References	133-134
Chapter 5: Results and Discussion (Part 2)	137-167
<i>5.1. Section A-Preparation and characterization of curcumin loaded chitosan/MMT nanoparticles for controlled drug delivery applications</i>	137-148
5.1.1. Effect of variation of MMT and genipin concentration on the different properties of curcumin loaded chitosan-MMT nanoparticles	137-139
5.1.2. Fourier Transform Infra-red Spectroscopy (FTIR) study	139-140
5.1.3. X-Ray Diffraction (XRD) Study	140

5.1.4. Scanning electron microscopy (SEM) study	141
5.1.5. Transmission electron microscopy (TEM) study	141
5.1.6. Swelling Study	142-143
5.1.7. <i>In vitro</i> Release Studies	143-144
5.1.8. Cell Viability Study	144-145
5.1.9. Study of toxicity related parameter (lipid peroxidation and lactate dehydrogenase (LDH) activity) and Antioxidant status	146
5.1.10 <i>In vitro</i> wash-off test for evaluation of mucoadhesive property	147
5.1.11. <i>Ex vivo</i> mucoadhesive test	148
<i>5.2. Section B-Preparation and characterization of curcumin loaded carboxymethyl chitosan/MMT nanoparticles for controlled drug delivery applications</i>	148-157
5.2.1. Effect of variation of MMT and genipin concentration on the different properties of curcumin loaded CMC-MMT nanoparticles	148-150
5.2.2. Fourier Transform Infra-red Spectroscopy (FTIR) study	150
5.2.3. X-Ray Diffraction (XRD) Study	151
5.2.4. Scanning electron microscopy (SEM) study	151-152
5.2.5. Transmission electron microscopy (TEM) study	152
5.2.6. Swelling Study	152-153
5.2.7. <i>In vitro</i> Release Studies	153-154
5.2.8. Cell Viability Study	154-156
5.2.9. <i>In vitro</i> wash-off test for evaluation of mucoadhesive property	156-157
5.2.10. <i>Ex vivo</i> mucoadhesive test	157
<i>5.3. Section C-Preparation and characterization of curcumin loaded phosphorylated chitosan/MMT nanoparticles for controlled drug delivery applications</i>	157-166

5 3 1 Effect of variation of MMT and genipin concentration on the different properties of curcumin loaded PCTS-MMT nanoparticles	157-159
5 3 2 Fourier Transform Infra-red Spectroscopy (FTIR) study	159
5 3 3 X-Ray Diffraction (XRD) Study	160
5 3 4 Scanning electron microscopy (SEM) study	160-161
5 3 5 Transmission electron microscopy (TEM) study	161
5 3 6 Swelling Study	161-162
5 3 7 <i>In vitro</i> Release Studies	162-163
5 3 8 Cytotoxicity Study	164-165
5 3 9 <i>In vitro</i> wash-off test for evaluation of mucoadhesive property	165
5 3 10 <i>Ex vivo</i> mucoadhesive test	166
References	167
Chapter 6: Conclusion and Future Scope	168-170
Appendices	171

List of Tables

Chapter	Table	Title	Page No.
1	1.1.	Composition of Soy flour	10-11
	1.2.	Amino acid contents in Soy flour	11-12
3	3.1.	Recipes for the formation of different isoniazid loaded chitosan-CW microparticles crosslinked with GA	65
	3.2.	Recipes for the formation of different isoniazid loaded chitosan- montmorillonite nanoparticles	67
	3.3.	Recipes for the formation of different isoniazid loaded CMC- montmorillonite nanoparticles	69
	3.4.	Recipes for the formation of different isoniazid loaded PCTS- montmorillonite nanoparticles	71
	3.5.	Recipes for the formation of different isoniazid loaded SF- montmorillonite nanoparticles	73
	3.6.	Recipes for the formation of different curcumin loaded chitosan- montmorillonite nanoparticles	74
	3.7.	Recipes for the formation of different curcumin loaded CMC- montmorillonite nanoparticles	75
	3.8.	Recipes for the formation of different curcumin loaded PCTS- montmorillonite nanoparticles	76
4	4.1	Effect of variation of CW and GA concentration on the different properties of chitosan microparticles	87
	4.2.	Effect of variation of surfactant concentration on the different properties of chitosan nanoparticle	96
	4.3.	Results of in vitro wash-off test to assess mucoadhesive properties of nanoparticles prepared	105
	4.4.	Weight required to detach the membrane at different time intervals	106
	4.5.	Effect of variation of MMT and GA concentration on the different properties of CMC nanoparticles	108
	4.6	Effect of variation of MMT and GA concentration on the different properties of PCTS nanoparticles	119
	4.7.	Effect of variation of MMT and GA concentration on the different properties of SF nanoparticles	127

5	5.1	Effect of variation of MMT and genipin concentration on the different properties of chitosan-MMT nanoparticles	138
	5.2	Results of in vitro wash-off test to assess mucoadhesive properties of nanoparticles prepared	147
	5.3	Weight required to detach the membrane at different time intervals	148
	5.4	Effect of variation of MMT and genipin concentration on the different properties of CMC-MMT nanoparticles	150
	5.5	Results of in vitro wash-off test to assess mucoadhesive properties of nanoparticles prepared	156
	5.6.	Weight required to detach the membrane at different time intervals	157
	5.7.	Effect of variation of MMT and genipin concentration on the different properties of PCTS-nanoparticles	159
	5.8.	Results of in vitro wash-off test to assess mucoadhesive properties of nanoparticles prepared	165
	5.9.	Weight required to detach the membrane at different time intervals	166

List of Figures

Chapter	Figure	Title	Page No
1	1 1	Drug levels in the blood plasma (a) traditional drug dosing, (b) controlled-delivery dosing	2
	1 2	Structure of chitosan	6
	1 3	Scheme of preparation of CMC from chitosan	8
	1 4	Preparation of phosphorylated chitosan from chitosan	8
	1 5	Structure of isoniazid	13
	1 6	Pharmaceutical properties of curcumin	14
	1 7	Composition of curcumin	15
	1 8	Structure of montmorillonite	16
	1 9	Structure of cellulose	17
	1 10	Schematic diagram showing the hydrogen bonding within and between cellulose molecules alongwith the amorphous and crystalline region in cellulose	18
	1 11	Structures of several crosslinking agents	20
	1 12	Schematic diagram showing important stems in simple coacervation method (a) Dispersion of the core material in aqueous solution of polymer, (b) deposition of the coacervate around the core and (c) hardening of the nanoparticles	24
	1 13	Example of complex coacervation involving (a) dispersion of the core, (b) initial coacervation after addition of coacervation agent, (c) coacervation on the surface of the core and (d) formation of the cross-linked shell by reticulation of the interface	25
	1 14	Processing scheme for nanoparticle-preparation by single emulsion technique	26
	1 15	Processing scheme for nanoparticle-preparation by double emulsion technique	27
	1 16	Important steps of ionotropic gelation	28
	1 17	Schematic diagram of desolvation technique	29
	1 18	Schemation diagram of spray drying technique	30

3	3.1	Schematic diagram of preparation of CW	63
	3.2	Flowchart diagram showing the main steps in the preparation of isoniazid loaded chitosan-MMT nanoparticles	66
	3.3	Flowchart diagram showing the main steps in the preparation of isoniazid loaded CMC-MMT nanoparticles	68
	3.4	Flowchart diagram showing the main steps in the preparation of isoniazid loaded PCTS-MMT nanoparticles	70
	3.5	Flowchart diagram showing the main steps in the preparation of isoniazid loaded SF-MMT nanoparticles	72
4	4.1	FTIR spectra of (a) Cellulose, (b) CW, (c) Chitosan, (d) Isoniazid, and (e) C/CW5/GA50	89
	4.2	XRD patterns of (a) Cellulose, (b) CW, (c) chitosan, (d) Isoniazid, and (e) C/CW5/GA50	90
	4.3	SEM micrographs of (a) Untreated filter paper, (b) CW, (c) C/CW0/GA50 and (d) C/CW5/GA50	91
	4.4	TEM micrographs of chitosan microparticles (a) without CW range and (b) with CW at 50 nm scale respectively	92
	4.5	Percentage swelling degree at pH 1.2 and 7.4 ,(A){ (a)C/CW0/GA50, (b) C /CW1/GA50, (c) C/CW3/GA50, (d) C/CW5/GA50, (e) C/CW0/GA50, (f) C /CW1/GA50, (g) C/CW3/GA50, (h) C/CW5/GA50} and (B) {(a) C/CWM5/GA10, (b) C/CW5/GA30, (c) C /CW5/GA50, (d) C /CW5/GA70, (e) C/CWM5/GA10, (f) C/CW5/GA30, (g) C /CW5/GA50, (h) C /CW5/GA70}	93
	4.6	Cumulative release (%) at pH 1.2 and 7.4 ,(A){ (a)C/CW0/GA50, (b) C /CW1/GA50, (c) C/CW3/GA50, (d) C/CW5/GA50, (e) C/CW0/GA50, (f) C /CW1/GA50, (g) C/CW3/GA50, (h) C/CW5/GA50} and (B) {(a) C/CWM5/GA10, (b) C/CW5/GA30, (c) C /CW5/GA50,	94

	(d) C /CW5/GA70, (e) C/CWM5/GA10, (f) C/CW5/GA30, (g) C /CW5/GA50, (h) C /CW5/GA70}	
4.7	Cell viability study with variation of (a) Chitosan, (b) CW, (c) isoniazid, and (d) C/CW0/GA50 (e) C/CW1/GA50 (f) C/CW5/GA50 at 6 h, 12 h, and 24 h	95
4.8	FTIR spectra of (a) Pure chitosan, (b) MMT, (c) Isoniazid, and (d) NPV	98
4.9	XRD patterns of (a) Isoniazid, (b) Chitosan, (c) MMT, and (d) NPV	99
4.10	SEM micrographs of (a) Chitosan- MMT nanoparticles without isoniazid, (b) NPV, and TEM micrographs of (c) NPVI, and (d) NPV	100
4.11	Percentage swelling degree at pH 1.2 of (a) NPV, (b) NPV, (c) NPV, (d)NPV, (e) NPI, and at pH 7.4 of (f) NPV, (g) NPV, (h) NPV, (i) NPV, (j) NPI	101
4.12	Cumulative percentage drug release at (A) pH 1.2 of (a) NPV, (b) NPV, (c) NPV, (d)NPV, (e) NPI, and at (B) pH 7.4 of (a) NPV, (b) NPV, (c) NPV, (d) NPV, (e) NPI	102
4.13	Figure 4.13. Cell viability study with variation of (a) surfactant, (b) clay, (c) isoniazid, and (d) drug embedded nanoparticles, (e) NPI, (f) NPV, (g) NPV, (h) NPV at 6 h, 12 h, and 24 h	104
4.14	¹ H NMR spectra of CMC	107
4.15	FTIR spectra of (a) Chitosan, (b) CMC, (c) MMT, (d) Isoniazid, and (e) CMC/M5/GA50	109
4.16	XRD patterns of (a) Isoniazid, (b) MMT, (c) chitosan, (d) CMC, and (e) CMC/M5/GA50	111
4.17	SEM micrographs of (a) CMC /M0/GA50, (b) CMC/M5/GA50, and (c) EDX of CMC/M5/GA50	112

4.18	TEM micrographs of CMC nanoparticles (a) without MMT range and (b) with MMT at 100 nm scale respectively	113
4.19	Percentage swelling degree at pH 1.2 and 7.4: (A) {(a)CMC/M0/GA50, (b) CMC /M1/GA50, (c) CMC /M3/GA50, (d) CMC /M5/GA50, (e) CMC /M0/GA50, (f) CMC /M1/GA50, (g) CMC /M3/GA50, (h) CMC /M5/GA50} and (B) {(a) CMC M5/GA10, (b) CMC /M5/GA30, (c) CMC /M5/GA50, (d) CMC /M5/GA70, (e) CMC /M5/GA10, (f) CMC /M5/GA30, (g) CMC /M5/GA50, (h) CMC /M5/GA70}	114
4.20	. Cumulative release at (A) with variation of MMT at pH =1.2 {(a)CMC/M0/GA50, (b) CMC /M1/GA50, (c) CMC /M3/GA50, (d) CMC /M5/GA50}, (B) with variation of MMT at pH=7.4 {(a)CMC/M0/GA50, (b) CMC /M1/GA50, (c) CMC /M3/GA50, (d) CMC /M5/GA50}, (C) with variation of GA at pH= 1.2{(a) CMC M5/GA10, (b) CMC /M5/GA30, (c) CMC /M5/GA50, (d) CMC /M5/GA70} and (D) with variation of GA at pH= 7.4 {(a) CMC M5/GA10, (b) CMC /M5/GA30, (c) CMC /M5/GA50, (d) CMC /M5/GA70}	115
4.21	Cell viability study with variation of (a) CMC, (b) MMT, (c) isoniazid, and (d) CMC/M0/GA50 (e) CMC/M1/GA50 (f) CMC/M5/GA50 at 6 h, 12 h, and 24 h	116
4.22	³¹ P NMR spectra of PCTS	117
4.23	FTIR spectra of (a) Chitosan, (b) PCTS, (c) MMT, (d) Isoniazid, and (e) PCTS/M5/GA50	120
4.24	XRD patterns of (a) Isoniazid, (b) MMT, (c) chitosan, (d) PCTS, and (e) PCTS/M5/GA50	121
4.25	SEM micrographs of (a) PCTS /M0/GA50 and (b) PCTS/M5/GA50	122

4.26	TEM micrographs of PCTS nanoparticles (a) without MMT range and (b) with MMT at 100 nm scale respectively	122
4.27	Percentage swelling degree at pH 1.2 and 7.4: (A) {(a)PCTS/M0/GA50, (b) PCTS /M1/GA50, (c) PCTS /M3/GA50, (d) PCTS /M5/GA50, (e) PCTS /M0/GA50, (f) PCTS /M1/GA50, (g) PCTS /M3/GA50, (h) PCTS /M5/GA50} and (B) {(a) PCTS M5/GA10, (b) PCTS /M5/GA30, (c) PCTS /M5/GA50, (d) PCTS /M5/GA70, (e) PCTS /M5/GA10, (f) PCTS /M5/GA30, (g) PCTS /M5/GA50, (h) PCTS /M5/GA70}	123
4.28	Cumulative release at (A) with variation of MMT at pH =1.2 and 7.4 {(a)PCTS/M0/GA50, (b) PCTS /M1/GA50, (c) PCTS /M3/GA50, (d) PCTS /M5/GA50, (e)PCTS/M0/GA50, (f) PCTS /M1/GA50, (g) PCTS /M3/GA50, (h) PCTS /M5/GA50}, (B) with variation of GA at pH= 1.2 and 7.4 {(a) PCTS M5/GA10, (b) PCTS /M5/GA30, (c) PCTS /M5/GA50, (d) PCTS /M5/GA70 (e) PCTS M5/GA10, (f) PCTS /M5/GA30, (g) PCTS /M5/GA50, (h) PCTS /M5/GA70}	124
4.29	Cell viability study with variation of (a) PCTS, (b) MMT, (c) isoniazid, and (d) PCTS/M0/GA50 (e) PCTS/M1/GA50 (f) PCTS/M5/GA50 at 6 h, 12 h, and 24 h	125
4.30	FTIR spectra of (a) Pure SF, (b) MMT, (c) Isoniazid, and (d) SF/M5/GA50	128
4.31	XRD patterns of (a) Isoniazid, (b) MMT, (c) SF, and (d) SF/M5/GA50	129
4.32	SEM micrographs of (a) SF /M0/GA50, (b) SF/M5/GA50, and (c) EDX of SF/M5/GA50	130
4.33	TEM micrographs of (a) SF/M0/GA50, and (b) SF/M5/GA50	131

	4.34	Percentage swelling degree at A1, B1= pH 1.2 and A2, B2=pH 7.4 of (a) SF/M0/GA50, (b) SF/M1/GA50, (c) SF/M3/GA50, (d) SF/M5/GA50, (e) SF/M5/GA10, (f) SF/M5/GA30, (g) SF/M5/GA50, (h)SF/M5/GA70	132
	4.35	Cumulative percentage drug release at (A), (C) = pH 1.2 and (D), (E) = pH 7.4 of (a) SF/M0/GA50, (b) SF/M1/GA50, (c) SF/M3/GA50, (d) SF/M5/GA50, (e) SF/M5/GA10, (f) SF/M5/GA30, (g) SF/M5/GA50, (h)SF/M5/GA70	133
	4.36	Cell viability study with variation of (a) MMT, (b) SF, (c) isoniazid, and (d)SF/M0/GA50, (e)SF/M1/GA50, (f) SF/M5/GA50 at 6 h, 12 h, and 24	134
5	5.1	FTIR spectra of (a) Chitosan, (c) MMT, (d) curcumin, and (e) C/M5/Gen50	139
	5.2	XRD patterns of (a) Curcumin, (b) MMT, (c) chitosan, (d) C/M5/Gen50	140
	5.3	SEM micrographs of (a) C /M0/Gen50 and (b) C/M5/Gen50	141
	5.4	TEM micrographs of Chitosan nanoparticles (a) without MMT range and (b) with MMT at 100 nm scale respectively	141
	5.5	Figure 5.5. Percentage swelling degree at pH 1.2 and 7.4 ,(A){ (a)C/MMT0/Gen50, (b) C /MMT1/Gen50, (c) C/MMT3/Gen50, (d) C/MMT5/Gen50, (e) C/MMT0/Gen50, (f) C /MMT1/Gen50, (g) C/MMT3/GA50, (h) C/MMT5/GA50} and (B) {(a) C/MMT5/Gen10, (b) C/MMT5/Gen30, (c) C /MMT5/Gen50, (d) C /MMT5/Gen70, (e) C/MMT5/Gen10, (f) C/MMT5/Gen30, (g) C /MMT5/Gen50, (h) C /MMT5/Gen70}	142
	5.6	Cumulative release (%) at pH 1.2 and 7.4 ,(A){ (a)C/MMT0/Gen50, (b) C /MMT1/Gen50, (c)	144

	C/MMT3/Gen50, (d) C/MMT5/Gen50, (e) C/MMT0/Gen50, (f) C /MMT1/Gen50, (g) C/MMT3/Gen50, (h) C/MMT5/Gen50} and (B) {(a) C/MMT5/Gen10, (b) C/MMT5/Gen30, (c) C /MMT5/Gen50, (d) C /MMT5/Gen70, (e) C/MMT5/Gen10, (f) C/MMT5/Gen30, (g) C /MMT5/Gen50, (h) C /MMT5/Gen70}	
5.7	Cytotoxicity study of chitosan, MMT, curcumin, C/M1/Gen5, C/M3/Gen5 and C/M5/Gen5 at different concentrations on (a) normal lymphocytes, (b) MCF-7 and (c) HepG2 cell lines at different concentrations. [S4=C/M0/Gen50, S5=C/M3/Gen50, S6=C/M5/Gen50]	145
5.8	Effects of curcumin loaded chitosan-MMT nanoparticles on toxicity related parameters and antioxidants. Values of all the parameters are expressed as fold changes of mean in comparison to control. Level of GSH is calculated as nMole/g protein; Specific activity of SOD is expressed as μ Mole/mg Protein; Specific activity of catalase is expressed as μ Mole H ₂ O ₂ /min/mg Protein; Level of lipid peroxidation is calculated as nMole/g protein	146
5.9	FTIR spectra of (a) CMC, (b) MMT, (c) curcumin, and (d) CMC/M5/Gen50	150
5.10	XRD patterns of (a) Curcumin, (b) MMT, (c) CMC, (d) CMC/M5/Gen50	151
5.11	SEM micrographs of (a) CMC /M0/Gen50 and (b) CMC/M5/Gen50	152
5.12	TEM micrographs of CMC nanoparticles (a) without MMT range and (b) with MMT at 100 nm scale respectively	152
5.13	Percentage swelling degree at pH 1.2 and 7.4 ,(A){	153

	(a)CMC/MMT0/Gen50, (b) CMC /MMT1/Gen50, (c) CMC/MMT3/Gen50, (d) CMC/MMT5/Gen50, (e) CMC/MMT0/Gen50, (f) CMC /MMT1/Gen50, (g) CMC/MMT3/GA50, (h) CMC/MMT5/GA50} and (B) {(a) CMC/MMT5/Gen10, (b) CMC/MMT5/Gen30, (c) CMC/MMT5/Gen50, (d) CMC/MMT5/Gen70, (e) CMC/MMT5/Gen10, (f) CMC/MMT5/Gen30, (g) CMC /MMT5/Gen50, (h) CMC /MMT5/Gen70}	
5.14	Cumulative release (%) at pH 1.2 and 7.4 ,(A){ (a)CMC/MMT0/Gen50, (b) CMC/MMT1/Gen50, (c) CMC/MMT3/Gen50, (d) CMC/MMT5/Gen50, (e) CMC/MMT0/Gen50, (f) CMC/MMT1/Gen50, (g) CMC/MMT3/Gen50, (h) CMC/MMT5/Gen50} and (B) {(a) CMC/MMT5/Gen10, (b) CMC/MMT5/Gen30, (c) CMC/MMT5/Gen50, (d) CMC/MMT5/Gen70, (e) CMC/MMT5/Gen10, (f) CMC/MMT5/Gen30, (g) CMC/MMT5/Gen50, (h) CMC/MMT5/Gen70}	154
5.15	Cytotoxicity study of CMC, chitosan, MMT, curcumin, CMC/M1/Gen5, CMC/M3/Gen5 and CMC/M5/Gen5 at different concentrations on(a) normal lymphocytes, (b) MCF-7 and (c) HepG2 cell lines at different concentrations.[5=C/M5/Gen50, 3=CMC/M3/Gen50, 0=C/M0/Gen50]	156
5.16.	FTIR spectra of (a)PCTS, (b) MMT, (c) curcumin, and (d) PCTS/M5/Gen50.	159
5.17	XRD patterns of (a) Curcumin, (b) MMT, (c) PCTS, (d) PCTS/M5/Gen50	120
5.18	SEM micrographs of (a) PCTS /M0/Gen50 and (b) PCTS/M5/Gen50	161

- 5.19 TEM micrographs of PCTS nanoparticles (a) without MMT range and (b) with MMT at 100 nm scale respectively 161
- 5.20 Percentage swelling degree at pH 1.2 and 7.4 ,(A){ (a)PCTS/MMT0/Gen50, (b) PCTS/MMT1/Gen50, (c) PCTS/MMT3/Gen50, (d) PCTS/MMT5/Gen50, (e) PCTS/MMT0/Gen50, (f) PCTS/MMT1/Gen50, (g) PCTS/MMT3/GA50, (h) PCTS/MMT5/GA50} and (B) {(a) PCTS/MMT5/Gen10, (b) PCTS/MMT5/Gen30, (c) PCTS/MMT5/Gen50, (d) PCTS/MMT5/Gen70, (e) PCTS/MMT5/Gen10, (f) PCTS/MMT5/Gen30, (g) PCTS /MMT5/Gen50, (h) PCTS/MMT5/Gen70} 162
- 5.21 Cumulative release (%) at pH 1.2 and 7.4 ,(A){ (a)CMC/MMT0/Gen50, (b) CMC/MMT1/Gen50, (c) CMC/MMT3/Gen50, (d) CMC/MMT5/Gen50, (e) CMC/MMT0/Gen50, (f) CMC/MMT1/Gen50, (g) CMC/MMT3/Gen50, (h) CMC/MMT5/Gen50} and (B) {(a) CMC/MMT5/Gen10, (b) CMC/MMT5/Gen30, (c) CMC/MMT5/Gen50, (d) CMC/MMT5/Gen70, (e) CMC/MMT5/Gen10, (f) CMC/MMT5/Gen30, (g) CMC/MMT5/Gen50, (h) CMC/MMT5/Gen70} 163
- 5.22 Cytotoxicity study of PCTS, MMT, curcumin, PCTS/M1/Gen5, PCTS/M3/Gen5 and PCTS/M5/Gen5 at different concentrations on(a) normal lymphocytes, (b) MCF-7 and (c) HepG2 cell lines at different concentrations.[5=PCTS M5/Gen50, 3=PCTS/M3/Gen50, 0=PCTS/M0/Gen50] 164

Abbreviations

a.u.	Atomic unit
AFM	Atomic forced microscopy
API	Active pharmaceutical ingredient
CMC	Carboxymethyl chitosan
COX-2	Cyclooxygenase-2
CW	Cellulose whiskers
DIH	Drug induced hepatotoxicity
DMEM	Dulbecco's Modified Eagle Medium
DNA	Deoxyribonucleic acid
DS	Degree of substitution
DSC	Differential scanning calorimetry
EDX	Energy dispersive X-ray
FBS	Fatal bovine serum
FTIR	Fourier transform infrared spectroscopy
g	grams
GA	Glutaraldehyde
GSH	Glutathione
HDL	High density lipoprotein
kV	kilo Volt
LDH	Lactate dehydrogenase
LDL	Low density lipoprotein
LTBI	Latent tuberculosis infection
MDA	Malondialdehyde
mL	Milliliters
mmol	Mill moles
MMPs	Matrix metalloproteinases
MMT	Montmorillonite
MTT	(3-[4,5-dimethylthiazol-2-yl]-2,5 -diphenyl tetrazolium bromide)
mV	Millivolt
nm	Nanometer
NMR	Nuclear magnetic resonance

PBS	Phosphate buffer saline
PCTS	Phosphorylated chitosan
Rpm	Rotation per minute
SEM	Scanning electron microscopy
SF	Soy flour
TB	Tuberculosis
TEM	Transmission electron microscopy
TPP	Tripolyphosphate
UV-visible	Ultra violet-visible
v/v	volume/volume
w/v	weight/volume
WHO	World Health Organization
XRD	X-ray diffraction
SOD	Superoxide dismutase

CHAPTER 1

INTRODUCTION

CHAPTER 1

INTRODUCTION

1.1. Concept of Controlled Release Drug Delivery

Over the years, the treatment of patients has been accomplished by administering drugs to the body via various pharmaceutical dosages like tablets. These conventional drug delivery systems are still commonly used in the pharmaceutical industry. To maintain the drug level in the body within the therapeutic range, it is often necessary to take this type of drug delivery systems several times a day which sometimes results in undesirable and harmful level of drug in the body [1].

In the last few years conventional dosage forms of drugs are rapidly being replaced by the new and the novel drug delivery systems. Amongst, these the controlled release dosage forms have become exceptionally popular in present-day therapeutics. Controlled release may be defined as the technique or approach by which active agents are administered to specified target at a rate and duration designed to achieve the proposed result [2]. A typical controlled release system is designed to deliver the drug or active agents at a predetermined rate, locally or systemically, for a specified period of time. [3]. The release of the active agent may be constant or cyclic over a long period of time. The main purpose behind controlling the drug delivery is to achieve more effective therapies while eliminating the potential for both under- and overdosing. [4]. Controlled release drug administration means not only prolongation of the duration of drug delivery, but the term also implies the predictability and reproducibility of drug release kinetics. With traditional formulations, the drug level in the blood follows the profile shown in Figure 1.1a, in which the drug blood level rises after each administration of the drug and then decreases until the next administration. With traditional drug administration the blood level of the drug exceeds toxic level immediately after drug administration, and falls down below effective level after some time. Controlled drug delivery systems are designed for long-term administration where the drug level in the blood follows the profile shown in Figure 1.1(b), remaining constant, between the desired maximum and minimum, for an extended period of time [4].

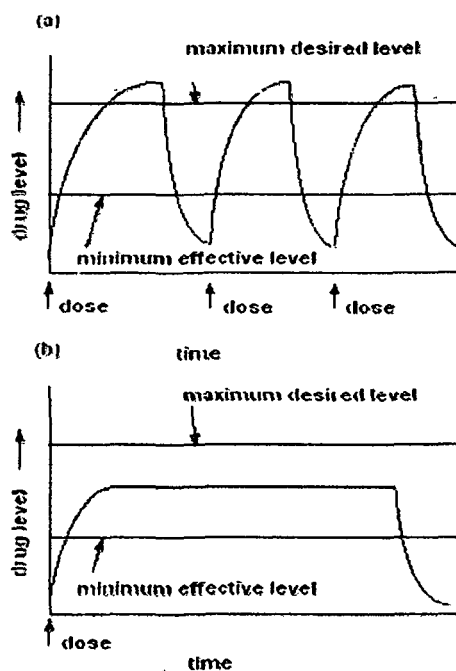


Figure 1.1. Drug levels in the blood plasma (a) traditional drug dosing, (b) controlled-delivery dosing

Nowadays, controlled release technologies are receiving immense attention in pharmaceutical industry, agricultural sector and academics. There is a growing awareness that substance in drugs and agricultural chemicals are highly toxic and sometimes, ineffective when applied by conventional methods. Controlled release technologies can provide a wide range of new therapeutic opportunities in pharmaceutical sectors like, product differentiation, market expansion and patent extension [5].

1.1.1. Need for Controlled Delivery Systems

Controlled drug delivery systems present numerous advantages compared to conventional drug delivery systems, which includes improved efficacy, reduced toxicity, and improved patient compliance and convenience [6]. Controlled drug delivery systems also increase the stability of drug by protecting it drug from hydrolysis or other derogative changes in gastrointestinal tract, it minimize the local and systemic side effects, reduces drug

accumulation with chronic dosing and most importantly, improve the bioavailability of some drugs [7,8].

Such systems often use synthetic or natural polymers as carriers for the drugs. All controlled release systems aim to improve the effectiveness of drug therapy [9,10]. This improvement can increase the therapeutic activity compared to the intensity of side effects, reducing the quantity of drug administrations required during treatment and eliminating the need for specialized drug administration.

1.1.2. Demerits of Controlled Release Systems

Controlled release systems have some disadvantages compared to conventional drug release systems which includes [11]

- Delay in commencement of drug action
- Possibility of dose dumping in the case of a poor formulation approach
- Greater dependence on gastrointestinal residence time of dosage form
- Likelihood of less precise dose tuning in some cases
- Cost per unit dose is higher when compared with conventional doses
- All drugs are not suitable for formulating controlled release systems.

In recent years, much advancement has occurred in the field of controlled delivery formulations. The polymers and fillers used in these systems have become much more sophisticated, with the capability to do more than simply extending the release period for a particular active agent (i.e. drug). Current controlled release systems can respond to changes in the biological environment and deliver or cease to deliver active agents based on these changes. Scientists are exploring the potential of the different technologies in the field of controlled release drug delivery.

1.2. Fundamental components of controlled delivery formulations

The most fundamental components of controlled delivery system include (a) the polymer matrix or matrices that regulate the release of the active components (b) the active agent i.e. drug, (c) reinforcing agent and (d) the crosslinking agents. Varieties of polymers,

active agents [12], and crosslinking agents are being used for the development of controlled delivery formulations.

1.2.1. Polymers

Polymers, both natural and synthetic, are highly beneficial in preparing controlled delivery formulations. Most of the drugs are low molecular weight compounds. Remarkable advancement in polymer science and technology has made it possible to combine a low molecular active agent species physically or chemically to a polymer. In controlled delivery technique, the active agent is allowed to release from the polymer-active agent combination over a period of time, most often to a specific target. In physical combinations, polymer acts as a rate-controlling device while in chemical combinations; it acts as a carrier for the active agent.

An important advantage of polymeric controlled delivery formulation is that the toxic natures of the chemicals are minimized. Many new drugs available are highly toxic. It poses risk to non-target organs also. But if it is encapsulated or distributed in a polymer, its toxicity will be much reduced, since the entire amount does not release at one time. Still another advantage is that the polymer combinations being solids are easy to handle [13].

The success of controlled delivery formulation relies on combining the active agent with the polymer in an economic manner alongwith time maintaining the desired release profile. These are often in opposition and one has to compromise in the ultimate cost/benefit ratio of controlled delivery formulations, [14]. However there are many classes of polymers which can be effectively employed in controlled delivery formulations. The efficiency of controlled delivery formulations depends on the following polymer properties-

- _ Solubility and distribution characteristics with the active agent.
- _ Solubility and distribution characteristics with the environmental agents.
- _ Good compatibility with the environment i.e., it should be non-toxic.
- _ Good compatibility with the active agent i.e., it should not produce undesirable products.
- _ Stability in the environment i.e., it should not degrade during the course of action.

Degradation is preferable after the completion of desired function. The degraded products should not harm the environment.

_ Ease of fabrication.

_ Cost.

1.2.1.1. Chitosan

Among the natural polymers, polysaccharides have received increasing attention because of their outstanding physical and biological properties [15]. Chitin is the second most omnipresent natural polysaccharide after cellulose and is composed of $\beta(1\rightarrow4)$ -linked 2-acetamido-2-deoxy- β -D-glucose (N-acetylglucosamine) which was first identified by Henri Braconnot (Director of botanical garden in Nancy, France) in 1811 [16,17]. The name chitin is derived from Greek, connotation "tunic" or "envelope". Chitin is structurally identical to cellulose, but has acetamide groups (NHCOCH_3) at the C-2 position. Chitin is a white, hard, inelastic, nitrogenous polysaccharide and occurs in nature as ordered crystalline microfibrils forming structural components in the exoskeleton of arthropods or in the cell walls of fungi and yeast. It is also produced by a number of other living organisms in the lower plant and animal kingdoms, serving in many functions where reinforcement and strength are required [18]. In 1843, Lassaigne demonstrated the presence of nitrogen in chitin. Depending upon the source from which it is obtained, chitin occurs as three different crystalline forms, namely α , β and γ forms [19-21]. It is found from studies that γ -chitin is a variant of α -chitin [22]. The strong inter- and intramolecular hydrogen bonding and crystalline structure are mainly responsible for limited solubility in common solvents.

After the discovery of chitin, the name "chitosan" came into sight. Rouget while experimenting with chitin first discovered it. Rouget observed that the compound of chitin could be maneuvered through chemical and temperature treatments for it to become soluble. Then, it was in 1878 when Ledderhose identified chitin to be made of glucosamine and acetic acid. By partial deacetylation under alkaline conditions, one obtains chitosan, which is the most important chitin derivative in terms of applications.

Chitosan plays an important role as drug delivery systems. In 1884, Rawls introduced chitosan as an attractive candidate for treating burns [23]. Chitosan is a linear aminopolysaccharide composed of randomly distributed (1→4) linked D-glucosamine and N-acetyl-D-glucosamine units and is obtained by the deacetylation of chitin, a prevalent natural polysaccharide found in the exoskeleton of crustaceans such as crab and shrimp [24]. It can also be obtained from some microorganisms and yeasts. Structure of chitosan is shown in Figure 1.2.

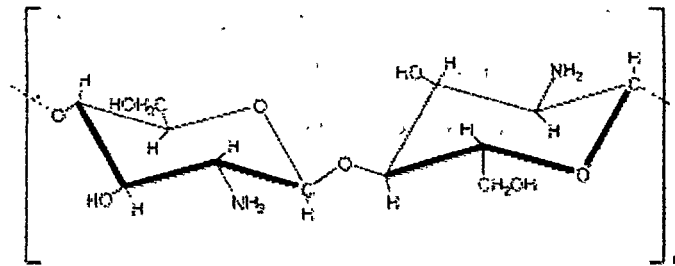


Figure 1.2. Structure of chitosan

Chitosan is a mucoadhesive polycation polymer at acidic pH which is not noxious and biocompatible [15, 25-27]. Chitosan has also fungicidal effect, wound healing properties and reduces cholesterol level [28]. Owing to its cationic nature chitosan has good mucoadhesive and membrane permeation enhancing properties [29]. Chitosan offer several advantages over other synthetic polymers and natural polymers.

- Like some plant fibers, it is not digestible; therefore it has no caloric value. This is a very important property for any weight loss product.
- Absorbs and binds fat and promote weight loss [30]
- Inhibits LDL cholesterol and boosts HDL cholesterol [31]
- Promote healing of ulcers/lesions [32,33]
- It has antibacterial and anticandida properties. It has also the ability to kill certain viruses [34-36]
- Acts as antacid [37,38]
- Inhibits the formation of plaque/tooth decay [39]
- Helps to control blood pressure
- May treat and prevent irritable bowel syndrome [40]

- Helps to prevent constipation [41]
- Helps to control blood pressure [42,43]
- Reduces uric acid level in blood [44]
- Anti-tumor action [45]
- Enzymatically biodegradable
- Non toxic and biocompatible

Beside biodegradability, natural polymer offers several advantages over synthetic polymers in terms of low cost, low density, low energy consumption, and wide availability.

So far, chitosan has been utilized in various fields of pharmaceutical technology, including the formulation of controlled release dosage forms, such as tablets, gels and microspheres, as mucoadhesive and/or permeation enhancing excipient for oral, nasal, ocular and buccal drug delivery and in non-viral gene delivery.

Even though chitosan has many advantages which make it useful in drug delivery system, it is also associated with the problem of solubility. Chitosan is a weak base and is insoluble in water, but soluble in dilute aqueous acidic solutions below $pK_a \sim 6.3$, in which the glucosamine units ($-NH_2$) gets converted into the soluble protonated form ($-NH_3^+$) [46]. To improve the solubility of chitosan, it is derivatized. The chitosan derivatives also have improved mucoadhesive and/or permeation enhancing properties in addition to improved solubility. The various derivatives which are used are trimethyl chitosan, phosphorylated chitosan, thiolated chitosan, etc. The strong cohesive properties of chitosan derivatives make them highly suitable excipients for prolonged controlled drug release dosage forms.

1.2.1.2. Carboxymethyl chitosan

Carboxymethyl chitosan is one of the water soluble derivatives of chitosan. Compared to other water-soluble derivatives of chitosan, carboxymethyl chitosan (CMC) has been widely studied because of its ease of synthesis, ampholytic character and possibilities of wide range of applications. The carboxymethylation procedure of both chitin and

chitosan has been reported by Muzzarelli [47]. Figure 1.3. shows the preparation process of CMC.

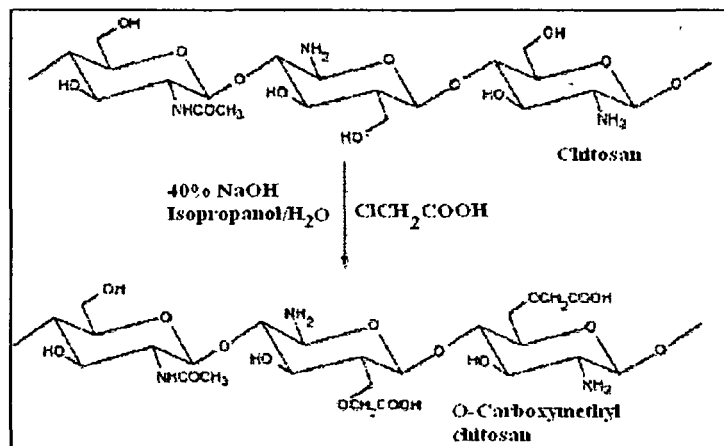


Figure 1.3. Scheme of preparation of CMC from chitosan

CMC has better solubility in water, superior antibacterial property [48] and enhanced biocompatibility [49,50]. CMC exhibits low toxicity [51].

1.2.1.3. Phosphorylated chitosan (PCTS)

Phosphorylated chitosan is one of the water soluble derivatives of chitosan which can be widely used in the field of drug delivery. Phosphorylated chitosan can be prepared by heating chitosan with orthophosphoric acid and urea in DMF or by the reaction of chitosan with phosphorus pentoxide in methane sulphonic acid [52-56]. Figure-1.4. shows the process of preparation of PCTS from chitosan. Phosphorylated chitosan of high degree of substitution (DS) was insoluble in water while those of low DS were soluble.

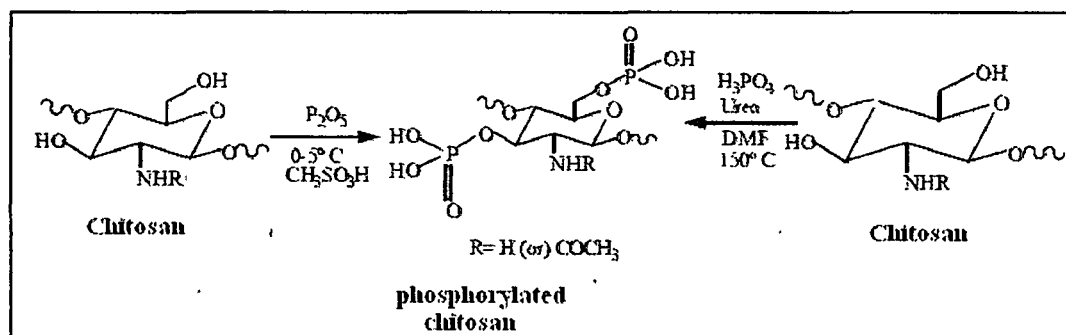


Figure 1.4. Preparation of phosphorylated chitosan from chitosan

The insolubility of Phosphorylated chitosan of high DS may be accredited to the formation of inter- or intramolecular salt linkage between amino and phosphate groups due to the formation of poly-ion complex [57]. Phosphorylated chitosan has a wide range of applications. Phosphorylated chitosan has strong metal binding capacity. They have very high adsorption capacity for Uranium than that of any other heavy metal [54]. Phosphorylated chitosan has ability to form chelate rings with transition metal ions as well as Calcium ions [58]. Phosphorylated chitosan gel beads are also used in controlled release drug delivery applications [59-61] Phosphorylated chitosan is used in the formation of biodegradable films, immobilization of enzymes, preservation of food from microbial deterioration, as additives (for clarification and deacidification of fruits and beverages, as emulsifying, thickening and stabilizing agents, for color stabilization etc.), and as dietary supplements. Phosphorylated chitosan is also used in tissue engineering as artificial bone scaffolds.

1.2.1.4. Soy flour

Soy (*Glycine max* (L.) Merr.) belongs to the leguminous family and contains nine different varieties. It was first used in United States in 1940 in bread formulations owing to its food and medicinal values [62]. Soybeans are classified as oil seeds, a staple food of nutritional value and a rich source of protein. Soy flour is made from soy beans by mechanically removing the hull, followed by extraction of the oil with hexane. Residual hexane is removed by flash desolventizer. The desolventized soy is then heat processed and ground to form the flour [63]. Soy flour is regarded as the most inexpensive vegetable protein of high quality which contains 50% protein and all of essential amino acids needed for human beings [64]. Soy flour has easy availability, good processability and is non toxic [65-68]. Soy flour lower cholesterol and thereby prevents heart attack, stroke and hypertension [69,70]. The protein and fibre in soyabeans can prevent high blood sugar level and help in keeping blood sugar levels control. Soyabean promote serum insulin production, reduce bone loss that typically occurs after menopause in women and inhibit cancer development [71-73]. The uses of soy flour as a drug delivery device have not been explored much. Table 1.1. shows the composition of soy flour and Table 1.2. shows the amino acid content of soy flour.

Table 1.1. Composition of Soy flour [74]

Content / 100 g	Unit	Content	Variation
Energy	kJ	1879	
Protein, total	g	37.2	36.3 - 38.0
Fat, total	g	22.2	20.6 - 23.8
saturated fatty acids	g	3.1	
monounsaturated fatty acids	g	5.4	
polyunsaturated fatty acids	g	12.6	
Carbohydrate, total	g	30.5	29.4 - 31.5
carbohydrate, available	g	20.1	
added sugar	g	0	
dietary fibre	g	10.4	9.8 - 11.0
Alcohol	g	0	
Vitamin A	RE	5.50	
retinol	µg	0	
β-carotene eq.	µg	66	
Vitamin D	µg	0	
D3 cholecalciferol	µg		
D2 ergocalciferol	µg		
25-hydroxycholecalciferol	µg		
Vitamin E	α-TE	21.0	
alpha-tocopherol	mg	21.0	
Vitamin K	µg	200	
Vitamin B1, thiamin	mg	0.75	
Vitamin B2, riboflavin	mg	0.31	
Niacin equivalents	NE	10.7	
Pantothenic Acid	mg	1.8	

Biotin	μg		
Folates	μg	800	
Vitamin B12	μg	0	
Vitamin C	mg	0	
L-Ascorbic Acid	mg		
L-Dehydroascorbic acid	mg		
Pantothenic Acid	mg	18	
Sodium, Na	mg	2	
Potassium, K	mg	1936	
Calcium, Ca	mg	150	
Magnesium, Mg	mg	240	
Phosphorus, P	mg	560	
Iron, Fe	mg	4	
Copper, Cu	mg	16	
Zinc, Zn	mg	5	
Iodine, I	μg	0.5	
Manganese, Mn	mg	2.3	
Chromium, Cr	μg	23	
Selenium, Se	μg	11	
Nickel, Ni	μg	390	

Table 1.2. Amino acid contents in Soy flour [74]

Amino acids	mg/100g	mg/g
Isoleucine	1800	280
Leucine	3200	490
Lysine	2600	400
Methionine	520	80
Cystine	650	100

Phenylalanine	2000	310
Tyrosine	1300	200
Threonine	1600	240
Tryptophan	520	80
Valine	2000	300
Arginine	2900	450
Histidine	1000	160
Alanine	1800	270
Aspartic acid	4800	730
Glutamic acid	7600	1170
Glycine	1700	260
Proline	2200	340
Serine	2100	320

1.2.2. Active Agents

The substance to be encapsulated or loaded is called active agent. It may be virtually any substance, natural or synthetic, that is entirely or partially soluble in the reaction medium or solvent. It may be solid, a hydrophobic or hydrophilic liquid, or a mixture of a solid and a hydrophobic or hydrophilic liquid. The major active agents include drugs, food products, agrochemicals and varieties of oils [75]. The loading substance may include a purified or partially purified substance depending on the requirements of application.

1.2.2.1. Isoniazid

Isoniazid (or 4-Pyridinecarboxylic acid hydrazide or isonicotinic acid hydrazide or INH), a first line drug used for tuberculosis chemotherapy [Figure 1.5]. Its molecular formula is $C_6H_7N_3O$. Isoniazid (INH) is one of the primary chemotherapeutic and prophylactic drugs used against *Mycobacterium tuberculosis*, the causative agent of tuberculosis, which is the one of the leading cause of death due to an infectious agent throughout the world [76].

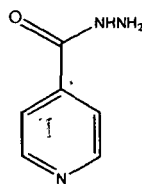


Fig.1.5. Structure of isoniazid

Isoniazid is soluble to the extent of 125 mg/mL of water at room temperature. Solubility in water varies as ~14% at 25°C, ~26% at 40°C; in ethanol: ~2% at 25°C, ~10% in boiling ethanol; in chloroform: ~0.1%. It is almost insoluble in ether and benzene. It has a melting point of 171.4°C. Isoniazid is one of the key active pharmaceutical ingredients (API) used in the combination treatment of tuberculosis (TB) recommended by the World Health Organization (WHO).

The WHO recommends a dosage range from 4 to 6 mg/kg, with the maximum daily dose not to exceed 300 mg. The 300 mg maximum daily dose is also used as preventive therapy for populations at high risk. At this dose, the antibiotic is well tolerated.

The most commonly occurring adverse effect in the treatment with isoniazid is hepatotoxicity. Serious toxic symptoms have been reported to occur at doses of 2–3 g or higher in adults. Doses of 10–15 g may be fatal without appropriate treatment [77].

1.2.2.2. Curcumin

Cancer is a familiar disease of old age. It is anticipated that the process of tumorigenesis initiates approximately at the age of 20 and detection of cancer is normally around the age of 50 or later. So, the estimated incubation time is around 20–30 years. Current studies indicate that in any given type of cancer 300–500 normal genes get modified somehow to result in the cancerous phenotype.

The ineffectiveness, lack of safety, and high cost of therapies have led to a lack of faith in anticancer approaches. Many plant-based products, however, achieve multitargeting naturally and, in addition, are low-priced and safe compared to synthetic agents. However, because pharmaceutical companies are not usually able to secure intellectual property rights to plant-based products, the development of plant-based anticancer

therapies has not been prioritized. Nonetheless, curcumin, a plant-based product, has shown significant promise against cancer and other inflammatory diseases.

Curcumin is one of the active components of Turmeric plant (*Curcuma longa*). Turmeric is a perennial herb of the Zingiberaceae family and is cultivated extensively in south and southeast tropical Asia [78].

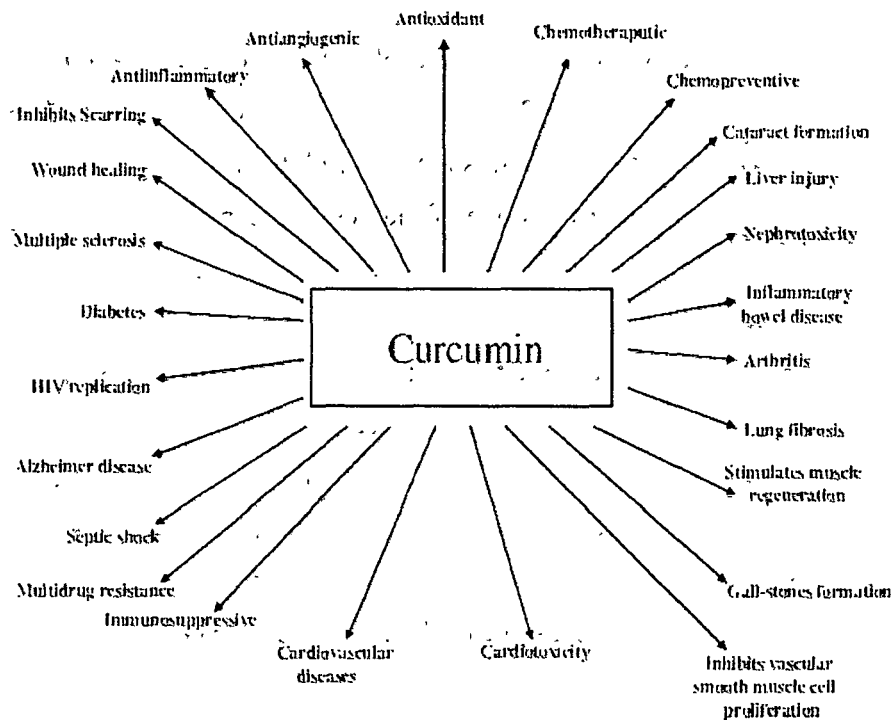


Figure 1.6. Pharmaceutical properties of curcumin

Turmeric, i.e., the ground rhizomes of *Curcuma longa*, has a long history of use in food as a spice, mainly as an ingredient in many diverse forms of curry powders and sauces, where curcumin is the main colouring substance. Curcumin is first identified in 1910 by Lampe and Milobedzka [79]. Curcumin has numerous pharmacological activities, including antioxidant, antimicrobial properties, anti-inflammatory effects and anti cancer activities [80-82]. Some other pharmaceutical properties of curcumin are described in figure 1.6.[83]. Chemically, curcumin is bis- α,β -unsaturated β -diketone (commonly called diferuloylmethane), which shows keto-enol tautomerism having a predominant keto form in acidic and neutral solutions and stable enol form in alkaline medium [84,85].

Commercial curcumin contains approximately 77% diferuloylmethane, 17% demethoxycurcumin, and 6% bisdemethoxycurcumin (Fig. 1.7.) [86].

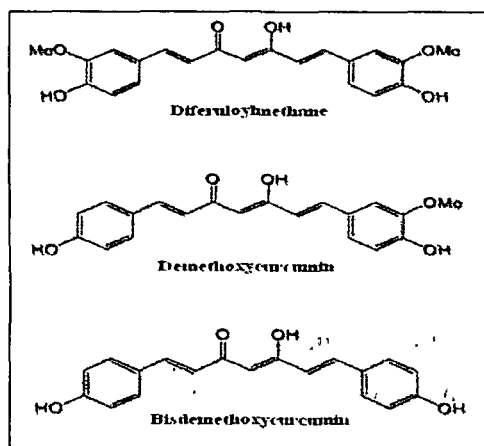


Figure 1.7. Composition of curcumin

The pharmacological safety and efficacy of curcumin makes it a budding compound for treatment and prevention of a wide variety of human diseases. But, in spite of all these advantages curcumin is not considered as the therapeutic agent due to its low bioavailability. The reasons for low bioavailability of curcumin within the body are poor absorption and high rate of metabolism. Animal studies have shown curcumin is rapidly metabolized, conjugated in the liver, and excreted in the feces, therefore having limited systemic bioavailability. A 40 mg/kg intravenous dose of curcumin given to rats resulted in complete plasma clearance at one hour post dose. An oral dose of 500 mg/kg given to rats resulted in a peak plasma concentration of only 1.8 ng/mL, with the major metabolites identified being curcumin sulfate and curcumin glucuronide [87]. To solve the problem of bioavailability curcumin can be complexed with other substances, such as alkaloid piperine, phospholipid, etc. [88,89] or curcumin can be incorporated in nanoparticles.

1.2.3. Reinforcing agents

In general, the reinforcing agent or the reinforcement is the discontinuous phase in the nanoparticles or microparticles which are much stronger and stiffer than the polymer

matrix. The reinforcing agents can either fibers, particles, laminae, whiskers, or flakes and they can either be organic, inorganic, metallic or ceramic materials. They are structural constituents. They determine the internal structure of the nanoparticles and provide strength and modulus to the nanoparticles. In controlled release drug delivery the properties of the nanoparticles can be controlled by varying the quantity of the reinforcing agent. The reinforcing agents used for the present study are montmorillonite and cellulose whisker.

1.2.3.1. Montmorillonite (MMT)

Montmorillonite was first described in 1847 for an occurrence in Montmorillon in the department of Vienne, France by Mauduyt [90]. He named the compound as “montmorillonite”. The name “montmorillonite” or the German form “Montmorillonit” appears to be first used by Naumann in 1850 [91]. Montmorillonite are sheet structured hydrous silicates which are referred to as phyllosilicates. Montmorillonite falls in the category of 2:1 smectite clay. The general formula for the chemical structure of this group is $(\text{Na,Ca})_{0,3}(\text{Al,Mg})_2\text{Si}_4\text{O}_{10}(\text{OH})_2 \cdot n(\text{H}_2\text{O})$ [Figure 1.8.]. Montmorillonite has layered structure where each layer is composed of two types of structural sheets: octahedral and tetrahedral. The tetrahedral sheet is composed of silicon-oxygen tetrahedra linked to neighboring tetrahedra by sharing three corners, resulting in a hexagonal network [92]. The remaining fourth corner of each tetrahedron forms a part to adjacent octahedral sheet. The octahedral sheet is usually composed of aluminum or magnesium in six-fold coordination with oxygen from the tetrahedral sheet and with hydroxyl.

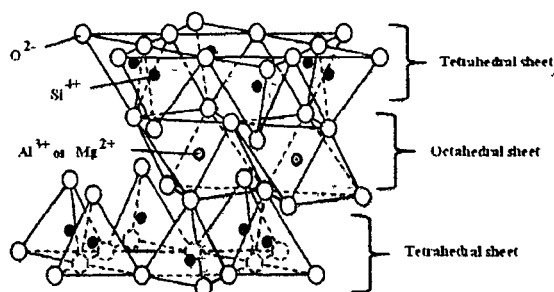


Figure 1.8. Structure of montmorillonite

The two sheets together form a layer, and several layers may be joined in a clay crystallite by interlayer cations, Van der Waals force, electrostatic force, or by hydrogen bonding. The presence of charge in tetrahedral and octahedral sheets influences the layered structure. Isomorphous substitution (i.e. the replacement of an element with another element in mineral crystal without modifying its chemical structure) in clay mineral mainly results in the charge development. For example, Al^{3+} can replace Si^{4+} in tetrahedral coordination, and replacement of Al^{3+} is possible by Mg^{2+} , Fe^{2+} in octahedral coordination. Montmorillonite is a hydrophilic clay with an aspect ratio of 1000:1 [93]. Montmorillonite can be used in pharmaceutical fields in creams and powders, baby powders, and as face packs and therapeutic muds [94]. Montmorillonite is used as a food additive for health and stamina [95] and for antibacterial activity against tooth and gum decay [96]. It can be used for the treatment of irritable bowel syndrome, prevention of constipation and prevents intestinal adsorption of cholesterol [97]. In controlled drug delivery applications, montmorillonite can control the release of the therapeutic agents as well as adsorb dietary toxins [98]. It has antibacterial effect and is non-toxic. Due to its biomedical properties, montmorillonite is also known as “medical clay” [99].

1.2.3.2. Cellulose whiskers (CW)

Cellulose is the most abundant biopolymer available on earth, and is present in a large variety of living species, such as animals, plants and bacteria. It is a renewable polymer which is biodegradable and biocompatible, and is being exponentially considered as a green alternative to fossil-fuel based polymers. Cellulose is a fibrous, tough, water-insoluble substance, which is found in the protective cell walls of plants, particularly in stalks, stems, trunks and all woody portions of plant tissues.

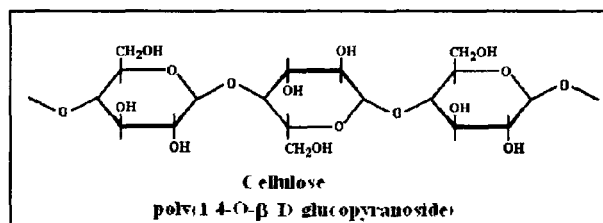


Figure 1.9. Structure of cellulose

Cellulose in the plants is composed of 1,4- β - glucopyranose units associated by hydrogen bonding [Figure 1.9.] and forming a semicrystalline structure where highly ordered regions (the crystallites) are distributed among disordered domains (the amorphous phase) [Figure 1.10.].

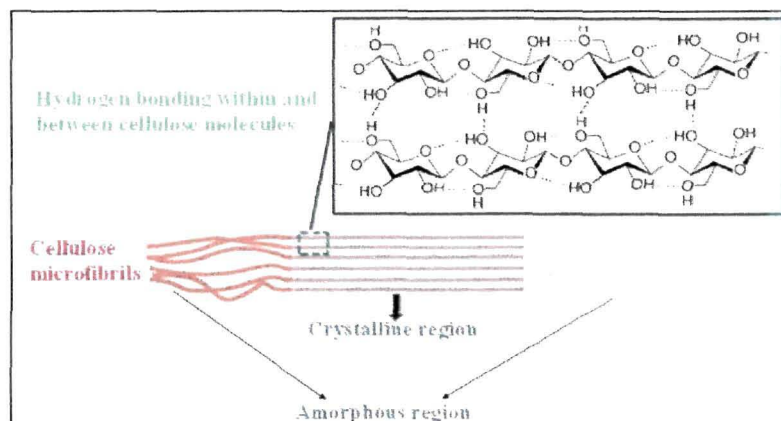


Figure 1.10. Schematic diagram showing the hydrogen bonding within and between cellulose molecules along with the amorphous and crystalline region in cellulose

Cellulose exists as four different polymorphs. They are cellulose I, II, III and IV. Cellulose I is the form usually found in nature and it occurs in two allomorphs I _{α} and I _{β} . Cellulose II is the crystalline form that appears after re-crystallization with aqueous sodium hydroxide, and it is thermodynamically the most stable crystalline form [100]. Cellulose III_I and III_{II} are obtained by a liquid ammonia treatment of cellulose I and II, respectively. Cellulose IV is obtained from heating cellulose III, the alteration being usually partial [101]. Cellulose has very high elastic modulus as well as high specific strength which make it an ideal candidate to reinforce polymer matrices in the form of macroscopic fibers.

Cellulose whiskers (CW) are usually obtained from cellulose fibers through an acid treatment combined with sonication. This process involves an acid hydrolysis of the fibers using concentrated sulfuric acid (H₂SO₄), which removes disordered regions of cellulose and leaves crystalline regions intact. After this treatment, rod-like shaped cellulose nanofibers, having anionic sulfate ester groups at their surface, are produced.

The geometrical dimensions of CW depend on the starting cellulose source, resulting in values for width varying from 5 to 20 nm, and for length from 100 nm to 1–2 μm [102]. CW has high specific strength, modulus and aspect ratio. Some other advantages of CW are their low density, renewable nature, abundance, biodegradability, and relatively low cost. As reinforcing agent, CW can significantly improve the mechanical properties of the polymers at low loading level [103]. Different types of value-added nanomaterials could be produced from CW. CW can be used to make aerogels, emulsion and foam stabilizer in food industry, DNA hybrid material, films, adhesives etc. [104-107]. CW is used in bone regeneration, artificial liver, regenerated cartilage, and suppression of action of matrix metalloproteinases (MMPs) in wound healing [108-110]. But much research has not been done in application of CW in controlled release drug delivery applications.

1.2.4. Crosslinking agents

Crosslinking is the formation of chemical links between molecular chains to form a three dimensional network of connected molecules. The crosslinking is used to control and enhance the properties of the resulting polymer system or interface. Crosslinking of polymers improves the mechanical properties as well as control release behaviour of the active agents. Depending on polymer and active agent properties, suitable crosslinkers are chosen for crosslinking. A large number of crosslinking agents, both natural and synthetic, are known to crosslink different natural and synthetic polymers. Synthetic crosslinkers such as formaldehyde, glutaraldehyde, glyceraldehydes [111-113], glyoxal [114,115], epichlorohydrin [112], sulfuric acid [111], sodium hexametaphosphate [114], sodium tripolyphosphate [116], diisocyanate, carbodiimides, tannic acid etc. All these chemical crosslinking agents are relatively cytotoxic. Nowadays, biocompatible crosslinking agents have received much attention in the field of biomedical application. For example, enzyme-catalyzed cross-linking methods have been developed to crosslink some biomaterials [117]. Genipin is a natural crosslinking agent, which is both non toxic and biocompatible [118]. Genipin can be obtained from its parent compound geniposide, which may be isolated from gardenia fruits. It has been reported that genipin can spontaneously react with amino acids or proteins to form dark blue pigments [119, 120]. In the present study, in order to improve the controlled release behaviour, synthetic

crosslinker, glutaraldehyde and natural crosslinker, genipin have been used for crosslinking of polymers. Figure 1.11. shows the structure of some of the available crosslinkers.

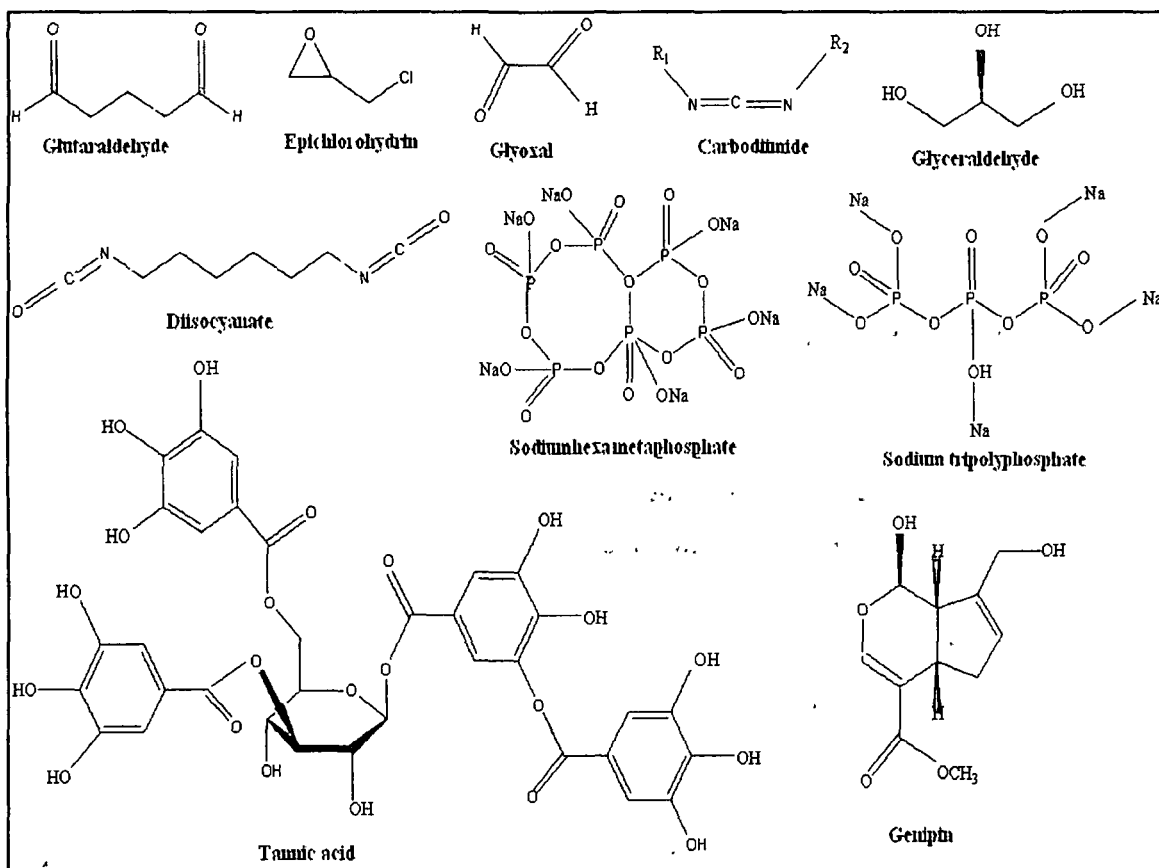


Figure 1.11. Structures of several crosslinking agents

1.3. Role of micro- and nanoparticles in controlled release drug delivery

Microparticles and nanoparticles are of considerable interest in the field of modern day drug delivery. Several methods are available for the preparation of nanoparticles and microparticles. The current situations, therefore, provides a practical basis for developing such type of controlled drug delivery systems for further applications. Although various applications of these micro and nanoparticles, e.g., for encapsulation of drugs, enzymes or fragrances, are discussed in some literatures [121] they are yet to be applied practically. Since the majority of the proposed applications are located in the

pharmaceutical field, most of the polymers used till now are not well-suited and nanoparticles composed of biocompatible and biodegradable natural polymers are required. Generally, many of the described approaches are rather unproductive (e.g., they require very low concentrations) and hence a further challenge will be to widen up the production of the nanoparticles.

The use of micro- and nanoparticles in drug delivery is also known as particulate drug delivery systems. Particulate drug delivery systems have traveled a long way from being used for research purposes to clinical applications in the last few decades. The terms “microparticle” and “nanoparticle” refer to particles where the dimensions of the particle are measured in micrometers and nanometer respectively. Most biologically active macromolecules and agents such as viruses, membranes and protein complexes are natural nanostructures; it is believed that nano-sized structures will be capable of enhanced interaction with cell membrane and proteins [122]. Owing to their very small size, micro- and nanoparticles drug delivery systems are easy to inject in the body, can be used for inhalation as dry powders or can be used for oral drug delivery purposes [123]. Nanoparticles were first developed around 1970 and were first formulated as carriers for vaccines and anticancer drugs [124]. Later on, nanoparticles were used for ophthalmic and oral drug delivery. The main advantages of nanoparticles in biomedical applications are listed below [125]

- Nanoparticles can improve the solubility of hydrophobic drug (eg. Curcumin)
- Nanoparticles with dual functionality can be used for diagnostic and therapeutic purposes (e.g., Fe₂O₃-Pt Nanoparticles)
- Nanoparticles can target tumors and can be used to reduce toxicity of the therapeutic drug
- Nanorobots can be used for drug release (e.g., photo- or pH-triggered drug release), thermal ablation, and hyperthermia.
- Increased surface area results in a faster dissolution of the active agent in the human body. Faster dissolution generally equates greater absorption and bioavailability

Polymer based micro-/nanoparticles are submicron size polymeric colloidal particles in which the active agents can be encapsulated within the polymeric matrix or adsorbed

onto the surface of the polymer [126]. These nanoparticles act as an excellent vehicle for delivery of a number of biomolecules, drugs, genes and vaccines to the specific sites. The prime advantages of polymeric nanoparticles are given below [127,128]

- Increases the stability of any volatile active agents
- Can be easily and cheaply fabricated in large quantities by a variety of methods
- Offer a significant improvement over traditional oral and intravenous methods of administration in terms of efficiency and effectiveness
- The choice of polymer and the ability to amend the release of active agents from polymeric nanoparticles have made them ideal contender for cancer therapy, delivery of vaccines, contraceptives and delivery of targeted antibiotics

1.4. Fabrication techniques of nanoparticles for controlled delivery formulations

Within the broad category of nanoparticles 'nanospheres' refer to spherical particles and 'nanocapsules' applies to particles which have a core surrounded by a material which is distinctly different from that of the core. The core may be solid, liquid or even gas. Nanoparticles usually refer to a homogeneous mixture of the polymer and active agent, whereas nanocapsules have at least one discrete domain of active agent. There are many methods of preparation of nanoparticles. Some methods for the preparation of nanoparticles include two main steps. The first step constitutes the preparation of an emulsified system while the nanoparticles are formed during the second step of the process. The second step is achieved either by the precipitation or the gelation of a polymer or by polymerization of monomers. In general, the principle of this second step gives its name to the method. In some cases, the nanoparticles form in the same time than the starting emulsified system. Suitable emulsified systems can be emulsions, mini-emulsions, nano-emulsions and microemulsions.

A few other methods do not require the preparation of an emulsion for obtaining the nanoparticles. They are based on the desolvation or precipitation of a polymer in conditions of spontaneous dispersion formation or by self assembly of macromolecules to form nanogels or polyelectrolyte complexes from a polymer solution. The methods are explained below.

1.4.1. Evaporation or Extraction of Solvent Based Process

In these methods the solvent in which the polymer is dissolved is eliminated. This elimination can be achieved by evaporation or by extraction. The formation of an emulsion is a necessary requirement. Aqueous and oily phases can be present, according to the nature of the continuum phase of the formed emulsion. The polymer is contained in the organic phase and the emulsifier is present in the aqueous phase. The emulsified organic drops containing the polymer and the active agent form micro-/ nanoparticles by the elimination of the organic solvent [129,130].

1.4.1.1. Coacervation phase separation method

Coacervation method is first developed by The National Cash Register (NCR) Corporation for carbonless copy paper as well as many other applications in 1950. This method involves the phenomenon of formation of liquid rich in polymer phase in equilibrium with another liquid phase. According to IUPAC, coacervation is defined as the separation into two liquid phases in colloidal systems. The phase more concentrated in colloid component is the coacervate, and the other phase is the equilibrium solution [131]. There are two methods of coacervation available, viz. simple coacervation and complex coacervation. Both the methods are almost identical except for the process in which phase separation is carried out.

1.4.1.1.1. Simple Coacervation Method

Simple coacervation is achieved when chemical compounds having high affinity for water such as salts and alcohols are added to the aqueous polymer solution. Simple coacervation can be brought about in any aqueous polymer solution if the pH, temperature, solvent and salt are properly chosen and adjusted [132]. The added compound cause two phases to be formed, one polymer rich phase and the other one poor. The whole process can be explained by the following three steps [133].

1. Dispersion of the core material in aqueous solution of polymer
2. Creation of insufficiency of water for hydrophilic colloid and the deposition of the coacervate around the core
3. Gelation of the coacervate and hardening of the nanoparticles

Figure 1.12. illustrates the preparation steps of nanoparticles by simple coacervation method. Microcapsules with different natural polymers have been produced by this method.

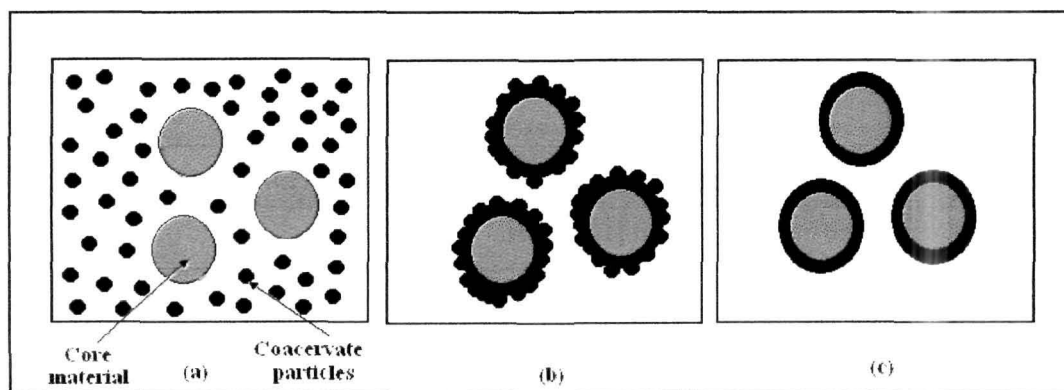


Figure 1.12. Schematic diagram showing important steps in simple coacervation method: (a) Dispersion of the core material in aqueous solution of polymer, (b) deposition of the coacervate around the core and (c) hardening of the nanoparticles

1.4.1.1.2. Complex Coacervation Method

Complex coacervation commonly refers to the liquid-liquid phase separation that results when solutions of two oppositely charged polymers are mixed, resulting in the formation of a dense polymer-rich phase, the precursors of which are soluble complexes [134]. The encapsulation process in complex coacervation involves four major steps:

1. Preparation of the hydrophilic colloid solution
2. Addition of second hydrophilic colloid solution of opposite charge to induce coacervation
3. Deposition around the core
4. Gelation of the coacervate and hardening of the nanoparticles

The core material (usually oil) is first dispersed into a polymer solution (e.g., a cationic aqueous polymer). The second polymer (water soluble, anionic) solution is then added to the prepared dispersion. Deposition of the shell material onto the core particles occurs when the two polymers form a complex. This process is initiated by the addition of salt or by changing the pH, temperature or by dilution of the medium. The shell thickness can be obtained as desired by controlled addition of the second polymer. Finally, the prepared

nanoparticles are stabilized by crosslinking, desolvation or thermal treatment. Complex coacervation is used to produce nanoparticles containing fragrant oils, liquid crystals, flavors, dyes or inks as the core material. Porous nanoparticles can also be prepared using this technique. When using this technique, certain conditions must be met to avoid agglomeration of the prepared capsules [135]. Figure – shows the steps of complex coacervation methods [136].

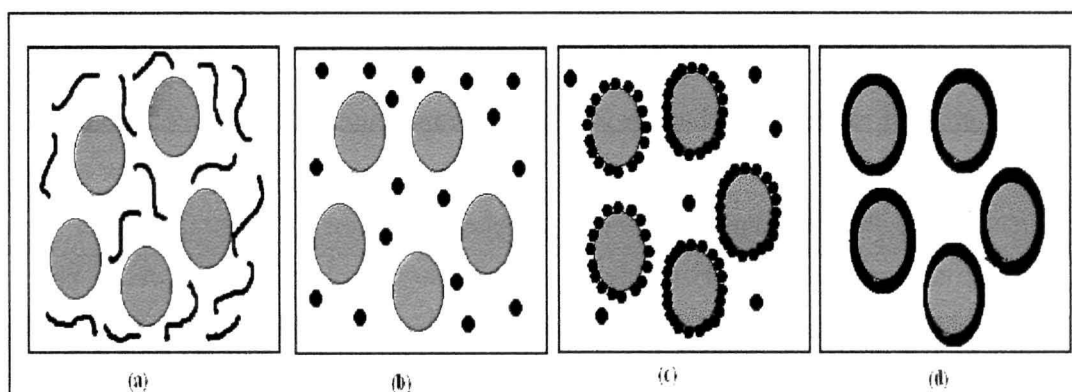


Figure 1.13. Example of complex coacervation involving (a) dispersion of the core, (b) initial coacervation after addition of coacervation agent, (c) coacervation on the surface of the core and (d) formation of the cross-linked shell by reticulation of the interface.

1.4. 2. Emulsion Based Process

1.4.2.1. Single emulsion

The particulate carriers of natural polymers, i.e. those of proteins and carbohydrates are prepared by single emulsion technique. In the first step the polymers are dissolved or dispersed in aqueous medium followed by dispersion in the non aqueous medium eg. Oil. In the second step, cross linking of the dispersed polymeric globule is carried out either by means of heat or by using chemical crosslinkers. The chemical cross linking agents used are gluteraldehyde, formaldehyde, terephthalate chloride, diacidchloride, etc. [137,138] Crosslinking by heat is accomplished by adding the dispersion to previously heated oil. Heat denaturation is not suitable for the thermolabile drugs while the chemical cross-linking suffers disadvantage of excessive exposure of active ingredient to chemicals if added at the time of preparation [139].

This process involves oil-in-water (o/w) emulsification. The o/w emulsion system consists of an organic phase comprised of a volatile solvent with dissolved polymer and the drug to be encapsulated, emulsified in an aqueous phase containing a dissolved surfactant. Once the emulsion is formed, it is subjected to solvent removal by either evaporation or extraction process to solidify the polymer droplets. In the case of solvent removal by evaporation, the emulsion is maintained at a reduced pressure or at atmospheric pressure and the stir rate is reduced to enable the volatile solvent to evaporate.

A major problem with this technique is a poor encapsulation efficiency of moderately water soluble and water soluble compounds, which partitioned out from the organic dispersed phase into the aqueous continuous phase. Successful entrapment of drug within the microspheres is thus highly dependent on solubility in the aqueous phase. Water soluble drugs (e.g. caffeine and salicylic acid) could not be entrapped within the poly (lactic acid) (PLA) microsphere using an Oil/Water emulsion method, while drugs with low water solubility, such as Diazepam, Hydrocortisone and Progesterone were successfully retained within the microspheres [140].

In order to increase the encapsulation efficiency of water soluble drugs, an oil-in-oil emulsion method was developed [141]. In this method, the drug may be dissolved or suspended in the oil phase before being dispersed in another oil phase. The processing scheme for nanoparticle-preparation by single emulsion technique shown in Figure 1.14. [142].

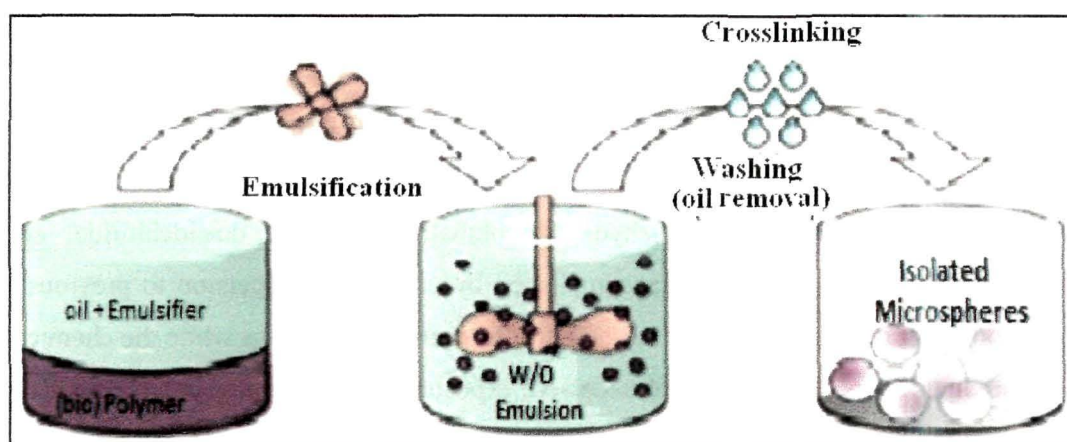


Figure 1.14. Processing scheme for nanoparticle-preparation by single emulsion technique

1.4.2.2. Double emulsion technique

This method for preparation of nanoparticles was reported to overcome the problem of low encapsulation efficiency of water soluble drug prepared by conventional water/oil emulsion solvent evaporation method.

This method involves the formation of the multiple emulsion or double emulsion of type w/o/w. It is best suited to water soluble drugs, peptides, proteins and vaccines. This method can be used with both the natural as well as the synthetic polymers. The aqueous protein solution is dispersed in a lipophilic organic continuous phase. This protein solution may contain the active constituents. The continuous phase is generally consisted of the polymer solution that eventually encapsulates of the protein contained in dispersed aqueous phase. The primary emulsion is then subjected to the homogenisation or the sonication before addition to the aqueous solution of the poly vinyl alcohol (PVA). This results in formation of a double emulsion. Emulsion is then subjected to solvent removal either by solvent evaporation or by solvent extraction process. The solvent evaporation is carried out by maintaining emulsion at reduced pressure or by stirring the emulsion so that the organic phase evaporates out. The emulsion is then added to large quantity of water into which organic phase diffuses out. The solid microspheres are subsequently obtained by filtration and washing with n-hexane, acetone or any organic solvent to remove traces of oil from the surface [143,144]. The Processing scheme for nanoparticle-preparation by double emulsion technique is shown in Figure 1.15. [142]

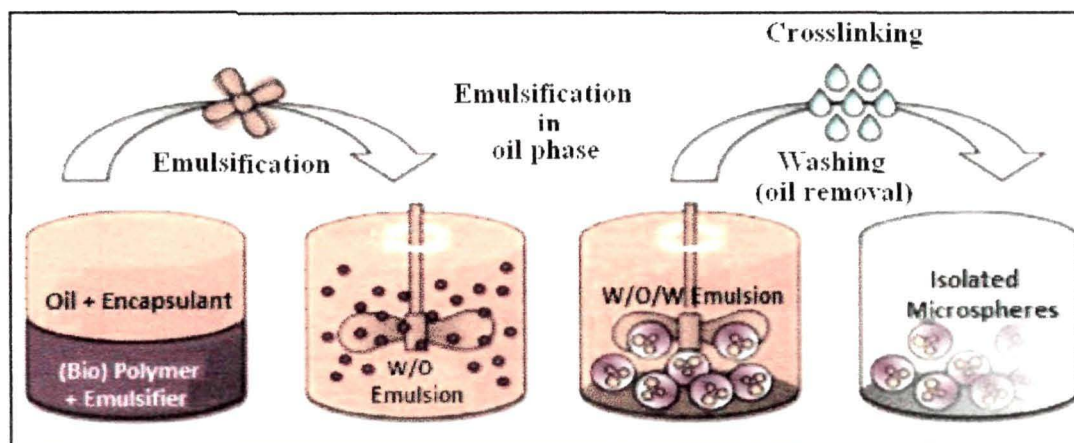


Figure 1.15. Processing scheme for nanoparticle-preparation by double emulsion technique

1.4.3. Ionotropic Gelation Technique

Ionotropic gelation is based on the ability of polyelectrolytes to crosslink in the presence of counter ions to form hydrogel beads known as gelspheres. Gelspheres are spherical crosslinked hydrophilic polymeric entity capable of extensive gelation and swelling in simulated biological fluids and the release of drug through it controlled by polymer relaxation. The hydrogel beads are produced by dropping a drug-loaded polymeric solution into the aqueous solution of polyvalent cations. The cations diffuse into the drug-loaded polymeric drops, forming a three dimensional lattice of ionically crosslinked moiety. Biomolecules can also be loaded into these gelspheres under mild conditions to retain their three dimensional structure [145,146]. In ionotropic gelation technique, there are natural polymers that can be used as drug carriers due to their biocompatibility and biodegradability. The natural or semisynthetic polymers i.e. Alginates, Gellan gum, Chitosan, Pectin and Carboxymethyl cellulose are widely used for the encapsulation of drug by this technique [147]. These natural polyelectrolytes contain certain anions/cations on their chemical structure which forms network structure by combining with the counter ions and induce gelation by cross linking. The important steps of ionotropic gelation are shown in figure 1.16 [148].

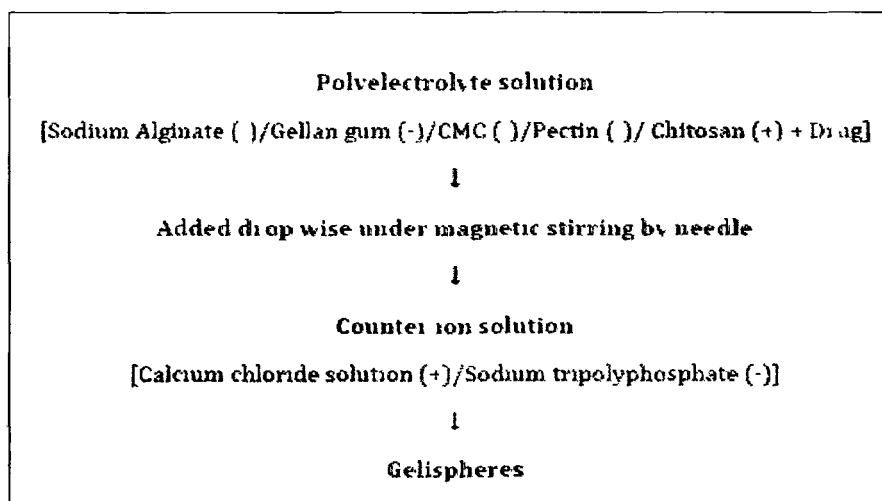


Figure 1.16. Important steps of ionotropic gelation

1.4.4. Desolvation method

Desolvation technique is mainly used for the preparation of nanoparticles for protein and polysaccharides [149]. Desolvation is a thermodynamically driven self assembly process for polymers to prepare nanoparticles. The polymer from an aqueous phase can be desolvated by pH change or change in temperature by suitable counter ions. Crosslinking can be done in the desolvation step. Desolvation technique involves three main steps: polymer dissolution, polymer aggregation and polymer deaggregation. Sodium sulphate, acetone, isopropanol, ethanol etc. can be added as desolvating agents. Both hydrophobic and hydrophilic drugs can be entrapped in nanoparticles using this technique [150]. The desolvation technique is illustrated in Figure 1.17.

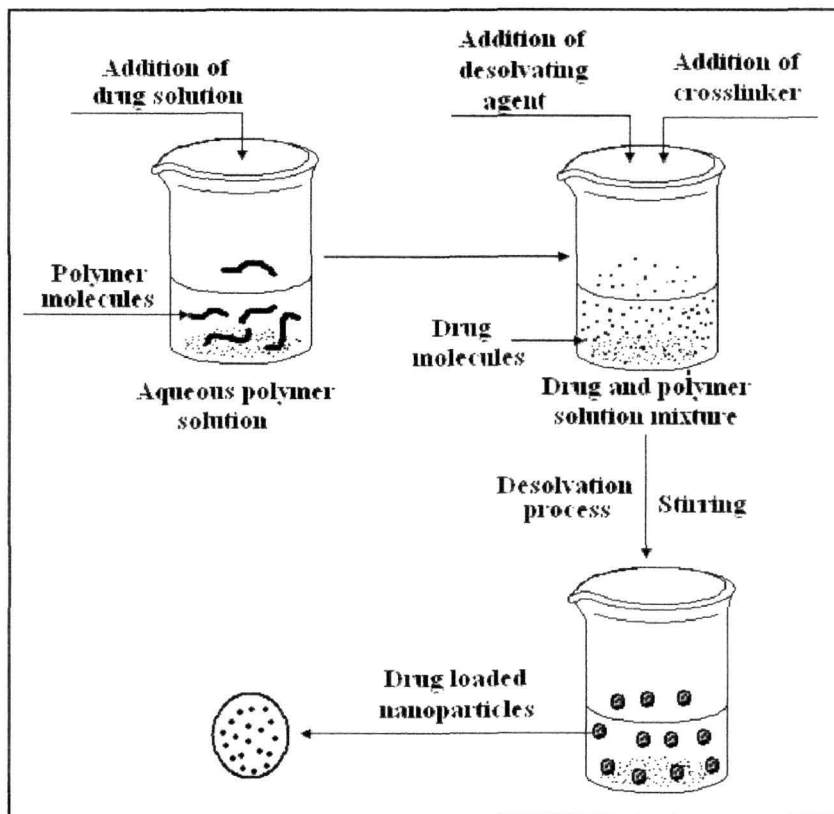


Figure 1.17. Schematic diagram of desolvation technique

1.4.5. Spray Drying

Spray drying is a technique used in pharmaceutical industry to produce dry powder from liquid phase by spraying in hot drying medium [151]. This technique has also been

employed as a microencapsulation method because it can be adapted to the development of different systems, microspheres or microcapsules, depending on the initial aqueous formulation, a solution, a suspension or an emulsion [152]. It is a continuous process which involves several steps, such as, atomization, mixing of spray with drying gas, evaporation and nanoparticle separation. The steps in spray drying is depicted in Figure 1.18. [153].

Polymers capable of forming a film over the surface of drying droplets have been included in formulations for spray drying to form microspheres. Among the applications, the suitability and ability of the polymer to modify the release characteristics by spray drying process can be identified as, for nasal drug delivery [154], modify mineral release in food fortification [155] and developing mucoadhesive delivery systems [156].

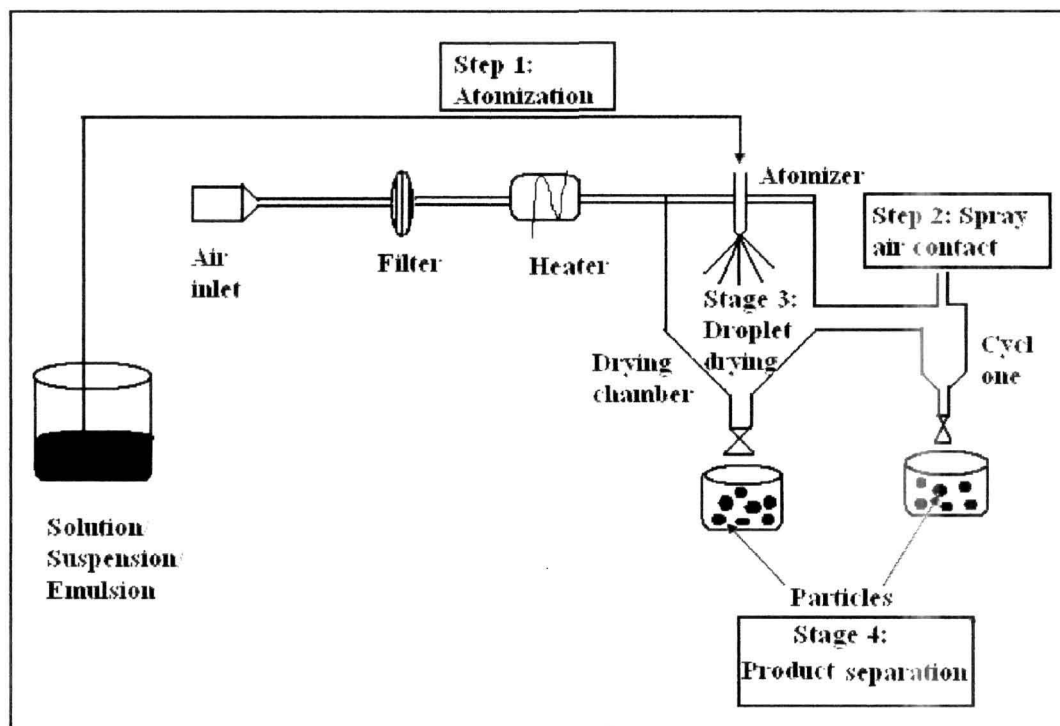


Figure 1.18. Schematic diagram of spray drying technique

1.4.5. Other fabrication techniques

Some other methods of nanoparticle preparation are also available which includes sol-gel method, pan coating, layer by layer (LBL) techniques, electrostatic encapsulation etc.

References

- [1] Chien, Y.W. & Lin, S. *Drug Delivery: Controlled Release*, Encyclopedia of Pharmaceutical Technology, 3rd ed. Informa Healthcare USA, Inc. 2007.
- [2] Kydonieus, A.F. IN: *Controlled Release Technology-Methods, Theory and Applications*. Kydonieus A.F. (ed) Vol1, CRC Press Inc., Boca Raton, 2, 1980.
- [3] Srikanth, P., et al. *Int. J. Adv. Pharm.*, **3**(1), 51-58, 2013.
- [4] L. Brannon-Peppas, Polymers in controlled drug delivery, in: *Medical Plastics and Biomaterials Magazine*, November, **34**, 1997.
- [5] Approved drug products with therapeutic equivalence evaluations, 18th Ed, US department of health and human services, 1998. 18th Edition of FDA's *Approved Drug Products with Therapeutic Equivalence Evaluations*, 1998.
- [6] Uhrich, K.E., et al. *Chem. Rev.* **99** (11), 3181--3198, 1999.
- [7] Patel, K., et al. *IJPRBS*, **1**(3), 1--26, 2012.
- [8] Madhusudhan P. & Nazeer S. *Int. J. Pharm. & Tech.* **2**, 625--684, 2010.
- [9] Langer, R. *Nature*, **392**, 5--10, 1998.
- [10] Brouwers, J. R. B. *J. Pharm. World Sci.* **18**(5), 153--162, 1996.
- [11] Bhowmik, et al. *The Pharma Innovation J.* **1** (10), 24--32, 2012.
- [12] Kydonieus, A.F. IN: *Controlled Release Technology-Methods, Theory and Applications*. Kydonieus A.F. (ed) Vol1, CRC Press Inc., Boca Raton, FL. 1980.

- [13] McCormick, C.L. *Polym. Prepr.* **28**(2), 90-91, 1987.
- [14] Paul, D.R. *IN: Controlled Release Polymeric Formulations*, D.R.Paul and F.W. Harris,(Ed), ACS Symposium Series Vol.33, American Chemical Society, Washington.D.C.1976.
- [15] Liu, Z., et al. *Adv. Drug Deliv. Rev.*, **60**, 1650--1662, **2008**.
- [16] Dutta P.K. & Kumar M. N. V. R. *JMS Polym. Rev.* **42**, 307, 2002.
- [17] Kavitha K., et al. *Int. J. Appl. Bio. & Pharma. Tech.* **2**(2), 249--258, 2011.
- [18] Van der Lubben, I.M. et al. *Biomater.* **22**(7), 68--694, 2001.
- [19] Rudall K. M., & Kenchington W. *Biol Rev.* **40**, 597--636, 1973.
- [20] Blackwell J., Chitin. *In: Walton AG*, Blackwell J, editors. *Biopolymers*. New York: Academic Press; 1973. 474--489.
- [21] Rudall, K. M. *J. Polym. Sci. Part C*, **28**, 83--102, 1969.
- [22] Atkins, E. D. T. *J Biosci.* **8**, 375--87, 1985.
- [23] Rawls, R. L. *C&EN.* **14**, 42--45, 1984.
- [24] Kumar, M.N., et al. *Chem. Rev.* **104**, 6017--6084, 2004.
- [25] Prabharan, M. *J. Biomater Appl.* **23**, 50--32, 2008.
- [26] Shirosakia, Y., et al. *Biomaterials* **26**, 485--493, 2005.

- [27] Venter, J.P., et al. *Int. J. Pharm.* **313**, 36--42, 2006.
- [28] Denkbaz, E.B., & Ottenbrite, R.M. *J. Bioact. Compat. Poly.* **21**, 351--368, 2006.
- [29] Pourshahab, P.S., et al. *J. Microencapsul.* **28**, 605--613, 2011.
- [30] Nauss J. L., et al. *Lipids* **18**(10), 714--719, 1983.
- [31] Ausar S F., et al *J Med Food* **6** (4), 397--399, 2003.
- [32] Kordestani S., et al. *J. Wound Care*, **17**(7), 323--327, 2008.
- [33] Sandoval M., et al. *J. Drugs Dermatol.* **10**(1), 75-79, 2011.
- [34] Rabea, E. I., et al. *Biomacromol.* **4**(6), 1457--1465, 2003.
- [35] Chen, C. S., et al. *J. Food Protec.* **61**(9), 1124--1128, 1998.
- [36] Hadrami A E. et al *Mar Drugs* **8**(4), 968--987, 2010
- [37] Hou, W.M., et al. *Chem. Pharm. Bull.* **33**, 3986--3992, 1985.
- [38] Ramachandran, S., et al. *Int. J. PharmTech Res.* **3**(1), 488--496, 2011..
- [39] Rajasree, R & Rahate, K.P. *IJPSR* **4**(11), 4175--4193, 2013.
- [40] Jain, S K. & Jain, A. *Expert opinion on drug delivery*, **5**(5), 483--498, 2008.
- [41] Chasanah, E., et al. *J. Coastal Dev.* **12**(2), 64 --72, 2009.
- [42] Giustina, A., & Ventura, P *Acta Toxicol Ther.* **16**, 199--214, 1995.

- [43] Scitutto, A M , & Colombo, P *Acta Toxicol Ther* **16**, 215--230, 1995
- [44] Maekawa, A , & Wada, M Food containing chitin or its derivatives for reduction of blood and urine uric acid *Jph Kokai Tokkyo Koho*, 1991
- [45] Qi, L F , et al *Bioorg Med Chem Lett* **15**, 1397--1399, 2005
- [46] Uma, G , & Shilpa, P *Int Res J of Science & Engineering*, **1**(1), 13--16, 2013
- [47] Muzzarelli, R A A *Carbo Polym* **8**, 1--21, 1988
- [48] Liu, X F , et al *J Appl Poly Sci* **79**(7), 1324--1335, 2001
- [49] Chen, X G , et al *Biomater* **23**, 4609--4614, 2002
- [50] Zhu, A , et al *Colloids and Surfaces B Biointerfaces*, **43**, 143--149, 2005
- [51] Tokura, S , et al *Macromol Symp* **101**(1), 389--396, 1996
- [52] Hamodrakas, S J , et al *Biochim Biophys Acta* **700**, 42--51, 1982
- [53] Hamodrakas, S J , et al *Biochim Biophys Acta* **703**(2), 216--222, 1982
- [54] Sakaguchi, T , et al *Agric Biol Chem* **45**(10); 2191--2195, 1984
- [55] Nishi, N , et al *Int J Bio Macromol* **6**(1), 53--54, 1984
- [56] Nishi, N , et al *Int J Bio Macromol* **8**(5), 311--317, 1986
- [57] Jayakumar, R , et al *e-Polymers*, **35**, 1--16, 2006

- [58] Ramos, V M , et al *Carbohydr Polym* **52**, 39--46, 2003
- [59] Jayakumar, R , et al *J Bioact Compat Polym* **21**(4), 327--340, 2006
- [60] Hadgraft, J & Valenta, C *Int J Pharm* **200**(2), 243--247, 2000
- [61] Win, P P , et al *Polym Int* **54**(3), 533--536, 2005
- [62] Hui, Y H , et al *Hand book of Food and Beverage Fermentation Technology*, Marcell Dekker, Inc, New York, 350--356, 2004
- [63] Porter, M A , & Jones, A. M *JAOCs*, **80**(6), 557--562, 2003
- [64] Akbari, N , et al *Annals of Biol Res* **3**(5), 2538--2544, 2012
- [65] Venter, C S *J Fam Eco & Consum Sci* **27**, 24--33, 1999
- [66] Fabiyi, E F *Pak J Nutr* **25**, 453--457, 2006
- [67] Porter, M A , & Jones, A M *J Am Oil Chem Soc* **80**, 557--562, 2003
- [68] Xiang, L C , et al *Chin J Polym Sci* **27**, 843--849, 2009
- [69] Desroches, S , et al *J Nutr* **134**, 574--579, 2004
- [70] Lijuan, Q , et al Evaluation and utilization of nutrient components of Chinese soyabean germplasm *The Third International Soyabean Processing and Utilization Conference (ISPUC-III) 2000 of the Innovative Era for Soyabeans*, Tsukuba, Ibaraki, Japan, 15--20, 2000

- [71] Fukushima, D., Recent Progress in Research and Technology for Processing and Utilization of Soyabeans. *The Third International Soyabean Processing and Utilization Conference (ISPUC-III): 2000 of the Innovative Era for Soyabeans*. Tsukuba, Ibaraki, Japan, 11--16, 2000.
- [72] Chen, Y.M., et al. *J. Clin. Endocrinol. Metab.* **88**, 4740--4747, 2003.
- [73] Symolon, H., et al. *J. Nutr.* **134** 1157--1161, 2004.
- [74] National Food Institute- Technical University of Denmark (DTU), Danish Food Composition Databank –ed 7.01, 2009
- [75] Kydonieus, A.F. *IN: Controlled Release Technology-Methods, Theory and Applications*. Kydonieus A.F. (ed) Vol1, CRC Press Inc., Boca Raton, FL., 1 1980.
- [76] Ramaswamy, S. V., et al. *Antimicrobial Agents And Chemotherapy*, **47**(4), 1241--1250, 2003.
- [77] Becker, C., et al. *J. Pharm. Sci.*, **96**(3), 522--531, 2007.
- [78] Bharat, B., et al. In:Curcumin-Biological and Medicinal Properties, 7034_book.fm, 2006.
- [79] Jurenka, J. S. *Altern. Med. Rev.* **14**(2), 141--153, 2009.
- [80] Lampe, V & Milobedzka, J. *Ber Dtsch Chem Ges* **46**, 2235, 1913.
- [81] Sharma, O. P. *Biochem. Pharmacol.* **25**, 1811--1812, 1976.
- [82] Negi, P. S., et al. *J. Agric. Food Chem.* **47**, 4297--4300, 1999.

- [83] Aggarwal, B. Curcumin — Biological and Medicinal Properties 7034_book.fm, 297-368, 2006.
- [84] Sharma R.A., et al. *Eur. J. Cancer* **41**, 1955--1968, 2005.
- [85] Wang, Y. J., et al. *J. Pharm. Biomed. Anal.* **15**, 1867--1876, 1997.
- [86] Anand, P., et al. *Mol. Pharm.* **4**(6), 807--818, 2007.
- [87] Ireson, C., et al. *Cancer Res.* **61**, 1058-1064, 2001.
- [88] Shoba, G., et al. *Planta Med.* **64**, 353--356, 1998.
- [89] Marczylo, T.H., et al. *Cancer Chemother. Pharmacol.* **60**, 171-177, 2007.
- [90] Mauduyt. *Bull. Soc. Geol. Fr.* **4**, 168-170, 1847.
- [91] Naumann, C. F. *Elemente der Mineralogie* (2nd ed.), Leipzig, 1850.
- [92] Clay Minerals—Sci-Tech Encyclopedia, McGraw Hill, 2007.
- [93] Gordon A & Keith F. *Polym. Bull.* **59**, 439--445, 2007.
- [94] Hartwell, J.M. *Clay Minerals* **6**, 111--118, 1965.
- [95] Anon.: *Terramin Clay—A California Living Clay*, Home Page: www.rawfoodinfo.com, 2007.
- [96] Anon.: *Cavities and Gum Diseases in Americans Increase at an Alarming Rate*, Home Page: www.topix.net, 2007.

- [97] Montazer, M., et al. *Asian J. Chem.* **25**(5), 2889--2892, 2013.
- [98] Patel, H.A., et al. *Bull. Mater. Sci.* **29**(2), 133--145, 2006.
- [99] Hua, S., et al. *Drug Dev. & Indus. Pharm.* **36**(9), 1106--1114, 2010.
- [100] O'Sullivan, A.C. *Cellulose*, **4**, 173--207, 1997.
- [101] Gardiner, E. S. & Sarko, A. *Can. J. Chem* **63**, 173--180, 1985.
- [102] Habibi, Y et al. *Chem. Rev.* **110**(6), 3479--3500, 2010.
- [103] Sebe, G. et al. *Biomacromol.* **13**, 570--578, 2012.
- [104] Gebald, C. J. A., et al. *Env. Sci. Tech.* **45**(20), 9101--9108, 2011.
- [105] Oza, K. P. & Frank, S. G. *J. Disp. Sci. Tech.* **7**, 543--561, 1986.
- [106] Thomas, W. R. *Prog. Food Nutr. Sci.* **6**, 341--351, 1982.
- [107] Lin, D. C., et al. *J. Mater. Res.* **20**(6), 1456--1464, 2005.
- [108] Czaja, W.K., et al. *Biomacromol.* **8**(1), 1--12, 2007.
- [109] Entcheva, E., et al. *Biomater.* **25**(26), 5753--5762, 2004.
- [110] Galgut, P.N. *Biomater.* **11**(8), 561--564, 1990.
- [111] Kumbar, S.G., et al. *J. Microencapsul.* **19**(2), 173--180, 2002.
- [112] Gonçalves, L.V., et al. *Polimeros: Ciência e Tecnologia*, **15**(1), 6--12, 2005.

- [113] Gupta, K. C., & Kumar, M. N. V. R., *J. App. Polym. Sci.* **76**(5), 672--683, 2000.
- [114] Gupta, K.C., & Jabrail, F.H. *Carbohydr. Polym.* **66**(1), 43--54, 2006.
- [115] Patel, V.R., & Amiji, M.M. *Pharma. Res.* **13**(4), 588--593, 1996.
- [116] Peniche, C., et al. *Macromol. Biosci.* **3**(10), 511--520, 2003.
- [117] Crescenzi, V., et al. *Biomacromol.* **3**(6), 1384--1391, 2002.
- [118] Sung H.W., et al. *J. Biomater. Sci. Polym. Ed.* **10**, 63--78, 1999.
- [119] Akao, T., et al. *Boil. Pharm. Bull.* **17**(12), 1573--1576, 1994.
- [120] Touyama, R., et al. *Chem. Pharm. Bull.* **42**(3), 668--673, 1994.
- [121] Meier, W. *Chem. Soc. Rev.* **29**, 295--303, 2000.
- [122] Mahapatro, A. & Singh, D.K. *J. Nanobiotech.* **9**(55), 1--11, 2011.
- [123] Kohane, D.S. *Biotech. & Bioeng.*, **96**(2), 204--209, 2007.
- [124] Couvreur, P., et al. *J. Pharm. Sci.* **71**(7), 790--792, 1982.
- [125] Gomez-Curet, I. *Nanoparticle Fabrication and Characterization for Biomedical Research Applications, Technical Summary*, Thermo Fisher Scientific Inc. Wilmington, USA, 2012.
- [126] Labhasetwar, V. et al. *Adv. Drug Del. Rev.* **24**(1), 63--85, 1997.
- [127] Abhilash M. *Int. J. Pharm. Bio. Sci.* **1**(1), 1--12, 2010.

- [128] Kayser, O., et al. *Cur. Pharm. Biotech.* **6**(1), 3--5, 2005.
- [129] Gomer, T. et al. *J. Control. Release* **57**(3), 259--268, 1999.
- [130] Freitas, S. et al. *J. Control. Release* **102**(2), 313--332, 2005.
- [131] IUPAC. *Compendium of Chemical Terminology*, 2nd ed. (the "Gold Book"). Compiled by A. D. McNaught and A. Wilkinson. Blackwell Scientific Publications, Oxford, 1997.
- [132] Ozer, A Y, & Hincal, A. A. *J. Microencapsul* **7**(3), 327--339, 1990.
- [133] NCR Microencapsulation-Pharmaceuticals, National Cash Register Co., Dayton, OH, 1-19, 1971.
- [134] Kizilay, E. *Adv Colloid Interface Sci.* **167**, 24--37, 2011.
- [135] Mathiowitz, E.; et al. IN: E. Mathiowitz ed., *Encyclopedia of Controlled Drug Delivery*, 2, John Wiley and Sons, Inc. New York, 1999.
- [136] Augustin, M. A. & Hemar, Y. *Chem. Soc. Rev.* **38**, 902--912, 2009.
- [137] Patel, N.R. et al. *Int. J. Pharm. & Life Sci.* **2**(8), 992--997, 2011.
- [138] Prasanth, V.V. et al. *Int. J. Pharm. & Biomedical Sci.* **2**(2), 332--338, 2011.
- [139] Alagusundaram, M., et al. *Int. J. ChemTech Res.* **1**(3), 526--534, 2009.
- [140] Tiwari, S., & Verma, P. *Int. J. Pharm. & Life Sci.* **2**(8), 998--1005, 2011

- [141] Tsai, D.C.; et al. *J. Microencapsul.* **3**(3), 181--193, 1986.
- [142] Singh, P. et al. *Ind. J. Novel Drug Del.* **3**(2), 70--82, 2011.
- [143] Vyas & Khar. *Targeted and Controlled drug delivery*, CBS Publishers and distributors, 2001.
- [144] Jain, D., et al. *AAPS Pharm. Sci. Tech.* **6**(1), 101--107, 2005.
- [145] Hemalatha, K., et al. *Int. J. Pharm. & Bio. Archives*, **2** (suppl. 3), 921--925, 2011.
- [146] Patil, J.S., et al. *Digest J. Nanomater. & Biostruc.* **5**(1), 241--248, 2010.
- [147] Raida, S.K., et al. *Int. J. Pharm.* **341**, 230--237, 2007.
- [148] Patil, P. et al. *Int. J. Pharm. Pharm. Sci.* **4**(4), 27--32, 2012.
- [149] Azarmi S.H. et al. *J. Pharm. Pharmaceut. Sci.* **9**(1), 124--132, 2006.
- [150] Sailaja, A.K. & Amareshwar, P. *Int. J. Pharm. Sci. Nanotech.* **5**(1), 1643--1647, 2012.
- [151] Broadhead, J., et al. *Drug, Dev. Ind. Pharm.* **18**(11), 1169--1206, 1992.
- [152] Re, M. I. *Dry. Technol.* **24**(4), 433--446, 2006.
- [153] Gohel, M. *Pharmainfo.net*, **7**(5), 2009.
- [154] Asada, M., et al. *Int. J. Pharm.* **270**(1-2), 167--174, 2004.
- [155] Oneda, F., & Ré, M.I. *Powder Technol.* **130**(1), 377--384, 2003.

[156] Gavini, E., et al. *J. Pharm. & Pharmacol.* 57(3), 287--294, 2005.

CHAPTER 2
LITERATURE SEARCH

CHAPTER 2

LITERATURE SEARCH

2.1. Isoniazid: An antituberculosis drug

Tuberculosis (TB) is a disease of antiquity which is thought to have evolved sometime between the seventh and sixth millennia BC [1]. In 1993, the World Health Organization (WHO) declared tuberculosis (TB) to be a 'global emergency' with more than a third of the world's population infected. Streptomycin discovered in 1944, was formerly considered to be a first-line drug used in the initial treatment of TB. But, an increasing resistance of TB causing bacteria to streptomycin in has decreased its overall usefulness. This problem was solved by the use of combination therapy with other agents discovered at around that time (isoniazid and *para*aminosalicylic acid). But, combination therapy encountered some problems. Patients had difficulty in adjusting to the lengthy treatment course associated with painful injections and toxic effects [2]. In 1960s, another antituberculosis drug was discovered which is known as rifampicin. Rifampicin can be orally administered to patients, which reduced the length of therapy from 18- 24 months to only 6 months [3]. Isoniazid, pyrazinamide and rifampicin, alongwith ethambutol are the most effective agents for the destruction of tubercle bacilli [4]. Anti-TB chemotherapy containing isoniazid, rifampicin and pyrazinamide has proved to be highly effective but hepatotoxic. Anti-TB drug induced hepatotoxicity (DIH) is the most common side-effect leading to interruption of therapy [5]. Nowadays, Isoniazid is one of the key active pharmaceutical ingredients (APIs) used in combination with rifampicin, pyrazinamide, and ethambutol for the treatment of tuberculosis [6-7]. The standard treatment regime for latent TB infection (LTBI) is nine month of daily intake of isoniazid. This regime is very effective for HIV-infected people taking antiretroviral therapy, and child aged 2-11years of age. In past only isoniazid was recommended for treatment of LTBI, but now there are three treatment options are available. One option recommends only isoniazid daily or twice daily for 9 months, second option recommends isoniazid daily or twice daily for 6 months and the third option recommends rifampicin alone for four months [8].

Isoniazid is carcinogenic in laboratory animals, most notably producing pulmonary tumors in mice by various routes of administration [9-10] Acute overdoses of isoniazid have been identified with a classical triad of symptoms including seizures refractory to standard anticonvulsants, metabolic acidosis, and coma [11] Chronic therapy leads to peripheral neuropathies, toxic encephalopathy, ataxia, stupor, memory impairment, toxic psychosis, optic neuritis and optic atrophy Isoniazid hepatotoxicity is a common complication of antituberculosis therapy that ranges in severity from asymptomatic elevation of serum transaminases to hepatic failure requiring liver transplantation [12] Angadi et al have reported the controlled release of isoniazid by inter penetrating polymer network blend microspheres derived from chitosan glutaraldehyde cross linked and hydroxy ethyl cellulose [13] Behera et al prepared poly- ϵ -caprolactone loaded isoniazid by water-in-oil-in-water double emulsion technique The prepared nanoparticles were characterized by atomic force microscopy (AFM), differential scanning calorimetry (DSC), fourier transform infrared spectroscopy (FTIR) study, and *in vitro* release kinetics study It was seen that percentage entrapment of isoniazid can be enhanced up to 63% by changing different formulation parameters [14] Rafeeq et al prepared isoniazid loaded chitosan nanoparticles by ionic gelation method to enhance the bioavailability and to reduce dose frequency of isoniazid [15] Ahmed et al prepared Alginate based nanoparticulate delivery system for controlled delivery of antiTB drugs High drug encapsulation efficiency was achieved in alginate nanoparticles, ranging from 70%-90% A single oral dose resulted in therapeutic drug concentrations in the plasma for 7-11 days and in the organs (lungs, liver and spleen) for 15 days In comparison to free drugs, there was a significant enhancement in the relative bioavailability of encapsulated drugs In TB-infected mice three oral doses of the formulation spaced 15 days apart resulted in complete bacterial clearance from the organs, compared to 45 conventional doses of orally administered free drugs [16]

2.2. Curcumin: An anticancer drug

Over the past decade, research into diet and cancer has concerned the scientists Chemicals derived from plants, known as phytochemicals, have garnered attention as potential cancer prevention agents Polyphenols are in the first line of phytochemicals

that have been studied for their potential preventive and therapeutic effects. Polyphenols are derived from many components of the human diet, including peanuts, green and black teas, red wine, olive oil, turmeric, etc. Some of these compounds are investigated for their cardiopreventive and anticancer properties [17].

Curcumin (or diferuloylmethane) is a polyphenol existing as a keto-enol tautomer, with the enol isomer more stable in both solid state and solution [18]. Curcumin is lipophilic consisting of two aromatic rings connected by two unsaturated carbonyl groups and therefore has poor water solubility. It is stabilized by hydrogen-bonding linked with the central hydroxyl group. This may be one of the important functional sites responsible for the assembly of molecular biological activities [19]. Curcumin is phototoxic to mammalian cells [20]. The observed phototoxicity makes curcumin a potential photosensitizing drug which can be applied for phototherapy.

Cancer is a hyperproliferative disorder that metastasizes into the vital organs of the body through attack followed by angiogenesis and distant metastasis. Much research is done on curcumin as an anticancer drug. Curcumin restrains the proliferation of a wide variety of tumor cells, such as breast cancer, colon cancer, renal cell cancer, hepatocellular cancer, T cell leukemia, B cell lymphoma, acute myelogenous leukemia, basal cell cancer, melanoma and prostate cancer [21-25]. Curcumin also induces apoptosis in a wide variety of cells [26-27]. It was observed that curcumin inhibits cyclooxygenase-2 (COX-2) as well as lipoxygenase (LOX), two enzymes involved in inflammation [28]. The antioxidant activity of curcumin was reported as early as 1975 [29]. Curcumin also exhibits antioxidant activities. Moreover, the hepato- and nephro-protective [30], thrombosis suppressing [31], myocardial infarction protective [32], hypoglycemic [33-34] and antirheumatic effects of curcumin are also well established.

In spite of its efficacy and safety, curcumin has not yet been approved as a therapeutic agent in part because of poor aqueous solubility, relatively low bioavailability, and intense staining color of curcumin have been highlighted as major problems [35]. Curcumin is formulated as nanosuspension [36], nanoemulsion [37], pH-sensitive nanoparticles [38], curcumin-loaded nanoparticles [39], curcumin-loaded solid lipid nanoparticles [40] etc. to increase its bioavailability and solubility. Curcumin-piperine nanoparticles coated with polyethylene glycol containing copolymer were prepared by

Moorthi et al. These nanoparticles had a minimum average particle size, excellent polydispersity index and optimal zeta potential which fall within the acceptable limits of the study. This dual nanoparticulate drug delivery system was found to be promising to overcome oral bioavailability and cancer cell targeting limitations in the treatment of cancer [41]. Bisht et al. synthesized polymeric nanoparticle encapsulated formulation of nanocurcumin utilizing the micellar aggregates of cross-linked and random copolymers of N-isopropylacrylamide (NIPAAm), with N-vinyl-2-pyrrolidone (VP) and poly(ethyleneglycol)monoacrylate (PEG-A). They observed that nanocurcumin, unlike free curcumin, is readily dispersed in aqueous media. Nanocurcumin demonstrated comparable *in vitro* therapeutic efficacy to free curcumin against a panel of human pancreatic cancer cell lines, as assessed by cell viability and clonogenicity assays in soft agar. Further, nanocurcumin's mechanisms of action on pancreatic cancer cells mirror that of free curcumin, including induction of cellular apoptosis, blockade of nuclear factor kappa B (NF κ B) activation, and downregulation of steady state levels of multiple pro inflammatory cytokines (IL-6, IL-8, and TNF α) [42].

2.3. Natural polymers for controlled drug delivery formulations

Though the controlled delivery formulations regarding the synthetic polymers were extensive and encouraging, the recent trend shifted towards natural polymers [43-44]. Chitosan and its water soluble derivatives are widely studied for controlled drug delivery applications. Chitosan nanoparticles have been prepared by several methods, such as the emulsion method, ionic gelation method [45-47], reverse micellar method, self-assembling method [48-49], etc.

Chitosan nanoparticles prepared by ionotropic gelation technique was first reported by Calvo *et al.* [50] and has been widely examined and developed. The mechanism of chitosan nanoparticle formation is based on electrostatic interaction between amine group of chitosan and negatively charge group of polyanion such as tripolyphosphate [51-52]. Nasti et al. studied the effect of a pH, concentration, ratios of components, and method of mixing, on the preparation of chitosan/TPP nanoparticles [53]. Lin et al. explored the relationship between free amino groups on the surface and the properties of chitosan nanoparticles prepared by the ionic gelation method [54]. Alishahi and coworkers

investigated the encapsulation of vitamin C into chitosan/TPP nanoparticles to extend its shelf life and achieve controlled release [55]. Katas et al. studied the antimicrobial activity of chitosan nanoparticles *in vitro* on *S. aureus* and *E. coli*. The nanoparticles were prepared by ionic gelation technique. They observed that smaller nanoparticles (± 400 nm) showed higher antibacterial activity compared to larger ones (± 700 nm) [56]. Basu et al. prepared chitosan/gelatin microspheres loaded with Ketorolac Tromethamine (KT) for oral delivery by complex coacervation and simple coacervation methods without the use of chemical cross-linking agent to avoid the toxic reactions and other undesirable effects of the chemical cross-linking agents [57]. Lucinda-Silva and Evangelista studied the chitosan and alginate microparticles formed by complex coacervation method in W/O emulsion. This method enabled the production of spherical particles, with slightly rough surface and narrow size distribution with maximal diameter of 10 μm [58]. Das et al. reported a nanoformulation of curcumin with a tripolymeric composite for delivery to cancer cells. The composite nanoparticles were prepared by using three biocompatible polymers—alginate, chitosan, and pluronic—by ionotropic gelation followed by polycationic cross-linking. Pluronic F127 was used to enhance the solubility of curcumin in the alginate-chitosan nanoparticles. Atomic force and scanning electron microscopic analysis showed that the particles were nearly spherical in shape with an average size of 100 ± 20 nm. A cytotoxicity assay showed that nanoparticles at a concentration of 500 $\mu\text{g/mL}$ were nontoxic to HeLa cells [59].

Due to the problem associated with the solubility of chitosan, some of its water soluble derivatives are also studied for drug delivery applications. One such water soluble derivative of chitosan is carboxymethyl chitosan. Farag and Mohammad prepared nanogels of a binary system of carboxymethyl chitosan (CMC) and poly-(vinyl alcohol) PVA by *in situ* process. The nanogels showed good pH-sensitivity swelling, improved surface property and good antibacterial activity against *Escherichia coli* (G⁻) and *Staphylococcus aureus* (G⁺). The swelling study showed water absorption up to 500% after 2 h [60]. Li et al. also prepared CMC and PVA blended hydrogels using freezing and thawing techniques. The results showed that addition of CMC can improve the physical properties of pure PVA hydrogels and could be efficiently applied as oral delivery systems for protein drugs [61].

Anitha et al. prepared chitosan, O-carboxymethyl chitosan (O-CMC) and N, O-carboxymethyl chitosan (N,O-CMC) nanoparticles by ionic gelation method using tripolyphosphate (TPP) and CaCl_2 . Cytotoxicity of the nanoparticles showed that the prepared nanoparticles were less cytotoxicity to breast cancer cells showing upto 98% cell viability. Antibacterial activities of these chitosan, O-CMC and N, O-CMC nanoparticles were also studied which revealed that chitosan nanoparticles showed less antibacterial activity compared to O-CMC and N, O-CMC nanoparticles. N, O-CMC nanoparticles demonstrated maximum antibacterial activity out of the three nanoparticles [62]. Later on, Anitha et al. prepared curcumin loaded N, O-CMC nanoparticles. The encapsulation efficiency of nanoparticle was found to be around 80%. Cytotoxicity studies using MTT assay indicated that curcumin-N, O-CMC nanoparticles showed specific toxicity towards cancer cells and non-toxicity to normal cells. These results indicated N,O-CMC is an efficient nanocarrier for delivering curcumin to cancer cells [63]. Anitha et al. further continued their research on CMC and prepared 5-fluorouracil (FU) in combination with curcumin loaded N, O-CMC nanoparticles. The prepared nanoparticles were found to be biocompatible. The *in vitro* drug release profile in pH 4.5 and 7.4 showed a sustained release profile over a period of 4 days. The exposure of the nanoparticles in colon cancer cells (HT 29) proved the enhanced anticancer effects *in vitro* and improved plasma concentrations under *in vivo* conditions [64]. Thu et al. developed $\text{Fe}_3\text{O}_4/\text{OCMCs}/\text{Cur}$ -based nanodrug system by *ex situ* grafting. This system was proven to successfully lead curcumin into HT29 cancer cells, and its effect on this cancer cell line was found to be much stronger than that of pure curcumin [65]. Another water soluble derivative of chitosan used for biomedical applications is phosphorylated chitosan. Wan et al. prepared phosphorylated chitosan (PCTS) membranes from the reaction of orthophosphoric acid and urea on the surface of chitosan membranes in N,N-dimethylformamide. It was also observed that the crystallinity of the phosphorylated chitosan membranes and the corresponding swelling indices were changed markedly, even though these membranes did not lose either their tensile strength or thermal stability to a significant degree in comparison with the unmodified chitosan membranes [66]. Nishi et al. reported that phosphorylated chitosan with low degree of substitution had shown increased solubility because of a strong interaction between the phosphoryl groups

and water [67]. Li and coworkers prepared phosphorylated chitosan/ chitosan/ hydroxyapatite composites which had a good compressive strength and can be used as a novel bio-composite for bone tissue engineering [68]. Pramanik and coworkers prepared hydroxyapatite (HAp)/chitosan phosphate nanocomposite solution-based chemical methodology with varying HAp contents from 10 to 60% (w/w). The mechanical properties of the composite improved significantly with increase in nanoparticle contents. Cytotoxicity study using murine L929 fibroblast validated that the nanocomposite was cytocompatible. Primary murine osteoblast cell culture study confirmed that the nanocomposite was osteocompatible and highly *in vitro* osteogenic. The prepared nanocomposite may be used in bone tissue engineering applications [69]. Phosphorylated chitosan membranes were reported to induce the biomimetic deposition of an apatite-like layer under simulated physiological conditions, after pre-incubation in calcium-containing solutions, due to chelation of calcium ions and partial hydrolysis of phosphate functionalities [70-71].

Win et al. prepared gel beads using phosphorylated chitosan by ionic gelation method using TPP to improve the controlled release system in a gastrointestinal fluid. This work studied the *in vitro* drug release profiles monitored at various pH media at 37 °C using ibuprofen (Ib) as a model drug [72]. Win et al. also investigated the effect of proteolytic enzymes on *in vitro* release of ibuprofen from phosphorylated chitosan microspheres in simulated gastric fluid (SGF) (pH 1.4) and simulated intestinal fluid (SIF) (pH 7.4). The release of ibuprofen from phosphorylated chitosan microspheres was found to be sustained more effectively than that from chitosan microspheres in the medium containing proteolytic enzymes [73].

Jayakumar and coworkers prepared phosphorylated chitosan beads by ionic gelation method using tripolyphosphate. The *in vitro* drug release behavior in various pH solutions was studied using indomethacin (IM) as a model drug at two different concentrations (0.3 and 0.6% w/w). The release rate of IM at pH 7.4 was higher than that at pH 1.4, due to the ionization of phosphorous groups and the high solubility of IM in the alkaline medium. These results indicated that PCTS beads have the potential to be used as controlled drug delivery systems through oral administration by avoiding the drug release in the highly acidic gastric fluid region of the stomach [74].

One of the highly cheap and easily available polymers is the soy flour and soy protein isolate. Soy flour (SF) and soy protein isolate (SPI) are edible protein which is tried to be exploited as one of the components of drug delivery systems. Liu and Tang explored the emulsifying properties of soy protein isolate nanoparticles and found that these nanoparticles can formulate Pickering emulsions with tailor-made properties [75]. Renu et al. studied the formulation of soy protein nanoparticles and its conjugation to antivenom. The nanoparticle was conjugated with antivenom immunoglobulins (F(ab')₂ fragments) using 1-ethyl-3-[3-dimethylaminopropyl]carbodiimide. *In vitro* studies indicated that conjugated antibodies inhibited the activity of protease, phospholipase and hyaluronidase enzymes of Bungarus caeruleus venom more efficiently than the free antivenom [76]. Teng and coworkers prepared SPI nanoparticle by desolvation method. They used curcumin as the model drug which was successfully encapsulated into the nanoparticles [77]. Teng et al. also prepared folic acid (FA) conjugated soy protein isolate (SPI) nanoparticles target specific drug delivery. Curcumin as a model drug was encapsulated successfully into FA-SPI nanoparticles. The highest encapsulation and loading efficiencies were around 92.7% and 5.4%, respectively, which were much higher than those with nonconjugated SPI nanoparticles. A faster release of curcumin was observed for FA-SPI nanoparticles in PBS/Tween 20 buffer. Cell culture study showed that conjugation of FA resulted in an increase in cellular uptake by at most 93% in Caco-2 cells. These results suggested that FA-SPI is a potential wall material for encapsulation and enhanced delivery of anticancer drugs [78]. Teng et al. prepared CMC-SPI nanoparticles by simple ionic gelation method for the encapsulation and controlled release of vitamin D₃ [79].

2.4. Montmorillonite (MMT) and Cellulose whisker (CW) in Biomedical Applications

Lee et al. used MMT to improve the mechanical properties of model scaffolds made of poly L-lactic acid (PLLA). The resulting polymer nanocomposite scaffolds had a 40% increase in tensile modulus when compared to pristine PLLA scaffolds [80]. Zhuang et al. observed that the intercalated structure of MMT-gelatin-chitosan has a lower degradation rate when compared to a gelatin-chitosan scaffold. The rate of degradation

can be modified by changing the MMT concentration. Improved cell adhesion and proliferation on the MMT-gelatin-chitosan nanocomposite film was also observed [81].

Wang et al. prepared quaternized chitosan/organically modified MMT nanocomposites by simple solution-mixing in aqueous media. Antimicrobial studies showed that the nanocomposites could strongly inhibit the growth of a wide variety of microorganisms, including Gram-positive bacteria, Gram-negative bacteria, and fungi. The antibacterial effect increased with the increase in the concentration of MMT [82]. Haerudin and coworkers developed nanocomposite film consisting of chitosan, montmorillonite (MMT) and cashew nut shell liquid (CNSL). FTIR spectroscopy of the nanocomposite films designated that, by addition of CNSL, amide groups of the chitosan are probably less attached and have more space for vibration. CNSL seems to provide intermolecular spaces between the chitosan molecules. Addition of CNSL as plasticizer improved the tensile strength by 10% and the elastic modulus by almost 18% and cell growth was observed on all the nanocomposite samples studied [83].

One of the problems associated with biomaterials for drug delivery is the burst release of encapsulated drugs from the system. MMT has a layered silicate structure which demonstrates good barrier properties to the system due to the tortuous diffusion pathways that small molecules (drug) must travel in order to pass through the system [84]. This property of MMT is highly useful in controlled release drug delivery applications. Cypes and coworkers prepared poly(ethylene-co-vinyl acetate)/organically modified MMT nanocomposites to study the release properties of dexamethasone. They found that the increase in MMT concentration provided a sustained release of dexamethasone [85].

Vaia et al. prepared poly(D, L-lactide-co-glycolide)/MMT nanoparticles loaded with paclitaxel by emulsion/solvent evaporation method. They studied the release kinetics of the drug and observed that there is an initial burst release of 22% drug on the first day. After which the release of drug was at a slower and constant rate [86]. Yuanichi et al. observed that drug release from MMT surface is promoted by the weak bonding between them and drug wettability is improved owing to the hydrophilic properties of MMT. They demonstrated that phenytoin-MMT adsorbates were able to improve the bioavailability of drug in comparison to phenytoin sodium capsules [87]. Das et al. developed gelatin/MMT nanocomposites for controlled delivery of paclitaxel [88]. Sahoo et al. prepared

gelatin/MMT hybrid nanocomposite loaded with paclitaxel for bladder cancer therapy. MMT was incorporated in the formulation as a matrix material component which also acts as a co-emulsifier in the nanocomposites preparation [89]. Liu et al. developed crosslinked alginate/quaternized carboxymethyl chitosan (QCMC)/OMMT microspheres by crosslinking with CaCl_2 . Bovine serum albumin (BSA) was used as the model drug. In vitro release results for BSA indicated that the prepared microsphere showed more excellent encapsulation and controlled release capacities than the microsphere without OMMT. The in vitro active cutaneous anaphylaxis test was carried out on Guinea pigs, which revealed that microsphere did not cause anaphylaxis. Therefore, the microspheres were suitable to apply as drug-controlled release carriers [90].

Cellulose and its derivatives have a long history as pharmaceutical excipients in various types of formulations. Mathew et al. used CWs as material for the development of artificial ligaments and tendons [91]. Cherian et al. produced polyurethane matrices that were reinforced with nanofibrillated cellulose for implantable purposes. They tested the application of the composites in design of prosthetic heart valves as well as vascular grafts [92]. Cellulose nanowhiskers have been found to be non toxic to cells and hence could be considered for delivery of biomolecules and therapeutics [93]. Dugan and coworkers studied the bioactivity of CW by interacting them with myoblast cells and observed that patterned CWs surfaces actively direct the growth of tissue leading to applications in tissue engineering, and also that CW exhibited non-cytotoxicity and nonimmunogenicity even at relatively high concentrations [94-95].

Although both MMT and CWs are widely used in nanocomposites, their use in nanoparticles for controlled drug delivery applications is very limited.

2.5. Glutaraldehyde and Genipin as Crosslinkers

Mirzaei et al. crosslinked chitosan with different amount of glutaraldehyde to prepare appropriate hydrogels to be used as drug delivery system. It was observed that with increasing crosslinking agent the swelling of the prepared samples degrees from 1200% to 600% and pore diameters change from 100 to 500 nm [96]. Gupta et al. have done different research on glutaraldehyde and glyoxal crosslinked microspheres for sustained release of centchroman under physiological conditions [97]. Ramachandran et al.

developed glutaraldehyde cross-linked chitosan microspheres loaded with famotidine for controlled delivery applications [98]. Distantina et al. developed glutaraldehyde-crosslinked kappa carrageenan hydrogel [99].

Harris et al. prepared chitosan hydrochloride-genipin microspheres for controlled release of three drugs, namely, clarithromycin, tramadol hydrochloride and heparin. Genipin was found to be an efficient chemical-crosslinking agent delaying the outflow of drugs from the microspheres [100]. Sung et al. reported that genipin was around 10,000 times less toxic than glutaraldehyde. Also, the proliferative capacity of cells after exposure to genipin was approximately 5000 times greater than that after exposure to glutaraldehyde. It was noted that the cells seeded on the surface of the glutaraldehyde-fixed tissue were not able to survive. In contrast, the surface of the genipin-fixed tissue was found to be filled with 3T3 fibroblasts. These results suggested that cellular compatibility of the genipin-fixed tissue was superior to that of glutaraldehyde [101]. Liang et al. prepared genipin-crosslinked gelatin microspheres as a drug carrier for intramuscular administration [102].

2.6. Objectives and plan of work

Tuberculosis (TB) and Cancer are two of the dreaded diseases that have affected the humankind from the very early time. Both the diseases are the leading cause of death worldwide. The major problems TB treatment is noncompliance of patients to prescribed regimens, primarily because effective chemotherapy of TB involves the daily administration of one or more drugs for a period of 6 months or longer. Clinical administration of the treatment is limited because of toxic side effects and degradation of drugs before reaching their target site, low permeability and poor patient compliance. Thus, the drawbacks of conventional chemotherapy required the development of a delivery or carrier system to release drugs slowly over extended time periods, which will also allow reduction in frequency and dosing numbers. Similar is the case of cancer treatment with curcumin. Even though, curcumin itself is non toxic and offer wide potential in cancer treatment, its applicability is limited by low aqueous solubility and poor bioavailability. These problems can be handled if both isoniazid and curcumin are encapsulated in suitable polymer nanoparticles.

Polymers, such as chitosan can be efficiently used in the preparation of the nanoparticles. But chitosan is soluble only in acidic pH. Hence, to solve the problem of solubility, chitosan derivatives, like carboxymethyl chitosan, phosphorylated chitosan, thiolated chitosan etc. are synthesized. These derivatives of chitosan are soluble in water at all pH. Furthermore, these derivatives increase the drug loading efficiency and also the mucoadhesion with the cell membranes.

Nanofillers like clay, cellulose whiskers etc. can be used in nanoparticle synthesis. The nanofillers can control the release of drug and provide mechanical stability to the nanoparticles. Crosslinkers, such as, glutaraldehyde, genipin, etc. can be used to give dimensional stability to the nanoparticles.

Keeping in view all the above backgrounds, the aim of the present investigation was set and had been undertaken. In the present research work nanoparticles were developed for encapsulation of isoniazid and curcumin. These nanoparticles were studied for controlled release applications. The polymeric material used were naturally occurring polymers such as chitosan, soy flour and water soluble derivatives of chitosan like carboxymethyl chitosan (CMC) and phosphorylated chitosan (PCTS). Montmorillonite (MMT) and cellulose whisker (CW) were used as the reinforcing agents. The nanoparticles were prepared by using different methods like, microencapsulation, ionic gelation and desolvation methods. Both synthetic and natural crosslinker were used for the preparation of the nanoparticles. Synthetic crosslinker used was glutaraldehyde and natural crosslinker was genipin.

The main objectives of the present investigation were:

- i) To develop nanoparticles employing, different natural biodegradable polymers like, soy flour, chitosan and its water soluble derivatives, either alone or in combination with filler (MMT, cellulose whisker), cross linking agents and other additives.
- ii) To study the effect of various parameters like amount of filler, polymer, percentage of cross linking agents, etc. on drug loading capacity, release characteristics, water absorption, etc.

- iii) To characterize the composite using FTIR, X-ray diffractometer, scanning electron microscope, transmission electron microscope, etc
- iv) To study the cytotoxicity effect of the nanoparticles on the living system

Reference

- [1]Manchester, K. *Med. His.* **28**, 162--173, 1984.
- [2]Onyebujoh, P., et al. *Bull. World Health Organ.* **83** (11) 857--865, 2005.
- [3]Mitchison, D. A. *Int. J. Tuberc. Lung Dis.* **4** (9), 796--806, 2000.
- [4]World Health Organization; Treatment of tuberculosis: guidelines for national programmes, 3rd ed., Geneva, 2003.
- [5]Schaberg, T., et al. *Eur. Respir. J.* **9**, 2026--2030, 1996.
- [6]Catalani, E. *Int. J. Tuberc. Lung Dis.* **3**, S289--S291, 1999.
- [7]Iseman, M.D. *Eur Respir. J.* **20** (36S), 87S--94S, 2002.
- [8]Latent Tuberculosis Infection (LTBI) – Targeted Testing and Treatment , 1--17, 2009.
- [9]IARC Monographs on the Evaluation of Carcinogenic Risk of Chemicals to Man, *International Agency for Research on Cancer*, Lyon, **14**, 159--172, 1974.
- [10]Bhide, S.V. et al. *Int. J. Cancer*, **21**, 381--386, 1978
- [11]Desai, V.A., & Agarwal, S.B. *J. Indian Acad. Clin. Med.* **5** (1), 83--85, 2004.
- [12] Pandit, A. et al. *J Appl. Pharm. Sci.* **2** (5), 233--243, 2012.
- [13]Angadi, S.C. et al. *Int. J. Biol. Macromol.* **47** (2), 171--179, 2010.
- [14]Behera, A.K. et al. *Der Pharmacia Lettre*, **5** (4), 43--50, 2013.
- [15]Muhammed, R.P.E, et al. *Res. J. Pharm. Biol. Chem. Sci.* **1** (4), 383--390, 2010.
- [16]Ahmad, Z., et al. *Indian J. Chest. Dis. Allied. Sci.* **48**, 171--176, 2006.
- [17]Strimpakos, A.S., & Sharma, R.A. *Antioxid. Redox Signal.* **10**, 511--545, 2008.
- [18]Balasubramanian, K. *J. Agric. Food Chem.* **54** (10) 3512--3520, 2006.
- [19]Priyadarsini K.I., et al. *Free. Radic. Biol. Med.* **35** (5), 475--484, 2003.
- [20]Dahl, T.A, et al. *Photochem. Photobiol.* **59**, 290--294, 1994.
- [21]Jiang M.C., et al. *Nutr. Cancer* **26**, 111--120, 1996.

- [22] Kuo M.L., et al. *Biochim. Biophys. Acta* **1317**, 95--100, 1996.
- [23] Aggarwal, B.B., et al. *Anticancer Res.* **23**, 363--398, 2003.
- [24] Chen, H. et al. *Anticancer Res.* **19**, 3675--3680, 1999.
- [25] Choudhuri, T., et al. *FEBS Lett.* **512**, 334--340, 2002.
- [26] Jaruga, E., et al. *FEBS Lett.* **433**, 287--293, 1998.
- [27] Piwocka, K., et al. *Exp. Cell. Res.* **249**, 299--307, 1999.
- [28] Huang, M.T., et al. *Cancer Res.* **51**, 813--819, 1991.
- [29] Chattopadhyay, I., et al. *Curr. Sci.* **87** (1), 44--53, 2004.
- [30] Kiso, Y., et al. *Planta Med.* **49** (3), 185--187, 1983.
- [31] Srivastava, R., et al. *Thromb. Res.* **40** (3), 413--417, 1985.
- [32] Nirmala, C., & Puvanakrishnan, R. *Mol. Cell. Biochem.* **159** (2), 85--93, 1996.
- [33] Babu, P.S., & Srinivasan, K. *Mol. Cell. Biochem.* **152** (1), 13--21, 1995.
- [34] Arun, N., & Nalini, N. *Plant Foods Hum. Nutr.* **57** (1), 41--52, 2002.
- [35] Anand, P., et al. *Mol. Pharm.* **4**, 807--818, 2007.
- [36] Naito, M., et al. *J. Atheroscler. Thromb.* **9** (5) 243--250, 2002.
- [37] Murugan, P., & Pari, L. *J. Basic Clin. Physiol. Pharmacol.* **17** (4), 231--244, 2006.
- [38] Sharma, R.A., et al. *Clin. Cancer Res.* **7** (7), 1894--1900, 2001.
- [39] Ryu, E.K., et al. *J. Med. Chem.* **49** (20), 6111--6119, 2006.
- [40] Kimura, T., et al. *Chem. Pharm. Bull.* **37** (2), 463--466, 1989.
- [41] Moorthi, C., et al. *Asian Pac. J. Trop. Biomed.* **2** (11), 841--848, 2012.
- [42] Bisht, S., et al. *J. Nanobiotech.* **5** (3), 1--18, 2007.
- [43] Kruij, C.G., et al. *Curr. Opin. Colloid Interface Sci.* **9** (5), 340--349, 2004.
- [44] Maji, T.K., et al. *Bioresource Technol.* **98** (4), 840--844, 2007

- [45] Ohya, Y , et al *Pure Appl Chem* , **31**, 629--642, 1994
- [46] Yokohama, M , et al *J Controlled Release* **50**, 79--92, 1998
- [47] Kataoka, K , et al *J Controlled Release* **64**, 143--153, 2000
- [48] Liu, C G , et al *Carbohydr Polym* **62**, 293--298, 2005
- [49] Chen, X G , et al *J Agric Food Chem* , **51**, 3135--3139, 2003
- [50] Calvo, P , et al *J Appl Poly Sci* **63**, 125--132, 1997
- [51] Bodmeier, R., et al *Pharm Res* **6**, 413--417, 1989
- [52] Xu, Y , & Du, Y *Int J Pharm* **250**, 215--226, 2003
- [53] Nasti, A , et al *Pharm Res* **26**, 1918--1930, 2009
- [54] Lin, A H , et al *Yao Xue Xue Bao* **42**, 323--328, 2007
- [55] Alishahi, A et al *Food Chem* **126**, 935--940, 2011
- [56] Katas, H et al *J Med Sci* **11** (4), 192--197, 2011
- [57] Basu, S K et al *Sci Pharm* **78**, 79--92, 2010
- [58] Lucinda-Silva, R M , & Evangelista, R C *Acta Farm Bonaerense* **24** (3), 366--370, 2005
- [59] Das, R K., et al *Nanomed Nanotech Biol Med* **6**, 153--160, 2010
- [60] Farag, R K , & Mohamed, R R *Molecules* **18**, 190--203, 2013
- [61] Li, Y , et al *Polym Int* **58**, 1120--1125, 2009
- [62] Anitha, A , et al *Carbo Pol* **78**, 672--677, 2009
- [63] Anitha, A , et al *J Biomater Sci* **23**, 1381--1400, 2012
- [64] Anitha, A , et al *Eur J Pharm Biopharm* **88**, 238--251, 2014
- [65] Thu, H P , et al *Chem Lett* **40** (11), 1--3, 2011
- [66] Wan, Y , et al *Macromol Chem Phys* **204** (5/6), 850--858 2003
- [67] Nishi, N et al *Int J Biol Macromol* **8** (5), 311--317, 1986

- [68]Li, B., et al. *Mater. Des* **32**, 4543--4547, 2011.
- [69] Pramanik, N., et al. *Int. J. Biomater*, **2009**, 1--8, 2009.
- [70]Yokogawa, Y., et al. *J. Mater. Sci. Mater. Med.* **8** (7), 407--412, 1997.
- [71]Varma, H.K., et al. *Biomater.* **20** (9), 879--884, 1999.
- [72]Win, P.P. *Carbohydr. Polym.* **53** (3), 305--310, 2003.
- [73] Win, P.P., et al. *Polym. Int.* **54** (3), 533--536, 2005.
- [74] Jayakumar, R., et al. *J. Bioact. Comp. Polym.* **21**, 327--340, 2006.
- [75]Liu, F., & Tang, C.H. *J. Agric. Food. Chem.* **62**, 2644--2654, 2014.
- [76] Renu, K., et al. *Appl. Biochem. Biotechnol.* 1--14, 2014, DOI 10.1007/s12010-014-1207-5.
- [77]Teng, Z., et al. *J. Agric. Food. Chem.* **60**, 2712--2720, 2012.
- [78] Teng, Z., et al. *J. Agric. Food. Chem.* **61**, 2556--2564, 2013.
- [79] Teng, Z., et al. *Food Chem.* **141**, 524--532, 2013.
- [80]Lee, J.H., et al. *Biomater.* **24**, 2773--2778, 2003.
- [81]Zhuang, H., et al. *J. Mater. Sci. Mater. Med.* **18**, 951--957, 2007.
- [82]Wang, X., et al. *J. Biomed. Mater. Res. Part A* **84** (2), 384--390, 2008.
- [83]Haerudin, H., et al. *Int. J. Tech* **1**, 65--73, 2010.
- [84]Yano, K., et al. *J. Polym. Sci. A-Polym. Chem.* **35**, 2289--2294, 2000.
- [85]Cypes, S.H., et al. *J. Control. Release* **90**, 163--169, 2003.
- [86]Vaia, R.A., et al. *Chem. Mater.* **8**, 26--28, 1996.
- [87]Yuanichi, S., et al. *Phys. Rev. Lett.* **93** (8), 88--90, 2004
- [88]Das, P.R., et al. *Int. Res. J. Biochem. Bioinfo.* **1** (2), 035--042, 2011.
- [89]Sahoo, R., et al. *Eur. J. Sci. Res.* **48** (3), 527--537, 2011.

- [90]Liu, B., et al. *J. Biomater. Sci., Polym. Ed.* **24** (5), 589--605, 2013.
- [91]Mathew, A.P., et al. *Carbohydr. Polym.* **87** (3), 2291--2298, 2012.
- [92]Cherian, B.M., et al. *Carbohydr. Polym.* **86** (4), 1790--1798, 2011.
- [93]Kovacs, T., et al. *Nanotoxicology* **4** (3), 255--270, 2010.
- [94]Dugan, J.M., et al. *Biomacromol.* **11**(9), 2498--2504, 2010.
- [95]Dugan, J., et al. *Eur. Cells Mater.* **22**, 41--42, 2011.
- [96] Mirzaei, E., et al. *Int. J. Polym. Mater. Polym. Biomater.* **62**, 605--611, 2013.
- [97]Gupta, K.C., & Jabrail, F.H. *Carbohydr. Res.* **341**, 744--756, 2006.
- [98]Ramachandran, S., et al. *Trop. J. Pharma. Res.* **10** (3), 309--316, 2011.
- [99]Distantina, S., et al. *Eng. J.* **17** (3), 57--66, 2012.
- [100] Harris, R., et al. *Mar. Drugs* **8**, 1750--1762, 2010.
- [101]Sung, H.W., et al. *J. Biomater. Sci. Polym. Ed.* **10** (1), 63--78, 1999.
- [102]Liang, H.C., et al. *J. Biomed. Mater. Res. Part A*, **65** (2), 271--282, 2003.

CHAPTER 3
EXPERIMENTAL

CHAPTER 3
EXPERIMENTAL

This chapter covers the materials and methods, which includes raw materials used, techniques for sample preparation, release studies and characterization of the products.

3.1. Materials used

The chemicals used in the present study and the manufacturers are listed below:

Materials	Suppliers
(i) Chitosan (Low molecular weight)	Sigma Aldrich, Germany
(ii) Soy flour (SF)	Raja Soya, Tezpur (Assam, India)
(iii) Montmorillonite K-10	Sigma Aldrich, Germany
(iv) Isoniazid	Sigma Aldrich, Germany
(v) Curcumin	Sigma Aldrich, Germany
(vi) Glacial Acetic Acid	Merck, India
(vii) Monochloroacetic acid	Sigma Aldrich, Germany
(viii) Orthophosphoric acid	Merck, India
(ix) Urea	Merck, India
(x) N,Ndimethylformamide	Sigma Aldrich, Germany
(xi) Histopaque 1077	Sigma Aldrich, Germany
(xii) NaHCO ₃	Merck, India
(xiii) (3-[4, 5-dimethylthiazol-2-yl]-2, 5-diphenyl tetrazolium bromide) (MTT).	Sigma Aldrich, Germany
(xiv) Tween 80	Merck, India
(xv) Sodium tripolyphosphate	Merck, India
(xvi) Calcium chloride (CaCl ₂)	Merck, India.
(xvii) Glutaraldehyde (GA)	Loba Chemi PvtLtd, Mumbai, India.
(xviii) Genipin	Challenge Bioproducts Co., Taiwan
(xix) RPMI 1640	HiMedia Laboratories (Mumbai, India)
(xx) Fatal bovine serum (FBS)	HiMedia Laboratories (Mumbai, India)

(xxi) Whatman filter paper No. 1	GE Healthcare, Chalfont St. Giles, Buckinghamshire, U.K.
(xxii) MCF-7 cell line	NCCS Pune, India
(xxiii) HepG2 cell line	NCCS Pune, India
(xxiv) DMEM	HiMedia Laboratories (Mumbai, India)
(xxv) Thiobarbituric acid	HiMedia Laboratories (Mumbai, India)
(xxvi) Trichloroacetic acid	HiMedia Laboratories (Mumbai, India)
(xxvii) Penicillin-streptomycin antibiotic	HiMedia Laboratories (Mumbai, India)
(xxviii) Dimethyl sulfoxide (DMSO)	Merck, India

The rest of the chemicals were of analytical grade and used as received.

3.2. Methods

3.2.1. Section A: Preparation of Nanoparticles/microparticles loaded with hydrophilic drug, Isoniazid

3.2.1.1. Preparation of Cellulose Whisker (CW)

Cellulose whisker was synthesized from whatman filter paper by following the method of Zhang et. al. with slight modification [1]. Whatman filter paper (No. 1) was sieved through a test sieve (Scientific Engineering Corporation, New Delhi, India) outfitted with 100 mesh screen to obtain very small size. The resultant cellulose powder (1g) was pretreated by taking into a beaker and was dispersed in 5 M NaOH solution. The mixture was stirred at 65° C for 6 h. The slurry thus obtained was filtered and thoroughly washed with distilled water until neutral pH was obtained and dried in vacuum oven. 100 mL of DMSO was added to the dried cellulose. The slurry was then sonicated for 1 h, filtered, washed with 500 mL of distilled water and vacuum dried in oven.

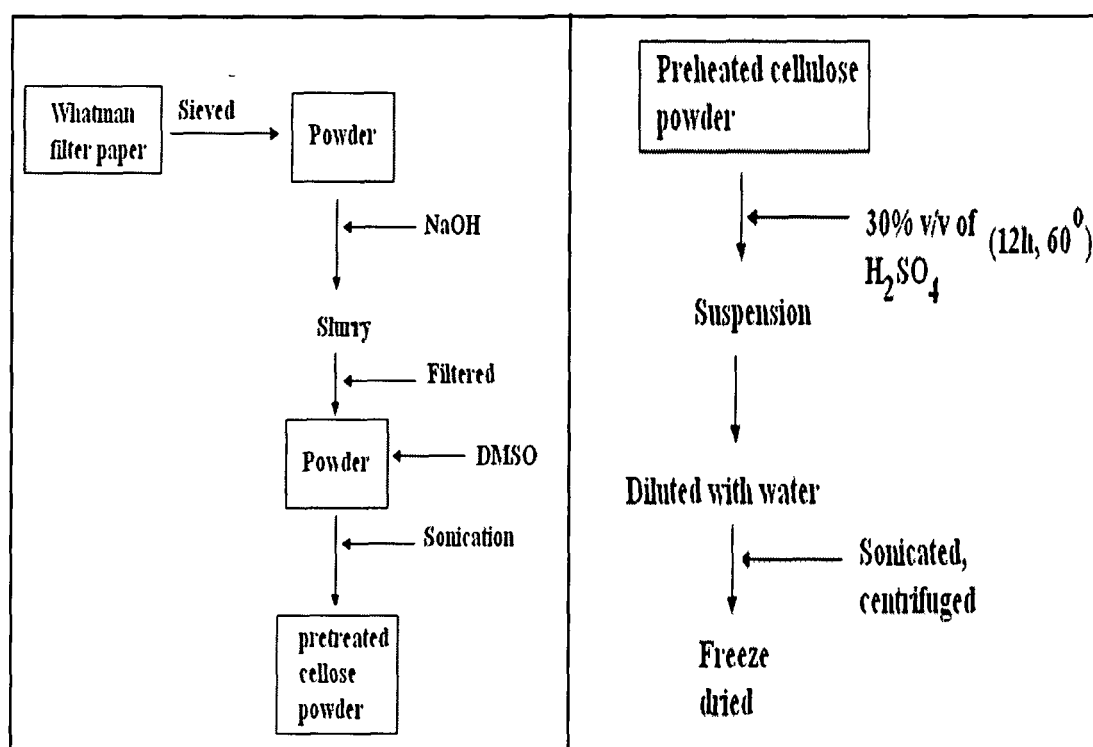


Figure 3.1. Schematic diagram of preparation of CW

Then, 1 g of the obtained cellulose was dispersed in 25 mL of 30% (v/v) H_2SO_4 in a three-necked (250 mL) round bottom flask equipped with a mechanical stirrer and a thermometer. The flask was then placed in a water bath, and its contents were stirred vigorously for 12 h while the temperature was maintained at $60^\circ C$. The suspension was then diluted with 75 mL of distilled water and sonicated for 1 h.

The dispersion was centrifuged at nearly 8000 rpm for 30 min and washed with distilled water until the pH of the supernatant liquid was nearly 7. The residues (cellulose whiskers) separated after high-speed centrifugation was collected and freeze-dried. Figure 3.1. shows the schematic diagram of preparation of CW.

These cellulose whiskers (CW) were further used for the preparation of the microparticles.

3.2.1.2. Preparation of Isoniazid loaded Chitosan–CW microparticles by microencapsulation method

Microspheres of Chitosan composite were made by microencapsulation method as reported by Devi et. al. with modifications [2]. In this method 1% (w/v) chitosan solution was prepared in water containing 0.5 % (v/v) acetic acid and measured amount of prepared cellulose whisker was dispersed in the chitosan solution along with 0.005 mL Tween 80 (surfactant) and stirred for 1 h and then sonicated for 20 min. In another beaker, known amount of (250 mL) sunflower oil was taken. This oil was stirred for approximately 10 min. Under stirring condition, 50 ml of 1% chitosan solution containing dispersed cellulose whisker was added drop wise to the beaker containing oil to form water in oil emulsion. After this, a known amount of Na_2SO_4 solution (20% w/v) was added slowly to the beaker to obtain the microparticles.

The optimum ratio of chitosan and Na_2SO_4 at which complete phase separation occurred was 1:2. The beaker containing the microspheres was left to rest for approximately 15mins under constant stirring condition. The system was then brought to $5-10^\circ C$ to harden the microsphere. Crosslinking of the microspheres was achieved by slow addition of certain amount of glutaraldehyde (GA) solution. The temperature of the beaker was then raised to $45^\circ C$ and stirring was continued for another 6 h to complete the crosslinking reaction. The beaker was then brought down to room temperature slowly

while stirring. The microspheres were filtered through 300-mesh nylon cloth, washed with acetone rapidly to remove oil, if any, adhered to the surface of microspheres. This was further washed with distilled water until the pH of filtrate reached neutrality. The microspheres were then dried in open air. The dried microspheres were then dipped in isoniazid solution (0.5% w/v) for 120 min., filtered through 300-mesh nylon cloth, and quickly washed with water to remove isoniazid, if any, adhered to the surface. The isoniazid-encapsulated microspheres were again freeze-dried and stored in a glass ampule in a refrigerator.

A series of seven samples were prepared for the present study.

Table 3.1. Recipes for the formation of different isoniazid loaded chitosan-CW microparticles crosslinked with GA

Sample code	(Chitosan) % w/v (amount in g in 50 ml water)	CW (% w/w) w.r.t Chitosan (amount in g in 50 mL water)	GA (% v/w) w.r.t chitosan (amount in mL)	Isoniazid (g)	Tween 80 (mL)
C/CW0/GA50	1 (0.5)	0 (0.00)	0.25	0.1	0.005
C/CW1/GA50	1 (0.5)	1 (0.005)	0.25	0.1	0.005
C/CW3/GA50	1 (0.5)	3 (0.015)	0.25	0.1	0.005
C/CW5/GA50	1 (0.5)	5 (0.025)	0.25	0.1	0.005
C/CW5/GA10	1 (0.5)	1 (0.025)	0.05	0.1	0.005
C/CW5/GA30	1 (0.5)	1 (0.025)	0.15	0.1	0.005
C/CW5/GA70	1 (0.5)	1 (0.025)	0.35	0.1	0.005

3.2.1.3. Preparation of Isoniazid loaded Chitosan Montmorillonite nanoparticles using ionic gelation method

Chitosan nanoparticles were prepared by ionic crosslinking of chitosan with sodium tripolyphosphate (TPP) and employing the process as reported by Calvo [3]. 1% (w/v) chitosan solution was prepared in water containing 0.5 % (v/v) acetic acid. 0.005g of MMT was swelled in 50 mL of water for 24h. It was then stirred vigorously by mechanical stirrer for 48h and sonicated for 30 min. This dispersed MMT solution was added to 50 mL of 1 % (w/v) chitosan solution. To this solution, isoniazid (0.01 g) and

Tween 80 (0.5-5% v/w of chitosan i.e. 0.0025-0.025 mL) were added, stirred and sonicated for 15 min. Now, 1% (w/v) TPP solution was prepared in water. Nanoparticles were obtained by slow addition of 15 mL of TPP solution to 100 mL of isoniazid containing chitosan-MMT solution under constant magnetic stirring at room temperature for 30 min. The temperature of the container containing nanoparticles was brought down to 5-10°C to harden the nanoparticles. Now GA (0.1 mmol) was added and the temperature was increased to 45°C. The reaction was continued for 45 min. The nanoparticles were separated by centrifuging the solution for 30 min. The product was washed several times with water and dried. The dried nanoparticles were kept in ampule, stored in refrigerator and redispersed in deionised water for further use. Figure 3.2. depict the preparation process of formation of isoniazid loaded chitosan- MMT nanoparticles.

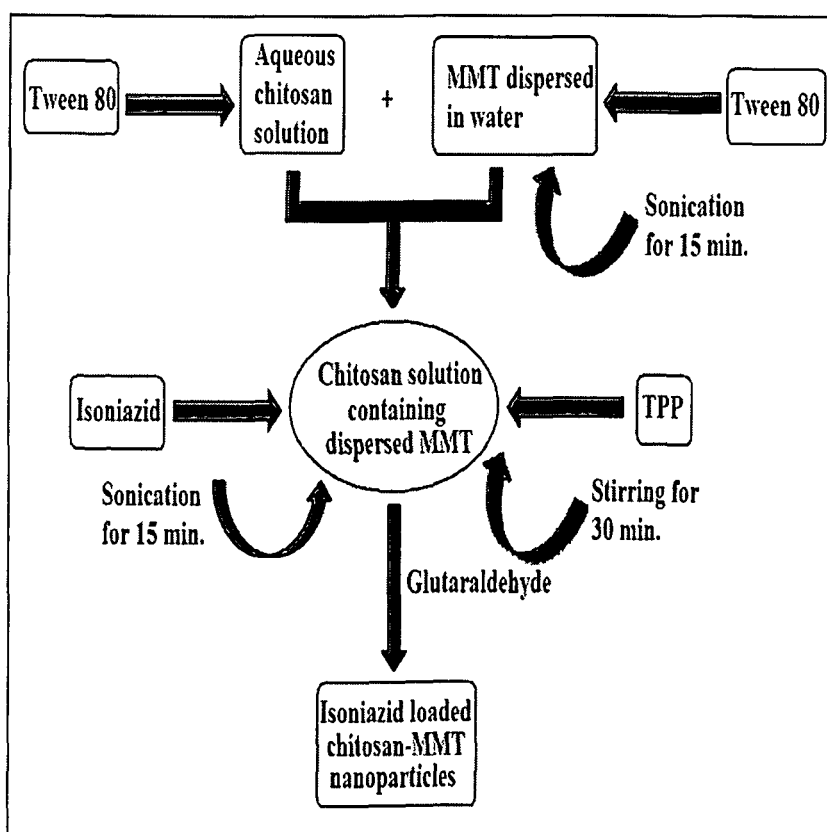


Figure 3.2. Flowchart diagram showing the main steps in the preparation of isoniazid loaded chitosan-MMT nanoparticles

A series of six samples were prepared for the present study.

Table 3.2. Recipes for the formation of different isoniazid loaded chitosan-montmorillonite nanoparticles

Sample code	Chitosan % w/v(amount in g in 50mL water)	MMT % w/v w.r.t chitosan (amount in g in 50 mL water)	Tween 80 %v/w w.r.t.chitosan (amount in mL)	Isoniazid (g)	TPP % w/v w.r.t water (amount in g in 100 mL water)	GA (mmol)
NPI	1 (0.5)	1(0.005)	0 (0.0)	0.01	1 (1)	0.1
NPII	1 (0.5)	1(0.005)	0.5 (0.0025)	0.01	1 (1)	0.1
NPIII	1 (0.5)	1(0.005)	1(0.005)	0.01	1 (1)	0.1
NPIV	1 (0.5)	1(0.005)	3(0.015)	0.01	1 (1)	0.1
NPV	1 (0.5)	1(0.005)	5 (0.025)	0.01	1 (1)	0.1
NPVI	1 (0.5)	0 (0.00)	5 (0.025)	0.01	1 (1)	0.1

3.2.1.4. Synthesis of carboxymethyl chitosan

Carboxymethyl chitosan derivatives were prepared as described in the literature [4]. Chitosan (1gm) was swollen in 100 ml of water for 24 h. To this, monochloroacetic acid (4gm) was added and mixture was vigorously stirred until all chitosan was dissolved in water to give a homogenous solution. After that, the pH of the solution was adjusted to 8.0 by slow addition of 5% NaHCO₃ with continuous stirring. The reaction medium becomes opaque due to precipitation of chitosan caused by the rise of pH but reverted to homogenous solution on heating at 90°C. After heating at 90°C for 6 h, the solution cooled to ambient temperature and the pH was adjusted to 6.0 by using 1% HCl solution. The precipitate was then filtered off and the product was washed and brought to neutral pH with 90% ethanol solution. It was then dissolved in dilute sodium hydroxide solution to get the neutral sodium-salt of carboxymethyl chitosan, which was separated by being lyophilized.

3.2.1.5. Preparation of Isoniazid loaded CMC-MMT nanoparticles by ionic gelation method

Isoniazid loaded CMC-MMT nanoparticles were prepared by ionic crosslinking of CMC with CaCl_2 and employing the process as reported by Tavakol et al. with modifications [5]. 1% (w/v) CMC solution was prepared in water at 45°C . and stirred for 1 h at room temperature in a beaker. Varying percentage of MMT (1-5% w/w of CMC) was swelled in 50 mL of water along with 0.005 ml Tween 80 (surfactant) for 24h. It was then stirred vigorously by mechanical stirrer for 48h and sonicated for 30 min. This dispersed MMT solution was added to 50 mL of 1 % (w/v) CMC solution.

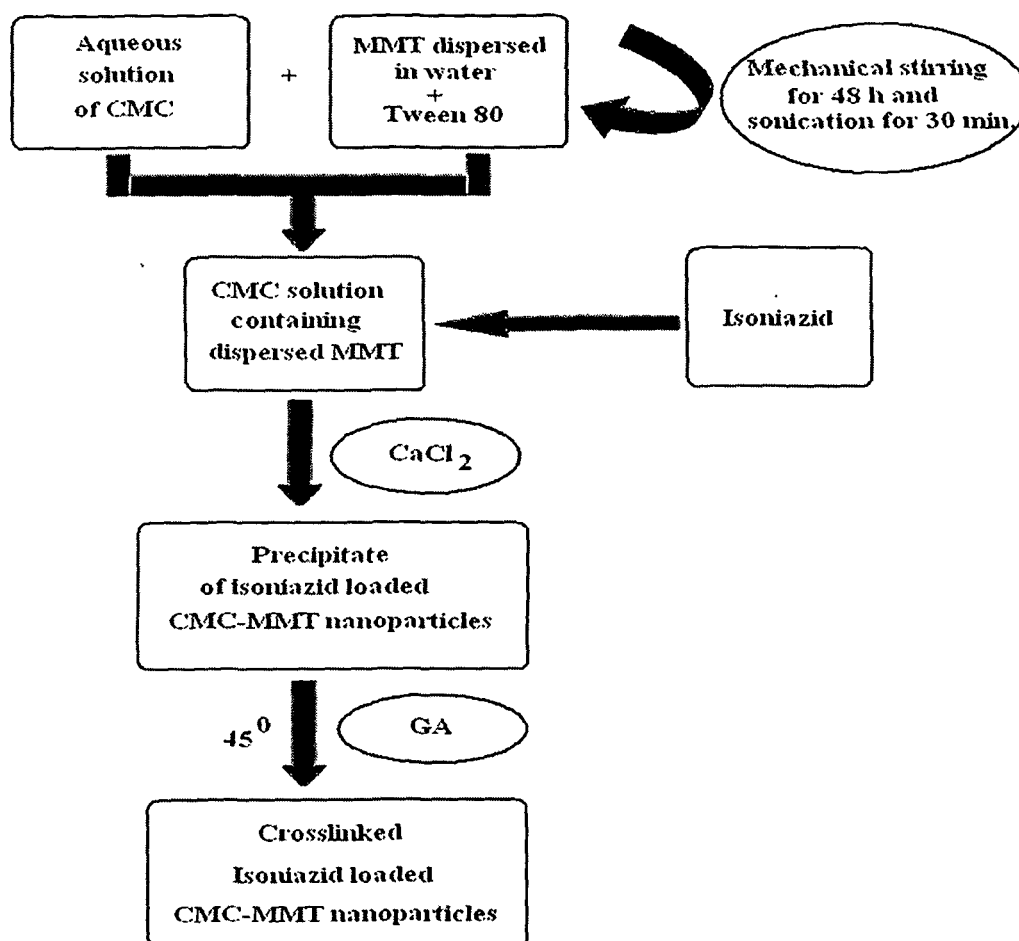


Figure 3.3. Flowchart diagram showing the main steps in the preparation of isoniazid loaded CMC-MMT nanoparticles

This was followed by addition of isoniazid (0.01g) to the beaker under stirring condition. 1 wt% of CaCl₂ solution was added slowly to the beaker till complete precipitation of CMC–MMT nanoparticles occurred. After 1h, the temperature of the system was brought down to 5-10° C to harden the nanoparticles. GA (10-70% v/w w.r.t. CMC) was added as a cross-linker and the temperature was increased to 45° C. The reaction was contained for 30 minutes. The precipitate was then separated by centrifuge and freeze dried. The dried nanoparticles were kept in ampule, stored in refrigerator and redispersed in deionised water for further use. Figure 3.3. depicts the preparation process of formation of isoniazid loaded CMC- MMT nanoparticles.

A series of seven samples were prepared by varying the MMT and GA concentration.

Table 3.3. Recipes for the formation of different isoniazid loaded CMC- montmorillonite nanoparticles

Sample code	(CMC) % w/v (amount in g in 50 ml water)	MMT % w/w w.r.t CMC (amount in g in 50 mL water)	GA% v/w w.r.t. CMC (amount in mL)	Isoniazid (g)	TPP % w/v w.r.t water (amount in g in 100 mL water)
CMC/M0/GA50	1 (0.5)	0 (0.00)	0.25	0.01	1 (1)
CMC/M1/GA50	1 (0.5)	1 (0.005)	0.25	0.01	1 (1)
CMC/M3/GA50	1 (0.5)	3 (0.015)	0.25	0.01	1 (1)
CMC/M5/GA50	1 (0.5)	5 (0.025)	0.25	0.01	1 (1)
CMC/M5/GA10	1 (0.5)	1 (0.025)	0.05	0.01	1 (1)
CMC/M5/GA30	1 (0.5)	1 (0.025)	0.15	0.01	1 (1)
CMC/M5/GA70	1 (0.5)	1 (0.025)	0.35	0.01	1 (1)

3.2.1.6. Synthesis of phosphorylated chitosan (PCTS)

PCTS was prepared by the following method of Li et al. with modifications [6]. 5% w/v of aqueous chitosan solution was mixed with 25 g of urea and 50 ml of N,Ndimethylformamide. Then 6 g of 85% orthophosphoric acid was added to the chitosan solution. The mixture was reacted at 150° C for 1 h. After cooling, the reaction

mixture was filtered. The obtained precipitate was washed thoroughly with deionized water and then dried at room temperature for 48 h.

3.2.1.7. Preparation of Isoniazid loaded PCTS-MMT nanoparticles by ionic gelation method

PCTS nanoparticles were prepared using ionotropic gelation process with the counter polyanion sodium triphosphate (TPP). PCTS (1 g) was dissolved in 100 mL distilled water with slight heating and stirred for 3h to obtain a transparent homogeneous solution. Varying percentage of MMT (1-5% w/w of PCTS) was swelled in 50 mL of water along with 0.005 ml Tween 80 (surfactant) for 24h. It was then stirred vigorously by mechanical stirrer for 48h and sonicated for 30 min. This dispersed MMT solution was added to 50 mL of 1 % (w/v) PCTS solution.

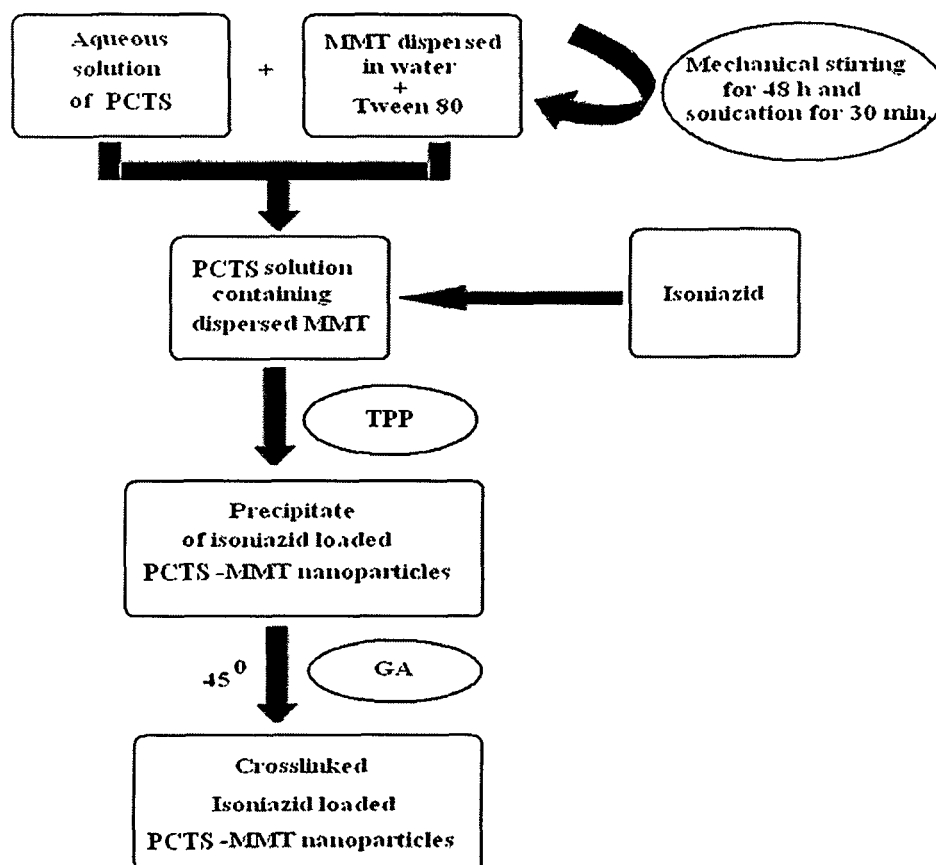


Figure 3.4. Flowchart diagram showing the main steps in the preparation of isoniazid loaded PCTS-MMT nanoparticles

This was followed by addition of isoniazid (0.01g) to the beaker under stirring condition. Now, 1% (w/v) TPP solution was prepared in water. Nanoparticles were obtained by slow addition of 15 mL of TPP solution to 100 mL of isoniazid containing PCTS-MMT solution under constant magnetic stirring at room temperature for 30 min. The temperature of the container containing nanoparticles was brought down to 5-10°C to harden the nanoparticles. Now varying amount of GA (10-70% v/w w.r.t. PCTS) was added and the temperature was increased to 45°C. The reaction was continued for 45 min. The nanoparticles were separated by centrifuging the solution for 30 min. The product was washed several times with water and dried. The dried nanoparticles were kept in ampule, stored in refrigerator and redispersed in deionised water for further use. Figure 3.4. depicts the preparation process of formation of isoniazid loaded PCTS- MMT nanoparticles.

A series of seven samples were prepared for the present study.

Table 3.4. Recipes for the formation of different isoniazid loaded PCTS- montmorillonite nanoparticles

Sample code	(PCTS) % w/v (amount in g in 50 ml water)	MMT % w/w w.r.t PCTS (amount in g in 50 mL water)	GA% v/w w.r.t. PCTS (amount in mL)	Isoniazid (g)	TPP % w/v w.r.t water (amount in g in 100 mL water)
PCTS/M0/GA50	1 (0.5)	0 (0.00)	0.25	0.01	1 (1)
PCTS/M1/GA50	1 (0.5)	1 (0.005)	0.25	0.01	1 (1)
PCTS/M3/GA50	1 (0.5)	3 (0.015)	0.25	0.01	1 (1)
PCTS/M5/GA50	1 (0.5)	5 (0.025)	0.25	0.01	1 (1)
PCTS/M5/GA10	1 (0.5)	1 (0.025)	0.05	0.01	1 (1)
PCTS/M5/GA30	1 (0.5)	1 (0.025)	0.15	0.01	1 (1)
PCTS/M5/GA70	1 (0.5)	1 (0.025)	0.35	0.01	1 (1)

3.2.1.8. Preparation of isoniazid-loaded SF nanoparticles by desolvation method

Nanoparticles were prepared with SF following a desolvation method with modifications [7]. 0.5 g of SF was dissolved in 50 mL deionized water and stirred for 1 h at room temperature in a beaker by varying the percentage of MMT viz. 0, 1, 3, 5% (dry weight of SF) was swelled in 50 mL of water along with 0.005 mL Tween 80 (surfactant) for 24 h. It was then stirred vigorously by a mechanical stirrer for 48 h and sonicated for 30 min.

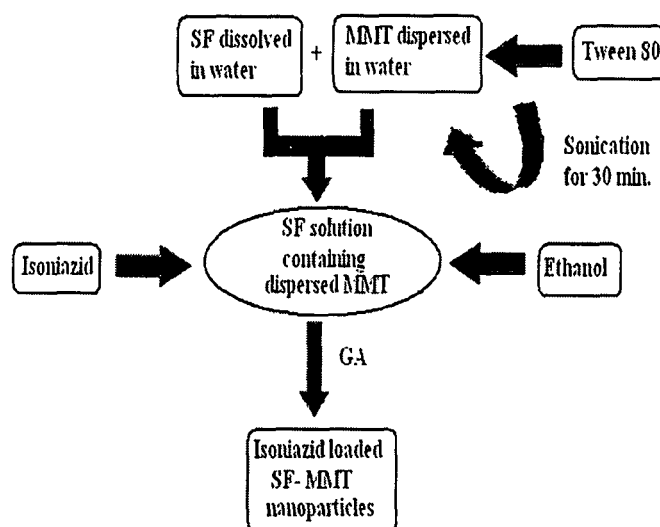


Figure 3.5. Flowchart diagram showing the main steps in the preparation of isoniazid loaded SF-MMT nanoparticles

This dispersed MMT solution was added to 50 mL of 1% (w/v) SF solution. This was followed by the addition of isoniazid (0.01 g) to the beaker under stirring. SF–MMT nanoparticles form on addition of ethanol (50 mL) dropwise into the dispersion. Ethanol acts as a desolvating agent. After 1 h, the temperature of the system was brought down to 5–10°C to harden the nanoparticles. GA was added as a cross-linker and the temperature was increased to 45 °C. Thereafter, rotary evaporation was applied using a Buchi Rotavapor R114 at 30 °C (BUCHI Labortechnik AG, Flawil, Switzerland) to remove ethanol, which was then replaced with the same volume of deionized water. The nanoparticles were separated by centrifuging the solution for 30 min. The product was washed several times with water and dried. The dried nanoparticles were kept in an

ampule, stored in a refrigerator and redispersed in deionised water for further use. Figure 3.5. depicts the preparation process of isoniazid loaded SF–MMT nanoparticles.

A series of 7 samples was prepared using the formulation by varying the concentration of MMT and GA.

Table 3.5. Recipes for the formation of different isoniazid loaded SF- montmorillonite nanoparticles

Sample code	(SF) % w/v (amount in g in 50 ml water)	MMT % w/v w.r.t SF (amount in g in 50 mL water)	Tween 80 %v/w w.r.t. SF (amount in mL)	Isoniazid (g)	Ethanol (ml)	GA % v/v of 100 mL solution
SF/M0/GA50	1 (0.5)	0 (0.00)	1 (0.005)	0.01	50	50
SF/M1/GA50	1 (0.5)	1 (0.005)	1(0.005)	0.01	50	50
SF/M3/GA50	1 (0.5)	3 (0.015)	1(0.005)	0.01	50	50
SF/M5/GA50	1 (0.5)	5 (0.025)	1(0.005)	0.01	50	50
SF/M5/GA10	1 (0.5)	1 (0.025)	1(0.005)	0.01	50	0
SF/M5/GA30	1 (0.5)	1 (0.025)	1(0.005)	0.01	50	10
SF/M5/GA70	1 (0.5)	1 (0.025)	1(0.005)	0.01	50	70

3.2.2. Section B: Preparation of nanoparticles loaded with hydrophobic drug, Curcumin.

3.2.2.1. Preparation and characterization of curcumin loaded chitosan/MMT nanoparticles for controlled drug delivery applications.

Chitosan nanoparticles were prepared by ionic crosslinking of chitosan with tripolyphosphate. 1% chitosan solution was prepared in water containing 0.5 % acetic acid. MMT is swelled in 50 ml water for 24 hours. The solution was stirred vigorously by mechanical stirrer for two days and sonicated for 30 minutes. The MMT solution was added to 50 ml of 1 % chitosan solution. 0.01 g curcumin is solubilized in ethanol-water

mixture and was added to the aqueous solution of chitosan and MMT. 0.005 ml Surfactant (Tween 80) was added. 1% TPP solution was prepared in water. Nanoparticles were obtained by addition of 15 ml of TPP in 100 ml chitosan clay solution under constant stirring at room temperature for 30 minutes. The nanoparticles were chemically crosslinked using genipin. The nanoparticles were separated by centrifuging the solution for 30 minutes and the resulting nanoparticles were washed with water and dried. The amount of MMT and genipin was varied to obtain different set of nanoparticles. A total seven samples were prepared.

Table 3.6. Recipes for the formation of different curcumin loaded chitosan-montmorillonite nanoparticles

Sample code	Chitosan % w/v (amount in g in 50mL water)	MMT % w/v w.r.t chitosan (amount in g in 50 mL water)	Tween 80 %v/w w.r.t. chitosan (amount in mL)	Curcumin (g)	TPP % w/v w.r.t water (amount in g in 100 mL water)	genipin %v/w w.r.t. Chitosan (amount in mL)
C/M0/Gen50	1 (0.5)	0 (0.00)	1 (0.005)	0.01	1 (1)	0.25
C/M1/Gen50	1 (0.5)	1 (0.005)	1(0.005)	0.01	1 (1)	0.25
C/M3/Gen50	1 (0.5)	3 (0.015)	1(0.005)	0.01	1 (1)	0.25
C/M5/Gen50	1 (0.5)	5 (0.025)	1(0.005)	0.01	1 (1)	0.25
C/M5/Gen10	1 (0.5)	1 (0.025)	1(0.005)	0.01	1 (1)	0.05
C/M5/Gen30	1 (0.5)	1 (0.025)	1(0.005)	0.01	1 (1)	0.15
C/M5/Gen70	1 (0.5)	1 (0.025)	1(0.005)	0.01	1 (1)	0.35

3.2.2.2. Preparation and characterization of curcumin loaded carboxymethyl chitosan/MMT nanoparticles for controlled drug delivery applications.

Curcumin loaded CMC-MMT nanoparticles were prepared by ionic crosslinking of CMC with CaCl₂. 1% (w/v) CMC solution was prepared in water at 45° C. and stirred for 1 h at room temperature in a beaker. Varying percentage of MMT (1-5% w/w of CMC) was

swelled in 50 mL of water along with 0.005 ml Tween 80 (surfactant) for 24h. It was then stirred vigorously by mechanical stirrer for 48h and sonicated for 30 min. This dispersed MMT solution was added to 50 mL of 1 % (w/v) CMC solution. 0.01 g curcumin is solubilized in ethanol-water mixture and was added to the aqueous solution. This was followed by addition of curcumin to the aqueous solution of CMC - MMT mixture under stirring condition. 1 wt% of CaCl₂ solution was added slowly to the beaker till complete precipitation of CMC–MMT nanoparticles occurred. After 1h, the temperature of the system was brought down to 5-10° C to harden the nanoparticles. GA (10-70% v/w w.r.t. CMC) was added as a cross-linker and the temperature was increased to 45° C. The reaction was contained for 30 minutes. The precipitate was then separated by centrifuge and freeze dried. The dried nanoparticles were kept in ampule, stored in refrigerator and redispersed in deionised water for further use. Overall seven samples were prepared by varying the amount of MMT and genipin.

Table 3.7. Recipes for the formation of different curcumin loaded CMC- montmorillonite nanoparticles

Sample code	(CMC) % w/v (amount in g in 50 ml water)	MMT % w/w w.r.t CMC (amount in g in 50 mL water)	Genipin v/w w.r.t. CMC (amount in mL)	Curcumin (g)	TPP % w/v w.r.t water (amount in g in 100 mL water)
CMC/M0/Gen50	1 (0.5)	0 (0.00)	0.25	0.01	1 (1)
CMC/M1/Gen 50	1 (0.5)	1 (0.005)	0.25	0.01	1 (1)
CMC/M3/Gen50	1 (0.5)	3 (0.015)	0.25	0.01	1 (1)
CMC/M5/Gen50	1 (0.5)	5 (0.025)	0.25	0.01	1 (1)
CMC/M5/Gen10	1 (0.5)	1 (0.025)	0.05	0.01	1 (1)
CMC/M5/Gen30	1 (0.5)	1 (0.025)	0.15	0.01	1 (1)
CMC/M5/Gen70	1 (0.5)	1 (0.025)	0.35	0.01	1 (1)

3.2.2.3. Preparation and characterization of curcumin loaded phosphorylated chitosan/MMT nanoparticles for controlled drug delivery applications.

Table 3.8. Recipes for the formation of different curcumin loaded PCTS-montmorillonite nanoparticles

Sample code	(PCTS) % w/v (amount in g in 50 ml water)	MMT % w/w w.r.t PCTS (amount in g in 50 mL water)	genipin% v/w w.r.t. PCTS (amount in mL)	Curcumin (g)	TPP % w/v w.r.t water (amount in g in 100 mL water)
PCTS/M0/Gen50	1 (0.5)	0 (0.00)	0.25	0.01	1 (1)
PCTS /M1/Gen50	1 (0.5)	1 (0.005)	0.25	0.01	1 (1)
PCTS /M3/Gen50	1 (0.5)	3 (0.015)	0.25	0.01	1 (1)
PCTS /M5/Gen50	1 (0.5)	5 (0.025)	0.25	0.01	1 (1)
PCTS /M5/Gen10	1 (0.5)	1 (0.025)	0.05	0.01	1 (1)
PCTS /M5/Gen30	1 (0.5)	1 (0.025)	0.15	0.01	1 (1)
PCTS /M5/Gen70	1 (0.5)	1 (0.025)	0.35	0.01	1 (1)

PCTS nanoparticles were prepared using ionotropic gelation process with the counter polyanion sodium tripolyphosphate (TPP). PCTS (1 g) was dissolved in 100 mL distilled water with slight heating and stirred for 3h to obtain a transparent homogeneous solution. Varying percentage of MMT (1-5% w/w of PCTS) was swelled in 50 mL of water along with 0.005 ml Tween 80 (surfactant) for 24h. It was then stirred vigorously by mechanical stirrer for 48h and sonicated for 30 min. This dispersed MMT solution was added to 50 mL of 1 % (w/v) PCTS solution. 0.01 g curcumin is solubilized in ethanol-water mixture and was added to the aqueous solution. This was followed by addition of curcumin to the aqueous solution of PCTS - MMT mixture under stirring condition. Now, 1% (w/v) TPP solution was prepared in water. Nanoparticles were obtained by slow addition of 15 mL of TPP solution to 100 mL of isoniazid containing PCTS-MMT solution under constant magnetic stirring at room temperature for 30 min. The

temperature of the container containing nanoparticles was brought down to 5-10°C to harden the nanoparticles. Now varying amount of genipin (10-70% v/w w.r.t. PCTS) was added and the temperature was increased to 45°C. The reaction was continued for 45 min. The nanoparticles were separated by centrifuging the solution for 30 min. The product was washed several times with water and dried. The dried nanoparticles were kept in ampule, stored in refrigerator and redispersed in deionised water for further use. A series of seven samples were prepared for the present study.

3.2.3. Preparation of calibration curve

3.2.3.1. Calibration curve of Isoniazid

A calibration curve is essential to estimate the release rate of drug from nanoparticles in the suitable solvent medium. Calibration curve was drawn as per the procedure [2]. A known concentration of isoniazid (in double distilled water) was scanned in the range 200 – 400 nm by using UV-Visible spectrophotometer (UV-2001Hitachi, Tokyo, Japan). A sharp peak at 262 nm was observed for isoniazid having concentration in the range of 0.001 – 0.01g/100 mL. The absorbance values at 262 nm obtained with respective concentration were recorded and plotted. From this calibration curve, the unknown concentration of isoniazid was obtained by knowing the absorbance value.

3.2.3.2. Calibration curve of Curcumin

A calibration curve is essential to estimate the release rate of drug from nanoparticles in the suitable solvent medium. A known concentration of curcumin (in distilled water-ethanol mixture) was scanned in the range 400-500nm) by using UV-Visible spectrophotometer. A sharp peak at 430 nm was noticed for curcumin having concentration in the range of 0.001 – 0.01g/100 mL). The absorbance values at 430 nm obtained with respective concentration were recorded and plotted. From this calibration curve, the unknown concentration of curcumin was obtained by knowing the absorbance value.

3.2.4. Calculation of Process Yield

Process yield was calculated using the following equation as described in the literature [8].

$$\text{Process Yield (\%)} = \frac{[\text{Weight of nanoparticles} \times 100]}{[\text{Weight of (drug + clay + polymer)}]}$$

3.2.5. Calculation of Drug loading efficiency and Encapsulation efficiency of the nanoparticles

The drug loading efficiency of nanoparticles with different formulations was determined by ultracentrifugation of samples at room temperature for 30 min. The amount of free isoniazid was determined by noting the absorbance value of the supernatant at 262 nm using UV-Visible spectrophotometer. The drug loading efficiency (LE) of the nanoparticles was calculated using the following equations [3].

$$\text{Loading efficiency (LE) in (\%)} = \frac{(\text{Total amount of drug} - \text{Free amount of drug})}{\text{Total amount of drug}} \times 100$$

$$\text{Encapsulation efficiency (EE) (\%)} = \frac{(\text{Total amount of drug} - \text{Free amount of drug})}{\text{Weight of dry nanoparticles}} \times 100$$

3.2.6. Fourier Transform Infra-red Spectroscopy (FTIR) study

FTIR spectra of nanoparticles were taken in Nicolet (model Impact-410) spectrophotometer. The nanoparticles were grounded to powder, mixed with KBr and spectra were recorded in the range of 4000 – 400 cm^{-1} .

3.2.7. X-ray diffraction (XRD) study

The degree of intercalation of MMT and distribution of isoniazid in SF-MMT nanoparticles were examined by X-ray diffractometry. It was carried out in a Rigaku X-ray diffractometer (Miniflex, UK) using $\text{CuK}\alpha$ ($\lambda=0.154$ nm) radiation at a scanning rate of 1°/min with an angle ranging from 2° to 70° of 2θ .

3.2.8. Particle size determination

Particle size was determined by dynamic light scattering (DLS) analyzer (model DLS—Nano ZS, Zetasizer, Nanoseries, Malvern Instruments).

3.2.9. Scanning electron microscopy (SEM) study

The samples were mounted on a brass holder, sputtered with platinum. The surface morphologies of SF-MMT nanoparticles loaded with isoniazid were studied by using Scanning Electron Microscope (JEOL JSM – 6390LV) at an accelerated voltage of 5-10 KV.

3.2.10. Transmission electron microscopy (TEM) study

The dispersion of the silicate layers of clay in SF nanoparticles was examined by using Transmission Electron Microscope (JEOL JEM-2100) at an accelerated voltage of 100 KV

3.2.11. Water Uptake Studies

Water uptake studies were performed in both phosphate buffer (pH 7.4) and 0.1N HCl solution (pH 1.2) according to the procedure described in the literature [2].

Drug loaded nanoparticles (0.1 g) were taken in a pouch made of nylon cloth. The empty pouch was first conditioned by immersing it in either 0.1 N HCl (pH 1.2) or phosphate buffer (pH 7.4) for different time periods (1-8 h). The pouch containing the nanoparticles was immersed in a similar way in either 0.1 N HCl (pH 1.2) or phosphate buffer (pH 7.4) for the similar time periods. The weights of wet nanoparticles after a definite time period were determined by deducting the respective conditioned weight of the empty nylon pouch from this. Water uptake (%) was determined by measuring the change in the weight of the nanoparticles. The percentage of water uptake for each sample determined at time 't' was calculated using the following equation.

$$\text{Water uptake (\%)} = [(w_2 - w_1) / w_1] \times 100$$

Where, w_1 is initial weight of nanoparticles before swelling,

and w_2 is the final weight of nanoparticles after swelling for a predetermined time 't'.

The experiments were performed in triplicate and represented as a mean value.

3.2.12. *In vitro* drug release studies

To study the release profile of the nanoparticles, dried drug loaded samples were immersed in a solution of different pH namely 1.2 and 7.4 and stirred continuously. At scheduled time interval, 5mL solution was withdrawn, filtered and assayed spectrophotometrically at 262 nm by using UV-Visible spectrophotometer for the

determination of cumulative amount of drug release upto a time t . Each determination was carried out in triplicate. To maintain a constant volume, 5 ml of the solution having same pH was returned to the container [9].

3.2.13. Isolation of Lymphocytes, culture and treatment

Human blood was collected from suitable donor. It was diluted in the ratio of 1:1 with phosphate buffer saline (PBS) and layered 6 mL into 6 mL histopaque (1.077 g/mL). The isolation of lymphocytes and study of cell viability were done as per the procedure cited in the literature [10]. Lymphocytes were isolated from the sample after centrifugation for 30 min at 400 g, washed with PBS and finally with serum free media separately through centrifugation for 10 min at 250 g. Cell pellets were then suspended in PBS and cell viability was checked by Trypan blue exclusion method using haemocytometer. Cell viability more than 90 % was used for subsequent study.

Aliquots of 200 μ L of isolated cells were cultured plate in RPMI supplemented with 10% heat inactivated fetal bovine serum (FBS). Initially cells were maintained for 4 h in RPMI without FBS at 37^oC in 5 % CO₂ incubator. Cells were then treated with as per experimental requirements and maintained in presence of FBS for 6 h, 12h and 24 h.

3.2.14. Cytotoxicity experiments

Cytotoxicity assay was performed by measuring the viability of cells according to the method as described by Denizot and Lang [11]. The key component (3-[4, 5-dimethylthiazol-2-yl]-2, 5-diphenyl tetrazolium bromide) (MTT) is yellowish in color and mitochondrial dehydrogenase of viable cells cleave the tetrazolium ring, yielding purple insoluble formazan crystals which were dissolved in suitable solvent. The resulting purple solution was spectrophotometrically measured. An increase or decrease in cell number resulted in a concomitant change in the amount of formazan formed, indicating the degree of cytotoxicity caused by the test material. Briefly, after treatments, cells were treated with 10 % of MTT for 2 h followed by dissolving the formazan crystals in solvent and measuring the absorbance of solution at 570 nm. The absorbance of control cells at 6, 12 and 24 h were separately set as 100% viability and the values of treated cells were calculated as percentage of control.

3.2.15. Statistical analysis

All the data were expressed as means \pm SD. Results were statistically analyzed by student's t test for significant difference between group mean using GraphPad software [12]. The significant difference between the experimental and the control group was set at different levels as $p < 0.05$, $p < 0.01$ and $p < 0.001$.

3.2.16. Cell culture

MCF 7 and HepG2 cell lines were obtained from the NCCS Pune, India. Both cells were grown in DMEM supplemented with 10% fetal bovine serum, 100 μ g/ml penicillin-streptomycin antibiotics. Cells were maintained at 37°C and 5% CO₂ in a humidified incubator and were subcultured when they reached 80–90% confluence.

3.2.16.1. Preparation of the cell lysate

Cells were grown in 100-mm-diameter dishes to approximately 90% confluence. Cells were lysed by incubation in 5 mL of phenol red-free DMEM containing 1% Triton X-100 and protease inhibitor cocktail for 4 h on ice. Lysed cells were transferred to 1.5 mL microtubes and centrifuged at 16,000 rpm for 20 min. The supernatant was collected and pooled as a cell lysate.

3.2.16.2. Preparation of samples for LDH activity assay

Cell lysate was treated with nanoparticles at 37°C for the indicated time with mild agitation. The lysate was centrifuged at 16,000 rpm for 20 min to sediment nanoparticles. The supernatant was used for LDH activity assay.

3.2.16.3. LDH assay

LDH assay was done as previously described (Oh et al., 2013). MCF-7 and HepG2 cell lines were seeded in 96-well plates at a density of 2×10^5 cells/well and were grown for 24 h. Cells were treated with the curcumin loaded nanoparticles by substituting culture media with 200 μ L DMEM containing dispersed nanoparticles and incubated for 24 h. For the LDH assay, cell culture media were transferred to 1.5 mL microtubes and centrifuged at 16,000 rpm for 20 min to remove cell debris and nanoparticles. 20 μ L of supernatant was added to a 200 μ L aliquot of working reagent containing 0.2 mM NADH

and 2.5 mM sodium pyruvate in wells of 96-well plates. The decrease in absorbance at 340 nm was measured for 3 min with a SpectraMax M3 microplate reader (Molecular Devices, Sunnyvale, CA). Relative LDH activity was calculated from the slope of decreasing absorbance. LDH activities measured with the media from the untreated cells and the cells treated with 1% Triton X-100 were regarded as 100% and 0% viability, respectively. Assays were conducted in triplicate for each sample. The viability of cells treated with nanoparticles was expressed as a percentage of that of untreated cells.

3.2.16.4. Lipid Peroxidation Assay

Lipid peroxidation in the nanoparticles was estimated spectrophotometrically by using thiobarbituric acid reactive substance (TBARS) assay, as described in literature with modification [13]. It is estimated by determining the malondialdehyde (MDA) content per mg protein in the nanoparticles. 0.5 mL sample was mixed with 0.15 M Tris KCl buffer to which 0.625 mL of 30% Trichloroacetic acid (TCA) was added. To this whole system 0.625 mL of 52mM TBA was added and placed in a water bath for 45 min at 80°C, cooled in ice and centrifuged at room temperature for 10 min at 3,000 rpm. The absorbance of the clear supernatant was measured against blank of distilled water at 538.1 nm in spectrophotometer.

3.2.16.5. Reduced glutathione assay

Reduced glutathione was estimated as total non-protein sulphhydryl group by the method described by Dasgupta et al. with modification [14]. Homogenates were immediately precipitated with 0.1 ml of 25% trichloroacetic acid and the precipitate was removed after centrifugation. Free -SH groups were assayed in a total 3 ml volume by adding 2 ml of 0.6 mM DTNB prepared in 0.2 M sodium phosphate buffer (pH 8.0), to 0.1 ml of the supernatant and absorbance was read at 412 nm using a Shimadzu UV-160 spectrometer. GSH was used as a standard to calculate mmole of -SH content/g tissue.

3.2.16.6. Catalase assay

Catalase was estimated at 240 nm by monitoring the disappearance of H₂O₂ as described by Aebi [15]. The reaction mixture containing the nanoparticles (1 ml) containing 0.02

ml of s diluted cytosol in phosphate buffer (50 mM, pH 7.0) and 0.1 ml of 30 mM H₂O₂ in phosphate buffer. Catalase enzyme activity has been expressed as moles of H₂O₂ reduced/min/mg protein.

3.2.16.7. Superoxide dismutase

Superoxide dismutase was assayed utilizing the technique of Marklund and Marklund [16], which involves reticence of pyrogallol autoxidation at pH 8.0. A single unit of enzyme was defined as the quantity of superoxide dismutase required to produce 50% inhibition of autoxidation.

3.2.17. Mucoadhesion study

3.2.17.1. *In vitro* wash-off test

The mucoadhesive property of the nanoparticles was evaluated by an *in vitro* adhesion test method known as wash-off test method [17]. Freshly excised pieces of goat intestinal mucosa (5×5cm) were mounted with mucous side exposed on to glass slides with cotton thread. About 50 nanoparticles were spread on to each prepared glass slide and immediately thereafter the slides were hung to USP tablet disintegration test apparatus (Tab. Machines, Mumbai). When the test apparatus was operated, the sample was subjected to slow up and down movement in the test fluid at 37°C contained in a 1L vessel of the apparatus. Readings were taken at an interval of 30 min up to 5 h by stopping the machine and counting the number of nanoparticles still adhering to mucosal surface. The test was performed at intestinal (pH 7.4) and simulated gastric fluid (pH 1.2) condition.

3.2.17.2. *Ex vivo* mucoadhesive test

In this method, the force required to separate bio-adhesive sample from freshly excised goat intestine was determined [18]. Keeping the mucosal side out, the intestine was secured on to each glass vial using nylon thread. The diameter of each exposed mucosal membrane was 2 cm. The vials with the nasal tissue were kept at 37°C for 10 min. To the exposed tissue on this vial, a constant amount of nanoparticles was applied. The height of the vial was adjusted so that the nanoparticles could adhere to the mucosal

tissues of both vials. Water was added at a constant rate to the pan on the other side of the modified balance until the two vials were separated. The weight of water showed the weight required for displacement.

The adhesive force expressed as the detachment stress (dyne.cm^{-2}) is calculated using the following equation.

$$\text{Detachment stress (dyne.cm}^{-2}\text{)} = \text{mg/A}$$

where, 'm' is the mass (g) required to detach the membrane,

'g' is acceleration due to gravity taken as 980 cm sec^{-2} .

and 'A' is the area of tissue exposed which is equal to πr^2 (r is the radius of the exposed mucosal membrane)

References

- [1] Zhang, J., et al. *Carbo. Pol.*, **69**, 607--611, 2007.
- [2] Devi, N., & Maji, T.K. *Drug Dev. Ind. Pharm.*, **36**(1), 56--63, 2010.
- [3] Selvaraj, S., et al. *Der Pharmacia Lettre*, **2**(3), 420--431, 2010.
- [4] An, N.T., et al. *Carbo Pol.* **75**, 489--497, 2009.
- [5] Tavakol, M., et al. *Prog Biomater.* **2**, 1--10, 2013.
- [6] Li, B., et al. *Mater. & Designs.* **32**, 4543--4547, 2011.
- [7] Teng, Z., et al. *J. Agric. Food Chem.*, **60**(10), 2712--2720, 2012.
- [8] Adlin Jino Nesalin, J., et al. *Int. J. ChemTech Res.*, **1**(4), 1331--1334, 2009.
- [9] Cassano, R., et al. *J. Biomed. Mater. Res. Part A*, **100**(A), 536--542, 2012.
- [10] Hussain, A., et al. *Free Rad. Antiox.*, **2**(1), 9--12, 2012.
- [11] Denizot, F., & Lang, R. *J. Immunol. Methods*, **89**(2), 271--277, 1986.
- [12] Bourke, G.J., Daly, L.E., & McGilvary, J., *Interpretation and Uses of Medical Statistics*, 3rd ed., Blackwell Scientific Publication, Oxford, 1985.
- [13] Varshney, R., & Kale, R.K. *Int. J. Rad. Biol.* **58**, 733--743, 1990.
- [14] Dasgupta, T., et al. *Mol. & Cell. Biochem.* **245**, 11--22, 2003.
- [15] Aebi, H., et al., Catalase in Vitro. *Methods in Enzymology*. 105, Acad. Press, Florida, 1984.
- [16] Marklund, S., & Marklund, G. *Eur. J. Biochem.* **47**, 469--474, 1974.
- [17] Lehr, C.M., et al. *J. Control. Release*, **13**(1), 51--62, 1990.
- [18] Gandhi, R.B., & Robinson, J.R. *Ind. J. Pharma. Sci.*, **50**(3), 145--152, 1988.

CHAPTER 4
RESULTS AND
DISCUSSION
(PART 1)

CHAPTER 4

RESULTS AND DISCUSSION (PART 1)

Microencapsulation of hydrophilic drug Isoniazid in five different microparticle/nanoparticle systems, namely (i) chitosan-cellulose whisker microparticles, (ii) chitosan-montmorillonite(MMT) nanoparticles, (iii) carboxymethyl chitosan-MMT nanoparticles, (iv) phosphorylated chitosan-MMT nanoparticles and (iv) soy flour(SF)-MMT nanoparticles

In this part of work, the author has chosen complex coacervation (oil in water) and ionic gelation technique for the microencapsulation of Isoniazid. The effects of various parameters like surfactant concentration, filler concentration and crosslinker concentration on the microparticle/nanoparticle properties have been explained.

4.1. Section A-Preparation and characterization of isoniazid loaded chitosan/cellulose whisker microspheres for controlled drug delivery applications.

4.1.1. Effect of variation of CW and GA concentration on the different properties of isoniazid loaded chitosan CW microparticles

The results showing the effect of variation of CW and GA concentration on different properties of chitosan microparticles are shown in Table 4.1. The encapsulation efficiency and drug loading of CW free crosslinked microparticles were found to be higher compared to that of CW containing crosslinked microparticles. The encapsulation efficiency decreased with the increase in CW content in the microparticles. This could be attributed to the presence of the network structure of CW which restricts the diffusion of drug in the microparticles. The -OH groups of CW could interact with the -NH₂ group of chitosan and -CHO groups of GA resulting in extension of the polymer chains. The network structure of CW also hindered the movement of the intercalated polymer chains freely. The interference offered by the network structure of CW layers was absent in CW free crosslinked microparticles. Hence, it showed higher encapsulation efficiency.

Similarly, at a fixed CW content, the encapsulation efficiency of microparticles was found to further decrease with the increase in the glutaraldehyde (GA) concentration.

With the increase in GA content, the crosslinking increased and the surface of the microparticles get hardened. As a result, less amount of drug can diffuse through the microparticles and consequently the encapsulation efficiency and drug loading decreased. The average diameters of the microparticles were obtained in the range 823-919 nm. The variation in CW concentration did not significantly affect the particle size. However, the average diameter showed a decreasing trend on increasing the GA concentration. The amino groups present in chitosan interacted with the hydroxyl group of CW and GA. With the increase in the concentration of GA, the availability of free amino groups on microparticles reduces due to which the microparticles became more compact and hence the diameter would be less.

Zeta potential values of the microparticles were found in the range 43 to 55 mV indicating good stability of the microparticles. The surface of the microparticles was positively charged due to the presence of residual amino groups. With the incorporation of CW in chitosan matrix the surface charge decreases. The reduction in surface charge might be due to the increased electrostatic interaction between the protonated amino groups of chitosan and hydroxyl groups of CW.

Table 4.1. Effect of variation of CW and GA concentration on the different properties of chitosan microparticles

Sample code	Encapsulation efficiency (%)	Drug loading efficiency (%)	Average diameter (nm)	Zeta potential (mV)	Zeta potential of the same formulations without drug (mV)	Zeta potential of nanoparticles after 3 hours of drug release (mV)
C/CW0/GA50	72.10 (±0.02)	29.39(±0.08)	889.4 (± 15)	55.32 (± 0.03)	35.05 (± 0.01)	48.23(± 0.04)
C/CW1/GA50	69.83(±0.04)	26.61(±0.04)	889.7(± 12)	53.49(± 0.1)	34.12(± 0.03)	48.07(± 0.08)
C/CW3/GA50	67.43(±0.04)	24.18(±0.01)	886.1 (± 19)	53.21 (± 0.1)	34.08(± 0.07)	46.23(± 0.01)
C/CW5/GA50	67.10(±0.01)	22.27(±0.01)	856.3 (± 13)	51.92(± 0.03)	36.22(± 0.06)	47.34(± 0.03)
C/CW5/GA10	70.21(±0.03)	25.63(±0.02)	919.2 (± 15)	43.87(± 0.03)	32.11(± 0.06)	41.23(± 0.04)
C/CW5/GA30	70.09(±0.02)	22.58(±0.01)	902.9(± 16)	50.63 (± 0.06)	33.90(± 0.01)	45.12 (± 0.04)
C/CW5/GA70	65.13(±0.02)	19.19(±0.01)	823.7(± 10)	52.13 (± 0.01)	36.41(± 0.03)	48.34(± 0.01)

each value represents average of five readings, standard deviation in parenthesis

However, the zeta potential values increased as the GA concentration increased from 10 to 70%. The increase in the zeta potential indicated that the stability of the microparticles increased with the increase in the concentration of GA and they would not aggregate in acidic or basic medium [1]. All the zeta potential values were in the stable zone indicating that the synthesized microparticles are highly stable. The zeta potential values of the microparticles without drug showed lower value compared to the zeta potential of the microparticles after loading of drug. This showed that the stability and surface charge of the microparticles enhances on the incorporation of the drug. The increase in the zeta potential with the incorporation of the drug suggested that some of the drug polymer association was surface-adsorbed. Thus, a part of the drug was encapsulated within the chitosan matrix and the rest was adsorbed on the surface of the microparticles.

4.1.2. Fourier Transform Infra-red Spectroscopy (FTIR) study

FTIR spectra of Cellulose (ground filter paper), chitosan, CW, isoniazid and isoniazid loaded chitosan-CW microparticles are shown in Figure 4.1.

The successful synthesis of CW from Whatman filter paper was confirmed by FTIR analysis. The FTIR spectra of ground Whatman filter paper (curve a) shows a broad peak at 3426 cm^{-1} which is attributed to OH stretching. The peak at 2905 cm^{-1} was due to symmetric -CH stretching. A strong band at 1639 cm^{-1} was observed which is attributed to stretching vibration resulting from H-O-H intermolecular linkages. Bands at 1447 cm^{-1} and 1333 cm^{-1} were due to symmetric CH_2 bending and wagging respectively. Peaks at 1379 and 1259 cm^{-1} were attributed to C-H bending vibrations. Band at 1179 cm^{-1} and 896 cm^{-1} were assigned for C-O-C stretching frequency at the β -(1 \rightarrow 4) glycosidic linkages. A small peak at 1119 cm^{-1} is observed due to the in plane ring of the β -(1 \rightarrow 4) glycosidic linkages. Strong peak at 1049 cm^{-1} was attributed to the C-O stretching at C-3. The peaks assigned at 789 cm^{-1} and 712 cm^{-1} were the characteristic absorption of cellulose I_α and I_β , respectively [2].

The FTIR spectra of CW (curve b) showed that the peaks were almost similar to that of the untreated ground filter paper. The changes are observed only in the intensities of the peaks. The intensities of the same peaks appeared at 1379 cm^{-1} , 1119 cm^{-1} and 896 cm^{-1}

increased whereas the intensities of the peaks found at 2905 cm^{-1} , 1259 cm^{-1} , 1639 cm^{-1} and 1333 cm^{-1} did not alter much [2].

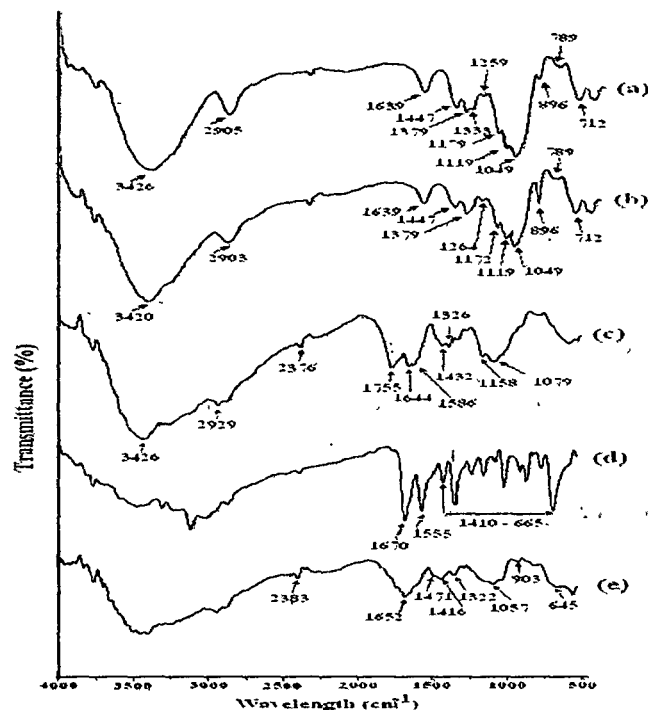


Figure 4.1. FTIR spectra of (a) Cellulose, (b) CW, (c) Chitosan, (d) Isoniazid, and (e) C/CW5/GA50

The basic absorption bands of chitosan (curve c) appeared at 3442 cm^{-1} (OH stretching and NH stretching, overlapped), 2939 cm^{-1} (CH stretching). The absorption peaks of amide I and amide II appeared at 1639 cm^{-1} (C=O stretching) and 1455 cm^{-1} (N-H in plane deformation coupled with C≡N stretching) respectively. The other notable peaks were found to appear at 1156 cm^{-1} (bridge -O- stretching), and 1062 cm^{-1} (-CO stretching) [3].

Curve d represents the spectrum of isoniazid. The absorption peaks appeared at 1664 and 1551 cm^{-1} were due to the amide I (C=O stretching) and amide II (N-H bending of secondary amide group) respectively. Besides this, multiple peaks appeared in the range $1410\text{--}669\text{ cm}^{-1}$ [1].

The appearance of all the characteristic peaks of chitosan, CW and isoniazid in the spectrum of isoniazid loaded chitosan-CW microparticles (curve e) suggested the incorporation of isoniazid and CW into the microparticles.

4.1.3. X-ray diffraction (XRD) study

The XRD diffractograms of the ground filter paper, CW, Chitosan, isoniazid and isoniazid loaded chitosan-CW microparticles are shown in Figure 4.2.

For CW, diffraction peaks were obtained at 2θ angles of 15.8° , 16.1° , 22.4° , and 34.4° corresponding to the (1-10), (110), (002), and (004) crystallographic planes, respectively. The intensity of peak for the (002) plane ($2\theta = 22.4^\circ$) of CW was much sharper than that of the untreated ground filter paper. The intensity of the peak appearing at $2\theta = 16.1^\circ$ (110 plane) for CWs is sharper than that of the peak of ordinary filter paper [2]. From the diffractograms, it was observed that the crystallinity of CW increased, as the peak intensity of the CWs was greater than that of the untreated ground filter paper.

The crystallinity index of CW was calculated from the formula

$$C_{I_r} (\%) = [(I_{002} - I_{am}) / I_{am}] \times 100$$

where I_{002} is the intensity of lattice peak diffraction at 22.4° and I_{am} is the peak intensity of the amorphous fraction at 16.1° . The crystallinity index was found to be 72.8%

Chitosan showed two distinct crystalline peaks at $2\theta = 10^\circ$ and 20.2° due to (020) and (100) plane, respectively [Figure 4.2. c] [3].

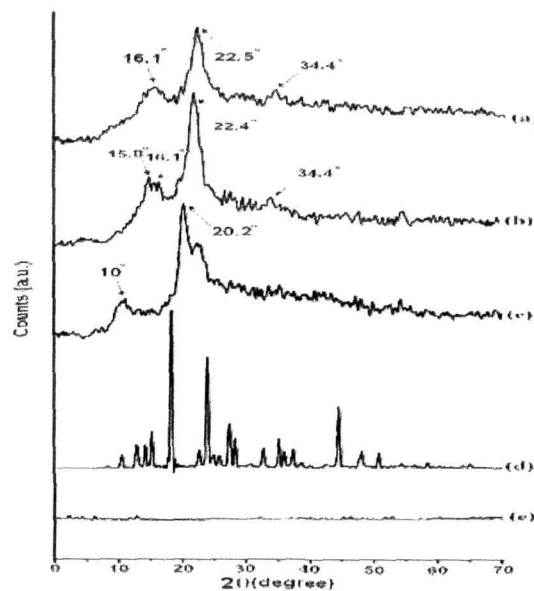


Figure 4.2. XRD patterns of (a) Cellulose, (b) CW, (c) chitosan, (d) Isoniazid, and (e) C/CW5/GA50

Isoniazid (curve 2d) shows multiple peaks at $2\theta=12^\circ$ to 50° due to its crystalline nature. Similar type of diffractogram was reported by Banik et.al.[4].

The characteristic peaks for CW and isoniazid were found to disappear in the diffractogram of chitosan-CW microparticles (curve 4.2. e). These findings indicated that CW lost its structure in the microparticles either due to vigorous stirring or due to the presence of chitosan matrix. The findings also suggested the occurrence of a molecular level dispersion of isoniazid in isoniazid loaded chitosan-CW microparticles.

4.1.4. Scanning electron microscopy (SEM) study

SEM analysis was performed to study the surface morphology of CW, chitosan microparticles and chitosan-CW microparticles loaded with isoniazid. Figure 4.3(a-d) represents the SEM micrographs of filter paper, CW, isoniazid loaded chitosan microparticles and isoniazid loaded chitosan-CW microparticles respectively. The surface of the untreated filter paper is agglomerated [Figure 4.3.(a)]. The surface of CW (Figure3b) was found to appear as small rod shaped and aggregated in nature [5]. Both isoniazid loaded chitosan microparticles which are devoid of CW [Figure 4.3. (c)] and which are incorporated with CW [Figure 4.3.(d)] showed spherical shapes. But the surface of isoniazid loaded chitosan-CW microparticles was rougher compared to isoniazid loaded chitosan microparticles suggesting good adhesion between CW and chitosan matrix.

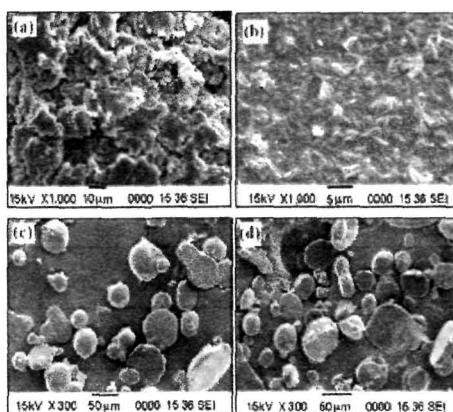


Figure 4.3. SEM micrographs of (a) Untreated filter paper, (b) CW, (c) C/CW0/GA50 and (d) C/CW5/GA50

4.1.5. Transmission electron microscopy (TEM) study

TEM micrographs of isoniazid loaded chitosan microparticles devoid of CW and with CW are shown in Figure 4.4.a and 4.4.b respectively. Figure 4.4.b showed the presence of network structure of CW in the chitosan matrix and the CW chains are bundled together. This could be ascribed to the formation of hydrogen bonding between the CW and the chitosan matrix. These types of structure were not observed in Figure 4.4a. The results indicated that CW were incorporated and dispersed in the chitosan matrix. Similar results were obtained by Iman et. al. [2].

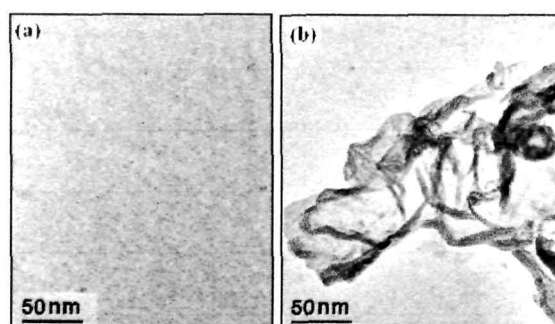


Figure 4.4. TEM micrographs of chitosan microparticles (a) without CW range and (b) with CW at 50 nm scale respectively

4.1.6. Swelling Study

The effect of pH on the percentage swelling of isoniazid loaded microparticles at pH 1.2 and 7.4 are shown in Figure 4.5. It was observed that the swelling of isoniazid loaded chitosan-CW microparticles was more in gastric pH (1.2) than in intestinal pH (7.4). At lower pH, the free amine groups become protonated and generated a repulsive force between the adjacent positively charged polymer chains causing the swelling of the polymer and consequently diffusion of more amount of drug out of the polymer matrix. In alkaline pH, the inbuilt hydrophobicity of chitosan nanoparticles prevented them from faster swelling [6].

Figure 4.5. (A) showed that with the increase in the concentration of CW, the percentage swelling degree decreased. Water absorption decreased by the presence of dispersed phase of CW into the chitosan matrix of the microparticles. CW particles acted as a blockade for water molecules and decreased the water diffusion through the crosslinked

chitosan-CW microparticles. Similarly, microparticles containing higher concentration of GA (Figure 4.5.B) swelled less due to higher crosslinking densities and less availability of the polar groups [2].

Furthermore, the percentage swelling degree was found to increase with the increase in time. With the increase in the time period, higher amount of the solvents can penetrate into the chitosan matrix, resulting in the increase in the percentage swelling degree.

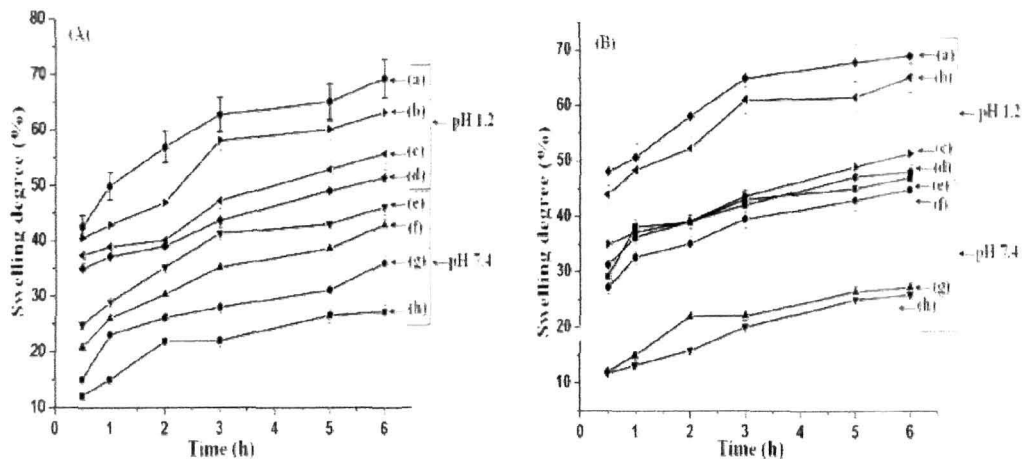


Figure 4.5. Percentage swelling degree at pH 1.2 and 7.4, (A) { (a) C/CW0/GA50, (b) C/CW1/GA50, (c) C/CW3/GA50, (d) C/CW5/GA50, (e) C/CW0/GA50, (f) C/CW1/GA50, (g) C/CW3/GA50, (h) C/CW5/GA50 } and (B) { (a) C/CW5/GA10, (b) C/CW5/GA30, (c) C/CW5/GA50, (d) C/CW5/GA70, (e) C/CW5/GA10, (f) C/CW5/GA30, (g) C/CW5/GA50, (h) C/CW5/GA70 }

4.1.7. *In vitro* Release Studies

The drug release profile of the microparticles at two different pH namely 1.2 and 7.4 are shown in Figure 4.6. The cumulative release (%) of isoniazid from chitosan-CW microparticles was pH dependent. The cumulative release (%) of isoniazid decreased with the increase in the pH of the medium. The major factors governing the release of isoniazid from microparticles were the swelling nature of the polymer and solubility of the drug in the solvent medium. The difference in release profile was due to the difference in the swelling behavior of chitosan in gastric and intestinal pH [7]. Chitosan swelled more in gastric pH compared to intestinal pH medium. The faster drug release rate in lower pH medium was due to the unstable microparticles structure, caused by the

protonation of amino groups of chitosan in lower pH [8]. The solubility of isoniazid increased at acidic pH due to its basic nature as reported in literature [10]. Acidic pH of the medium favored both the swelling of the polymer and solubility of the drug.

It was also observed that the cumulative release (%) of isoniazid decreased with the increase in CW content (Figure 4.6. A) and increased with the increase in the period of time. The percentage swelling of the microparticles decreased with the increase in the concentration of CW as stated earlier. Therefore, in order to aid the release of isoniazid the solvent particles could not diffuse properly to interact with the isoniazid molecules encapsulated in the microparticles. With the increase in time, the percentage degree of swelling increased and more and more solvent molecules could reach the drug molecule facilitated the release the isoniazid from the microparticles.

It was also seen that the cumulative release (%) of isoniazid decreased with the increase in the concentration of GA (Figure 4.6. B). This was due to the increase in crosslinking density of the microparticles. With higher crosslinking, the surfaces of the microparticles get hardened. The solvent molecules cannot easily penetrate the surface of the microparticles to reach the drug and thus decreases in cumulative release (%) were observed.

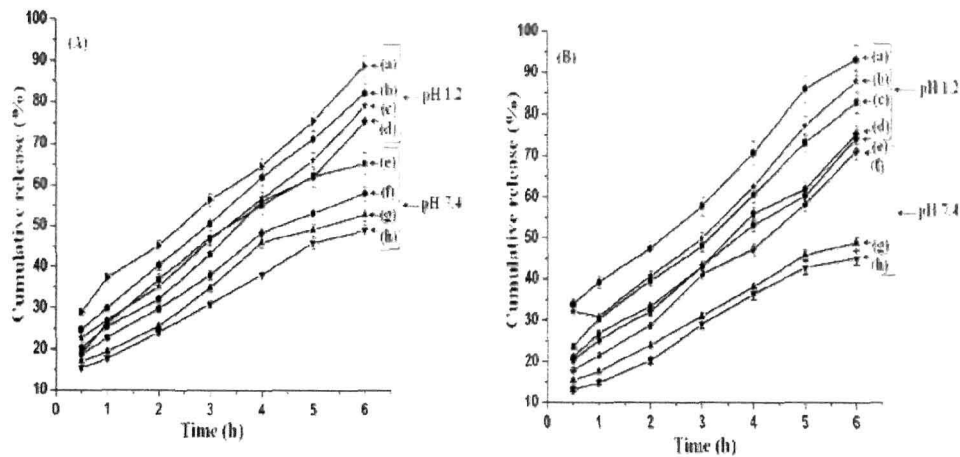


Figure 4.6. Cumulative release (%) at pH 1.2 and 7.4 ,(A) { (a) C/CW0/GA50, (b) C /CW1/GA50, (c) C/CW3/GA50, (d) C/CW5/GA50, (e) C/CW0/GA50, (f) C /CW1/GA50, (g) C/CW3/GA50, (h) C/CW5/GA50} and (B) { (a) C/CW5/GA10, (b) C/CW5/GA30, (c) C /CW5/GA50, (d) C /CW5/GA70, (e) C/CW5/GA10, (f) C/CW5/GA30, (g) C /CW5/GA50, (h) C /CW5/GA70}

4.1.8. Cell Viability Study

The effect of varying CW concentration (0-5%) and time (6, 12, and 24 h) on cell viability is shown in Fig 4.7. Figure 4.7.(a) showed that chitosan was not cytotoxic. Chitosan is used in pharmaceutical field due to its non toxic nature. It had high cell viability of around 98%. The synthesized CW was also found to be cell compatible and cell viability of CW was found around 92%. CW [Figure 4.7. (b)] was not at all cytotoxic to the cells as it was derived from cellulose. Similar types of observations were reported by Clift et. al. [10]. The in vitro cytotoxicity study of Isoniazid [Figure 4.7. (c)] showed that Isoniazid was highly cytotoxic to the cells with a cell viability of only around 40%.

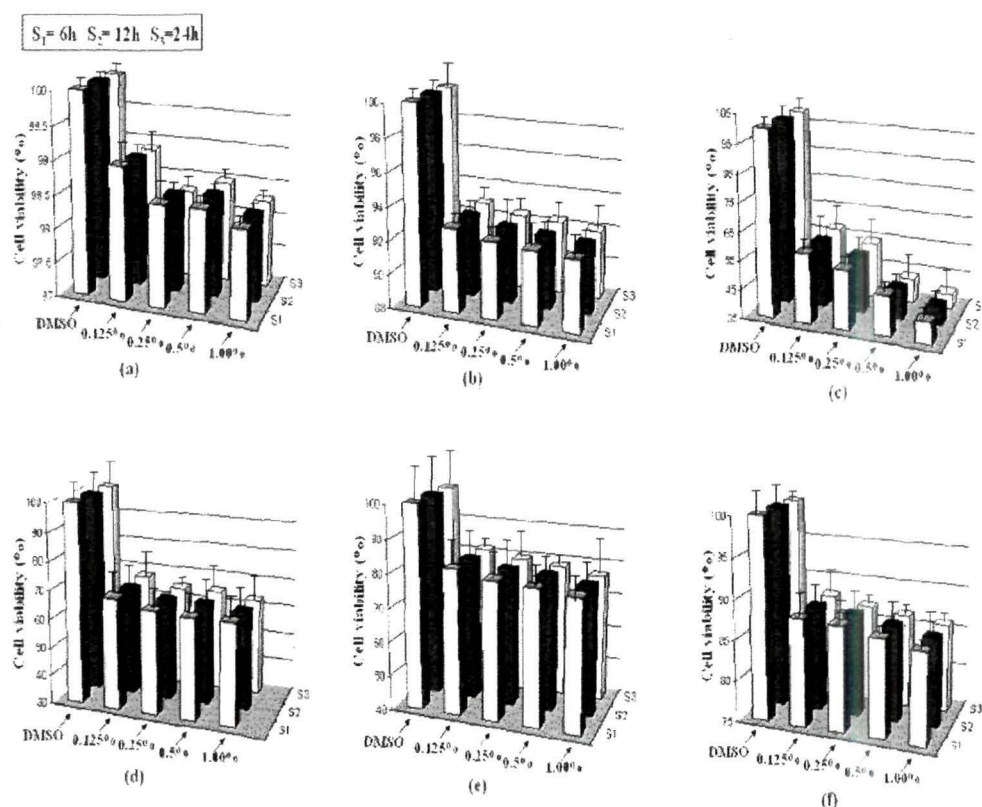


Figure 4.7. Cell viability study with variation of (a) Chitosan, (b) CW, (c) isoniazid, and (d) C/CW0/GA50 (e) C/CW1/GA50 (f) C/CW5/GA50 at 6 h, 12 h, and 24 h

This cell viability decreased with the increase of time (6 - 24h). It was observed that the cytotoxicity isoniazid loaded chitosan-CW microparticles decreased and cell viability

increased. The cell viability increased with the increase in the CW [Figure 4.7.(d-f)] in the microparticles. Owing to the network structure of CW, the drug could not easily diffuse out to interact with the cell and hence an increase in cell viability was observed. As per expectation, the cell viability decreased with the increase in the time due to diffusion of more and more drug from the microparticles to the cell environment.

4.2. Section B-Preparation and characterization of isoniazid loaded chitosan /montmorillonite nanoparticles for controlled drug delivery applications.

4.2.1. Effect of variation of surfactant concentration on the different properties of chitosan nanoparticles

Table 4.2. Effect of variation of surfactant concentration on the different properties of chitosan nanoparticle

Sample code.	Yield of nanoparticle (%)	Encapsulation efficiency (%)	Drug loading efficiency (%)	Average diameter (nm)	Zeta potential (mV)	Zeta potential of the same formulations without drug (mV)	Zeta potential of nanoparticles after 3 hours of drug release (mV)
NPI	92.81(±0.01)	73.10(±0.02)	25.39(±0.08)	451.8 (± 15)	21.22 (± 0.03)	17.05 (± 0.01)	18.53(± 0.04)
NPII	91.27(±0.05)	72.98(±0.04)	25.61(±0.04)	-	-	-	-
NPIII	91.38(±0.01)	73.32(±0.04)	28.18(±0.01)	322.4 (± 12)	28.24 (± 0.1)	21.67(± 0.07)	23.89(± 0.01)
NPIV	91.19(±0.01)	73.48(±0.01)	29.27(±0.01)	305.7 (± 13)	30.01 (± 0.06)	23.12(± 0.01)	26.33 (± 0.04)
NPV	92.52(±0.05)	73.41(±0.03)	31.63(±0.02)	282.2 (± 15)	36.93 (± 0.01)	30.41(± 0.03)	33.12(± 0.01)
NPVI	86.16(±0.08)	73.60(±0.02)	25.58(±0.01)	-	-	-	-

*each value represents average of five readings, standard deviation in parenthesis

The result showing the effect of variation of surfactant concentration on different properties of chitosan nanoparticles are shown in Table 4.2. In the case of MMT containing chitosan nanoparticles, yield (%) remained almost unchanged irrespective of surfactant concentration. Encapsulation efficiency (%) was also found to remain same.

It was also observed that neither the surfactant nor the MMT alone produced any significant effect on the drug loading efficiency except the yield. Surfactant alone provided somewhat low yield which might be due to the loss during isolation. At a fixed level of MMT concentration, drug loading efficiency showed an increasing trend while particle size exhibited a decreasing trend as the concentration of the surfactant increased. The presence of surfactant could increase the interlayer distance of silicate layers of MMT. The higher the concentration of surfactant, the higher was the interlayer distance to accommodate the polymer as well as drug. This resulted in an increase in drug loading efficiency. As the surfactant was soluble in water, it could decrease the solubility of ionically crosslinked chitosan in water and thus favoring the solid particle formation and consequently decrease the viscosity of dispersing phase. The lower dispersion phase viscosity facilitated the formation of lower particle size. The dispersing effect of the surfactant also favored the formation of lower particle size as the concentration of surfactant increased. Besides this, the physical interaction between the chitosan macromolecules might be destructed due to shear resulting in the formation of a dispersing phase of lower viscosity [11] which favors the formation of lower particle size. Zeta potential values of the nanoparticles showed that the zeta potential increased with the decrease in particle size. The zeta potential of nanoparticles which did not contain Tween 80 and Isoniazid was found to be less than that of the formulations containing both Tween 80 and Isoniazid. The zeta potential was found to be positive for all the formulations. Nanoparticles prepared without surfactant had a zeta potential less indicating that they would aggregate in acidic or basic medium. On the other hand, particles prepared with surfactant exhibited a higher zeta potential probably because the surfactant prevented the counter-ions from binding within chitosan. Such particles would be expected to be stable.

Isoniazid has normally three pKa values: 1.8 based on hydrazine nitrogen, 3.5 based on pyridine nitrogen and 10.8 based on acidic group [12]. In pH 1.2, the pKa of Isoniazid is found to be around 2 due to protonation of hydrazine nitrogen whereas in basic pH of 7.4 it is found to be around 12. The increase in the zeta potential with the incorporation of drug suggests that at least a part of the drug-polymer association was surface-adsorbed.

Thus, a part of the drug was embedded within the chitosan matrix and the rest was adsorbed on the surface of the nanoparticles.

4.2.2. Fourier Transform Infra-red Spectroscopy (FTIR) study:

In the spectrum of pure chitosan (Figure 4.8. a), the broad absorption band appeared in the range $3200-3450\text{ cm}^{-1}$ was due to the hydrogen-bonded OH stretching and NH_2 asymmetric stretching. The characteristic peaks of amide I and amide II appeared at 1646 cm^{-1} ($\text{C}=\text{O}$ stretching) and 1569 cm^{-1} (N-H in plane deformation coupled with $\text{C}\equiv\text{N}$ stretching) respectively [13]. The peaks exhibited in the spectrum for MMT (Figure 4.8.b) at 3435 , 1639 and $1051-544\text{ cm}^{-1}$ were for $-\text{OH}$ stretching, $-\text{OH}$ bending and oxide bands of metals like Si, Al, Mg, etc. Figure 4.8.c. represents the spectrum of isoniazid. The absorption peaks appeared at 1664 and 1551 cm^{-1} were due to the amide I ($\text{C}=\text{O}$ stretching) and amide II (N-H bending of secondary amide group) respectively. Besides this, multiple peaks appeared in the range $1410-669\text{ cm}^{-1}$ [14].

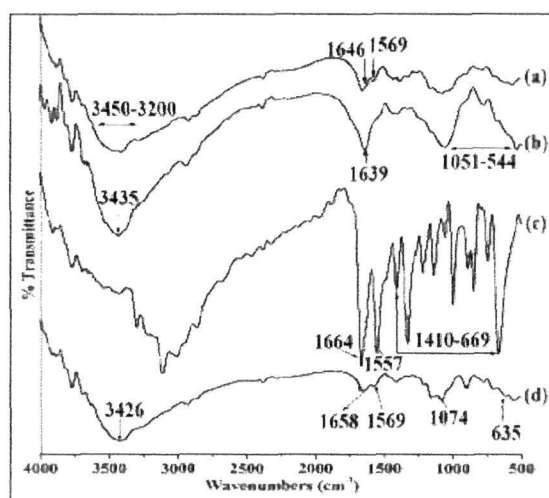


Figure 4.8. FTIR spectra of (a) Pure chitosan, (b) MMT, (c) Isoniazid, and (d) NPV

All the characteristic peaks of chitosan, MMT and isoniazid appeared and their intensities decreased in the spectrum of isoniazid loaded chitosan-MMT nanoparticles (Figure 4.8.d). Moreover, the intensity of the peak appeared in the range $3450-3200\text{ cm}^{-1}$ (Figure 4.8.a) decreased and shifted to lower wave number. This indicated an interaction

between MMT and chitosan. The decrease in hydroxyl peak intensity was reported by Deka et al. [15] while studying the properties of wood polymer nanocomposites. All these indicated a better dispersion of MMT and isoniazid in the chitosan-MMT nanoparticles.

4.2.3. X-ray diffraction (XRD) study

Isoniazid (curve 2a) shows multiple peaks at $2\theta=12$ to 50° due to its crystalline nature. Similar type of diffractogram was reported by Fukuoka et al. [16]. Chitosan (curve 4.9.b) shows its characteristic diffraction peak at $2\theta=20.3^\circ$ which corresponds to the (100) plane of orthorhombic crystal [17]. MMT exhibits the two characteristic peaks at $2\theta=9.01^\circ$ and 26.7° which are assigned for (001) and (002) plane (curve 4.9.c) [18]. The characteristic peaks for MMT and isoniazid were found to disappear in the diffractogram of MMT/chitosan nanoparticles (curve 4.9.d). It could be said that either the full expansion of MMT gallery occurred which was not possible to detect by XRD or the MMT layers become delaminated and no crystal diffraction peak appeared [19]. These findings suggested the occurrence of a molecular level dispersion of isoniazid in isoniazid loaded chitosan-MMT nanoparticles. The molecular level dispersion of isoniazid in the chitosan-hydroxyethyl cellulose blended microsphere was reported by Aminabhavi et al. [20].

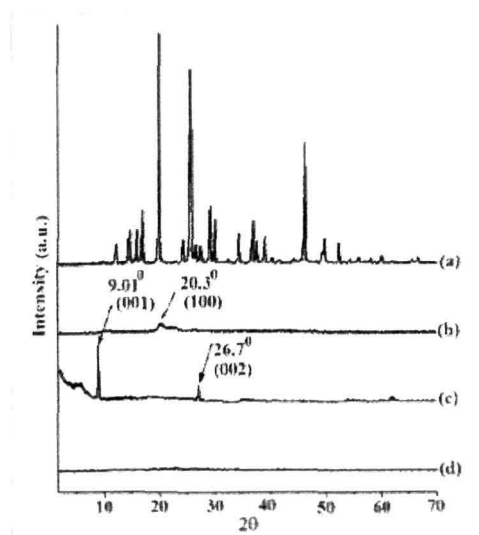


Figure 4.9. XRD patterns of (a) Isoniazid, (b) Chitosan, (c) MMT, and (d) NPV

4.2.4. Scanning electron microscopy (SEM) study

SEM micrographs of chitosan- MMT nanoparticles and isoniazid loaded nanoparticles are shown in Figure 4.10. a and 4.10. b respectively. The surface of the nanoparticles without isoniazid appeared less smooth and agglomerated as compared to isoniazid loaded nanoparticles. Isoniazid loaded nanoparticles had spherical shape and smooth surface. Selvaraj et. al. [21] reported that acyclovir loaded chitosan nanoparticles had solid dense structure with smooth spherical shape.

4.2.5. Transmission electron microscopy (TEM) study

TEM micrographs of isoniazid loaded chitosan nanoparticles devoid of MMT and with MMT are shown in Figure 4.10.c and 4.10.d respectively. Figure 4.10.d showed the presence of platelets of MMT tactoids in which the dark lines were the intersection of MMT layers. The bright areas were for polymer matrix and isoniazid. Similar observation was reported by Wang et. al. [22] while studying the biopolymer/montmorillonite structure by TEM. The results indicated that MMT was incorporated and dispersed in the chitosan matrix.

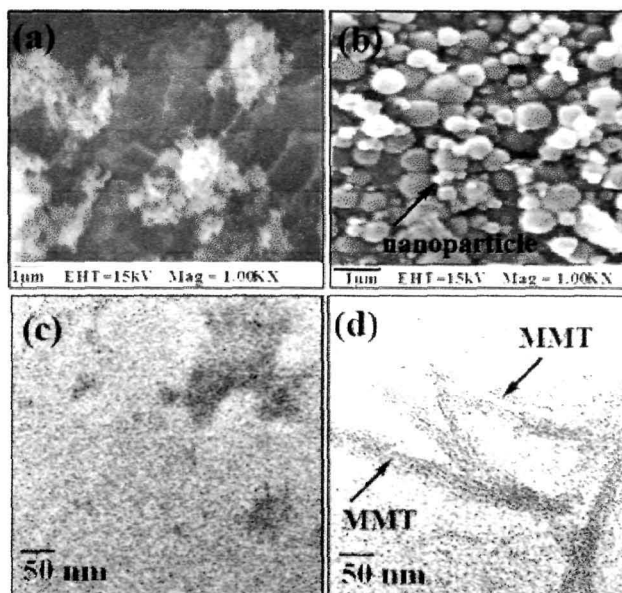


Figure 4.10. SEM micrographs of (a) Chitosan- MMT nanoparticles without isoniazid, (b) NPV, and TEM micrographs of (c) NPVI, and (d) NPV

4.2.6. Swelling Study

The effect of pH on the percentage swelling of isoniazid loaded nanoparticles at two different pH namely, 1.2 and 7.4 are shown in Figure 4.11. It was observed that the swelling of isoniazid loaded chitosan-MMT nanoparticles was more in gastric pH (1.2) than in intestinal pH (7.4). In acidic medium, the amine groups of chitosan molecules were ionized to ammonium ions. These cationic charges acted as repulsive forces between the polymer molecules [8] and hence increased the swelling. In alkaline pH, the inherent hydrophobicity of chitosan nanoparticles prevented them from faster swelling [6]. Furthermore, the percentage swelling degree was found to increase with the increase in time and decrease in particle size of the nanoparticles. The lower the particle size, the higher was the surface area. Higher surface area facilitated better contact of the nanoparticles with the solvent and thus improved swelling.

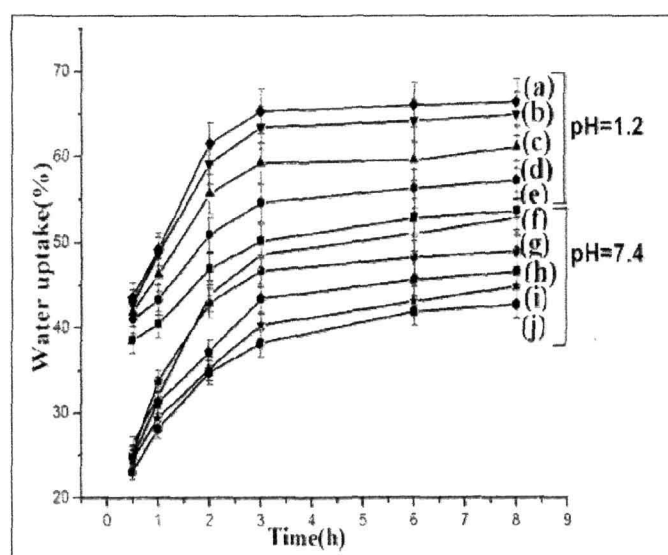


Figure 4.11. Percentage swelling degree at pH 1.2 of (a) NPV, (b) NPV, (c) NPV, (d) NPV, (e) NPV, and at pH 7.4 of (f) NPV, (g) NPV, (h) NPV, (i) NPV, (j) NPV

4.2.7. In vitro Release Studies

The drug release profile of the nanoparticles at two different pH namely 1.2 and 7.4 are shown in Figure 4.12. (A) and 4.12. (B). The cumulative release (%) of isoniazid from chitosan-MMT nanoparticles was found to be pH dependent. The cumulative release (%) of isoniazid decreased with the increase in the pH of the medium. The two main factors

governing the release profile of isoniazid from nanoparticles were swelling nature of the polymer and solubility of the drug in the medium. The difference in release profile was due to the difference in the solubilities of chitosan in gastric and intestinal pH. Chitosan was more soluble in gastric pH compared to intestinal pH. Lower pH of the medium favoured both the swelling of the polymer and solubility of the drug. Cumulative release (%) of isoniazid was also found to increase with the increase in time and decrease in particle size of the nanoparticles. The explanation for this observation was similar to that of stated earlier.

Moreover, a burst release of about 50% drug was observed in the first 3 hours of the test. The lower diffusion path due to lower particle size along with other already stated factors played an important role in controlling the release rate. The adsorbed drug on the surface of nanoparticles might be main factor responsible for the initial burst release. This was supported by the zeta potential value [23].

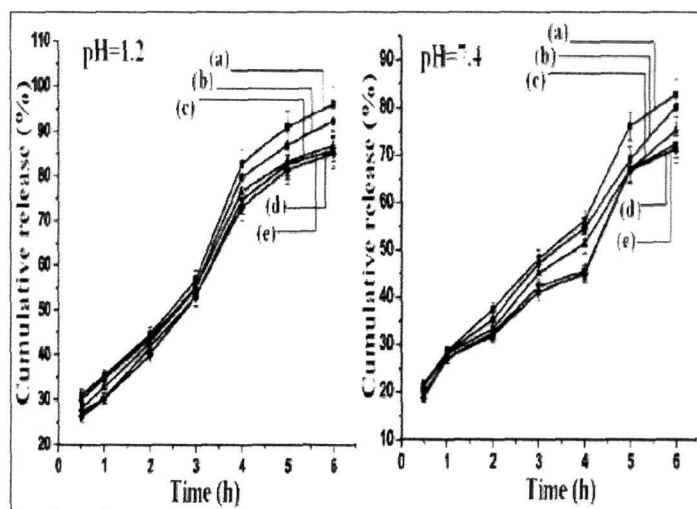


Figure 4.12. Cumulative percentage drug release at (A) pH 1.2 of (a) NPV, (b) NPV, (c) NPV, (d) NPV, (e) NPV, and at (B) pH 7.4 of (a) NPV, (b) NPV, (c) NPV, (d) NPV, (e) NPV

4.2.8. Cell viability Study

The results of the MTT-assay are shown in Figure 4.13. It was observed that the cell viability varied between 85-90% within the studied surfactant (Tween 80) concentration. This indicated that the surfactant was not highly cytotoxic to the cells (Figure 4.13.a).

Tween 80 did not exhibit any significant cytotoxicity when evaluated in CaCo-2 cells [24].

But in our case, a slight decrease in cell viability was observed as the concentration of surfactant increased. The nonionic surfactants were reported to be used as penetration enhancers due to their non irritating nature and low toxicity [25]. Addition of surfactant resulted in an increase in the dispersion of nanoparticles and enhanced their interaction with the cells leading to a decrease in cell viability. MMT showed very low cytotoxicity as evident from (Figure 4.13.b). Similar result was also reported by Wang et.al. [22]. Figure 4.13.c and 4.13.d showed the cell viability (%) of isoniazid alone and clay free isoniazid loaded nanoparticles. In both the cases, the cell viability decreased with the increase in the concentration of isoniazid. The cytotoxicity was found to be less in the case of isoniazid embedded polymeric nanoparticles compared to those of isoniazid alone. The polymer slowed down the release of isoniazid and hence decreased the interaction of drug with the cell. It was observed further (Figure 4.13.d and 4.13.e) that the cell viability of nanoparticles containing clay was more compared to clay free nanoparticles. This might be due to the fact that the silicate layers hindered the release of drug in the cell because of its tortuous path. Figure 4.13.(e-h) shows the results of cell viability of nanoparticles prepared under different concentration of surfactants (0-0.025ml). Nanoparticles prepared by using surfactant exhibited higher cytotoxicity than those of prepared without surfactant. The cytotoxicity of nanoparticles increased upto the use of 3% (v/w) surfactant, beyond that the value remained almost unchanged. The nanoparticles prepared without Tween 80 had large particle size compared to nanoparticles prepared with Tween 80. The higher the surfactant concentration, the lower was the particle size and higher was the surface area. Due to higher surface area, the contact of the nanoparticles with the cell increased and hence the cytotoxicity also increased. The increase of cytotoxicity value with time was due to more contact of drug with cell wall. The cell viability of the nanoparticles synthesized with and without surfactant was within the range of 70-90%.

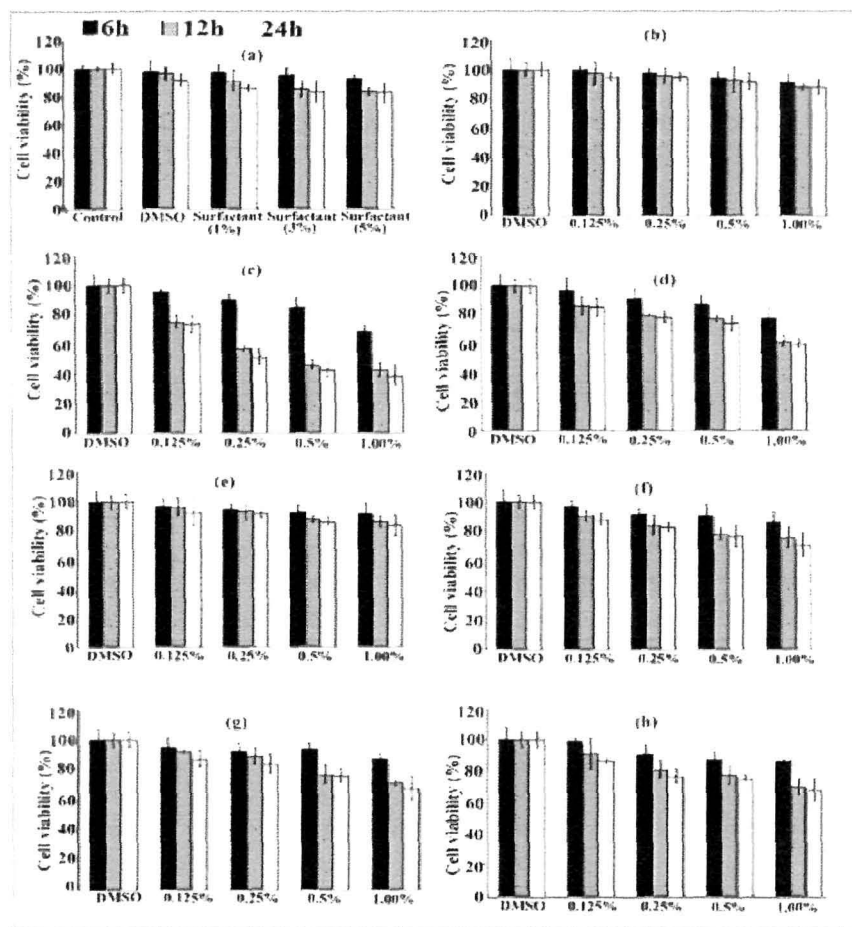


Figure 4.13. Cell viability study with variation of (a) surfactant, (b) clay, (c) isoniazid, and (d) drug embedded nanoparticles, (e) NPI, (f) NPIII, (g) NPV, (h) NPV at 6 h, 12 h, and 24 h

4.2.9. In vitro wash-off test for evaluation of mucoadhesive property

Results of the in vitro wash off test of chitosan-MMT nanoparticles containing isoniazid are given in Table 4.3. The results represented in table are the average readings of five samples. The test was carried out in gastric (pH=1.2) and intestinal pH (pH=7.4) environment. The mucoadhesion was found to be higher in gastric pH than in intestinal pH. The mucoadhesion properties were also enhanced with the decrease in the particle size of the nanoparticles.

At acidic pH, the free amino groups of chitosan nanoparticles might get protonated and became positively charged. This could strongly bind to the negatively charged mucus layer. The higher surface area of the nanoparticles was responsible for the observed

higher mucoadhesion property exhibited by chitosan nanoparticles having lower particle size. Sabitha et al. reported that the chitosan-alginate microcapsules showed lower mucoadhesive properties in intestinal pH compared to gastric pH [26].

Table 4.3. Results of in vitro wash-off test to assess mucoadhesive properties of nanoparticles prepared

pH	Sample Code	No. of particle taken	Reading after every 30 min									
			1	2	3	4	5	6	7	8	9	10
1.2	NPI	50	35.4 (±0.5)	32.4 (±0.5)	25.4 (±1.0)	20.4 (±0.5)	12.2 (±0.7)	10.8 (±0.7)	8.6 (±0.5)	5.0 (±0.6)	0	0
	NPIII	50	44 (±0.6)	42 (±0.9)	40 (±1.4)	35 (±0.6)	30 (±0.6)	20.4 (±0.5)	15 (±0.6)	12.4 (±0.5)	10.2 (±0.7)	4.8 (±0.4)
	NPIV	50	52.8 (±1.3)	50 (±0.6)	46.8 (±1.2)	45 (±0.6)	42.8 (±0.7)	37.8 (±1.0)	32 (±0.6)	23.2 (±0.4)	21.6 (±0.5)	17 (±1.3)
	NPVI	65	60 (±0.9)	58 (±0.6)	57 (±0.9)	55.4 (±0.8)	51.4 (±0.5)	47.2 (±0.4)	35.2 (±0.4)	30 (±0.6)	22.4 (±0.8)	14 (±1.3)
7.4	NPI	50	25 (±1.4)	20.2 (±0.7)	10.2 (±7.4)	8 (±0.6)	4 (±0.6)	2.2 (±0.4)	0	0	0	0
	NPIII	50	36 (±0.9)	33 (±0.9)	28.4 (±0.5)	22.4 (±0.5)	16 (±0.6)	14.8 (±0.4)	12 (±0.6)	7.6 (±1.0)	2.8 (±0.4)	0
	NPIV	50	44 (±0.9)	35 (±0.6)	32.2 (±0.7)	26 (±1.1)	21 (±0.6)	18.4 (±1.0)	11.2 (±0.4)	8.8 (±0.4)	5.4 (±0.5)	0
	NPVI	50	45.2 (±0.7)	43.8 (±0.7)	42 (±0.6)	40.8 (±0.4)	37.2 (±1.0)	35.4 (±0.5)	31.8 (±0.4)	28 (±0.6)	22.8 (±0.4)	16.6 (±0.5)

*each value represents average of five readings, standard deviation in parenthesis

4.2.10. Ex vivo mucoadhesive test

Table 4.4. shows the results of ex vivo mucoadhesion test. The results are the mean value of five readings. It was observed that the detachment force increased with the decrease in particle size of the nanoparticles. The lower the particle size, the higher was the surface area and hence the nanoparticles could strongly adhere to the mucosal surface. Rekha et al. reported that mucoadhesive properties of the succinyl chitosan particles enhanced due to better penetration of smaller size particles into the mucus layers [27].

Table 4.4. Weight required to detach the membrane at different time intervals.

Sample Code	Mass required to detach after 5 min (g)	Detachment force (dyne/cm ²)	Mass required to detach after 10 min (g)	Detachment force (dyne/cm ²)	Mass required to detach after 15 min (g)	Detachment force (dyne/cm ²)	Mass required to detach after 20 min (g)	Detachment force (dyne/cm ²)
NPI	9.95 (±0.05)	3103.8 (±12.7)	16.5 (±0.03)	5147.0 (±2.6)	21.1 (±0.03)	6582 (±7.6)	21.8 (±0.01)	6800.4 (±2.5)
NPIII	16.5 (±0.01)	5147.0 (±2.6)	19.6 (±0.05)	6124.1 (±19.0)	21.3 (±0.01)	6644.4 (±2.5)	22.0 (±0.02)	6862.8 (±5.1)
NPIV	17.85 (±0.05)	5568.2 (±12.7)	20.2 (±0.01)	6301.3 (±2.6)	21.6 (±0.04)	6737.9 (±10.2)	22.2 (±0.02)	6925.1 (±5.1)
NPVI	18.25 (±0.02)	5692.9 (±5.1)	22.1 (±0.01)	6893.9 (±2.6)	22.5 (±0.03)	7018.7 (±7.6)	23.5 (±0.01)	7330.7 (±2.5)

*each value represents average of five readings, standard deviation in parenthesis

4.3. Section C-Preparation and characterization of isoniazid loaded carboxymethyl chitosan /montmorillonite nanoparticles for controlled drug delivery applications.

4.3.1. Nuclear Magnetic Resonance (NMR) study

The ¹H NMR spectrum for CMC in D₂O is shown in Figure 4.14. The basic assignment of the chitosan resonance is that: 'a' is the resonance of H-1D (4.72 ppm), 'b' is H-1A (4.65 ppm), 'h' is the resonance of 3 acetyl-protons (2.0 ppm), 'e' is H3-6 protons (3.6–3.7 ppm), 'g' is H-2D proton resonance (3.1 ppm). In the region between 4.05 and 4.55 ppm, the resonances are the protons of 3- and 6-substituted carboxymethyl (–O–CH₂COOD) of CMC, 'd' is the resonance of 3 protons from H-6' (2 protons) and H-3' (1 proton), 'c' is the resonance of 1 proton from H-3. The resonance signal of the protons from N–CH₂COOD group can be found at f = 3.25 ppm. The result indicated that the amino groups were partly carboxymethylated along with the hydroxyl groups [28, 29].

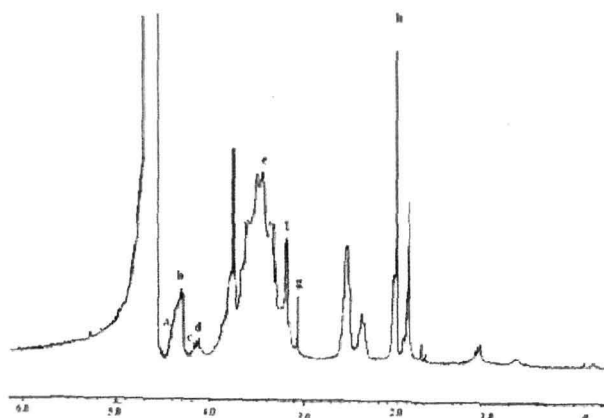


Figure 4.14. ^1H NMR spectra of CMC

4.3.2. Effect of variation of MMT and GA concentration on the different properties of isoniazid loaded CMC-MMT nanoparticles

The results showing the effect of variation of MMT and GA concentration on different properties of CMC nanoparticles are shown in Table 4.5. The encapsulation efficiency of MMT free crosslinked nanoparticles was found to be higher compared to that of MMT containing crosslinked nanoparticles. The encapsulation efficiency decreased with the increase in MMT content in the nanoparticles. This could be attributed to the presence of the silicate layers of MMT. The $-\text{OH}$ groups of MMT could interact with the residual $-\text{NH}_2$ group of CMC and $-\text{CHO}$ groups of GA resulting in extension of the polymer chains. The silicate layers of MMT also hindered the movement of the intercalated polymer chains freely and might assist the formation of fine channels from inner to outer surface of the nanoparticles during drying process. The more the encapsulation of MMT, the higher is the chance formation of fine channels. Thus, part of the drug might get diffused from the particles to the external medium resulting in the decrease of encapsulation efficiency. The interference offered by the MMT layers was absent in MMT free crosslinked nanoparticles. Hence, it showed higher encapsulation efficiency. Similarly, at a fixed MMT content, the encapsulation efficiency of nanoparticles was found to further decrease with the increase in the glutaraldehyde (GA) concentration. GA

might further restrict the free motion of the intercalated polymer chains and thus assist the formation of porous structure.

The average diameter of the nanoparticles was obtained in the range 541-570 nm. The variation in MMT concentration did not significantly affect the particle size. However, the average diameter showed a decreasing trend on increasing the GA concentration. The residual amino groups present in CMC interacted with the hydroxyl group of MMT and GA. With the increase in the concentration of GA, the availability of free amino groups on nanoparticles reduces due to which the nanoparticles became more compact and hence the diameter would be less.

Table 4.5. Effect of variation of MMT and GA concentration on the different properties of CMC nanoparticles

Sample code	Yield of nanoparticle (%)	Encapsulation efficiency (%)	Average diameter (nm)	Zeta potential (mV)
CMC/M0/GA50	92.76(±0.01)	68.12(±0.04)	543.7 (± 11)	47.21(± 0.02)
CMC/M1/GA50	92.09(±0.04)	64.38(±0.01)	546.3(± 11)	44.08(± 0.07)
CMC/M3/GA50	92.32 (±0.01)	62.11(±0.01)	544.1(± 8)	42.92(± 0.3)
CMC/M5/GA50	91.98(±0.03)	60.31(±0.03)	548.9(± 10)	37.63(± 0.02)
CMC/M5/GA10	91.62(±0.03)	61.77 (±0.02)	570.2(± 11)	35.35(± 0.01)
CMC/M5/GA30	91.20(±0.01)	61.03(±0.01)	564.7(± 14)	35.94(± 0.01)
CMC/M5/GA70	91.93(±0.02)	59.46 (±0.01)	541.1(± 13)	37.83(± 0.03)

* each value represents average of five readings, standard deviation in parenthesis

Zeta potential values of the nanoparticles were found in the range 39 to 47 mV indicating good stability of the nanoparticles. The surface of the nanoparticles was positively charged due to the presence of residual amino groups. With the incorporation of MMT in CMC matrix the surface charge decreases. The reduction in surface charge might be due to the increased electrostatic interaction between the protonated amino groups of CMC and hydroxyl groups of MMT [30].

However, the zeta potential values increased as the GA concentration increased from 10 to 70%. The increase in the zeta potential indicated that the stability of the nanoparticles

increased with the increase in the concentration of GA and they would not aggregate in acidic or basic medium. All the zeta potential values were in the stable zone indicating that the synthesized nanoparticles are highly stable.

4.3.3. Fourier Transform Infra-red Spectroscopy (FTIR) study:

FTIR spectra of chitosan, CMC, MMT, Isoniazid and isoniazid loaded CMC-MMT nanoparticles are shown in Figure 4.15. The basic absorption bands of chitosan (curve a) appeared at 3442 cm^{-1} (OH stretching and NH stretching, overlapped), 2939 cm^{-1} (CH stretching). The characteristics peaks of amide I and amide II appeared at 1639 cm^{-1} (C=O stretching) and 1455 cm^{-1} (N-H in plane deformation coupled with C≡N stretching) respectively. The other peaks appeared at 1156 cm^{-1} (bridge -O- stretching), and 1062 cm^{-1} (-CO stretching) were also shown [3].

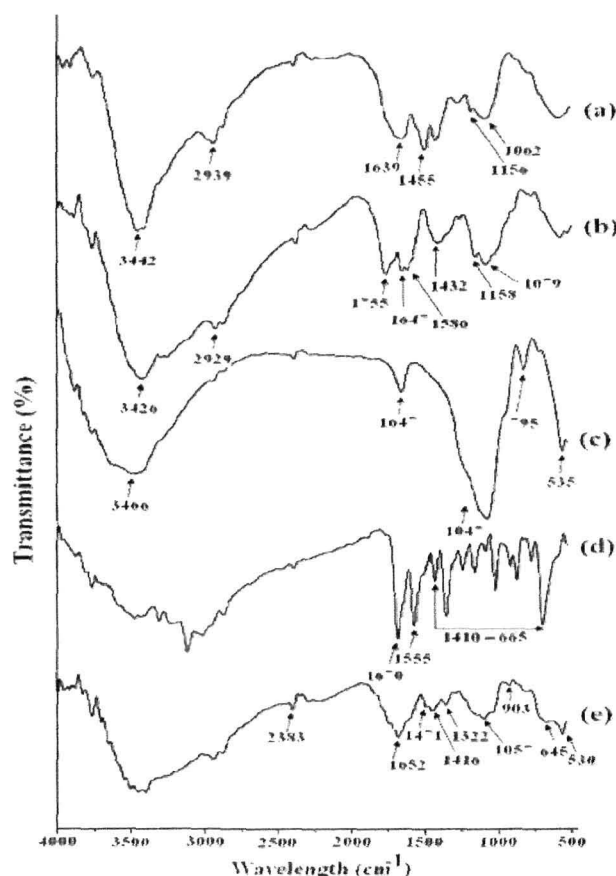


Figure 4.15. FTIR spectra of (a) Chitosan, (b) CMC, (c) MMT, (d) Isoniazid, and (e) CMC/M5/GA50

Curve b shows the IR spectrum of the sodium salt of CMC, where the strong peaks were found to appear at 1586 cm^{-1} and 1432 cm^{-1} corresponded to the respective asymmetric and symmetric stretching vibrations of COO^- group, 1755 cm^{-1} (for carboxylic acids, $-\text{COOH}$) and 1647 cm^{-1} (for deforming NH_2 vibration). The C–O absorption peak of the secondary hydroxyl group became stronger and shifted to 1079 cm^{-1} . The broad peak in CMC at $3400\text{--}3200\text{ cm}^{-1}$ was due to both O–H and N–H stretching vibrations and the peak at 2929 cm^{-1} was due to the C–H stretching vibrations [31]. From the IR spectra, we concluded that the carboxymethyl group was successfully attached to the chitosan backbone.

Curve c represents the spectra of MMT. The peaks exhibited in the spectrum for MMT at 3435 , 1639 and $1051\text{--}544\text{ cm}^{-1}$ were for $-\text{OH}$ stretching, $-\text{OH}$ bending and oxide bands of metals like Si, Al, Mg, etc. Curve d represents the spectrum of isoniazid. The absorption peaks appeared at 1664 and 1551 cm^{-1} were due to the amide I (C=O stretching) and amide II (N-H bending of secondary amide group) respectively. Besides this, multiple peaks appeared in the range $1410\text{--}669\text{ cm}^{-1}$ [1].

All the characteristic peaks of CMC, MMT and isoniazid appeared and their intensities decreased in the spectrum of isoniazid loaded chitosan-MMT nanoparticles (curve e). In isoniazid loaded CMC-MMT nanoparticles, no absorption band was found in the region of 1755 cm^{-1} . But a new peak at 1322 cm^{-1} was observed. This peak along with peak at 1652 cm^{-1} can be credited to the stretching vibrations of calcium cross-linked carboxyl groups of CMC [30].

Moreover, the intensity of the peak appeared at 3426 cm^{-1} for curve (b) decreased and shifted to lower wave number side isoniazid loaded CMC-MMT nanoparticles (curve e). This indicated an interaction between the hydroxyl groups of MMT and CMC. The decrease in hydroxyl peak intensity was reported by Deka et. al. [15] while studying the properties of wood polymer nanocomposites. All these indicated a better dispersion of MMT and isoniazid in the chitosan-MMT nanoparticles.

4.3.4. X-ray diffraction (XRD) study

The carboxymethylation of chitosan was also confirmed by XRD study. The XRD diffractograms of the Chitosan, CMC, MMT, isoniazid and isoniazid loaded CMC-MMT

nanoparticles are shown in Figure 4.16. Chitosan showed two distinct crystalline peaks at $2\theta=10^\circ$ and 20.2° due to (020) and (100) plane, respectively [Figure 4.16.c] [4,3]. Conversely, in the case of CMC, the peak at 10° disappeared, and the intensity of the peak at $2\theta=20^\circ$ diminished [Figure 4.16.d]. The reason for the desertion and weakening of the peaks might due to the demolition of the intermolecular hydrogen bonds and the crystalline regions of chitosan which signify the formation of CMC by the process of the carboxymethylation of chitosan [3].

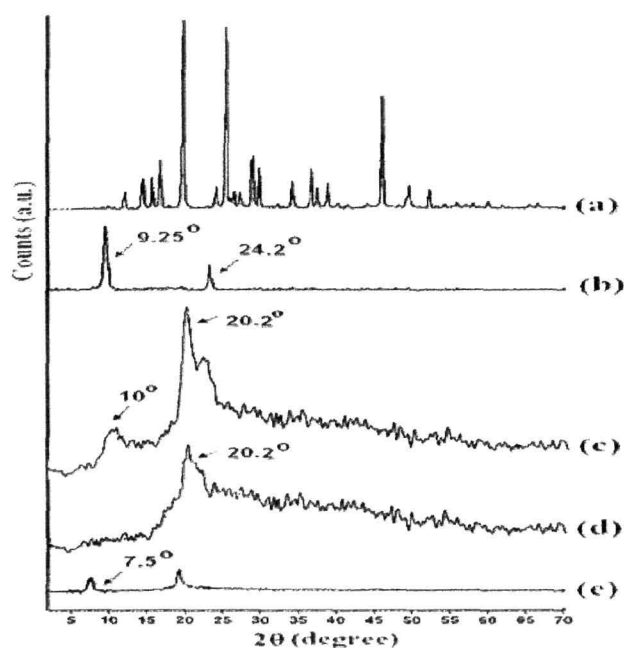


Figure 4.16. XRD patterns of (a) Isoniazid, (b) MMT, (c) chitosan, (d) CMC, and (e) CMC/M5/GA50

Isoniazid (curve 4.16. a) shows multiple peaks at $2\theta=12^\circ$ to 50° due to its crystalline nature. MMT exhibits the two characteristic peaks at $2\theta=9.25^\circ$ and 24.2° which are assigned for (001) and (002) plane (figure 4.16. b). The characteristic peaks for isoniazid were found to disappear in the diffractogram of MMT-CMC nanoparticles (curve 4.16. e). The intensity of both the characteristic peaks for MMT was found to decrease. Further, the peak corresponding to $2\theta=9.25^\circ$ was found to shift to $2\theta=7.5^\circ$. These findings suggested an increase in gallery spacing of MMT due to intercalation and occurrence of a molecular level dispersion of isoniazid in isoniazid loaded CMC-MMT nanoparticles.

4.3.5. Scanning electron microscopy (SEM) study

SEM analysis was performed to study the surface morphology of CMC nanoparticles and CMC-MMT nanoparticles loaded with isoniazid. Figure 4.17.a and 4.17. b represents the SEM micrographs of CMC nanoparticles and CMC-MMT nanoparticles respectively. The surface of CMC nanoparticles (Figure 4.17. a) appeared rough and slightly agglomerated. However, on addition of MMT into CMC nanoparticles the roughness as well as the agglomeration decreased (Figure 4.17. b). MMT acted as a physical crosslinking agents which enhanced the dimensional stability and hence the smoothness [32].

Further work was done through energy dispersive X-ray (EDX) analysis of clay loaded nanoparticles as shown in Figure 4.17.c. Elements such as Al, Na and Si, which are mainly from the silicate MMT, were detected demonstrating the effective incorporation of MMT into the nanoparticles [33].

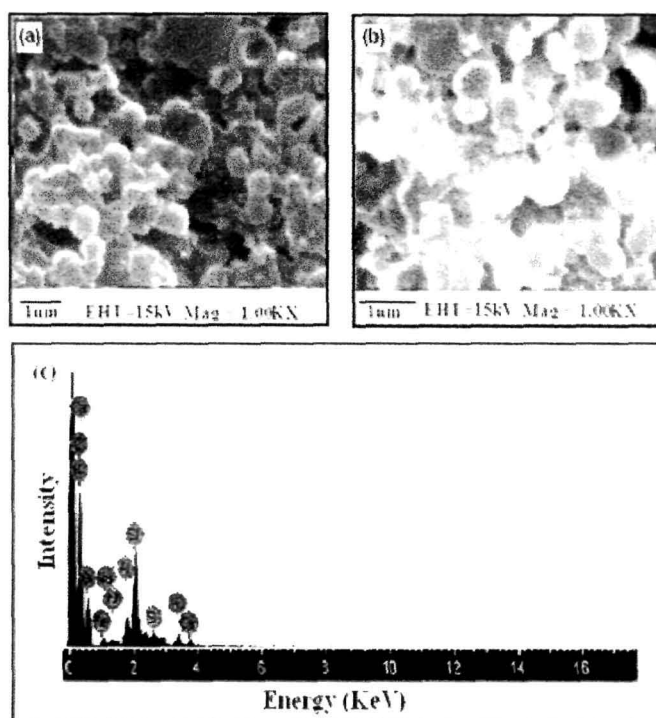


Figure 4.17. SEM micrographs of (a) CMC /M0/GA50, (b) CMC/M5/GA50, and (c) EDX of CMC/M5/GA50

4.3.5. Transmission electron microscopy (TEM) study

TEM micrographs of isoniazid loaded carboxymethyl chitosan nanoparticles devoid of MMT and with MMT are shown in Figure 4.18.a and 4.18. b respectively. Figure 4.18.b showed the presence of platelets of MMT tactoids in which the dark lines were the intersection of MMT layers. The bright areas were for polymer matrix and isoniazid. The results indicated that MMT was incorporated and dispersed in the CMC matrix.

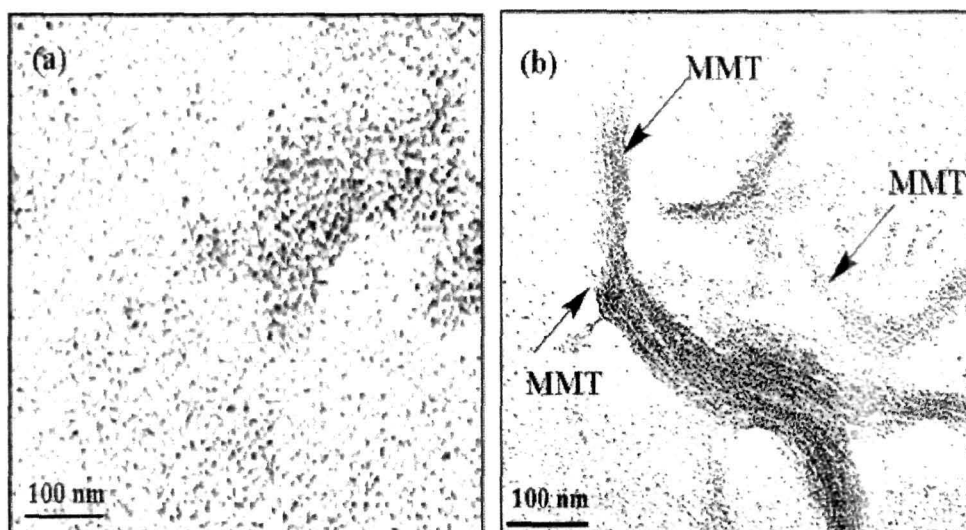


Figure 4.18. TEM micrographs of CMC nanoparticles (a) without MMT range and (b) with MMT at 100 nm scale respectively

4.3.6. Swelling Study

The effect of pH on the percentage swelling of isoniazid loaded nanoparticles at two different pH namely, 1.2 and 7.4 are shown in Figure 4.19. It was observed that the swelling of isoniazid loaded carboxymethyl chitosan-MMT nanoparticles was more in gastric pH (1.2) than in intestinal pH (7.4). At lower pH, the free amine groups become protonated and generated a repulsive force between the adjacent positively charged polymer chains causing the swelling of the polymer and consequently diffusion of more amount of drug out of the polymer matrix [34, 35]. In alkaline pH, protonation was prevented and hence swelling decreased.

Figure 4.19. (A) showed that with the increase in the concentration of MMT, the percentage swelling degree decreased. Water absorption decreased by the presence of

dispersed phase of MMT into the CMC matrix of the nanoparticles. MMT particles acted as a barricade for water molecules and decreased the water transmission through the crosslinked CMC-MMT nanoparticles. Similarly, nanoparticles containing higher concentration of GA (Figure 4.19B) swelled less due to higher crosslinking densities and less availability of the polar groups.

Furthermore, the percentage swelling degree was found to increase with the increase in time. With the increase in the time period, higher amount of the solvents can penetrate into the CMC matrix, resulting in the increase in the percentage swelling degree.

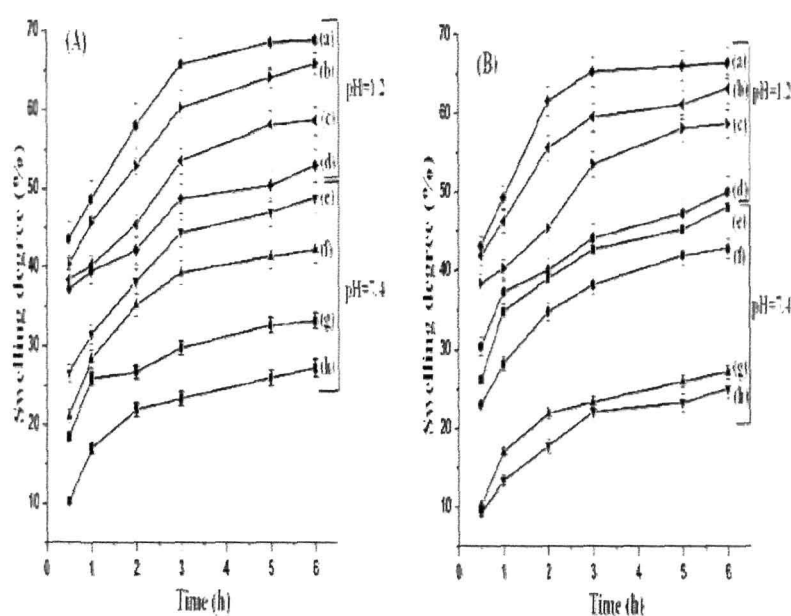


Figure 4.19. Percentage swelling degree at pH 1.2 and 7.4: (A) {(a)CMC/M0/GA50, (b) CMC /M1/GA50, (c) CMC /M3/GA50, (d) CMC /M5/GA50, (e) CMC /M0/GA50, (f) CMC /M1/GA50, (g) CMC /M3/GA50, (h) CMC /M5/GA50} and (B) {(a) CMC M5/GA10, (b) CMC /M5/GA30, (c) CMC /M5/GA50, (d) CMC /M5/GA70, (e) CMC /M5/GA10, (f) CMC /M5/GA30, (g) CMC /M5/GA50, (h) CMC /M5/GA70}

4.3.7. *In vitro* Release Studies

The drug release profile of the nanoparticles at two different pH namely 1.2 and 7.4 are shown in Figure 4.20. The cumulative release (%) of isoniazid from CMC-MMT nanoparticles was found to be pH dependent. The cumulative release (%) of isoniazid

decreased with the increase in the pH of the medium. The major factors controlling the release profile of isoniazid from nanoparticles were swelling nature of the polymer and solubility of the drug in the medium. The difference in release profile was due to the difference in the swelling of CMC in gastric and intestinal pH. CMC was swelled more in gastric pH compared to intestinal pH medium. The faster drug release rate in lower pH medium was due to the wobbly nanoparticles structure, caused by the protonation of residual amino groups of CMC in lower pH [34]. The solubility of isoniazid increased at acidic pH due to its basic nature. Lower pH of the medium favored both the swelling of the polymer and solubility of the drug.

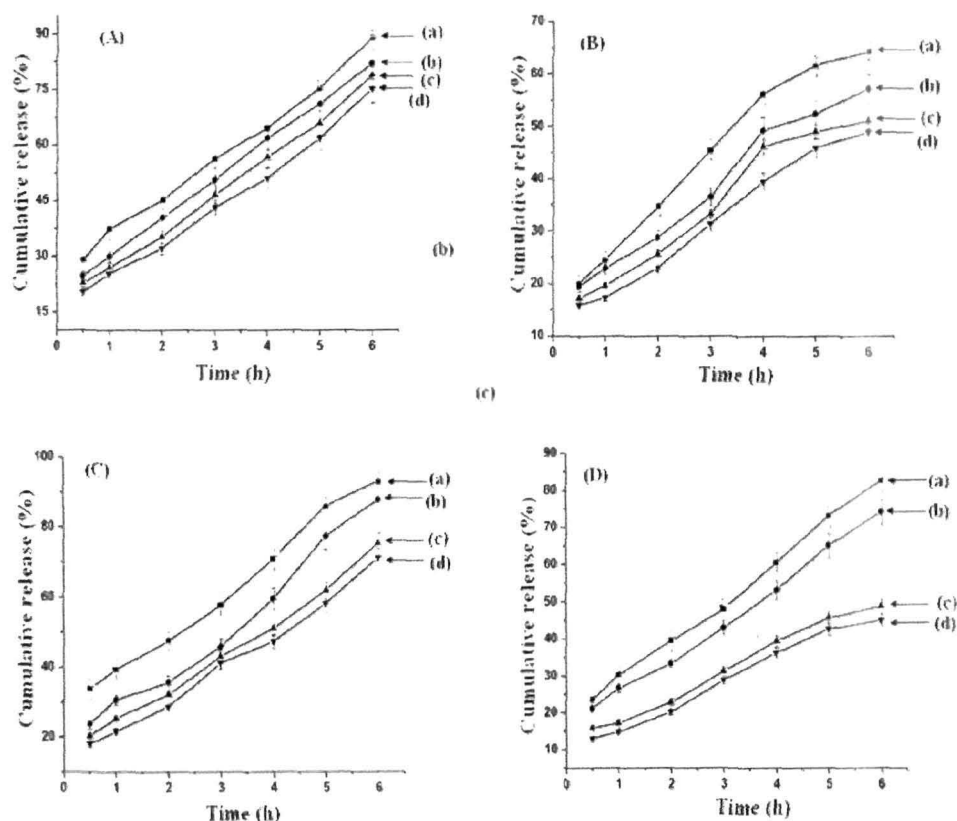


Figure 4.20. Cumulative release at (A) with variation of MMT at pH =1.2 {(a)CMC/M0/GA50, (b) CMC /M1/GA50, (c) CMC /M3/GA50, (d) CMC /M5/GA50}, (B) with variation of MMT at pH=7.4 {(a)CMC/M0/GA50, (b) CMC /M1/GA50, (c) CMC /M3/GA50, (d) CMC /M5/GA50}, (C) with variation of GA at pH= 1.2{(a) CMC M5/GA10, (b) CMC /M5/GA30, (c) CMC /M5/GA50, (d) CMC /M5/GA70} and (D) with variation of GA at pH= 7.4 {(a) CMC M5/GA10, (b) CMC /M5/GA30, (c) CMC /M5/GA50, (d) CMC /M5/GA70}

It was also observed that the cumulative release (%) of isoniazid decreased with the increase in MMT content (Figure 4.20. A and B) and increased with the increase in the period of time. The percentage swelling of the nanoparticles decreased with the increase in the concentration of MMT. Therefore, in order to facilitate the release of isoniazid the solvent particles could not diffuse properly to interact with the isoniazid molecules encapsulated in the nanoparticles. With the increase in time, the percentage degree of swelling increased and more and more solvent molecules could reach the drug molecule and hence helped to release the isoniazid from the nanoparticles.

It was also seen that the cumulative release (%) of isoniazid decreased with the increase in the concentration of GA (Figure 4.20.C and D). This was due to the increase in crosslinking density of the nanoparticles. The more the crosslinking, less the accessibility of solvent to penetrate into the CMC-MMT nanoparticles and thus a decrease in cumulative release (%) were observed.

4.3.8. Cell Viability Study

The effect of varying MMT concentration (0-5%) and time (6, 12, and 24 h) on cell viability is shown in Figure 4.21. Figure 4.21. (a) showed that CMC was non toxic. It had high cell viability of around 97%.

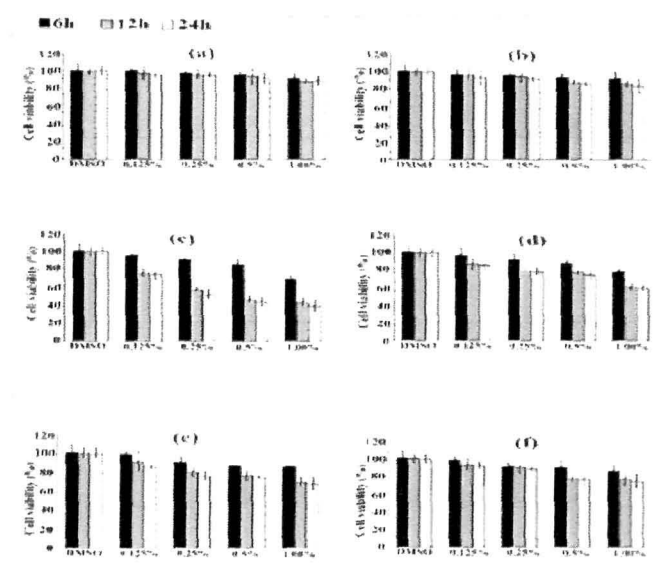


Figure 4.21. Cell viability study with variation of (a) CMC, (b) MMT, (c) isoniazid, and (d) CMC/M0/GA50 (e) CMC/M1/GA50 (f) CMC/M5/GA50 at 6 h, 12 h, and 24 h

It was also observed that the cell viability varied between 84-100% within the studied MMT concentration (Figure 4.21. b). This indicated that the MMT was not cytotoxic to the cells. The cell viability decreased with the increase in the concentration of the nanoparticles and time interval.

Isoniazid was found to be highly cytotoxic. The cell viability for 1% isoniazid at 24h is only 40% (Figure 4.21.c). The cytotoxicity was found to be less for isoniazid loaded CMC-MMT nanoparticles compared to those of isoniazid alone. The MMT containing CMC nanoparticles hindered the release of isoniazid due to its tortuous path and hence reduced the interaction of drug with the cell. It was observed further { Figure 4.21. (d-f)} that the cell viability of MMT containing nanoparticles was more compared to MMT free nanoparticles. This might be due to the fact that the silicate layers of clay stalled the release of drug in the cell because of its meandering path.

4.4. Section D-Preparation and characterization of isoniazid loaded phosphorylated chitosan /montmorillonite nanoparticles for controlled drug delivery applications.

4.4.1. Nuclear Magnetic Resonance (NMR) study

Phosphorylation of chitosan can be confirmed by ^{31}P NMR. The position of phosphorylation can also be distinguished from the signals of proton-decoupled ^{31}P NMR spectra in Figure 4.22.

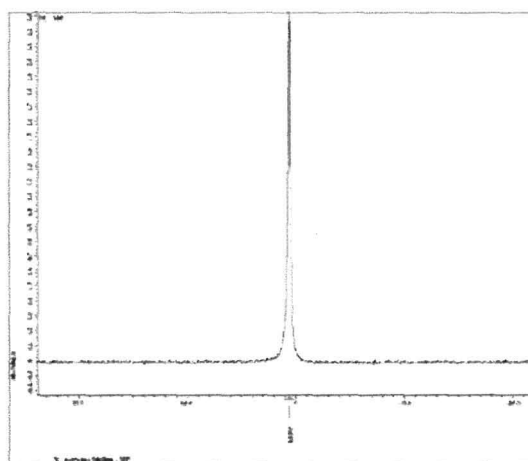


Figure 4.22. ^{31}P NMR spectra of PCTS

The appearance of a peak at 0.6135 ppm indicates that some groups in chitosan is phosphorylated. It is observed that some amino groups in chitosan could undergo the reaction to form phosphorylamide groups according to Wang et al. [36].

4.4.2. Effect of variation of MMT and GA concentration on the different properties of isoniazid loaded CMC-MMT nanoparticles

The results showing the effect of variation of MMT and GA concentration on different properties of PCTS nanoparticles are shown in Table 4.6. The encapsulation efficiency of MMT free crosslinked nanoparticles was found to be higher compared to that of MMT containing crosslinked nanoparticles. The encapsulation efficiency decreased with the increase in MMT content in the nanoparticles. This could be attributed to the presence of the silicate layers of MMT. The –OH groups of MMT could interact with the residual –NH₂ group of PCTS and –CHO groups of GA resulting in extension of the polymer chains. The silicate layers of MMT also hindered the movement of the intercalated polymer chains freely and might assist the formation of fine channels from inner to outer surface of the nanoparticles during drying process. The more the encapsulation of MMT, the higher is the chance formation of fine channels. Thus, part of the drug might get diffused from the particles to the external medium resulting in the decrease of encapsulation efficiency. The interference offered by the MMT layers was absent in MMT free crosslinked nanoparticles. Hence, it showed higher encapsulation efficiency. The high encapsulation efficiency of the nanoparticles can also be attributed to the hydrophilic bulky phosphate groups of PCTS. Due to these hydrophilic groups in PCTS, the nanoparticles swelled more and so the drug can easily enter in the nanoparticles.

Similarly, at a fixed MMT content, the encapsulation efficiency of nanoparticles was found to further decrease with the increase in the glutaraldehyde (GA) concentration. GA might further restrict the free motion of the intercalated polymer chains and thus assist the formation of porous structure.

The average diameter of the nanoparticles was obtained in the range 421-451 nm. The variation in MMT concentration did not significantly affect the particle size. However, the average diameter showed a decreasing trend on increasing the GA concentration. The

residual amino groups present in PCTS interacted with the hydroxyl group of MMT and GA. With the increase in the concentration of GA, the availability of free residual amino groups on nanoparticles reduces due to which the nanoparticles became more compact and hence the diameter would be less.

Table 4.6. Effect of variation of MMT and GA concentration on the different properties of PCTS nanoparticles

Sample code	Yield of nanoparticle (%)	Encapsulation efficiency (%)	Average diameter (nm)	Zeta potential (mV)
PCTS/M0/GA50	94.77(±0.03)	89.11(±0.01)	451.2(±9)	35.11(±0.01)
PCTS/M1/GA50	94.39(±0.01)	87.18(±0.02)	463.5(±10)	32.89(±0.03)
PCTS/M3/GA50	94.62(±0.03)	84.49(±0.02)	467.2(±9)	31.32(±0.01)
PCTS/M5/GA50	93.91(±0.01)	82.80(±0.01)	462.1(±8)	31.03(±0.01)
PCTS/M5/GA10	94.25(±0.04)	84.15(±0.02)	473.4(±9)	38.41(±0.01)
PCTS/M5/GA30	94.81(±0.04)	83.63(±0.03)	468.1(±8)	37.20(±0.02)
PCTS/M5/GA70	94.49(±0.02)	81.51(±0.01)	421.9(±9)	29.99(±0.02)

*each value represents average of five readings, standard deviation in parenthesis

4.4.3. Fourier Transform Infra-red Spectroscopy (FTIR) study

FTIR spectra of chitosan, PCTS, MMT, Isoniazid and isoniazid loaded PCTS-MMT nanoparticles are shown in Figure 4.23. As described earlier in the previous section, the basic absorption bands of chitosan (curve a) appeared at 3442 cm^{-1} (OH stretching and NH stretching, overlapped), 2939 cm^{-1} (CH stretching). The characteristic peaks of amide I and amide II appeared at 1639 cm^{-1} (C=O stretching) and 1455 cm^{-1} (N-H in plane deformation coupled with C≡N stretching) respectively. The other peaks appeared at 1156 cm^{-1} (bridge -O- stretching), and 1062 cm^{-1} (-CO stretching) were also shown. The spectrum of PCTS showed that the peaks at 1639 cm^{-1} and 1455 cm^{-1} from amide absorption still remain while new peaks for the stretching vibrations of P=O and P-O near 1258 and 1025 cm^{-1} have appeared [37]. These results suggest that some hydroxyl groups in chitosan are phosphorylated.

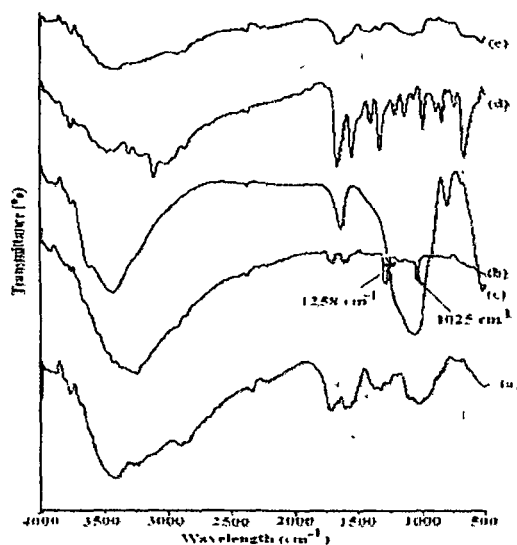


Figure 4.23. FTIR spectra of (a) Chitosan, (b) PCTS, (c) MMT, (d) Isoniazid, and (e) PCTS/MS/GA50

Curve c represents the spectra of MMT. The peaks exhibited in the spectrum for MMT at 3435, 1639 and 1051-544 cm^{-1} were for -OH stretching, -OH bending and oxide bands of metals like Si, Al, Mg, etc. Curve d represents the spectrum of isoniazid. The absorption peaks appeared at 1664 and 1551 cm^{-1} were due to the amide I (C=O stretching) and amide II (N-H bending of secondary amide group) respectively. Besides this, multiple peaks appeared in the range 1410-669 cm^{-1} .

All the characteristic peaks of PCTS, MMT and isoniazid appeared and their intensities decreased in the spectrum of isoniazid loaded chitosan-MMT nanoparticles (curve e).

4.4.4. X-ray diffraction (XRD) study

The phosphorylation of chitosan was also confirmed by XRD study. The XRD diffractograms of the Chitosan, PCTS, MMT, isoniazid and isoniazid loaded PCTS-MMT nanoparticles are shown in Figure 4.24. Chitosan showed two distinct crystalline peaks at $2\theta = 10^\circ$ and 20.2° due to (020) and (100) plane, respectively [Figure 4.24.c]. Conversely, in the case of PCTS [Figure 4.24 d], the peak at 10° disappeared, and the intensity of the peak at $2\theta = 20^\circ$ diminished [37].

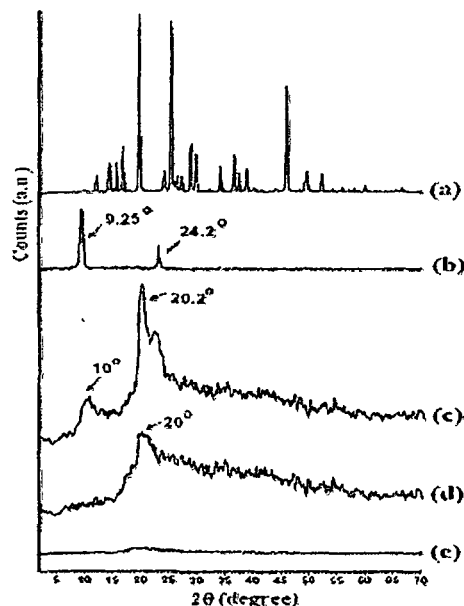


Figure 4.24. XRD patterns of (a) Isoniazid, (b) MMT, (c) chitosan, (d) PCTS, and (e) PCTS/MS/GA50

Isoniazid (curve 4.24.a) shows multiple peaks at $2\theta=12^\circ$ to 50° due to its crystalline nature. MMT exhibits the two characteristic peaks at $2\theta=9.25^\circ$ and 24.2° which are assigned for (001) and (002) plane (figure 4.24. b). The characteristic peaks for isoniazid and MMT were found to disappear in the diffractogram of PCTS-MMT nanoparticles (curve 4.24. e). These findings suggested an increase in gallery spacing of MMT due to intercalation and occurrence of a molecular level dispersion of isoniazid in isoniazid loaded PCTS-MMT nanoparticles.

4.4.5. Scanning electron microscopy (SEM) study

SEM analysis was performed to study the surface morphology of PCTS nanoparticles and PCTS-MMT nanoparticles loaded with isoniazid. Figure 4.25.a and 4.25. b represents the SEM micrographs of PCTS nanoparticles and PCTS-MMT nanoparticles respectively. The surface of PCTS nanoparticles (Figure 4.25. a) appeared rough and slightly agglomerated. However, on addition of MMT into PCTS nanoparticles the smoothness as well as the agglomeration decreased (Figure 4.25. b).

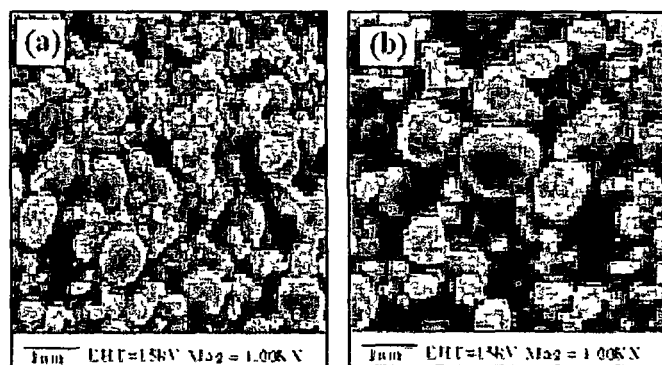


Figure 4.25. SEM micrographs of (a) PCTS/M0/GA50 and (b) PCTS/M5/GA50

4.4.6. Transmission electron microscopy (TEM) study

TEM micrographs of isoniazid loaded PCTS nanoparticles devoid of MMT and with MMT are shown in Figure 4.26.a and 4.26. b respectively. Figure 4.26.b showed the presence of platelets of MMT tactoids in which the dark lines were the intersection of MMT layers. The bright areas were for polymer matrix and isoniazid. The results indicated that MMT was incorporated and dispersed in the PCTS matrix.

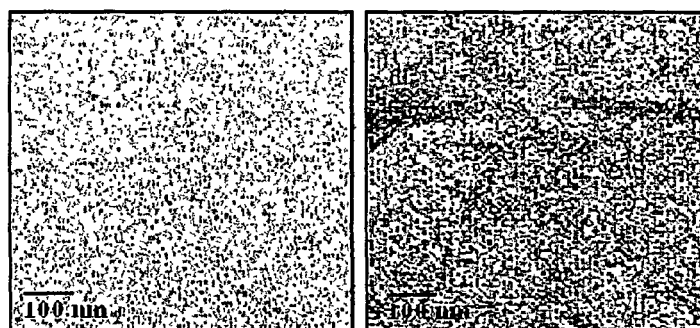


Figure 4.26. TEM micrographs of PCTS nanoparticles (a) without MMT range and (b) with MMT at 100 nm scale respectively

4.4.7. Swelling Study

The effect of pH on the percentage swelling of isoniazid loaded nanoparticles at two different pH namely, 1.2 and 7.4 are shown in Figure 4.27. It was observed that the swelling of isoniazid loaded PCTS-MMT nanoparticles was more in gastric pH (1.2) than in intestinal pH (7.4). At lower pH, the residual free amine groups and phosphate groups

become protonated and generated a repulsive force between the adjacent positively charged polymer chains causing the swelling of the polymer and consequently diffusion of more amount of drug out of the polymer matrix. In alkaline pH, protonation was prevented and hence swelling decreased.

Figure 4.27. (A) showed that with the increase in the concentration of MMT, the percentage swelling degree decreased. Water absorption decreased by the presence of dispersed phase of MMT into the PCTS matrix of the nanoparticles. MMT particles acted as a barricade for water molecules and decreased the water transmission through the crosslinked PCTS-MMT nanoparticles. Similarly, nanoparticles containing higher concentration of GA (Figure 4.27. B) swelled less due to higher crosslinking densities and less availability of the polar groups.

Furthermore, the percentage swelling degree was found to increase with the increase in time. With the increase in the time period, higher amount of the solvents can penetrate into the PCTS matrix, resulting in the increase in the percentage swelling degree.

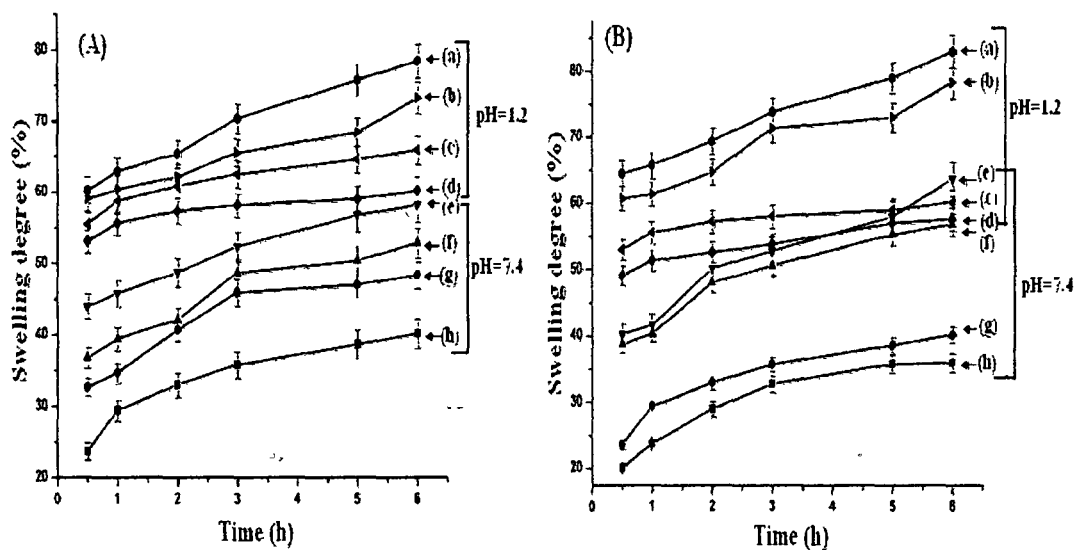


Figure 4.27. Percentage swelling degree at pH 1.2 and 7.4: (A) {(a)PCTS/M0/GA50, (b) PCTS /M1/GA50, (c) PCTS /M3/GA50, (d) PCTS /M5/GA50, (e) PCTS /M0/GA50, (f) PCTS /M1/GA50, (g) PCTS /M3/GA50, (h) PCTS /M5/GA50} and (B) {(a) PCTS M5/GA10, (b) PCTS /M5/GA30, (c) PCTS /M5/GA50, (d) PCTS /M5/GA70, (e) PCTS /M5/GA10, (f) PCTS /M5/GA30, (g) PCTS /M5/GA50, (h) PCTS /M5/GA70}

4.4.8. *In vitro* Release Studies

The drug release profile of the nanoparticles at two different pH namely 1.2 and 7.4 are shown in Figure 4.28. The cumulative release (%) of isoniazid from PCTS-MMT nanoparticles was found to be pH dependent. The cumulative release (%) of isoniazid decreased with the increase in the pH of the medium. The difference in release profile was due to the difference in the swelling of PCTS in gastric and intestinal pH. PCTS was swelled more in gastric pH compared to intestinal pH medium. The faster drug release rate in lower pH medium was due to the wobbly nanoparticles structure, caused by the protonation of residual amino groups and phosphate groups of PCTS in lower pH.

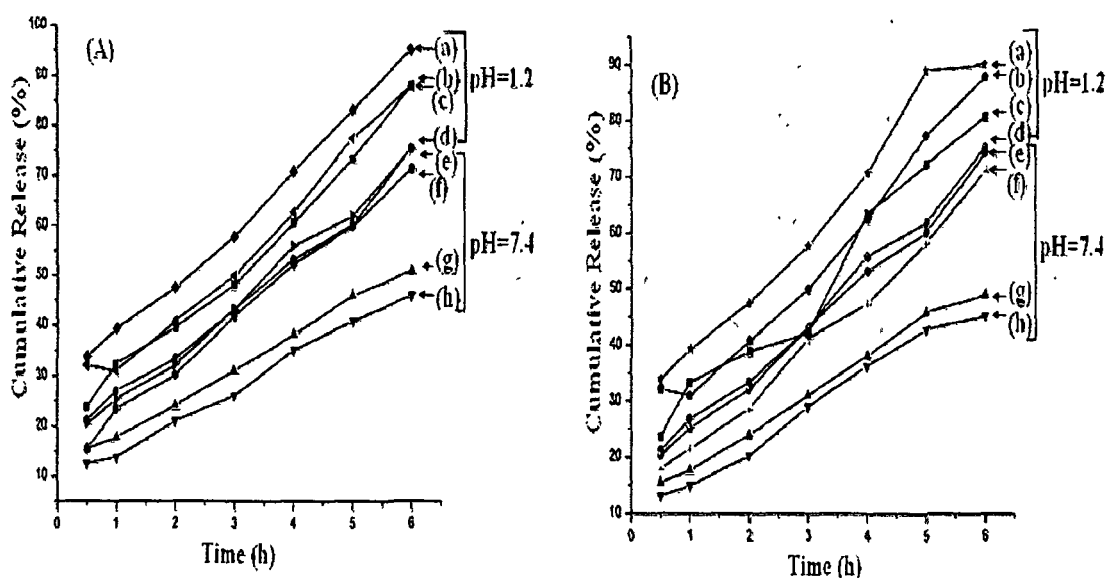


Figure 4.28. Cumulative release at (A) with variation of MMT at pH =1.2 and 7.4 {(a)PCTS/M0/GA50, (b) PCTS /M1/GA50, (c) PCTS /M3/GA50, (d) PCTS /M5/GA50, (e)PCTS/M0/GA50, (f) PCTS /M1/GA50, (g) PCTS /M3/GA50, (h) PCTS /M5/GA50}, (B) with variation of GA at pH= 1.2 and 7.4 {(a) PCTS M5/GA10, (b) PCTS /M5/GA30, (c) PCTS /M5/GA50, (d) PCTS /M5/GA70 (e) PCTS M5/GA10, (f) PCTS /M5/GA30, (g) PCTS /M5/GA50, (h) PCTS /M5/GA70}

It was also observed that the cumulative release (%) of isoniazid decreased with the increase in MMT content (Figure 4.28. A) and increased with the increase in the period of time. The percentage swelling of the nanoparticles decreased with the increase in the concentration of MMT. Therefore, in order to facilitate the release of isoniazid the solvent particles could not diffuse properly to interact with the isoniazid molecules

encapsulated in the nanoparticles. With the increase in time, the percentage degree of swelling increased and more and more solvent molecules could reach the drug molecule and hence helped to release the isoniazid from the nanoparticles.

It was also seen that the cumulative release (%) of isoniazid decreased with the increase in the concentration of GA (Figure 4.28.B). This was due to the increase in crosslinking density of the nanoparticles. The more the crosslinking, less the accessibility of solvent to penetrate into the PCTS-MMT nanoparticles and thus a decrease in cumulative release (%) were observed.

4.4.9. Cell Viability Study

The effect of varying MMT concentration (0-5%) and time (6, 12, and 24 h) on cell viability is shown in Figure 4.29. Figure 4.29. (a) showed that PCTS was non toxic. It had high cell viability of around 95%. It was also observed that the cell viability varied between 82-100% within the studied MMT concentration (Figure 4.29. b). This indicated that the MMT was not cytotoxic to the cells. The cell viability decreased with the increase in the concentration of the nanoparticles and time interval.

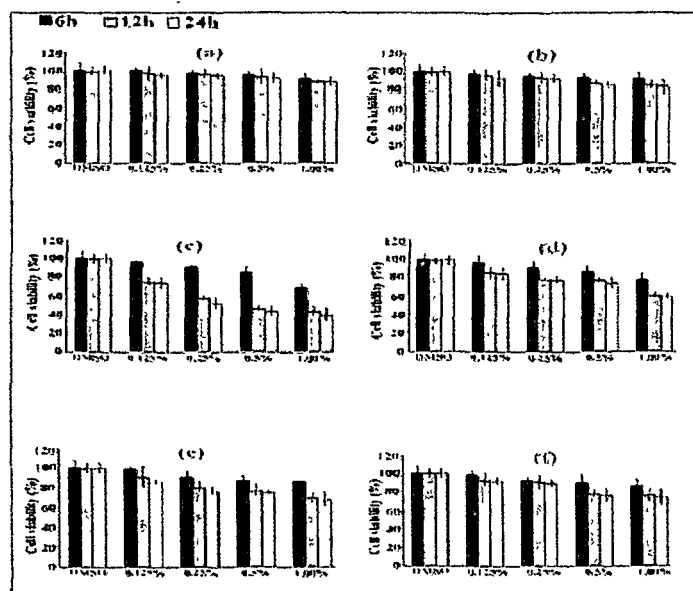


Figure 4.29. Cell viability study with variation of (a) PCTS, (b) MMT, (c) isoniazid, and (d) PCTS/M0/GA50 (e) PCTS/M1/GA50 (f) PCTS/M5/GA50 at 6 h, 12 h, and 24 h

Isoniazid was found to be highly cytotoxic. The cell viability for 1% isoniazid at 24h is only 40% (Figure 4.29.c). The cytotoxicity was found to be less for isoniazid loaded CMC-MMT nanoparticles compared to those of isoniazid alone. The MMT containing CMC nanoparticles hindered the release of isoniazid due to its tortuous path and hence reduced the interaction of drug with the cell. It was observed further { Figure 4.29. (d-f)} that the cell viability of MMT containing nanoparticles was more compared to MMT free nanoparticles. This might be due to the fact that the silicate layers of clay stalled the release of drug in the cell because of its meandering path.

4.5. Section E-Preparation and characterization of isoniazid loaded soy flour /montmorillonite nanoparticles for controlled drug delivery applications.

4.5.1. Effect of variation of MMT and GA concentration on the different properties of SF nanoparticles

The result showing the effect of variation of MMT and GA concentration on different properties of SF nanoparticles are shown in Table 4.7. Encapsulation efficiency and drug loading efficiency of crosslinked nanoparticles without MMT exhibited a higher value compared to that of MMT containing crosslinked nanoparticles. Both the encapsulation efficiency and drug loading efficiency were found to decrease with the increase in MMT content in the nanoparticles. This could be attributed to the presence of the silicate layers of MMT. The silicate layers of MMT restricted the movement of the intercalated polymer chains freely. As a result, the formation of porous structure might take place during dehydration force. This in turn would produce many fine channels from the interior to the surface of the particles. Thus, part of the drug might get diffused from the particles to the external medium resulting in the decrease of both encapsulation and drug loading efficiency. Hua et. al prepared oflotoxin /MMT/chitosan microspheres and reported that the collapse of polymeric network structure at higher MMT loading might be responsible for lower loading of oflotoxin. [38]. The hindrance offered by the MMT layers was absent in MMT free crosslinked nanoparticles. Hence, it showed high encapsulation and drug loading efficiency.

Similarly, at a fixed MMT content, the drug loading efficiency and encapsulation efficiency of nanoparticles were found to decrease with the increase in the GA concentration. GA, a crosslinker, might further restrict the free motion of the intercalated polymer chains and thus facilitating the formation of porous structure. The drug could migrate from the interior of the nanoparticles to the outer surface or preparing medium through the channels.

Table 4.7. Effect of variation of MMT and GA concentration on the different properties of SF nanoparticles

Sample code.	Yield of nanoparticle (%)	Encapsulation efficiency (%)	Drug loading efficiency (%)	Average diameter (nm)	Zeta potential (mV)
SF/M0/GA50	90.54(±0.05)	60.93(±0.02)	82.23(±0.05)	642.2(±12)	-41.32(±0.03)
SF/M1/GA50	90.82(±0.01)	57.41(±0.04)	80.71(±0.01)	641.7(±15)	-40.13(±0.08)
SF/M3/GA50	91.26(±0.03)	54.53(±0.04)	76.12(±0.03)	647.4(±12)	-42.29(±0.03)
SF/M5/GA50	91.12(±0.05)	52.12(±0.01)	71.33(±0.01)	632.9(±10)	-39.16(±0.04)
SF/M5/GA10	91.13(±0.01)	53.62(±0.03)	72.93(±0.04)	648.2(±10)	-43.88(±0.03)
SF/M5/GA30	91.66(±0.03)	52.91(±0.01)	72.03(±0.05)	638.1(±12)	-40.25(±0.01)
SF/M5/GA70	90.81(±0.01)	50.69(±0.04)	71.01(±0.03)	629.6(±14)	-34.72(±0.01)

The average diameter of the nanoparticles was obtained in the range 633–648 nm. The variation in MMT concentration did not affect the particle size. However, the average diameter showed a decreasing trend on increasing the GA concentration. The amino groups present in soy flour interacted with the hydroxyl group of MMT and GA. The availability of free amino groups on nanoparticles reduced with the increase in the

concentration of GA due to which the nanoparticles became more compact and hence the diameter would be less

Zeta potential values of the nanoparticles were found in the range -35 to -44mV indicating good stability of the nanoparticles. The variation of MMT did not show significant effect on the zeta potential. However, the zeta potential values increased as the GA concentration increased from 0 to 70%. The increase in the zeta potential indicated that the stability of the nanoparticles increased with the increase in the concentration of GA and they would not aggregate in acidic or basic medium.

4.5.2. Fourier Transform Infra-red Spectroscopy (FTIR) study

In the spectrum of pure soy flour (SF) (Figure 4.30. a), the broad absorption band appeared at around 3450 cm^{-1} due to the hydrogen-bonded OH stretching and NH_2 asymmetric stretching vibrations. The characteristic peaks of amide I, amide II and amide III appeared at 1648 cm^{-1} ($\text{C}=\text{O}$ stretching), 1548 cm^{-1} (N-H bending) and 1240 cm^{-1} ($\text{C}=\text{N}$ stretching) respectively [39].

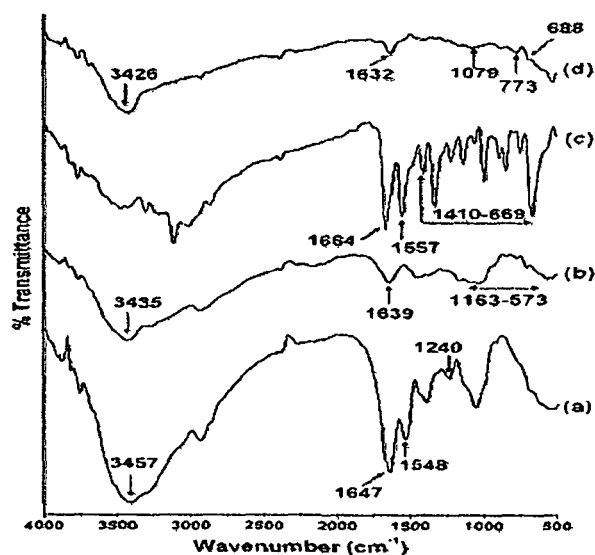


Figure 4.30. FTIR spectra of (a) Pure SF, (b) MMT, (c) Isoniazid, and (d) SF/MS/GA50

The peaks exhibited in the spectrum for MMT (Figure 4.30.b) at 3435 , 1639 and $1163\text{-}573\text{ cm}^{-1}$ were for -OH stretching, -OH bending and oxide bands of metals like Si, Al,

Mg, etc. Figure 4.30 c represents the spectrum of isoniazid. The absorption peaks appeared at 1664 and 1557cm^{-1} were due to the amide I (C=O stretching) and amide II (N-H bending of secondary amide group) respectively. Besides this, multiple peaks appeared in the range $1410\text{-}669\text{ cm}^{-1}$.

All the characteristic peaks of SF, MMT and isoniazid appeared and their intensities decreased in the spectrum of isoniazid loaded SF-MMT nanoparticles (Figure 4.30 d). The intensity of the peak of soy flour appeared in the range $3450\text{-}3200\text{ cm}^{-1}$ (Figure 4.30 a) decreased and shifted to lower wave number. This indicated an interaction between the hydroxyl group of NH_2 group of MMT and SF.

4.5.3. X-ray diffraction (XRD) study

Figure 4.31 (a-d) represents the XRD diffraction pattern of isoniazid, MMT, pure SF and isoniazid loaded SF nanoparticles. Curve 4.31 (a) showed multiple peaks at $2\theta=12$ to 50° which was due to its crystalline nature of isoniazid. Soy flour (curve 4.31 b) shows its characteristic diffraction peak at $2\theta=200$ [28].

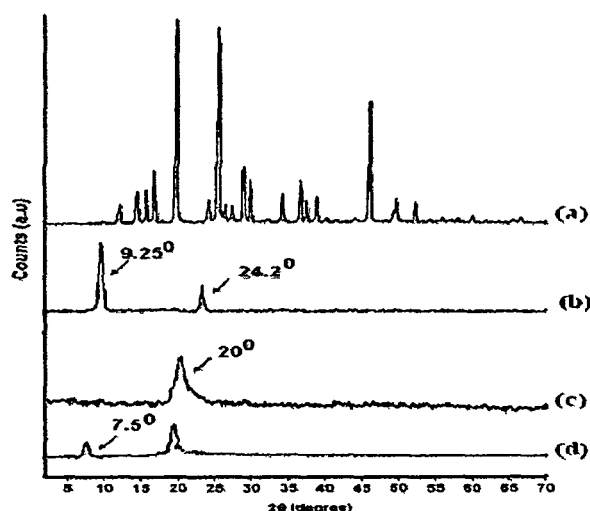


Figure 4.31. XRD patterns of (a) Isoniazid, (b) MMT, (c) SF, and (d) SF/M5/GA50

MMT exhibits the two characteristic peaks at $2\theta=9.25^\circ$ and 24.2° which are assigned for (001) and (002) plane (curve 4.31 b) [39]. The peak of isoniazid was found to disappear in the diffractogram of MMT/ SF nanoparticles (curve 4.30 d).

However, after the incorporation of MMT the intensity of the peak at $2\theta = 20^\circ$ decreased in intensity and shifted to lower 2θ value. Furthermore, a new peak corresponding to MMT with decreased intensity appeared at around $2\theta = 7.5^\circ$. This indicated that the MMT layers were partially exfoliated and dispersed into the nanocomposite. The subordination of intensity of the peak at $2\theta = 9.25^\circ$ to $2\theta = 7.5^\circ$ indicated the collapse of the layered structure of MMT incorporated nanoparticles.

4.5.4. Scanning electron microscopy (SEM) study

SEM micrographs of SF nanoparticles and SF-MMT nanoparticles are shown in Figure 4.32.a and 4.32.b respectively. The surface of the nanoparticles without MMT appeared less smooth and agglomerated as compared to only SF nanoparticles. Similar results were reported by Dong et.al. [40] while studying the morphology of paclitaxel loaded PLGA/MMT nanoparticles.

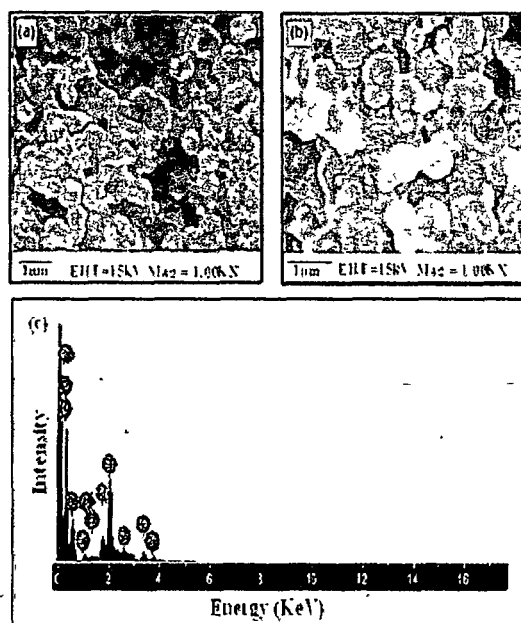


Figure 4.32. SEM micrographs of (a) SF/M0/GA50, (b) SF/M5/GA50, and (c) EDX of SF/M5/GA50

Further work was done through energy dispersive X-ray (EDX) analysis of the nanoparticles observed in the fracture for the clay loaded nanoparticles as shown in Figure 4.32.c. Elements such as Al, Na and Si, which are mainly from the silicate

nanoclay, were detected indicating that the MMT had been successfully incorporated into the composite [41]

4.5.5. Transmission electron microscopy (TEM) study

TEM micrographs of isoniazid loaded SF nanoparticles devoid of MMT and with MMT are shown in Figure 4.33 (a) and 4.33 (b) respectively. Figure 4.33 (b) showed the presence of platelets of MMT tactoids in which the dark lines were the intersection of MMT layers. The bright areas were for SF matrix and isoniazid. Similar observation was reported by Choi et al. while studying the anionic MMT (cloisite Na⁺) and PVA composite structure by TEM [42]. The results indicated that MMT was incorporated and dispersed in the SF matrix.

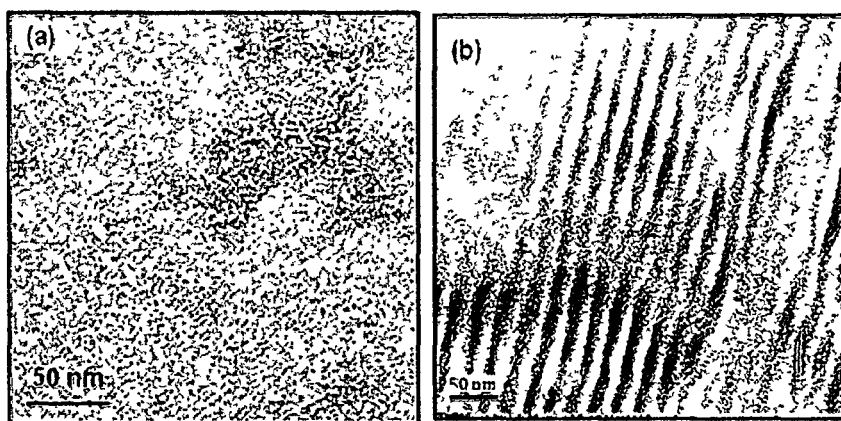


Figure 4.33. TEM micrographs of (a) SF/M0/GA50, and (b) SF/M5/GA50

4.5.6. Swelling Study

The effect of pH on the percentage swelling of isoniazid loaded nanoparticles at two different pH namely, 1.2 and 7.4 are shown in Figure 4.34. It was observed that the swelling of isoniazid loaded SF-MMT nanoparticles was more in intestinal pH (7.4) than in gastric pH (1.2). Under acidic pH values, most of the carboxylate anions of SF become protonated. The main anion-anion repulsive forces were diminished and accordingly a decrease in swelling values was observed. At alkaline pH values, some of carboxylate groups are ionized and the electrostatic repulsion between COO⁻ groups

caused an augmentation of the swelling degree [43]. Furthermore, the percentage swelling degree was found to increase with the increase in time.

With the increase in the concentration of MMT, the percentage swelling degree decreased. This is due to the fact that the silicate layers of MMT provided torturous pathway for the diffusion of water through the nanoparticles. Similarly, nanoparticles containing higher concentration of GA swelled less due to higher crosslinking densities and less availability of the polar groups.

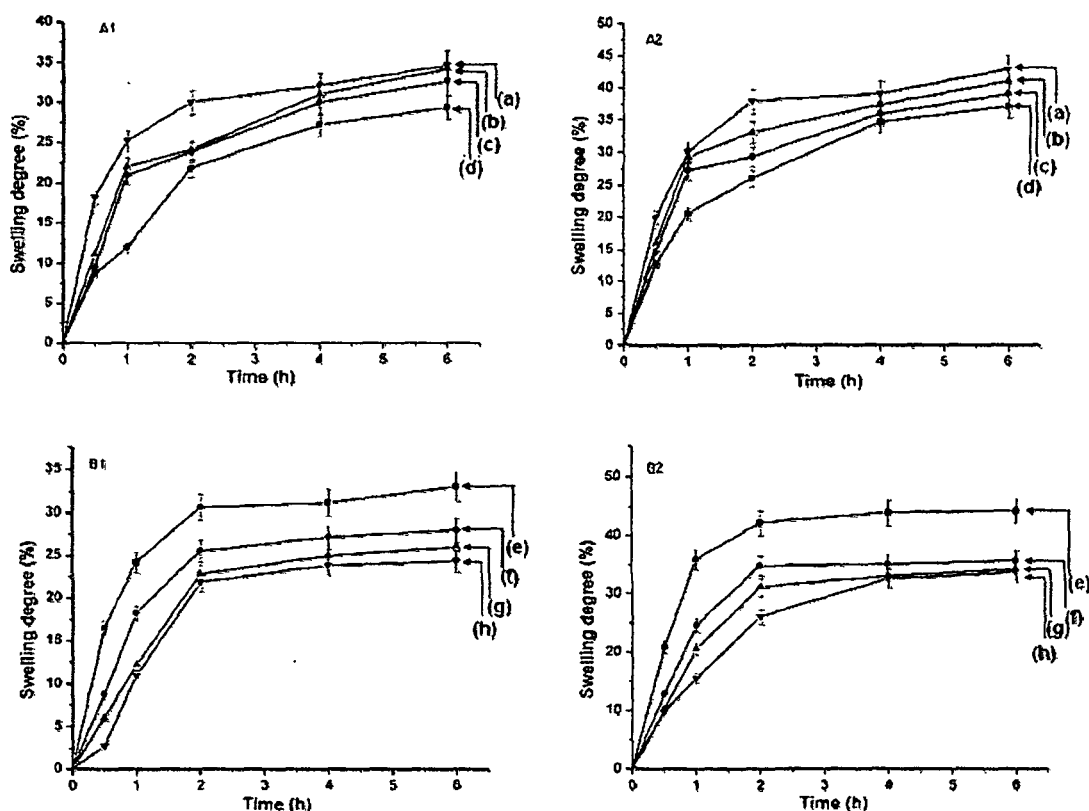


Figure 4.34. Percentage swelling degree at A1, B1= pH 1.2 and A2, B2= pH 7.4 of (a) SF/M0/GA50, (b) SF/M1/GA50, (c) SF/M3/GA50, (d) SF/M5/GA50, (e) SF/M5/GA10, (f) SF/M5/GA30, (g) SF/M5/GA50, (h) SF/M5/GA70

4.5.7. *In vitro* Release Studies

The drug release profile of the nanoparticles at two different pH namely 1.2 and 7.4 are shown in Figure 4.35. (A-D). The cumulative release (%) of isoniazid from SF-MMT nanoparticles was found to be pH dependent. The cumulative release (%) of isoniazid

increased with the increase in the pH of the medium. In alkaline medium, the breaking of hydrogen bonding between the SF and isoniazid facilitated the release of the drug and thus enhanced the cumulative release [44].

Cumulative release (%) of isoniazid was also found to increase with the increase in time, decrease in MMT content and decrease in GA concentration of the nanoparticles. The explanation for this observation was similar to that of stated earlier.

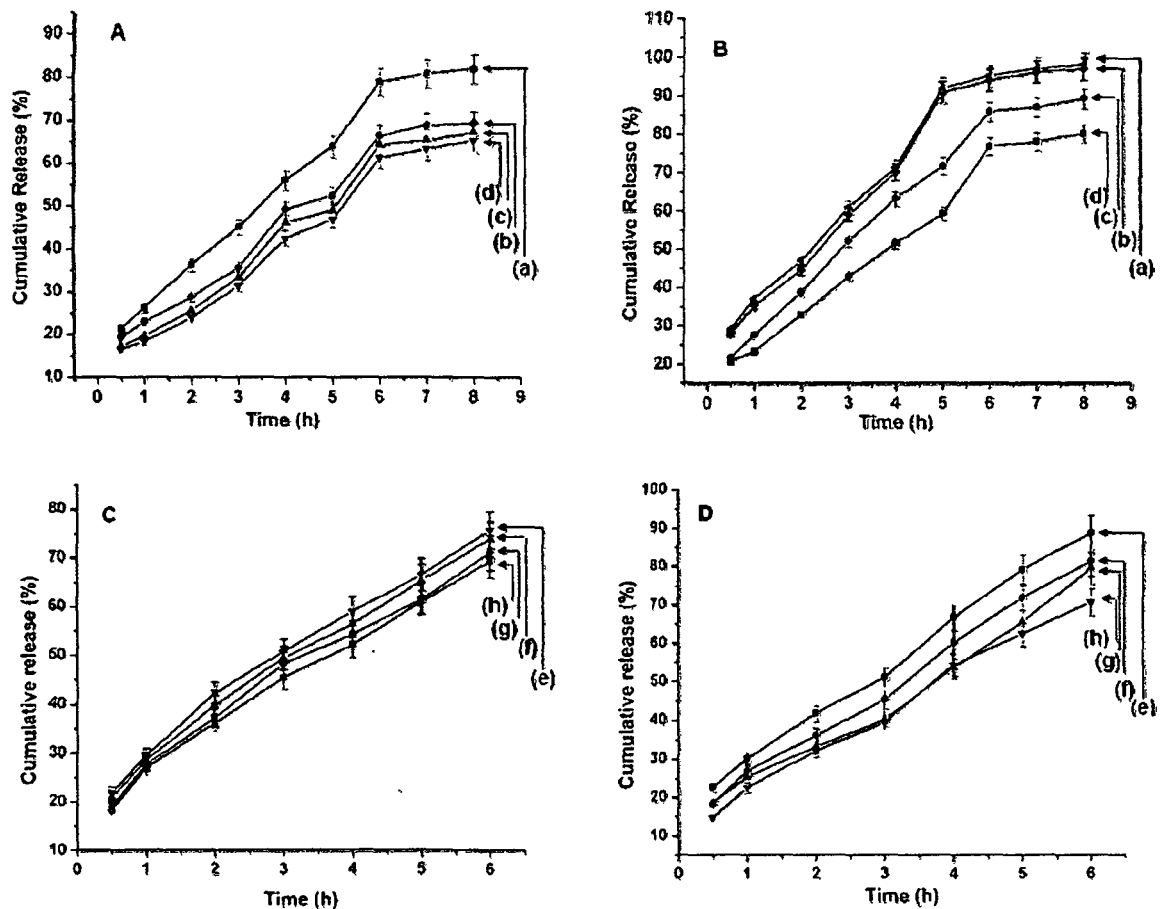


Figure 4.35. Cumulative percentage drug release at (A), (C) = pH 1.2 and (D), (E) = pH 7.4 of (a) SF/M0/GA50, (b) SF/M1/GA50, (c) SF/M3/GA50, (d) SF/M5/GA50, (e) SF/M5/GA10, (f) SF/M5/GA30, (g) SF/M5/GA50, (h) SF/M5/GA70

4.5.8. Cell Viability Study

The results of the MTT-assay are shown in Figure 4.36. It was observed that the cell viability varied between 85-95% within the studied MMT concentration. This indicated

that the MMT was not cytotoxic to the cells (Figure 4.36 a). SF showed very low cytotoxicity as evident from (Figure 4.36.b). Figure 4.36. c and 4.36. d showed the cell viability (%) of isoniazid alone and clay free isoniazid loaded nanoparticles. In both the cases, the cell viability decreased with the increase in the concentration of isoniazid. The cytotoxicity was found to be less in the case of isoniazid loaded polymeric nanoparticles compared to those of isoniazid alone. The polymer slowed down the release of isoniazid and hence decreased the interaction of drug with the cell. It was observed further (Figure 4.36.d, 4.36.e and 4.36f) that the cell viability of clay containing nanoparticles was more compared to clay free nanoparticles. This might be due to the fact that the silicate layers of clay hindered the release of drug in the cell because of its tortuous path.

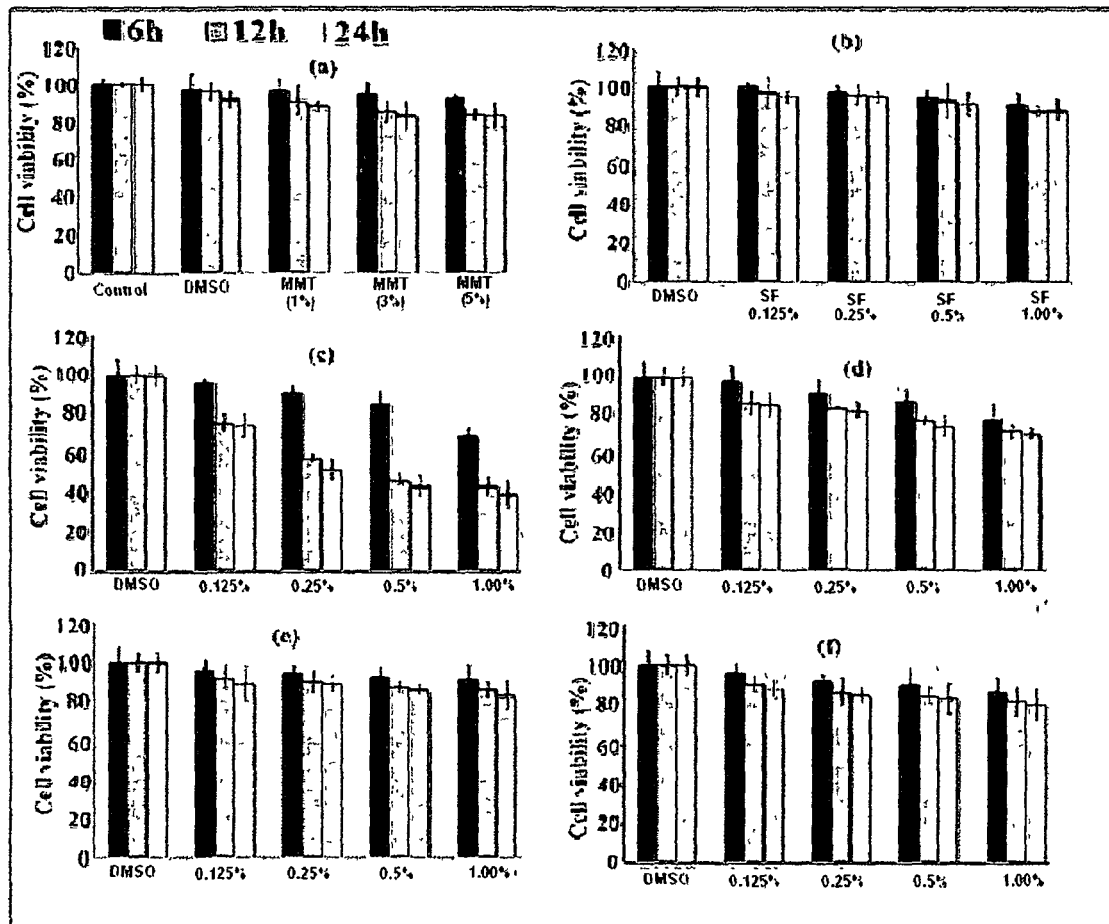


Figure 4.36. Cell viability study with variation of (a) MMT, (b) SF, (c) isoniazid, and (d) SF/M0/GA50, (e) SF/M1/GA50, (f) SF/M5/GA50 at 6 h, 12 h, and 24 h

Reference

- [1] Banik, N., et al. *New J. Chem.* **37**, 3981--3990, 2013.
- [2] Iman, M., et al. *Ind. Eng. Chem. Res.* **52**, 6969--6983, 2013.
- [3] Mukhopadhyay, P., et al. *J. App. Polym. Sci.* **129**, 835--845, 2013.
- [4] Banik, N., et al. *RSC Adv.* **2**, 10519--10528, 2012.
- [5] Lu, P. & Hsieh, Y. *Carbohydr. Pol.* **82**(2), 329--336, 2010.
- [6] Gupta K.C. & Ravi Kumar, M.N. *J. Mater. Sci.: Mater. Med.* **12**(9), 753--759, 2001.
- [7] Guliyeva, U., et al. *Eur. J. Pharm. Biopharm.* **62**(1), 17--25, 2006.
- [8] Gupta N.V. & Shivakumar, H.G., *Trop. J. Pharm. Res.* **9**(3), 257--264, 2010.
- [9] Bceker, C., et al. *J. Pharm. Sci.* **96**, 522--531, 2007.
- [10] Clift, M.J.D. et al. *Biomacromol.* **12**, 3666--3673, 2011.
- [11] da Trindade Neto, C. G., et al. *Polym. Int.* **54**, 659--666, 2005.
- [12] Atta, N. F., et al. *Int. J. Electrochem. Sci.* **6**, 5097--5113, 2011.
- [13] Amaral, I.F., et al. *J. Biomater. Sci., Polym. Ed.* **16**, 1575--1593, 2005.
- [14] Devi, N. & Maji, T.K. *Drug Dev. Indus. Pharma.* **36**, 56--63, 2010.
- [15] Deka, B.K. & Maji, T.K. *Compos. Sci. Technol.* **70**, 1755--1761, 2010.
- [16] Fukuoka, E., et al. *Chem. Pharm. Bull.* **41**, 2166--2171, 1993.
- [17] Zong, Z., et al. *Polym.* **41**, 899--906, 2000.
- [18] Bahari, A., et al. *Afr. J. Pure Appl. Chem.* **5**, 429--435, 2011.
- [19] Lu, W.H., et al. *Forestry Studies in China*, **8**, 35--40, 2006.
- [20] Angadi, S.C., et al. *Int. J. Biol. Macromol.* **47**, 171--179, 2010.
- [21] Selvaraj, S., et al. *Der Pharmacia Lettre* **2**, 420--431, 2010.
- [22] Wang, X., et al. *Nanotech.* **19**, 1-7, 2008.

- [23] Pourshahab, P. S., et al. *J. Microencapsul.* **28**, 605--613, 2011.
- [24] O'Sullivan, S.M., et al. *Brit. J. Nutr.* **91**, 757--764, 2004.
- [25] Monteiro-Riviere, N.A., et al. *Nanomed.: Nanotechnol. Biol. Med.* **1**, 293--299, 2005.
- [26] Sabitha, P., et al. *Int. J. Chem. Tech. Res.* **2**, 88--98, 2010.
- [27] Rekha, M.R. & Sharma, C.P. *Trends Biomater. Artif. Organs.* **21**, 107--115, 2007.
- [28] Mourya, V.K., et al. *Adv. Mat. Lett.* **1**(1), 11--33, 2010.
- [29] Lusiana, R. A., et al. *Int. J. of Chem. Eng. Appl.* **4**(4), 229--233, 2013.
- [30] Anitha, A., et al. *J. Biomat. Sci.* **23**, 1381--1400, 2012.
- [31] Farag, R. K. & Mohamed, R. R. *Molecules* **18**(1), 190--203, 2013.
- [32] Zheng, J. et al. *J. Wuhan University of Technology-Mater. Sci. Ed.* **26**(4), 628--633, 2011.
- [33] Cai, X., et al. *Compos. Part A*, **39**, 727--737, 2008.
- [34] Sahu, S.K., et al. *J. Mater. Sci.: Mater. Med.* **21**, 1587--1597, 2010.
- [35] Anitha, A., et al. *Carbo. Pol.* **83**, 452--461, 2011.
- [36] Wang, X., et al. *Biomater.* **22**(16), 2247--2255, 2001.
- [37] Wan, Y. *Macromol. Chem. Phys.* **204**, 850--858, 2003.
- [39] Hua, S., et al. *Drug Dev. Indus. Pharm.* **36**, 1106--1114, 2010.
- [40] Iman, M. & Maji, T. K. *J. Appl. Polym. Sci.* **127**, 3987--3996, 2013.
- [41] Dong, Y., & Feng, S. *Biomater.* **26**, 6068--6076, 2005.
- [42] Cai, X., et al. *Composites, Part A*, **39**, 727--737, 2008.
- [43] Choi, J. H., et al. *Langmuir*, **28**, 6826--6831, 2012.
- [44] Pourjavadi, A., et al. *Polym. Bull.*, **57**, 813--824, 2006.
- [45] Sasmal, A., et al. *Int. J. Plastics Tech.* **13**, 8--21, 2009.

CHAPTER 5
RESULTS AND
DISCUSSION
(PART 2)

Microencapsulation of hydrophobic drug curcumin in three different nanoparticle systems, namely (i) chitosan-montmorillonite(MMT) nanoparticles, (ii) carboxymethyl chitosan-MMT nanoparticles and (iii) phosphorylated chitosan-MMT nanoparticles

In this part of work, the author has chosen ionic gelation technique for the microencapsulation of curcumin. The effects of various parameters like filler concentration and crosslinker concentration on the nanoparticle properties have been explained.

5.1. Section A-Preparation and characterization of curcumin loaded chitosan/MMT nanoparticles for controlled drug delivery applications.

5.1.1. Effect of variation of MMT and genipin concentration on the different properties of curcumin loaded chitosan-MMT nanoparticles

The results showing the effect of variation of MMT and genipin concentration on different properties of chitosan nanoparticles are shown in Table 5.1. The encapsulation efficiency of MMT free crosslinked nanoparticles was found to be higher compared to that of MMT containing crosslinked nanoparticles. The encapsulation efficiency decreased with the increase in MMT content in the nanoparticles. This could be attributed to the presence of the silicate layers of MMT. The –OH groups of MMT could interact with the -OH group and –NH₂ group of chitosan and –OH groups of genipin which resulted in the elongation of the polymer chains. The silicate layers of MMT also hindered the movement of the intercalated polymer chains freely and might assist the formation of fine channels from inner to outer surface of the nanoparticles during drying process. The more the encapsulation of MMT, the higher is the chance of formation of fine channels. Thus, part of the drug might get diffused from the particles to the external medium resulting in the decrease of encapsulation efficiency. The interference offered by the MMT layers was absent in MMT free crosslinked nanoparticles. Hence, it showed higher encapsulation efficiency. Similarly, at a fixed MMT content, the encapsulation efficiency of nanoparticles was found to further decrease with the increase in the genipin

concentration. Genipin might further restrict the free motion of the intercalated polymer chains and thus assist the formation of porous structure.

The average diameter of the nanoparticles was obtained in the range 430-560 nm. The variation in MMT concentration did not significantly affect the particle size. However, the average diameter showed a decreasing trend on increasing the genipin concentration. The amino groups present in chitosan interacted with the hydroxyl group of MMT and genipin. With the increase in the concentration of genipin, the availability of free amino groups on nanoparticles reduced. As a result, the nanoparticles became more compact and hence the diameter would be less.

Zeta potential values of the nanoparticles were found in the range 32 to 47 mV indicating good stability of the nanoparticles. The surface of the nanoparticles was positively charged due to the presence of amino groups. With the incorporation of MMT in chitosan matrix the surface charge decreased. The reduction in surface charge might be due to the increased electrostatic interaction between the protonated amino groups of chitosan and hydroxyl groups of MMT.

Table 5.1. Effect of variation of MMT and genipin concentration on the different properties of chitosan-MMT nanoparticles

Sample code	Yield of nanoparticle (%)	Encapsulation efficiency (%)	Average diameter (nm)	Zeta potential (mV)
C/M0/Gen50	94.76 (±0.01)	69.12 (±0.04)	430.7 (± 9)	47.21 (± 0.02)
C/M1/Gen50	92.08 (±0.04)	65.38 (±0.01)	457.8 (±7)	44.08 (± 0.07)
C/M3/Gen50	92.11 (±0.01)	63.11 (±0.01)	510.8 (± 98)	42.92 (± 0.3)
C/M5/Gen50	92.09 (±0.03)	60.31 (±0.03)	543.2 (± 10)	37.63 (± 0.02)
C/M5/Gen10	94.54 (±0.01)	63.25 (±0.04)	560.2 (±12)	32.12 (±0.1)
C/M5/Gen30	93.45 (±0.03)	62.65 (±0.09)	546.8 (±9)	35.34 (±0.3)
C/M5/Gen70	92.11 (±0.01)	58.55 (±0.01)	480.4 (±10)	42.54 (±0.02)

each value represents average of five readings, standard deviation in parenthesis

However, the zeta potential values increased as the genipin concentration increased from 10 to 70%. The increase in the zeta potential values indicated that the stability of the nanoparticles increased with the increase in the concentration of genipin and they would not aggregate in acidic or basic medium. Moreover, the increase in the zeta potential values with the increase in the concentration of genipin showed that there is some interaction of the polymer with genipin [1]. All the zeta potential values were in the stable zone indicating that the synthesized nanoparticles are highly stable.

5.1.2. Fourier Transform Infra-red Spectroscopy (FTIR) study

The appearance of important peaks of chitosan [Figure 5.1. (a)] and MMT [Figure 5.1. (b)] in FTIR study was already discussed in Chapter 4. Figure 5.1. (c) showed the FTIR spectra of curcumin. The bands at 708, 835 and 1000 cm^{-1} were attributed to the bending vibrations of the C-H bond of alkene groups ($\text{RCH}=\text{CH}_2$).

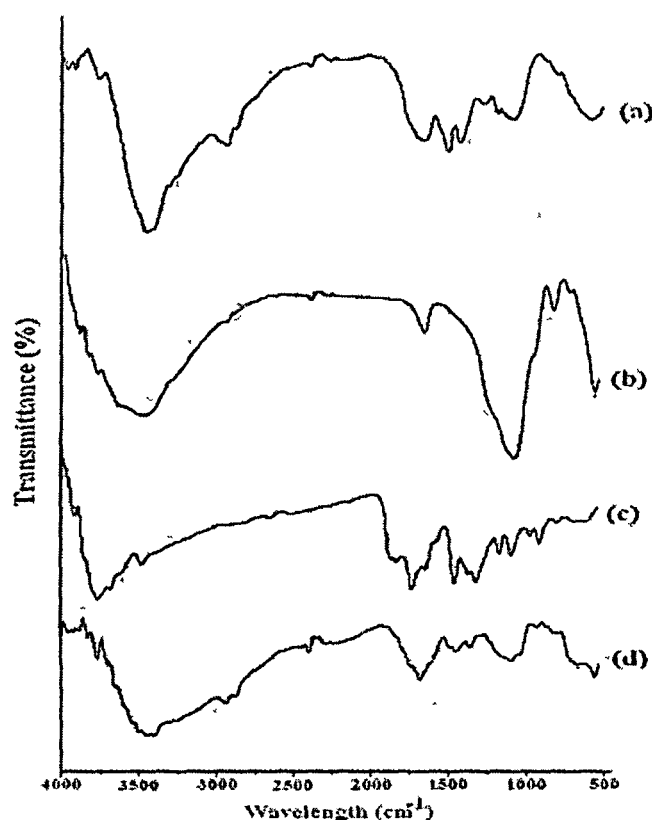


Figure 5.1. FTIR spectra of (a) Chitosan, (b) MMT, (c) curcumin, and (d) C/M5/Gen50

An intense band at 1720 cm^{-1} was assigned to the vibration of the carbonyl bond ($\text{C}=\text{O}$). The band appearing as a small shoulder at 1708 cm^{-1} was attributed to the Keto-enol tautomerism of curcumin. The bands appeared at 1440 and 1328 cm^{-1} were due to the vibrational mode of $\text{C}-\text{O}$ elongation of the alcohol and phenol groups [2]. All the important peaks of chitosan, MMT and curcumin were observed in the prepared nanoparticles [Figure 5.1. (d)] with reduced intensity.

5.1.3. X-Ray Diffraction (XRD) Study

The X-ray diffractograms of chitosan and MMT is already given and studied in chapter 4. Figure 5.2. (c) showed the X-ray diffractogram of curcumin. Appearance of multiplets in the region $2\theta=2$ to 70° demonstrate the crystalline nature of the drug [3]. The characteristic peaks for MMT and curcumin were found to disappear in the diffractogram of MMT/ chitosan nanoparticles (curve 5.2.2. d). It could be said that either the full expansion of MMT gallery occurred which was not possible to detect by XRD or the MMT layers become delaminated and no crystal diffraction peak appeared.

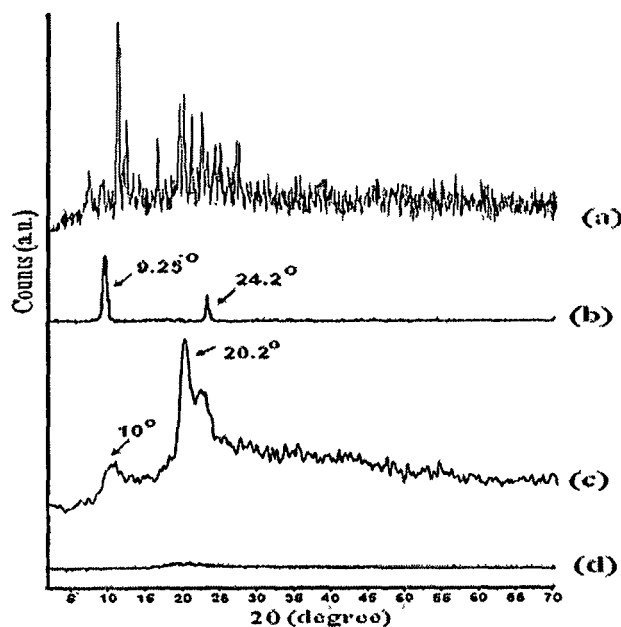


Figure 5.2. XRD patterns of (a) Curcumin, (b) MMT, (c) chitosan, (d) C/M5/Gen50

5.1.4. Scanning electron microscopy (SEM) study

SEM analysis was performed to study the surface morphology of chitosan nanoparticles and chitosan-MMT nanoparticles loaded with curcumin. Figure 5.3. a and 5.3. b represents the SEM micrographs of curcumin loaded chitosan nanoparticles and curcumin loaded chitosan-MMT nanoparticles respectively. The surface of curcumin loaded chitosan nanoparticles (Figure 5.3.a) appeared rough and slightly agglomerated. However, on addition of MMT into chitosan nanoparticles the roughness as well as the agglomeration decreased (Figure 5.3.b)

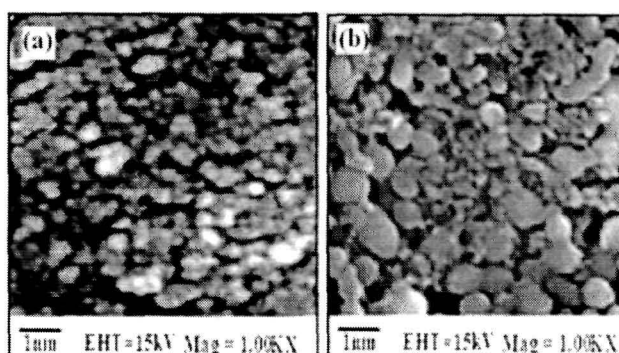


Figure 5.3. SEM micrographs of (a) C/M0/Gen50 and (b) C/M5/Gen50

5.1.5. Transmission electron microscopy (TEM) study

TEM micrographs of curcumin loaded chitosan nanoparticles devoid of MMT and with MMT are shown in Figure 5.4.a and 5.4. b respectively. Figure 5.4. b showed the presence of platelets of MMT tactoids in which the dark lines were the intersection of MMT layers. The bright areas were for polymer matrix and curcumin.

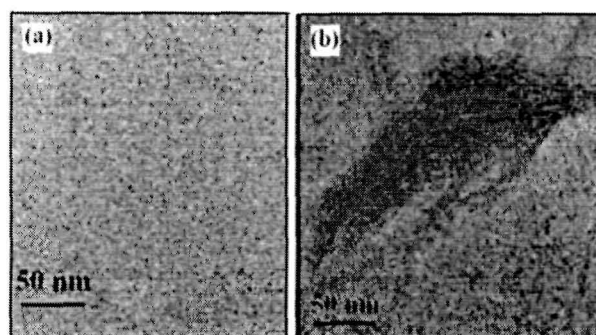


Figure 5.4. TEM micrographs of Chitosan nanoparticles (a) without MMT range and (b) with MMT at 100 nm scale respectively

5.1.6. Swelling Study

The effect of pH on the percentage swelling of curcumin loaded nanoparticles at two different pH namely, 1.2 and 7.4 are shown in Figure 5.5. It was observed that the swelling of curcumin loaded chitosan-MMT nanoparticles was more in gastric pH (1.2) than in intestinal pH (7.4). At lower pH, the free amine groups become protonated and generated a repulsive force between the adjacent positively charged polymer chains causing the swelling of the polymer and consequently diffusion of more amount of drug out of the polymer matrix. In alkaline pH, protonation was prevented and hence swelling decreased [4].

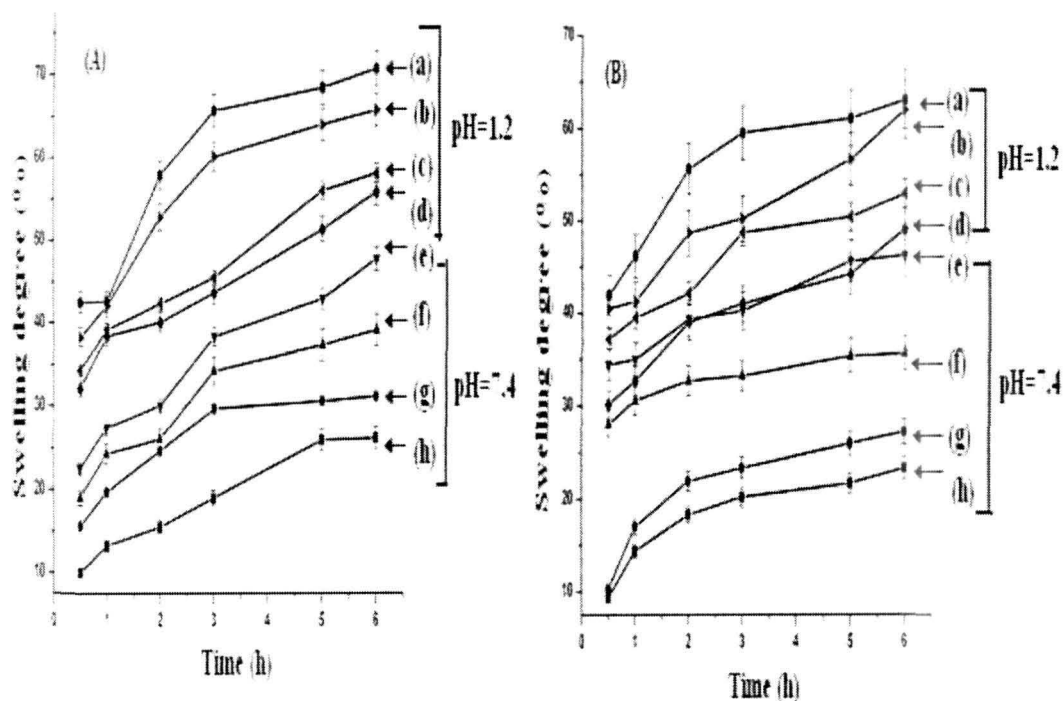


Figure 5.5. Percentage swelling degree at pH 1.2 and 7.4, (A) { (a) C/MMT0/Gen50, (b) C/MMT1/Gen50, (c) C/MMT3/Gen50, (d) C/MMT5/Gen50, (e) C/MMT0/Gen50, (f) C/MMT1/Gen50, (g) C/MMT3/GA50, (h) C/MMT5/GA50} and (B) { (a) C/MMT5/Gen10, (b) C/MMT5/Gen30, (c) C/MMT5/Gen50, (d) C/MMT5/Gen70, (e) C/MMT5/Gen10, (f) C/MMT5/Gen30, (g) C/MMT5/Gen50, (h) C/MMT5/Gen70}

Figure 5.5. (A) showed that with the increase in the concentration of MMT, the percentage swelling degree decreased. Water absorption decreased by the presence of dispersed phase of MMT into the chitosan matrix of the nanoparticles. MMT particles

acted as a barricade for water molecules and decreased the water transmission through the crosslinked chitosan-MMT nanoparticles. Similarly, nanoparticles containing higher concentration of genipin (Figure 5.5.B) swelled less due to higher crosslinking densities and less availability of the polar groups.

Furthermore, the percentage swelling degree was found to increase with the increase in time. With the increase in the time period, higher amount of the solvents can penetrate into the chitosan matrix, resulting in the increase in the percentage swelling degree.

5.1.7. *In vitro* Release Studies

The drug release profile of the nanoparticles at two different pH namely 1.2 and 7.4 are shown in Figure 5.6. The cumulative release (%) of curcumin from chitosan-MMT nanoparticles was found to be pH dependent. The cumulative release (%) of curcumin decreased with the increase in the pH of the medium. The difference in release profile was due to the difference in the swelling of chitosan in gastric and intestinal pH. Chitosan was swelled more in gastric pH compared to intestinal pH medium. The faster drug release rate in lower pH medium was due to the unstable nanoparticles structure, caused by the protonation of residual amino groups of chitosan in lower pH. It was also observed that the cumulative release (%) of curcumin decreased with the increase in MMT content (Figure 5.6. A) and increased with the increase in the period of time. The percentage swelling of the nanoparticles decreased with the increase in the concentration of MMT. Therefore, in order to facilitate the release of curcumin the solvent particles could not diffuse properly to interact with the curcumin molecules encapsulated in the nanoparticles. With the increase in time, the percentage degree of swelling increased and more and more solvent molecules could reach the drug molecule and hence helped to release the curcumin from the nanoparticles.

It was also seen that the cumulative release (%) of curcumin decreased with the increase in the concentration of genipin (Figure 5.6. B). When genipin content of nanoparticles increases the polymer density also increases. This leads to less free space availability for drug diffusion and consequently the release rate decreases [5].

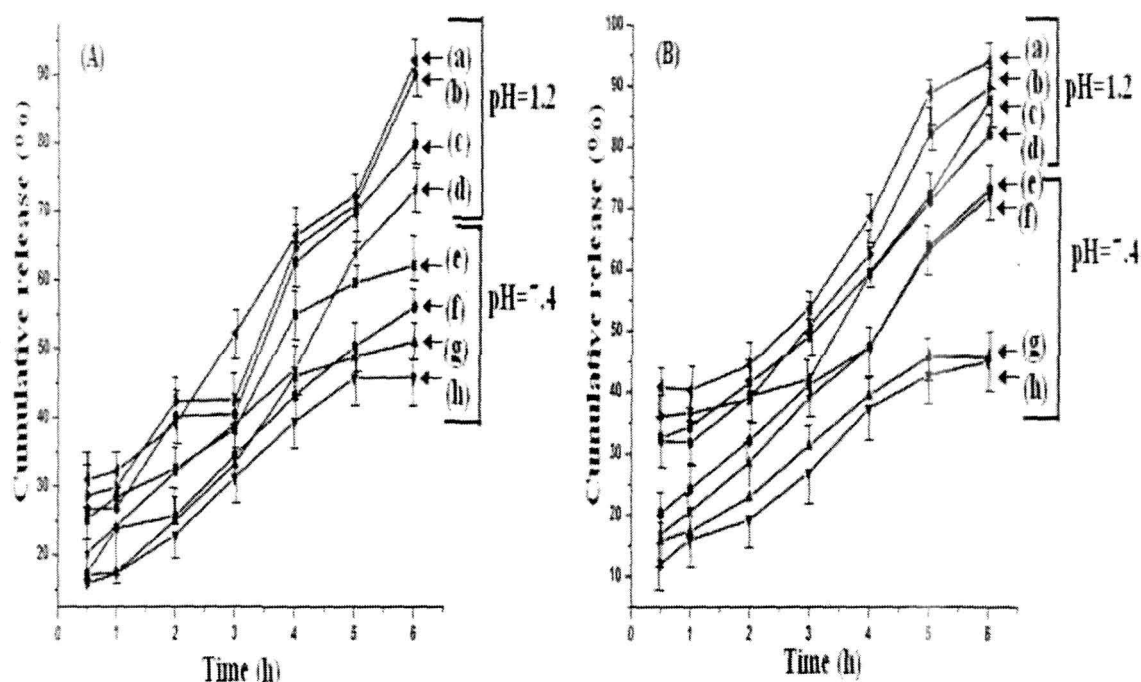


Figure 5.6. Cumulative release (%) at pH 1.2 and 7.4, (A) { (a) C/MMT0/Gen50, (b) C/MMT1/Gen50, (c) C/MMT3/Gen50, (d) C/MMT5/Gen50, (e) C/MMT0/Gen50, (f) C/MMT1/Gen50, (g) C/MMT3/Gen50, (h) C/MMT5/Gen50 } and (B) { (a) C/MMT5/Gen10, (b) C/MMT5/Gen30, (c) C/MMT5/Gen50, (d) C/MMT5/Gen70, (e) C/MMT5/Gen10, (f) C/MMT5/Gen30, (g) C/MMT5/Gen50, (h) C/MMT5/Gen70 }

5.1.8. Cell viability study

The effect of varying MMT concentration (0-5%) and time (6, 12, and 24 h) on cell viability is shown in Figure 5.7. Figure 5.7. showed that chitosan, MMT, curcumin and the nanoparticles were not at all cytotoxic to normal lymphocyte cells. Infact, all these components have the ability to induce cell proliferation. The cell viability of the normal cells increased from 100% to around 400%.

But, when MTT assay was conducted on two cancer cell lines MCF-7 and HepG2, it was observed that the nanoparticles were highly cytotoxic to the cancer cell lines. With the increase in MMT concentration, the cell viability decreased from 100-60%. So, around 40% killing of the cancer cell lines was observed. The higher the concentration of MMT, the slower was the release of the drug from the nanoparticles. The cancer cell killing activity of curcumin loaded nanoparticles were also observed by Anitha et.al. [6]

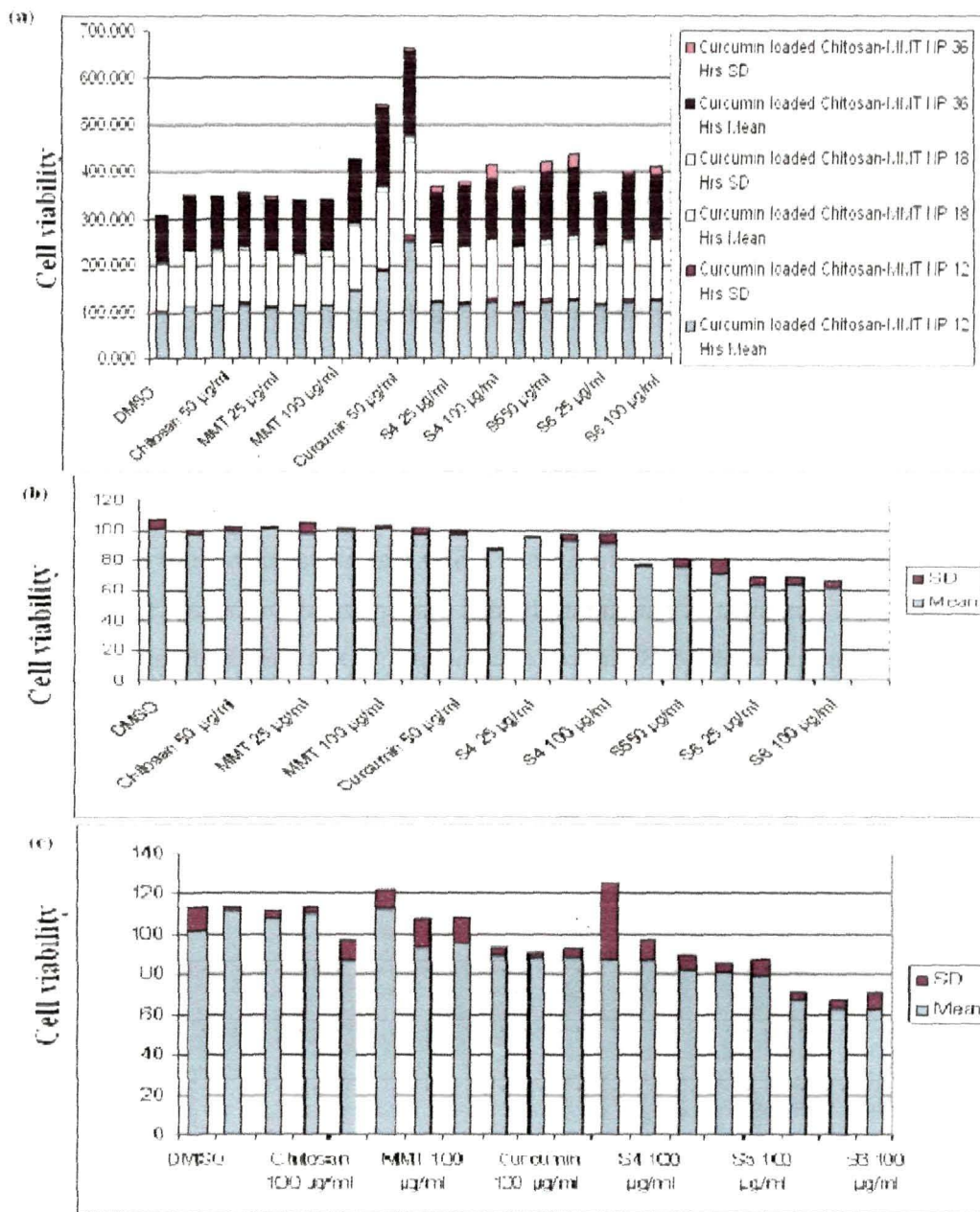


Figure 5.7. Cytotoxicity study of chitosan, MMT, curcumin, C/M1/Gen5, C/M3/Gen5 and C/M5/Gen5 at different concentrations on (a) normal lymphocytes, (b) MCF-7 and (c) HepG2 cell lines at different concentrations. [S4=C/M0/Gen50, S5=C/M3/Gen50, S6=C/M5/Gen50]

5.1.9. Study of toxicity related parameter (lipid peroxidation and lactate dehydrogenase (LDH) activity) and Antioxidant status

The lymphocyte toxicity profile of chitosan, MMT, curcumin and different formulations [Figure 5.8.] were studied by measuring the lipid peroxidation and lactate dehydrogenase (LDH) activity. Treatment of lymphocytes with chitosan, MMT, curcumin and the different formulation decreased the malondialdehyde (MDA) formation. The level of MDA formation in different formulations was slightly higher than that of curcumin alone. Similar pattern was also observed in the case of LDH activity measured in the cell free medium. The decrease in the LDH activity suggested that there was no membrane damage in the cells and the MDA level suggested the lacking of cellular damage. Reduced glutathione (GSH), the non-enzymatic component of antioxidant system measured as acid soluble sulfahydryl group (-SH) was elevated by only chitosan, MMT and curcumin treatment. Curcumin loaded nanoparticle increased the GSH level compared to curcumin alone. Superoxide dismutase (SOD) and catalase, the two major enzymatic component of antioxidant system also enhanced by the different treatments. The increased activity was found more compared to curcumin alone. The elevated level of antioxidants in the lymphocytes confers protective function against cellular damage.

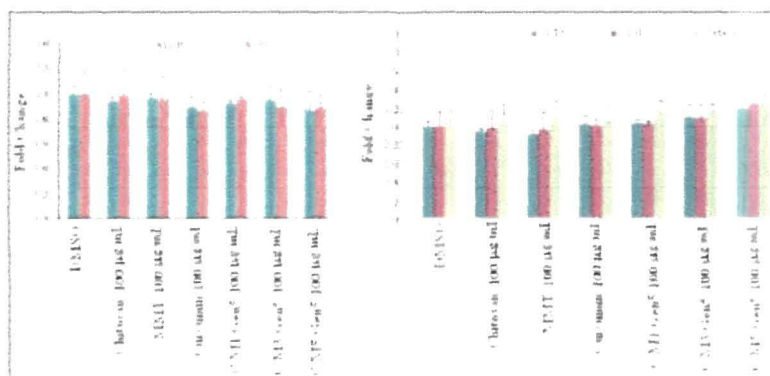


Figure 5.8. Effects of curcumin loaded chitosan-MMT nanoparticles on toxicity related parameters and antioxidants. Values of all the parameters are expressed as fold changes of mean in comparison to control. Level of GSH is calculated as nMole/g protein; Specific activity of SOD is expressed as $\mu\text{Mole}/\text{mg Protein}$; Specific activity of catalase is expressed as $\mu\text{Mole H}_2\text{O}/\text{min}/\text{mg Protein}$; Level of lipid peroxidation is calculated as nMole/g protein

5.1.10 In vitro wash-off test for evaluation of mucoadhesive property

Table 5.2. Results of in vitro wash-off test to assess mucoadhesive properties of nanoparticles prepared

pH	Sample Code	No. of particle taken	Reading after every 30 min									
			1	2	3	4	5	6	7	8	9	10
1.2	C/MMT0/Gen50	50	32.1 (±0.5)	31.8 (±0.5)	22.1 (±1.0)	20.4 (±0.5)	17.8 (±0.7)	15.3 (±0.7)	12.4 (±0.5)	9.4 (±0.6)	5.9 (±0.7)	0
	C/MMT1/Gen50	50	37.6 (±0.6)	35.2 (±0.9)	32.6 (±1.4)	35 (±0.6)	31.2 (±0.6)	25.3 (±0.5)	14.3 (±0.6)	13.7 (±0.5)	12.9 (±0.7)	5.8 (±0.4)
		60	54.8 (±1.3)	52.4 (±0.6)	51.9 (±0.5)	45.3 (±0.6)	42.6 (±0.7)	35.6 (±1.0)	32.4 (±0.6)	29.5 (±0.4)	26.4 (±0.5)	19.6 (±1.3)
	C/MMT5/Gen50	65	62.5 (±0.9)	61.5 (±0.6)	56.3 (±0.9)	52.4 (±0.5)	50.3 (±0.5)	48.4 (±0.4)	42.8 (±0.4)	38.2 (±0.6)	35.7 (±0.8)	25.1 (±0.5)
7.4	C/MMT0/Gen50	50	25.3 (±1.4)	22.7 (±0.5)	17.6 (±0.4)	14.3 (±0.6)	10.5 (±0.6)	8.5 (±0.4)	5.2 (±0.4)	0	0	0
	C/MMT1/Gen50	50	31.4 (±0.9)	31.1 (±0.9)	29.3 (±0.5)	27.4 (±0.5)	16.4 (±0.6)	13.2 (±0.4)	11.3 (±0.6)	9.6 (±1.0)	0	0
	C/MMT3/Gen50	50	41.3 (±0.9)	36.7 (±0.6)	30.1 (±0.7)	27.9 (±1.1)	25.8 (±0.6)	19.4 (±1.0)	9.4 (±0.4)	5.4 (±0.4)	1.2 (±0.5)	0
	C/MMT5/Gen50	50	46.8 (±0.7)	42.3 (±0.7)	39.9 (±0.6)	39.5 (±0.4)	38.5 (±1.0)	30.6 (±0.5)	28.8 (±0.4)	24 (±0.6)	22.8 (±0.4)	12.3 (±0.5)

*each value represents average of five readings, standard deviation in parenthesis

Results of the in vitro wash off test of chitosan-MMT nanoparticles containing curcumin are given in Table 5.2. The results represented in table are the average readings of five samples. The test was carried out in gastric (pH=1.2) and intestinal pH (pH=7.4) environment. The mucoadhesion was found to be higher in gastric pH than in intestinal pH. At acidic pH, the free amino groups of chitosan nanoparticles might get protonated and became positively charged. This could strongly bind to the negatively charged mucus layer. Sabitha et al. reported that the chitosan-alginate microcapsules showed lower mucoadhesive properties in intestinal pH compared to gastric pH [7]. The mucoadhesion further increased with the increase in the MMT content. This might be due to the interaction of the hydroxyl group of MMT with the mucin layer. But, the exact reason of increase in mucoadhesivity with the increase in MMT content is inexplicable. Similar types of observations were done by Zhuang et al. [8]

5.1.11. *Ex vivo* mucoadhesive test

Table 5.3. shows the results of *ex vivo* mucoadhesion test. The results are the mean value of five readings. It was observed that the detachment force increased with the increase in the MMT content in the nanoparticles which showed the mucoadhesive property of MMT along with chitosan in the nanoparticles.

Table 5.3. Weight required to detach the membrane at different time intervals

Sample Code	Mass required to detach after 5 min (g)	Detachment force (dyne/cm ²)	Mass required to detach after 10 min (g)	Detachment force (dyne/cm ²)	Mass required to detach after 15 min (g)	Detachment force (dyne/cm ²)	Mass required to detach after 20 min (g)	Detachment force (dyne/cm ²)
C/MMT1/Gen50	12.43 (±0.01)	3879.4 (±13.7)	14.52 (±0.01)	4531.7 (±0.6)	19.93 (±0.03)	6220.2 (±1.6)	24.7 (±0.01)	7708.9 (±1.5)
C/MMT1/Gen50	14.32 (±0.03)	4469 (±1.9)	20.37 (±0.04)	6357.5 (±0.9)	22.83 (±0.01)	6644.4 (±2.5)	25.3 (±0.02)	6862.8 (±5.1)
C/MMT3/Gen50	18.55 (±0.02)	5789.5 (±1.8)	23.54 (±0.04)	7346.9 (±1.5)	27.5 (±0.04)	7125.2 (±18.2)	28.03 (±0.02)	7896.2 (±6.1)
C/MMT5/Gen50	19.03 (±0.02)	5939.2 (±11.5)	25.65 (±0.06)	8005.4 (±0.4)	27.9 (±0.03)	8707.6 (±1.6)	32.21 (±0.01)	10052.8 (±3.7)

*each value represents average of five readings, standard deviation in parenthesis

5.2. Section B-Preparation and characterization of curcumin loaded carboxymethyl chitosan/MMT nanoparticles for controlled drug delivery applications.

5.2.1. Effect of variation of MMT and genipin concentration on the different properties of curcumin loaded CMC-MMT nanoparticles

The results showing the effect of variation of MMT and genipin concentration on different properties of CMC nanoparticles are shown in Table 5.4. The encapsulation efficiency of MMT free crosslinked nanoparticles was found to be higher compared to that of MMT containing crosslinked nanoparticles. The encapsulation efficiency decreased with the increase in MMT content in the nanoparticles. This could be attributed to the presence of the silicate layers of MMT. The -OH groups of MMT could interact with the residual -NH₂ group of CMC and -OH groups of genipin resulting in extension of the polymer chains. The silicate layers of MMT also hindered the

movement of the intercalated polymer chains freely and might assist the formation of fine channels from inner to outer surface of the nanoparticles during drying process. The more the encapsulation of MMT, the higher is the chance formation of fine channels. Thus, part of the drug might get diffused from the particles to the external medium resulting in the decrease of encapsulation efficiency. The interference offered by the MMT layers was absent in MMT free crosslinked nanoparticles. Hence, it showed higher encapsulation efficiency.

Similarly, at a fixed MMT content, the encapsulation efficiency of nanoparticles was found to further decrease with the increase in the genipin concentration. Genipin might further restrict the free motion of the intercalated polymer chains and thus assist the formation of porous structure.

The average diameter of the nanoparticles was obtained in the range 435-474 nm. The variation in MMT concentration did not significantly affect the particle size. However, the average diameter showed a decreasing trend on increasing the genipin concentration. The residual amino groups present in CMC interacted with the hydroxyl group of MMT and genipin. With the increase in the concentration of genipin, the availability of free amino groups on nanoparticles reduces due to which the nanoparticles became more compact and hence the diameter would be less.

Zeta potential values of the nanoparticles were found in the range 32 to 50 mV indicating good stability of the nanoparticles. The surface of the nanoparticles was positively charged due to the presence of residual amino groups. With the incorporation of MMT in CMC matrix the surface charge decreases. The reduction in surface charge might be due to the increased electrostatic interaction between the protonated amino groups of CMC and hydroxyl groups of MMT.

However, the zeta potential values increased as the genipin concentration increased from 10 to 70%. The increase in the zeta potential values indicated that the stability of the nanoparticles enhanced with the increase in the concentration of genipin and they would not aggregate in acidic or basic medium. All the zeta potential values were in the stable zone indicating that the synthesized nanoparticles are highly stable.

Table 5.4. Effect of variation of MMT and genipin concentration on the different properties of CMC-MMT nanoparticles

Sample code	Yield of nanoparticle (%)	Encapsulation efficiency (%)	Average diameter (nm)	Zeta potential (mV)
CMC/M0/Gen50	92.76(±0.02)	70.22(±0.04)	435.7 (± 11)	50.21(± 0.02)
CMC/M1/Gen50	91.08(±0.01)	67.38(±0.02)	435.3(± 11)	48.08(± 0.07)
CMC/M3/Gen50	93.51 (±0.01)	61.13(±0.01)	467.1(± 8)	44.92(± 0.3)
CMC/M5/Gen50	94.09(±0.03)	59.54(±0.03)	469.9(± 10)	36.63(± 0.02)
CMC/M5/Gen10	91.67(±0.02)	62.19(±0.04)	474.1(±8)	32.11(±0.01)
CMC/M5/Gen30	93.50(±0.05)	60.22(±0.01)	470.2 (±7)	32.97(±0.05)
CMC/M5/Gen70	92.82(±0.01)	54.71(±0.05)	452.2(±9)	40.24(±0.01)

*each value represents average of five readings, standard deviation in parenthesis

5.2.2. Fourier Transform Infra-red Spectroscopy (FTIR) study

The appearance of important peaks of CMC [Figure 5.9. (d)] and MMT[Figure 5.9. (d)] in FTIR study has been already discussed in Chapter 4 and that of curcumin [Figure 5.9. (d)] has been discussed in Section A of this chapter. All the important peaks of CMC, MMT and curcumin were observed in the prepared nanoparticles [Figure 5.9. (d)] with reduced intensity.

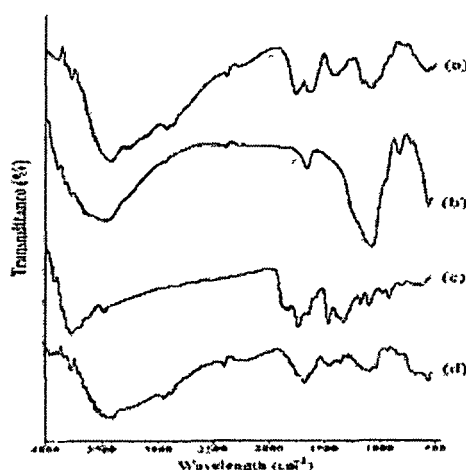


Figure 5.9. FTIR spectra of (a) CMC, (b) MMT, (c) curcumin, and (d) CMC/M5/Gen50

5.2.3. X-Ray Diffraction (XRD) Study

The X-ray diffractograms of CMC [Figure 5.10. (c)] and MMT [Figure 5.10 (b)] is already studied in chapter 4 and that of curcumin [Figure 5.10 (a)] is discussed in the Section A of this chapter. The characteristic peaks for MMT and curcumin were found to disappear in the diffractogram of MMT/ CMC nanoparticles (curve d). It could be said that either the full expansion of MMT gallery occurred which was not possible to detect by XRD or the MMT layers become delaminated and no crystal diffraction peak appeared.

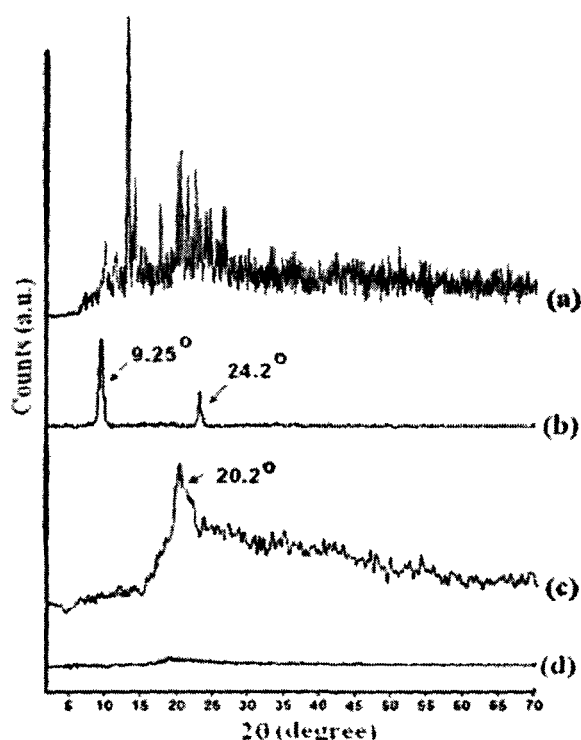


Figure 5.10. XRD patterns of (a) Curcumin, (b) MMT, (c) CMC, (d) CMC/M5/Gen50

5.2.4. Scanning electron microscopy (SEM) study

SEM analysis was performed to study the surface morphology of chitosan nanoparticles and CMC-MMT nanoparticles loaded with curcumin. Figure 5.11(a) and (b) represents the SEM micrographs of chitosan nanoparticles and CMC-MMT nanoparticles respectively. The surface of chitosan nanoparticles (Figure 5.11a) appeared smooth and slightly agglomerated. However, on addition of MMT into CMC nanoparticles the smoothness as well as the agglomeration decreased (Figure 5.11 b)

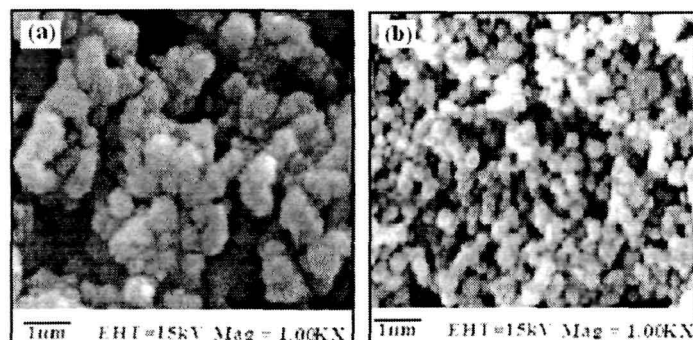


Figure 5.11. SEM micrographs of (a) CMC /M0/Gen50 and (b) CMC/M5/Gen50

5.2.5. Transmission electron microscopy (TEM) study

TEM micrographs of curcumin loaded CMC nanoparticles devoid of MMT and with MMT are shown in Figure 5.12 (a) and (b) respectively. Figure 5.12 (b) showed the presence of platelets of MMT tactoids in which the dark lines were the intersection of MMT layers. The bright areas were for polymer matrix and curcumin.

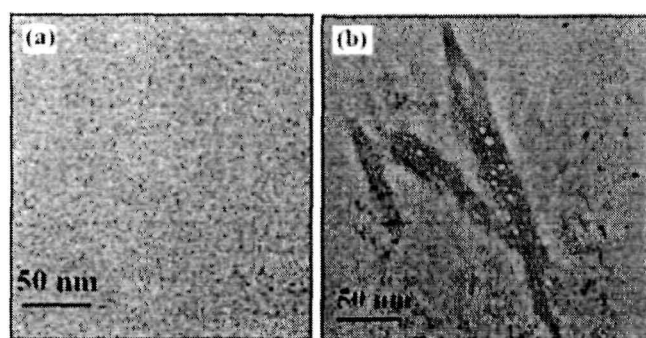


Figure 5.12. TEM micrographs of CMC nanoparticles (a) without MMT range and (b) with MMT at 100 nm scale respectively

5.2.6. Swelling Study

The effect of pH on the percentage swelling of curcumin loaded nanoparticles at two different pH namely, 1.2 and 7.4 are shown in Figure 5.13. It was observed that the swelling of curcumin loaded carboxymethyl chitosan-MMT nanoparticles was more in gastric pH (1.2) than in intestinal pH (7.4). At lower pH, the free amine groups become protonated and generated a repulsive force between the adjacent positively charged polymer chains causing the swelling of the polymer and consequently diffusion of more

amount of drug out of the polymer matrix. In alkaline pH, protonation was prevented and hence swelling decreased.

Figure 5.13. (A) showed that with the increase in the concentration of MMT, the percentage swelling degree decreased. Water absorption decreased by the presence of dispersed phase of MMT into the CMC matrix of the nanoparticles. MMT particles acted as a barricade for water molecules and decreased the water transmission through the crosslinked CMC-MMT nanoparticles. Similarly, nanoparticles containing higher concentration of genipin (Figure 5.13. B) swelled less due to higher crosslinking densities and less availability of the polar groups.

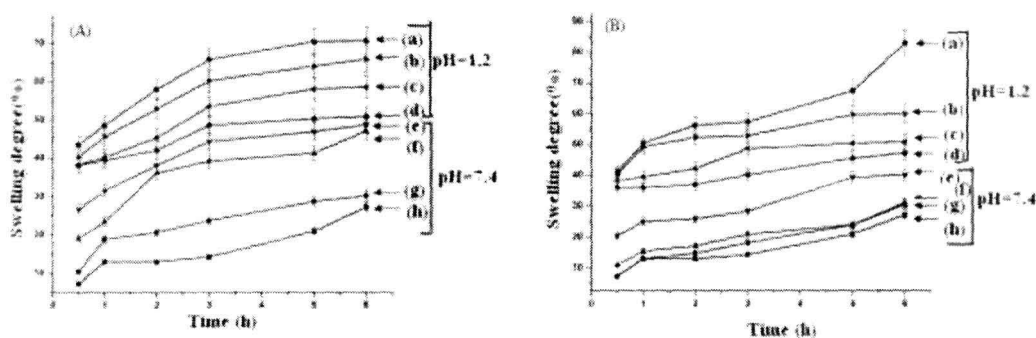


Figure 5.13. Percentage swelling degree at pH 1.2 and 7.4 ,(A) { (a) CMC/MMT0/Gen50, (b) CMC/MMT1/Gen50, (c) CMC/MMT3/Gen50, (d) CMC/MMT5/Gen50, (e) CMC/MMT0/Gen50, (f) CMC/MMT1/Gen50, (g) CMC/MMT3/Gen50, (h) CMC/MMT5/Gen50 } and (B) { (a) CMC/MMT5/Gen10, (b) CMC/MMT5/Gen30, (c) CMC/MMT5/Gen50, (d) CMC/MMT5/Gen70, (e) CMC/MMT5/Gen10, (f) CMC/MMT5/Gen30, (g) CMC/MMT5/Gen50, (h) CMC/MMT5/Gen70 }

Furthermore, the percentage swelling degree was found to increase with the increase in time. With the increase in the time period, higher amount of the solvents can penetrate into the CMC matrix, resulting in the increase in the percentage swelling degree.

5.2.7. In vitro Release Studies

The drug release profile of the nanoparticles at two different pH namely 1.2 and 7.4 are shown in Figure 5.14. The cumulative release (%) of curcumin from CMC-MMT nanoparticles was found to be pH dependent. The cumulative release (%) of curcumin decreased with the increase in the pH of the medium. The difference in release profile

was due to the difference in the swelling of CMC in gastric and intestinal pH. CMC was swelled more in gastric pH compared to intestinal pH medium. The faster drug release rate in lower pH medium was due to the wobbly nanoparticles structure, caused by the protonation of residual amino groups of CMC in lower pH.

It was also observed that the cumulative release (%) of curcumin decreased with the increase in MMT content (Figure 5.14. A) and increased with the increase in the period of time. The percentage swelling of the nanoparticles decreased with the increase in the concentration of MMT. Therefore, in order to facilitate the release of curcumin the solvent particles could not diffuse properly to interact with the curcumin molecules encapsulated in the nanoparticles. With the increase in time, the percentage degree of swelling increased and more and more solvent molecules could reach the drug molecule and hence helped to release the curcumin from the nanoparticles.

It was also seen that the cumulative release (%) of curcumin decreased with the increase in the concentration of genipin (Figure 5.14. B). This was due to the increase in crosslinking density of the nanoparticles. The more the crosslinking, less the accessibility of solvent to penetrate into the CMC-MMT nanoparticles and thus a decrease in cumulative release (%) were observed.

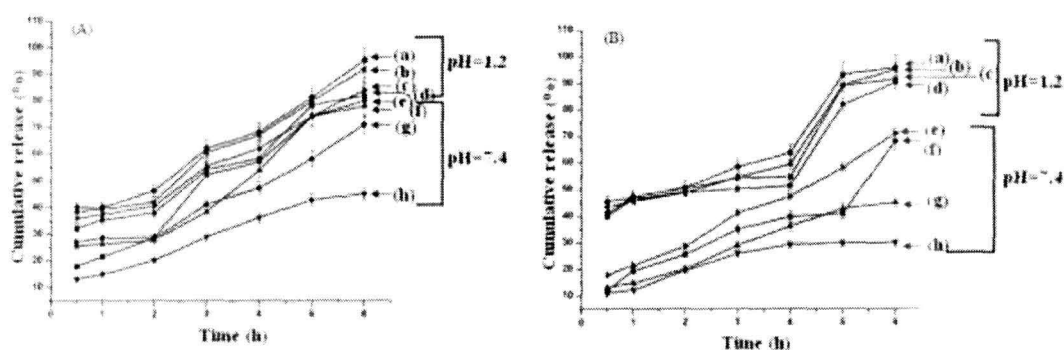


Figure 5.14. Cumulative release (%) at pH 1.2 and 7.4 ,(A) { (a) CMC/MMT0/Gen50, (b) CMC/MMT1/Gen50, (c) CMC/MMT3/Gen50, (d) CMC/MMT5/Gen50, (e) CMC/MMT0/Gen50, (f) CMC/MMT1/Gen50, (g) CMC/MMT3/Gen50, (h) CMC/MMT5/Gen50 } and (B) { (a) CMC/MMT5/Gen10, (b) CMC/MMT5/Gen30, (c) CMC/MMT5/Gen50, (d) CMC/MMT5/Gen70, (e) CMC/MMT5/Gen10, (f) CMC/MMT5/Gen30, (g) CMC/MMT5/Gen50, (h) CMC/MMT5/Gen70 }

5.2.8. Cytotoxicity Test

The effect of varying MMT concentration (0-5%) and time (6, 12, and 24 h) on cell viability is shown in Figure 5.15. Figure 5.15. (a) showed that CMC, MMT, curcumin and the nanoparticles was not at all cytotoxic to normal lymphocyte cells. Infact, all these components have the ability to induce cell proliferation. The cell viability of the normal cells increased from 100% to around 600%.

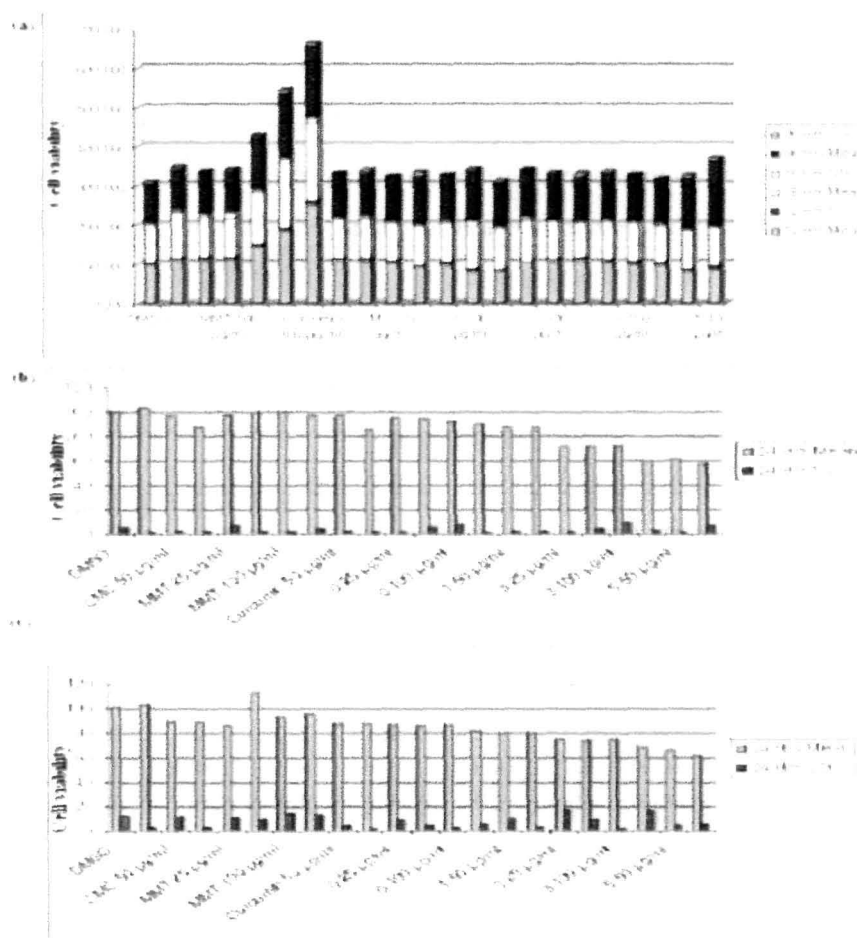


Figure 5.15. Cytotoxicity study of CMC, chitosan, MMT, curcumin, CMC/M1/Gen5, CMC/M3/Gen5 and CMC/M5/Gen5 at different concentrations on (a) normal lymphocytes, (b) MCF-7 and (c) HepG2 cell lines at different concentrations. [5=C/M5/Gen50, 3=CMC/M3/Gen50, 0=CM0/Gen50]

But, when MTT assay was conducted on two cancer cell lines MCF-7 and HepG2 (5.15 (b) and (c)), it was observed that the nanoparticles were highly cytotoxic to the cancer cell lines. With the increase in MMT concentration, the cell viability decreased from 100-60%. So, around 40% killing of the cancer cell lines was observed. The results showed

that the drug was released more slowly from the nanoparticles with the increase in the MMT concentration. This slow release of drug was more effective in effective killing of the cancer cell lines.

5.2.9. In vitro wash-off test for evaluation of mucoadhesive property

Results of the in vitro wash off test of chitosan-MMT nanoparticles containing curcumin are given in Table 5.5. The results represented in table are the average readings of five samples. The test was carried out in gastric (pH=1.2) and intestinal pH (pH=7.4) environment. The mucoadhesion was found to be higher in gastric pH than in intestinal pH. The mucoadhesion properties were also enhanced with the increase in the MMT content.

Table 5.5. Results of in vitro wash-off test to assess mucoadhesive properties of nanoparticles prepared

pH	Sample Code	No. of particle taken	Reading after every 30 min									
			1	2	3	4	5	6	7	8	9	10
1.2	CMC/MMT0/Gen50	50	34.1 (±0.5)	32.2 (±0.5)	28.8 (±1.0)	24.2 (±0.5)	25.3 (±0.7)	21.4 (±0.7)	15.3 (±0.5)	10.4 (±0.6)	9.7 (±0.7)	3.2 (±0.7)
	CMC/MMT1/Gen50	50	39.3 (±0.6)	35.2 (±0.9)	32.6 (±1.4)	31.1 (±0.6)	29.3 (±0.5)	24.3 (±0.5)	20.6 (±0.6)	19.7 (±0.5)	15.9 (±0.7)	7.2 (±0.4)
	CMC/MMT3/Gen50	60	58.2 (±1.3)	56.4 (±0.5)	51.9 (±0.5)	45.3 (±0.6)	42.6 (±0.7)	35.6 (±0.5)	32.4 (±0.6)	29.5 (±0.4)	26.4 (±0.5)	20.5 (±1.3)
	CMC/MMT5/Gen50	65	62.1 (±0.4)	60.3 (±0.6)	54.3 (±0.9)	51.8 (±0.5)	49.6 (±0.5)	43.2 (±0.4)	41.8 (±0.4)	36.9 (±0.6)	32.2 (±0.8)	29.3 (±0.5)
7.4	CMC/MMT0/Gen50	50	30.2 (±1.4)	27.7 (±0.5)	20.7 (±0.4)	19.7 (±0.6)	15.3 (±0.6)	10.4 (±0.4)	9.5 (±0.4)	1.3 (±0.6)	0	0
	CMC/MMT1/Gen50	50	34.9 (±0.9)	30.1 (±0.9)	25.5 (±0.5)	27.4 (±0.5)	16.4 (±0.6)	13.2 (±0.4)	11.3 (±0.6)	9.6 (±1.0)	4.3 (±0.4)	0
	CMC/MMT3/Gen50	50	42.8 (±0.9)	38.0 (±0.6)	34.1 (±0.5)	32.9 (±1.1)	27.4 (±0.6)	24.3 (±1.0)	18.7 (±0.4)	10.5 (±0.4)	5.3 (±0.5)	0
	CMC/MMT5/Gen50	50	44.6 (±0.7)	42.5 (±0.7)	38.6 (±0.4)	37.9 (±0.4)	37.5 (±0.6)	33.7 (±0.5)	29.2 (±0.4)	25.6 (±0.6)	23.7 (±0.4)	19.4 (±0.6)

At acidic pH, the free amino groups of chitosan nanoparticles might get protonated and became positively charged. This could strongly bind to the negatively charged mucus

layer. Moreover, the presence of a strong hydrogen bonding was due to hydrophilic carboxylic acid group of CMC and mucin increases the mucoadhesivity [9].

5.2.10. *Ex vivo* mucoadhesive test

Table 5.6. shows the results of *ex vivo* mucoadhesion test. The results are the mean value of five readings. It was observed that the detachment force increased with the decrease in particle size of the nanoparticles.

Table 5.6. Weight required to detach the membrane at different time intervals

Sample Code	Mass required to detach after 5 min (g)	Detachment force (dyne/cm ²)	Mass required to detach after 10 min (g)	Detachment force (dyne/cm ²)	Mass required to detach after 15 min (g)	Detachment force (dyne/cm ²)	Mass required to detach after 20 min (g)	Detachment force (dyne/cm ²)
CMC/MMT1/Gen50	14.23 (±0.03)	4441.2 (±11.8)	16.39 (±1.6)	5115.4 (±0.6)	20.11 (±0.03)	6276.4 (±1.6)	21.37 (±0.01)	6669.6 (±1.5)
CMC/MMT1/Gen50	17.88 (±1.6)	5580.4 (±1.9)	27.79 (±0.04)	8673.3 (±0.03)	27.84 (±0.01)	8688.9 (±0.03)	29.06 (±0.02)	9069.7 (±5.1)
CMC/MMT3/Gen50	20.63 (±0.02)	6438.7 (±1.8)	29.54 (±1.6)	9219.5 (±1.6)	30.01 (±0.04)	9366.2 (±18.2)	36.65 (±0.03)	11438.5 (±6.1)
CMC/MMT5/Gen50	23.33 (±0.02)	7281.3 (±11.5)	29.91 (±0.06)	9334.9 (±0.4)	31.97 (±0.03)	9977.9 (±1.6)	39.21 (±0.01)	12237.5 (±3.7)

5.3. Section C-Preparation and characterization of curcumin loaded phosphorylated chitosan/MMT nanoparticles for controlled drug delivery applications.

5.3.1. Effect of variation of MMT and Genipin concentration on the different properties of curcumin loaded PCTS-MMT nanoparticles

The results showing the effect of variation of MMT and genipin concentration on different properties of PCTS nanoparticles are shown in Table 5.7. The encapsulation efficiency of MMT free crosslinked nanoparticles was found to be higher compared to that of MMT containing crosslinked nanoparticles. The encapsulation efficiency

decreased with the increase in MMT content in the nanoparticles. This could be attributed to the presence of the silicate layers of MMT. The –OH groups of MMT could interact with the residual –NH₂ group of PCTS and –OH groups of genipin resulting in extension of the polymer chains. The silicate layers of MMT also hindered the movement of the intercalated polymer chains freely and might assist the formation of fine channels from inner to outer surface of the nanoparticles during drying process. The more the encapsulation of MMT, the higher is the chance formation of fine channels. Thus, part of the drug might get diffused from the particles to the external medium resulting in the decrease of encapsulation efficiency. The interference offered by the MMT layers was absent in MMT free crosslinked nanoparticles. Hence, it showed higher encapsulation efficiency. The high encapsulation efficiency of the nanoparticles can also be attributed to the hydrophilic bulky phosphate groups of PCTS. Due to these hydrophilic groups in PCTS, the nanoparticles swelled more and so the drug can easily enter in the nanoparticles.

Similarly, at a fixed MMT content, the encapsulation efficiency of nanoparticles was found to further decrease with the increase in the glutaraldehyde (GA) concentration. GA might further restrict the free motion of the intercalated polymer chains and thus assist the formation of porous structure.

The average diameter of the nanoparticles was obtained in the range 419-472 nm. The variation in MMT concentration did not significantly affect the particle size. However, the average diameter showed a decreasing trend on increasing the genipin concentration. The residual amino groups present in PCTS interacted with the hydroxyl group of MMT and genipin. With the increase in the concentration of GA, the availability of free residual amino groups on nanoparticles reduces due to which the nanoparticles became more compact and hence the diameter would be less. The zeta potential values showed that the nanoparticles are stable.

Table 5.7. Effect of variation of MMT and GA concentration on the different properties of PCTS nanoparticles

Sample code	Yield of nanoparticle (%)	Encapsulation efficiency (%)	Average diameter (nm)	Zeta potential (mV)
PCTS/M0/GA50	93.77(±0.03)	87.01(±0.01)	456.2 (± 3)	30.99(± 0.01)
PCTS /M1/GA50	93.59(±0.01)	85.54(±0.02)	458.3(± 6)	31.27(± 0.03)
PCTS /M3/GA50	93.42(±0.03)	83.19(±0.02)	462.1(± 1)	30.54(± 0.01)
PCTS /M5/GA50	93.41(±0.02)	81.54(±0.01)	468.4(± 6)	30.03(± 0.01)
PCTS /M5/GA10	92.75(±0.02)	84.54(±0.02)	472.4(± 4)	40.41(± 0.01)
PCTS /M5/GA30	92.71(±0.04)	83.63(±0.03)	454.3(± 9)	38.12(± 0.02)
PCTS /M5/GA70	91.09(±0.02)	81.51 (±0.01)	419.5(± 9)	26.88(± 0.02)

*each value represents average of five readings, standard deviation in parenthesis

5.3.2. Fourier Transform Infra-red Spectroscopy (FTIR) study

The appearance of important peaks of PCTS and MMT in FTIR study is already discussed in Chapter 4 and that of curcumin is discussed in Section A of this chapter. All the important peaks of PCS, MMT and curcumin were observed in the prepared nanoparticles [Figure 5.16. (d)] with reduced intensity.

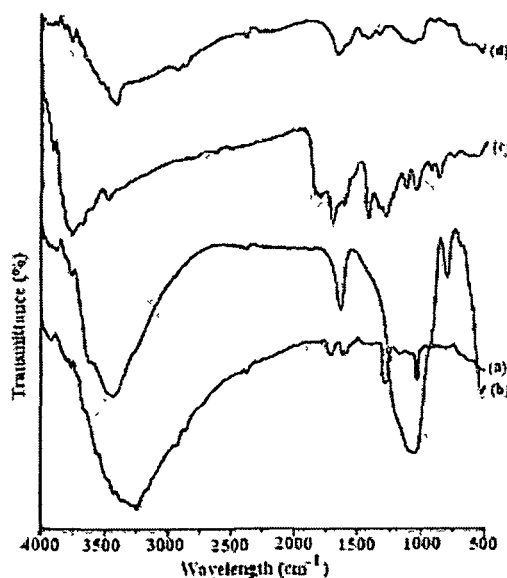


Figure 5.16. FTIR spectra of (a)PCTS, (b) MMT, (c) curcumin, and (d) PCTS/M5/Gen50

5.3.2. X-Ray Diffraction (XRD) Study

The X-ray diffractograms of PCTS and MMT is already studied in chapter 4 and that of curcumin is discussed in the Section A of this chapter. The characteristic peaks for MMT and curcumin were found to disappear in the diffractogram of MMT/ PCTS nanoparticles (curve 5.17. d). It could be said that either the full expansion of MMT gallery occurred which was not possible to detect by XRD or the MMT layers become delaminated and no crystal diffraction peak appeared.

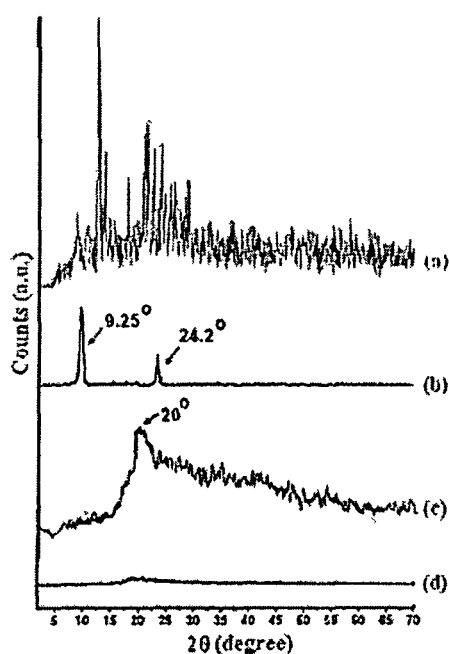


Figure 5.17. XRD patterns of (a) Curcumin, (b) MMT, (c) PCTS, (d) PCTS/MS/Gen50

5.3.3. Scanning electron microscopy (SEM) study

SEM analysis was performed to study the surface morphology of PCTS nanoparticles and PCTS-MMT nanoparticles loaded with curcumin. Figure 5.18 a and 4b represents the SEM micrographs of PCTS nanoparticles and PCTS-MMT nanoparticles respectively. The surface of PCTS nanoparticles (Figure4a) appeared smoother and slightly

agglomerated. However, on addition of MMT into PCTS nanoparticles the smoothness as well as the agglomeration decreased (Figure 5.18 b)

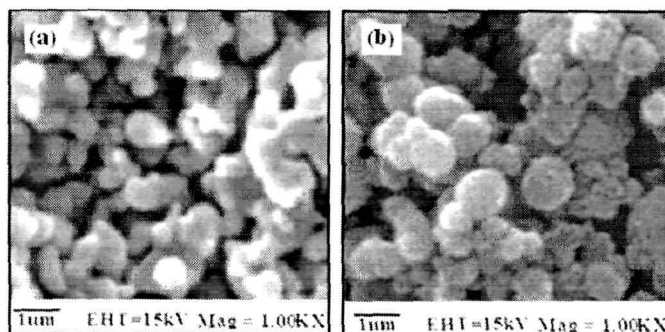


Figure 5.18. SEM micrographs of (a) PCTS/M0/Gen50 and (b) PCTS/M5/Gen50

5.3.4. Transmission electron microscopy (TEM) study

TEM micrographs of curcumin loaded PCTS nanoparticles devoid of MMT and with MMT are shown in Figure 5.19. (a) and 5.19. (b) respectively. Figure 5.19 (b) showed the presence of platelets of MMT tactoids in which the dark lines were the intersection of MMT layers. The bright areas were for polymer matrix and curcumin.

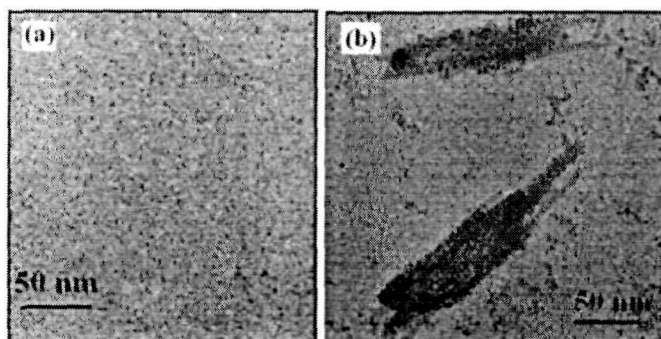


Figure 5.19. TEM micrographs of PCTS nanoparticles (a) without MMT range and (b) with MMT at 100 nm scale respectively

5.3.5. Swelling Study

The effect of pH on the percentage swelling of curcumin loaded nanoparticles at two different pH namely, 1.2 and 7.4 are shown in Figure 5.20. It was observed that the swelling of curcumin loaded PCTS-MMT nanoparticles was more in gastric pH (1.2) than in intestinal pH (7.4). At lower pH, the free amine groups become protonated and

generated a repulsive force between the adjacent positively charged polymer chains causing the swelling of the polymer and consequently diffusion of more amount of drug out of the polymer matrix.. In alkaline pH, protonation was prevented and hence swelling decreased.

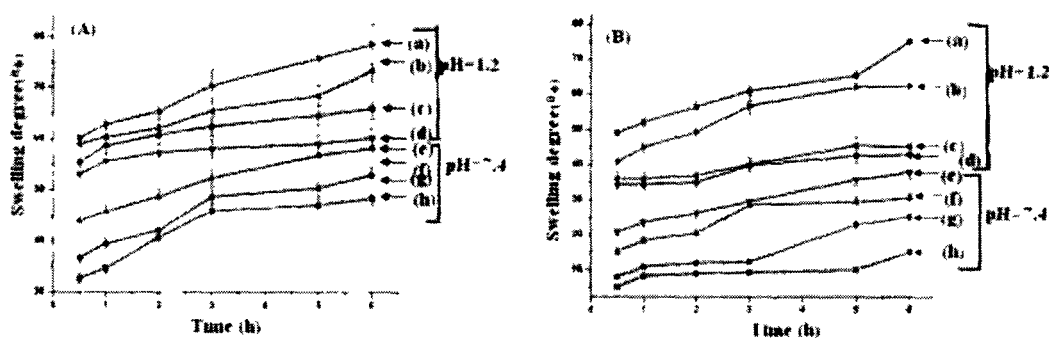


Figure 5.20. Percentage swelling degree at pH 1.2 and 7.4 ,(A) { (a)PCTS/MMT0/Gen50, (b) PCTS/MMT1/Gen50, (c) PCTS/MMT3/Gen50, (d) PCTS/MMT5/Gen50, (e) PCTS/MMT0/Gen50, (f) PCTS/MMT1/Gen50, (g) PCTS/MMT3/GA50, (h) PCTS/MMT5/GA50} and (B) {(a) PCTS/MMT5/Gen10, (b) PCTS/MMT5/Gen30, (c) PCTS/MMT5/Gen50, (d) PCTS/MMT5/Gen70, (e) PCTS/MMT5/Gen10, (f) PCTS/MMT5/Gen30, (g) PCTS /MMT5/Gen50, (h) PCTS/MMT5/Gen70}

Figure 5.20. (A) showed that with the increase in the concentration of MMT, the percentage swelling degree decreased. Water absorption decreased by the presence of dispersed phase of MMT into the PCTS matrix of the nanoparticles. MMT particles acted as a barricade for water molecules and decreased the water transmission through the crosslinked PCTS-MMT nanoparticles. Similarly, nanoparticles containing higher concentration of genipin (Figure 5.20. B) swelled less due to higher crosslinking densities and less availability of the polar groups.

Furthermore, the percentage swelling degree was found to increase with the increase in time. With the increase in the time period, higher amount of the solvents can penetrate into the CMC matrix, resulting in the increase in the percentage swelling degree.

5.3.6. *In vitro* Release Studies

The drug release profile of the nanoparticles at two different pH namely 1.2 and 7.4 are shown in Figure 5.21. The cumulative release (%) of curcumin from PCTS-MMT nanoparticles was found to be pH dependent. The cumulative release (%) of curcumin

decreased with the increase in the pH of the medium. The major factors controlling the release profile of curcumin from nanoparticles were swelling nature of the polymer and solubility of the drug in the medium. The difference in release profile was due to the difference in the swelling of PCTS in gastric and intestinal pH. PCTS was swelled more in gastric pH compared to intestinal pH medium.

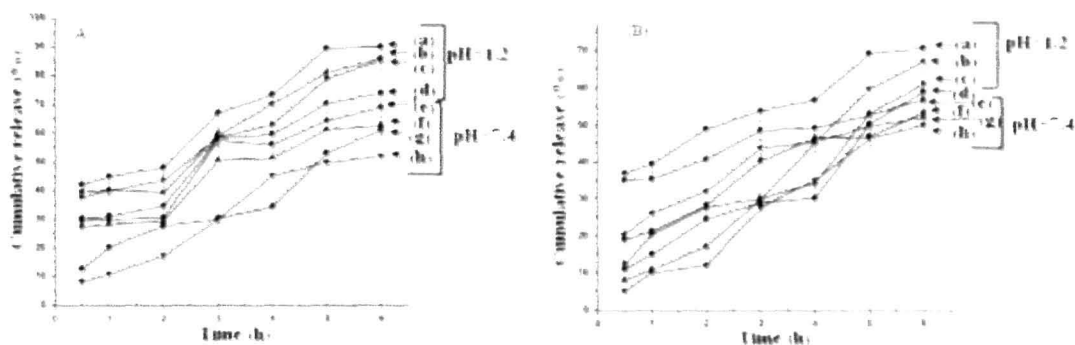


Figure 5.21. Cumulative release (%) at pH 1.2 and 7.4 (A) { (a) CMC/MMT0/Gen50, (b) CMC/MMT1/Gen50, (c) CMC/MMT3/Gen50, (d) CMC/MMT5/Gen50, (e) CMC/MMT0/Gen50, (f) CMC/MMT1/Gen50, (g) CMC/MMT3/Gen50, (h) CMC/MMT5/Gen50 } and (B) { (a) CMC/MMT5/Gen10, (b) CMC/MMT5/Gen30, (c) CMC/MMT5/Gen50, (d) CMC/MMT5/Gen70, (e) CMC/MMT5/Gen10, (f) CMC/MMT5/Gen30, (g) CMC/MMT5/Gen50, (h) CMC/MMT5/Gen70 }

It was also observed that the cumulative release (%) of curcumin decreased with the increase in MMT content (Figure 5.21. A) and increased with the increase in the period of time. The percentage swelling of the nanoparticles decreased with the increase in the concentration of MMT. Therefore, in order to facilitate the release of curcumin the solvent particles could not diffuse properly to interact with the curcumin molecules encapsulated in the nanoparticles. With the increase in time, the percentage degree of swelling increased and more and more solvent molecules could reach the drug molecule and hence helped to release the curcumin from the nanoparticles.

It was also seen that the cumulative release (%) of curcumin decreased with the increase in the concentration of genipin (Figure 5.21. B). This was due to the increase in crosslinking density of the nanoparticles. The more the crosslinking, less the accessibility of solvent to penetrate into the PCTS-MMT nanoparticles and thus a decrease in cumulative release (%) were observed.

5.3.7. Cytotoxicity Test

The effect of varying MMT concentration (0-5%) and time (6, 12, and 24 h) on cell viability is shown in Figure 5.22.

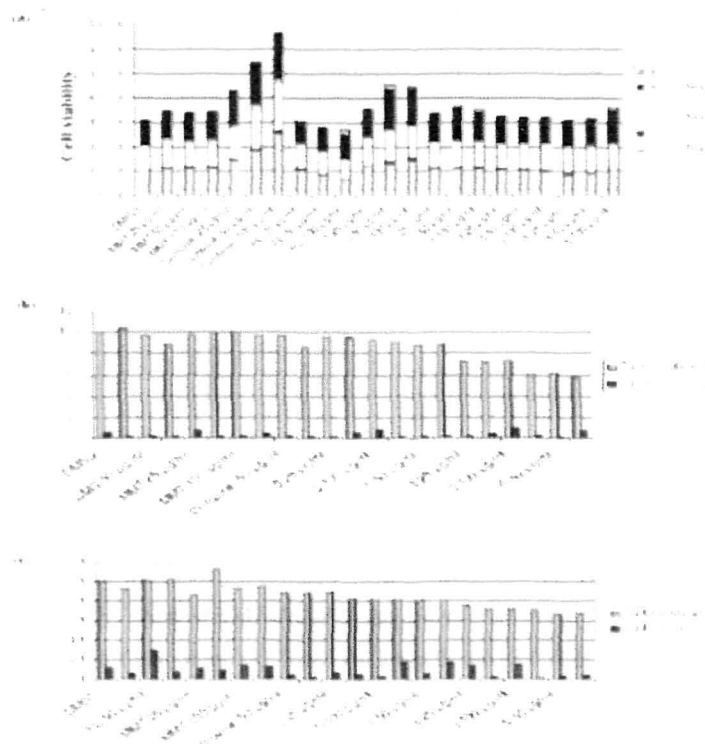


Figure 5.22. Cytotoxicity study of PCTS, MMT, curcumin, PCTS/M1/Gen5, PCTS/M3/Gen5 and PCTS/M5/Gen5 at different concentrations on (a) normal lymphocytes, (b) MCF-7 and (c) HepG2 cell lines at different concentrations. [5=PCTS M5/Gen50, 3=PCTS/M3/Gen50, 0=PCTS/M0/Gen50]

Figure 5.22. (a) showed that CMC, MMT, curcumin and the nanoparticles was not at all cytotoxic to normal lymphocyte cells. Infact, all these components have the ability to induce cell proliferation. The cell viability of the normal cells increased from 100% to around 600%.

But, when MTT assay was conducted on two cancer cell lines MCF-7 and HepG2 [5.22(b) and (c)], it was observed that the nanoparticles were highly cytotoxic to the cancer cell lines. With the increase in MMT concentration, the cell viability decreased from 100-65%. So, around 35% killing of the cancer cell lines was observed. The results showed that the drug was released more slowly from the nanoparticles with the increase

in the MMT concentration. This slow release of drug was more effective in effective killing of the cancer cell lines.

5.3.8. In vitro wash-off test for evaluation of mucoadhesive property

Results of the in vitro wash off test of chitosan-MMT nanoparticles containing curcumin are given in Table 5.8. The results represented in table are the average readings of five samples. The test was carried out in gastric (pH=1.2) and intestinal pH (pH=7.4) environment. The mucoadhesion was found to be higher in gastric pH than in intestinal pH. The mucoadhesion properties were also enhanced with the increase in MMT content.

At acidic pH, the free amino groups of chitosan nanoparticles might get protonated and became positively charged. This could strongly bind to the negatively charged mucus layer.

Table. 5.8. Results of in vitro wash-off test to assess mucoadhesive properties of nanoparticles prepared

pH	Sample Code	No. of particle taken	Reading after every 30 min									
			1	2	3	4	5	6	7	8	9	10
1.2	PCTS/MMT0/Gen50	50	36.2 (±0.5)	34.8 (±0.5)	31.1 (±1.0)	28.3 (±0.5)	25.3 (±0.7)	23.2 (±0.7)	20.4 (±0.5)	10.4 (±0.6)	9.7 (±0.7)	3.2 (±0.7)
	PCTS/MMT1/Gen50	50	42.8 (±0.6)	38.2 (±0.9)	34.9 (±1.4)	29.6 (±0.6)	29.3 (±0.5)	27.3 (±0.4)	21.5 (±0.6)	19.7 (±0.5)	15.9 (±0.7)	7.2 (±0.4)
	PCTS/MMT3/Gen50	60	58.3 (±1.3)	52.6 (±0.5)	46.3 (±0.5)	45.3 (±0.6)	42.6 (±0.7)	36.1 (±0.5)	34.9 (±0.6)	29.5 (±0.4)	26.4 (±0.5)	20.5 (±1.3)
	PCTS/MMT5/Gen50	65	64.3 (±0.4)	62.1 (±0.6)	56.4 (±0.4)	51.8 (±0.5)	49.6 (±0.4)	45.3 (±0.4)	42.7 (±0.4)	36.9 (±0.6)	32.2 (±0.8)	29.3 (±0.5)
7.4	PCTS/MMT0/Gen50	50	37.2 (±1.4)	31.9 (±0.5)	28.7 (±0.4)	19.7 (±0.6)	15.3 (±0.6)	12.8 (±0.4)	12.3 (±0.4)	6.3 (±0.6)	3.9 (±0.4)	0
	PCTS/MMT1/Gen50	50	38.3 (±0.9)	36.2 (±0.9)	32.8 (±0.5)	27.4 (±0.5)	16.4 (±0.6)	15.3 (±0.4)	10.3 (±0.6)	5.1 (±1.0)	4.8 (±0.4)	0
	PCTS/MMT3/Gen50	50	47.9 (±0.9)	42.3 (±0.6)	38.2 (±0.5)	32.9 (±1.1)	27.4 (±0.6)	23.3 (±1.0)	19.9 (±0.4)	9.81 (±0.4)	6.3 (±0.5)	1.9 (±0.4)
	PCTS/MMT5/Gen50	50	48.3 (±0.7)	41.6 (±0.7)	39.1 (±0.4)	42.5 (±0.4)	37.5 (±0.6)	35.9 (±0.5)	32.6 (±0.4)	22.5 (±0.6)	23.7 (±0.4)	19.4 (±0.6)

5.3.9. Ex vivo mucoadhesive test

Table 5.9. shows the results of ex vivo mucoadhesion test. The results are the mean value of five readings. It was observed that the detachment force increased with the decrease in particle size of the nanoparticles.

Table 5.6. Weight required to detach the membrane at different time intervals

Sample Code	Mass required to detach after 5 min (g)	Detachment force (dyne/cm ²)	Mass required to detach after 10 min (g)	Detachment force (dyne/cm ²)	Mass required to detach after 15 min (g)	Detachment force (dyne/cm ²)	Mass required to detach after 20 min (g)	Detachment force (dyne/cm ²)
PCTS/MMT1/Gen50	15.15 (±0.1)	4728.3 (±2.7)	29.09 (±0.01)	9331.8 (±1.6)	30.43 (±0.03)	9497.2 (±1.6)	31.82 (±0.01)	9931.1 (±3.5)
PCTS/MMT1/Gen50	18.65 (±0.8)	5820.7 (±1.3)	26.98 (±0.04)	6357.5 (±2.3)	31.45 (±0.09)	9815.6 (±2.5)	35.87 (±0.02)	11195.1 (±5.9)
PCTS/MMT3/Gen50	19.44 (±0.1)	6067.3 (±1.4)	28.13 (±0.04)	8420.5 (±4.5)	31.99 (±0.14)	9984.1 (±18.2)	35.92 (±0.02)	11210.7 (±5.4)
PCTS/MMT5/Gen50	23.98 (±0.8)	7484.2 (±6.5)	28.99 (±0.06)	9047.8 (±0.4)	32.87 (±1.2)	10258.8 (±1.6)	36.23 (±0.01)	11307.5 (±6.7)

References

- [1] Harris, R., et al. *Mar. Drugs*, **8**, 1750--1762, 2010.
- [2] Kim, H.J. et al, *Int. J. Electrochem. Sci.* **8**, 8320--8328, 2013.
- [3] Arun, G., et al. *Int J Pharm Pharm Sci*, **4**(5), 360--365, 2012.
- [4] Anitha, A. et al. *Carbohydr. Poly.* **83**, 452--461, 2011.
- [5] Sabitha, P., et al. *Int. J. Chem. Tech. Res.* **2**, 88--98, 2010.
- [6] Rekha, M.R. & Sharma, C.P. *Trends Biomater. Artif. Organs.* **21**, 107--115, 2007
- [7] Sabitha, P., et al. *Int. J. Chem. Tech. Res.* **2**, 88--98, 2010.
- [8] Zhuang, H. et al. *J. Mater.Sci. Mater. Med.* **18**, 951---957, 2007.
- [9] Shinde, U., et al. *J. Drug Del.* **2013**, 1--15, 2013

CHAPTER 6
CONCLUSION
AND
FUTURE SCOPE

In the present experimental work, it was found that isoniazid and curcumin could be encapsulated successfully inside glutaraldehyde and genipin cross-linked chitosan-CW microparticles, chitosan-MMT nanoparticles, CMC-MMT nanoparticles, PCS-MMT nanoparticles and SF-MMT nanoparticles. The nanoparticles were prepared by varying concentration of MMT and crosslinking agent using complex coacervation technique, ionic gelation technique and desolvation method.

The salient features that come out of the present study could be summarized as follows

- ❖ Isoniazid loaded biopolymer/MMT (or cellulose whisker) nanoparticles and Curcumin loaded biopolymer/MMT nanoparticles were prepared using glutaraldehyde and genipin as the crosslinkers and Tween 80 as the surfactant.
- ❖ NMR studies confirmed the synthesis of carboxymethyl chitosan and phosphorylated chitosan.
- ❖ FTIR and XRD studies established the successful synthesis of the nanoparticles. TEM studies showed the delamination/dispersion of MMT layers and cellulose whiskers inside the polymer matrix.
- ❖ Swelling and cumulative release study showed that the nanoparticles were pH dependent. All the systems, such as, Isoniazid loaded chitosan/cellulose whisker microparticles, isoniazid loaded chitosan/MMT nanoparticles, isoniazid loaded carboxymethyl chitosan/MMT nanoparticles, isoniazid loaded phosphorylated chitosan/MMT nanoparticles, curcumin loaded chitosan/MMT nanoparticles, curcumin loaded carboxymethyl chitosan/MMT nanoparticles and curcumin loaded phosphorylated chitosan/MMT nanoparticles showed higher swelling and cumulative release in gastric pH compared to intestinal pH. Whereas in the case of isoniazid loaded soy flour/MMT nanoparticles, both percentage swelling degree and cumulative release were more in intestinal pH compared to gastric pH.

- ❖ Cytotoxicity study demonstrated that except isoniazid all other components(chitosan, CMC, PCTS, CW, MMT) of the nanoparticles were non toxic. The toxicity of isoniazid was greatly reduced on encapsulation in the nanoparticles. Similarly, in case of curcumin loaded polymer-MMT nanoparticles, all the component were non toxic to normal human lymphocyte. Not only this, the components and the curcumin loaded nanoparticles induced cell growth in the normal cells. Contrary to this, the nanoparticles were highly cytotoxic to the cancer cell lines MCF-7 and HepG2. Cancer cell killing upto 40% was observed in the nanoparticles.
- ❖ *In vitro* and *ex vivo* mucoadhesion study showed that the prepared nanoparticles were mucoadhesive. The mucoadhesivity of chitosan, CMC and PCTS nanoparticles was more in gastric pH than in intestinal pH.

Future scope

- ❖ Both isoniazid and curcumin were found to be encapsulated within the crosslinked polymeric nanoparticles. The release rate can be varied by varying the type and concentration of polymer, nature and amount of crosslinker, nature and amount of reinforcing filler, etc.
- ❖ Although the present system exhibited a remarkable improvement in cell viability of the normal lymphocytes as well as killing of the cancer cells by using the curcumin loaded nanoparticles, further thorough studies in terms of repeatability and use of different cell lines are needed in order to authenticate the findings. Trial of the nanoparticles animal models and clinical trials are needed for better understanding of the anticancer activity and commercialization of the products.
- ❖ Studies relating to controlling of the particle size and their distribution may allow to produce monodisperse particles which may potentially open

up many opportunities in other biomedical and pharmaceutical applications.

- ❖ Nanoparticles prove effective in controlling drug release. However, there remains a challenge for nanoparticulate drug delivery in terms of the fate of particles and their interactions with biological systems. A methodical study is necessary which may shower some light on the interaction of the remaining polymer, filler, if any, after drug delivery with the biological system. This may help further to design the delivery system in a better way.

APPENDICES

List of Publications and Conference Attended**A. List of Publications**

1. Banik, N., et al. Soy flour nanoparticles for controlled drug delivery: effect of crosslinker and montmorillonite (MMT)". *New J. Chem.*, **37**, 3981-- 3990, 2013.
2. Banik, N., et al. Preparation and evaluation of the effect of particle size on the properties of chitosan-montmorillonite nanoparticles loaded with isoniazid. *RSC Advances* **2**, 10519--10528, 2012.
3. Banik, N., et al. Carboxymethyl chitosan-montmorillonitenanoparticles for controlled delivery of isoniazid: evaluation of the effect of theglutaraldehyde and montmorillonite, *Polym. Advan. Technol.* 2014, DOI: 10.1002/pat.3406.
4. Banik, N., et al. Synthesis and Evaluation of the Properties of Chitosan-Cellulose whisker Microparticles for Controlled Release of Isoniazid*J. Microencapsul. (Under review).*
5. Banik, N., et al. Phosphorylated chitosan-Montmorillonite Nanoparticles for Controlled Delivery of Isoniazid: Evaluation of the Effect of the Glutaraldehyde and Montmorillonite **(Communicated).**
6. Banik, N., et al. Preparation and evaluation of the effect of chitosan/montmorillonite nanoparticles for the controlled delivery of hydrophobic drug, Curcumin. **(Communicated).**
7. Banik, N., et al. A systematic study of carboxymethylchitosan/montmorillonite nanoparticles for controlled delivery of Curcumin. **(Communicated).**
8. Banik, N., et al. Study of phosphorylated chitosan/ MMT nanoparticles as an anticancer agent and for the controlled delivery of Curcumin. **(Communicated).**

List of Seminars/Conferences/Workshops/Symposium attended

1. Summer School on Green Chemistry, 2-22nd June, 2009, Tezpur University.
2. Frontier Lecture Series, 20-22nd November, 2009, Tezpur University.
3. Workshop on Intellectual Property Right Sensitization, 21st September, 2010, Tezpur University.

4. National Conference on Chemistry, Chemical Technology and Society, 11-12th November, 2012, Tezpur University.
5. Workshop on Spectroscopic tools and their Applications, 6th April, 2013, Tezpur University.

Cite this *RSC Advances*, 2012, 2, 10519–10528

www.rsc.org/advances

PAPER

Preparation and evaluation of the effect of particle size on the properties of chitosan-montmorillonite nanoparticles loaded with isoniazid

Nibedita Banik,^a Anowar Hussain,^b Anand Ramteke,^b Hemanta K. Sharma^c and Tarun K. Maji^{*a}

Received 18th April 2012, Accepted 25th August 2012

DOI: 10.1039/c2ra20702h

In this report, efforts have been made to develop isoniazid loaded chitosan-montmorillonite nanoparticles by ionic gelation of chitosan with pentasodium tripolyphosphate. The nanoparticles have been characterized by FTIR, XRD, SEM and TEM. The effect of surfactant and particle size on chitosan nanoparticles have been assessed with regard to swelling, encapsulation efficiency and release of isoniazid in different mediums. Swelling experiments provide important information on drug diffusion properties, which indicates that the chitosan nanoparticles are highly sensitive to the pH environment. The drug release mechanism has been studied during different time periods using a UV-visible spectrophotometer. Cytotoxicity has been assessed by MTT assay analysis. Mucoadhesion properties have been appraised by an *in vitro* wash off test and an *ex vivo* mucoadhesion test. The results imply that chitosan-montmorillonite nanoparticles can be exploited as potential drug carriers for controlled-release applications.

1. Introduction

In the current scenario of pharmaceutical research, polymers have been extensively used as an active agent for drug delivery. They can control the release of a drug over a prolonged period by forming a matrix, a membrane or (nano)carriers thereby avoiding repetitive dosing.¹ Generally, natural biodegradable polymers are preferred as controlled drug delivery systems due to their low toxicity, easy availability and cell biocompatibility.² Among the natural polymers, chitosan plays an important role in drug delivery systems. Chitosan is an omnipresent modified natural polymer obtained from partial deacetylation of the biopolymer chitin, which is present in the shells of crustacean, such as crabs and lobsters.³ It can also be obtained from some microorganisms and yeasts. Chitosan is a mucoadhesive polycation polymer at acidic pH which is not noxious and is biocompatible.^{4–6} Chitosan also has a fungicidal effect, wound healing properties and can reduce cholesterol level.⁷ Owing to its cationic nature, chitosan has good mucoadhesive and membrane permeation enhancing properties.⁸

Nanoparticles have evoked much interest recently for the delivery of drugs such as peptides, proteins and genes due to their ability to protect these from degradation by proteolytic enzymes in the gastrointestinal tract. They possess mucoadhesive properties

and are capable of being adhered to the mucosal tissues. Different bioactive compounds have been successfully encapsulated within polymers and have been tested for their therapeutic activity.⁹

Montmorillonite (MMT) clay is a smectite clay having silica tetrahedral sheets layered between alumina octahedral sheets. Due to its good physical and chemical properties, MMT has received considerable attention in recent years for drug delivery systems applications.¹⁰ Isoniazid is an antituberculosis drug which can be used as a model drug.

Various methods are used to prepare chitosan nanoparticles, such as coacervation, emulsion-droplet coalescence, reverse micelles, ionic gelation and self assembly chemical modification. Extensive research has been done to synthesize chitosan nanoparticles loaded with drugs by ionic gelation processes.^{11–14} The amine groups of chitosan are protonated to form ammonium ions in acidic media. These can be crosslinked either chemically with glutaraldehyde and genipin or physically with sodium tripolyphosphate, sulphate, citrate, *etc*. Varieties of crosslinkers are reported to be used for controlling the release behavior of drugs.^{14–16} The nanoparticles prepared by physical crosslinking swell faster in release media compared to those of chemically crosslinked nanoparticles. Therefore, a synergistic approach by using both physical and chemical crosslinking seems to be more viable to control the release behavior of a drug. A similar approach has reported by Gupta *et al*.¹⁷ To the best of our knowledge, there is no report on synthesizing drug loaded chitosan-MMT nanoparticles by using this method. In this paper, efforts have been made to prepare isoniazid loaded chitosan-MMT nanoparticles by an ionic gelation method followed by chemical crosslinking with glutaraldehyde (GA). This report aims at the study of the effect of clay and surfactant on various properties of nanoparticles

^aDepartment of Chemical Sciences, Tezpur University, Assam, India 784028. E-mail: tkm@tezu.ernet.in, Fax: +91 3712 267005, Tel: +91 3712 267007, Ext: 5053

^bDepartment of Molecular Biology and Biotechnology, Tezpur University, Assam, India 784028

^cDepartment of Pharmaceutical Sciences, Dibrugarh University, Assam, India 786004

2. Experimental section

2.1 Materials

Low molecular weight chitosan, montmorillonite K-10, isoniazid, histopaque 1077 and [3-(4, 5-dimethylthiazol-2-yl)-2,5-diphenyl tetrazolium bromide] (MTT) were obtained from Sigma Aldrich, Germany Tween 80, glutaraldehyde (25%) and sodium tripolyphosphate (TPP) were purchased from Merck, India RPMI 1640 and fetal bovine serum (FBS) were procured from HiMedia Laboratories (Mumbai, India) The rest of the chemicals were of analytical grade and used directly

2.2. Preparation of chitosan clay nanoparticles loaded with isoniazid

Chitosan nanoparticles were prepared by ionic crosslinking of chitosan with sodium TPP and employing the process as reported by Calvo¹¹ 1% (w/v) chitosan solution was prepared in water containing 0.5% (v/v) acetic acid 0.005 g of MMT was swelled in 50 mL of water for 24 h. It was then stirred vigorously by mechanical stirring for 48 h and sonicated for 30 min. This dispersed MMT solution was added to 50 mL of 1% (w/v) chitosan solution. To this solution, isoniazid (0.01 g) and Tween 80 (0.5–5% v/w of chitosan i.e. 0.0025–0.025 mL) were added, stirred and sonicated for 15 min. Then, 1% (w/v) TPP solution was prepared in water. Nanoparticles were obtained by the slow addition of 15 mL of TPP solution to 100 mL of isoniazid containing chitosan-MMT solution under constant magnetic stirring at room temperature for 30 min. The temperature of the container containing nanoparticles was brought down to 5–10 °C to harden the nanoparticles. GA (0.1 mmol) was added and the temperature was increased to 45 °C. The reaction was continued for 45 min. The nanoparticles were separated by centrifuging the solution for 30 min. The product was washed several times with water and dried. The dried nanoparticles were kept in an ampule, stored in a refrigerator and redispersed in deionised water for further use. Scheme 1 and Scheme 2 depict the preparation process and the plausible mechanism of formation of isoniazid loaded chitosan- MMT nanoparticles. A series of six samples were prepared for the present study as represented in Table 1.

2.3. Calculation of process yield

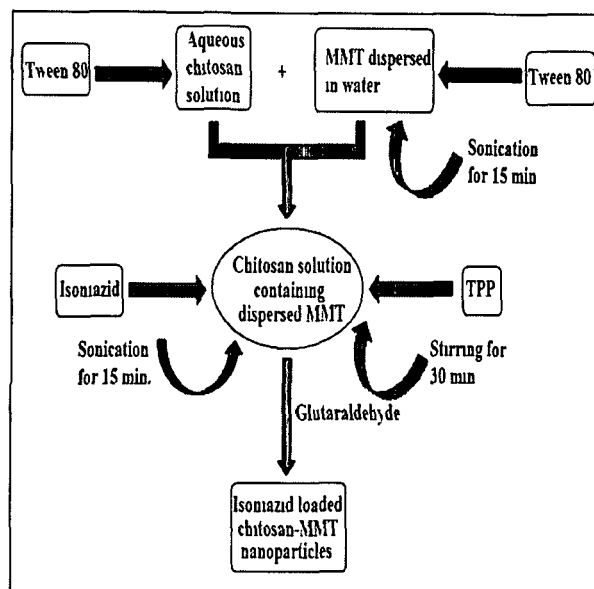
Process yield was calculated using the following equation as described in the literature¹⁸

$$\text{Process Yield (\%)} = \frac{[\text{Weight of nanoparticles} \times 100]}{[\text{Weight of (drug + clay + polymer)}]}$$

2.4. Calibration curve of isoniazid

A calibration curve is essential to estimate the release rate of drug from nanoparticles in a suitable solvent medium. The calibration curve was drawn as per a previously reported procedure¹⁹

A known concentration of isoniazid (in double distilled water) was scanned in the range 200–400 nm by using a UV-Visible spectrophotometer (UV-2001 Hitachi, Tokyo, Japan). A sharp peak at 262 nm was noticed for isoniazid having a concentration in the range of 0.001–0.01 g/100 mL. The absorbance values at



Scheme 1 Flowchart diagram showing the main steps in the preparation of isoniazid loaded chitosan nanoparticles

262 nm obtained with the respective concentration were recorded and plotted. From this calibration curve, the unknown concentration of isoniazid was obtained by knowing the absorbance value.

2.5. Calculation of drug loading efficiency and encapsulation efficiency of the nanoparticles

The drug loading efficiency of nanoparticles with different formulations was determined by ultracentrifugation of samples at room temperature for 30 min. The amount of free isoniazid was determined by noting the absorbance value of the supernatant at 262 nm using a UV-Visible spectrophotometer. The drug loading efficiency (LE) of the nanoparticles was calculated using the following equations¹¹

$$\text{Loading efficiency (LE) (\%)} = \frac{(\text{Total amount of drug} - \text{Free amount of drug}) \times 100}{\text{Total amount of drug}}$$

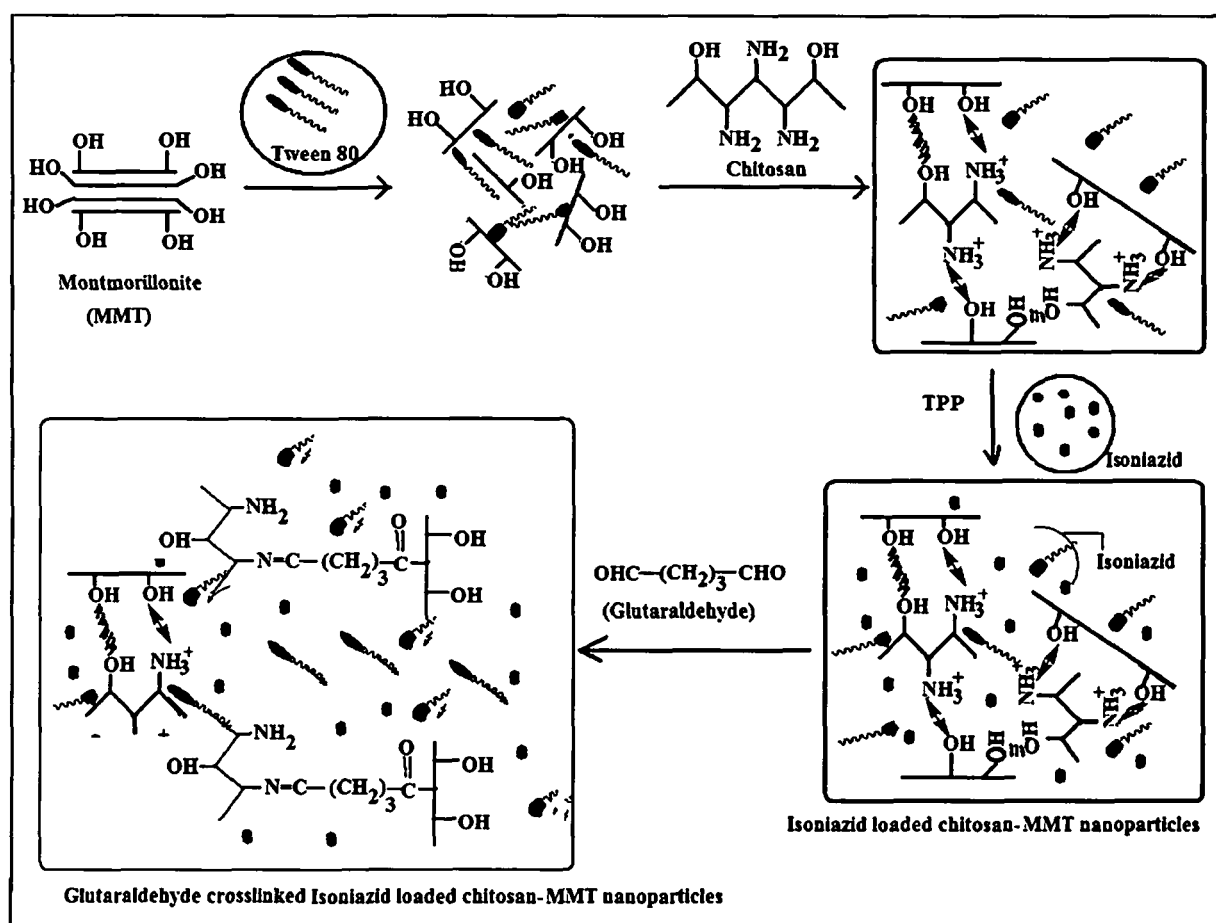
$$\text{Encapsulation efficiency (EE) (\%)} = \frac{(\text{Total amount of drug} - \text{Free amount of drug}) \times 100}{\text{Weight of dry nanoparticles}}$$

2.6. Fourier transmission infra-red spectroscopy (FTIR) study

FTIR spectra of nanoparticles were taken using a Nicolet (model Impact-410) spectrophotometer. The nanoparticles were ground to a powder, mixed with KBr and spectra were recorded in the range of 4000–400 cm^{-1} .

2.7. X-ray diffraction (XRD) study

The degree of intercalation of MMT and the distribution of isoniazid in chitosan-clay nanoparticles were examined by X-ray diffractometry. It was carried out in a Rigaku X-ray diffractometer.



Scheme 2 Plausible mechanism of formation of isoniazid loaded chitosan nanoparticles

(Miniflex, UK) using Cu-K α ($\lambda = 0.154$ nm) radiation at a scanning rate of 1°min^{-1} with an angle ranging from 2° to 70° of 2θ

2.8 Particle size determination

Particle size was determined by a dynamic light scattering (DLS) analyzer (model DLS—Nano ZS, Zetasizer, Nanoseries, Malvern Instruments)

2.9. Scanning electron microscopy (SEM) study

The samples were mounted on a brass holder sputtered with platinum. The surface morphologies of chitosan-MMT nanoparticles loaded with isoniazid were studied by using a scanning

electron microscope (JEOL JSM-6390LV) at an accelerated voltage of 5–10 KV

2.10. Transmission emission microscopy (TEM) study

The dispersion of the silicate layers of clay in chitosan nanoparticles was examined by using a transmission electron microscope (JEOL JEM-2100) at an accelerated voltage of 100 KV

2.11. Water uptake studies

Water uptake studies were performed in both phosphate buffer (pH 7.4) and 0.1 N HCl solution (pH 1.2) according to the procedure described in the literature²⁰

Table 1 Recipes for the formation of different isoniazid loaded chitosan-montmorillonite nanoparticles

Sample code	Chitosan (% w/v) (amount in g in 50 mL water)	MMT (% w/v) w r t chitosan (amount in g in 50 mL water)	Tween 80 (% v/v) w r t chitosan (amount in mL)	Isoniazid/g	TPP (% w/v) w r t water (amount in g in 100 mL water)	GA/mmol
NPI	1 (0.5)	1 (0.005)	0 (0.0)	0.01	1 (1)	0.1
NPII	1 (0.5)	1 (0.005)	0.5 (0.0025)	0.01	1 (1)	0.1
NPIII	1 (0.5)	1 (0.005)	1 (0.005)	0.01	1 (1)	0.1
NPV	1 (0.5)	1 (0.005)	3 (0.015)	0.01	1 (1)	0.1
NPV	1 (0.5)	1 (0.005)	5 (0.025)	0.01	1 (1)	0.1
NPVI	1 (0.5)	0 (0.00)	5 (0.025)	0.01	1 (1)	0.1

Nanoparticles (0.1 g) were taken in a pouch made of nylon cloth. The empty pouch was first conditioned by immersing it in either 0.1 N HCl (pH 1.2) or phosphate buffer (pH 7.4) for different time periods (1–8 h). The pouch containing the nanoparticles was immersed in a similar way in either 0.1 N HCl (pH 1.2) or phosphate buffer (pH 7.4) for similar time periods. The weights of wet nanoparticles after a definite time period were determined by deducting the respective conditioned weight of the empty nylon pouch from this. Water uptake (%) was determined by measuring the change in the weight of the nanoparticles. The percentage of water uptake for each sample determined at time t was calculated using the following equation:

$$\text{Water uptake (\%)} = [(w_2 - w_1)/w_1] \times 100$$

where, w_1 is initial weight of nanoparticles before swelling, and w_2 is the final weight of nanoparticles after swelling for a predetermined time t .

The experiments were performed in triplicate and represented as a mean value.

2.12. *In vitro* drug release studies

To study the release profile of the isoniazid loaded chitosan-MMT nanoparticles, dried drug loaded samples were immersed in a solution of different pH, namely 1.2 and 7.4, and stirred continuously. At scheduled time intervals, 5 mL solution was withdrawn, filtered and assayed spectrophotometrically at 262 nm by using a UV-Visible spectrophotometer for the determination of the cumulative amount of drug release up to a time t . To maintain a constant volume, 5 mL of the solution having same pH was returned to the container.^{21,22} Each determination was carried out in triplicate.

2.13. Isolation of lymphocytes, culture and treatment

Chicken blood was collected from source. It was diluted in a 1:1 ratio with phosphate buffer saline (PBS) and 6 mL was layered into 6 mL histopaque (1.077 g mL⁻¹). The isolation of lymphocytes and the study of cell viability were done as per the procedure cited in the literature.²³ Lymphocytes were isolated from the sample after centrifugation for 30 min at 400 g, washed with PBS and finally with serum free media separately through centrifugation for 10 min at 250 g. Cell pellets were then suspended in PBS and cell viability was checked by the Trypan blue exclusion method using a haemocytometer. Cell viability more than 90% was used for subsequent study.

Aliquots of 200 μ L of isolated cells were cultured in RPMI supplemented with 10% heat inactivated FBS. Initially cells were maintained for 4 h in RPMI without FBS at 37 °C in 5% CO₂ in an incubator. Cells were then treated as per experimental requirements and maintained in the presence of FBS for 6 h, 12 h and 24 h.

2.14. Cytotoxicity experiments

A cytotoxicity assay was performed by measuring the viability of cells according to the method as described by Denizot and Lang.²⁴ The key component [3-(4, 5-dimethylthiazol-2-yl)-2, 5-diphenyl tetrazolium bromide] (MTT) is yellowish in color and mitochondrial dehydrogenase of viable cells cleave the tetra-

zolium ring, yielding purple insoluble formazan crystals, which were dissolved in a suitable solvent. In this report, DMSO is used as the control solvent. The resulting purple solution was spectrophotometrically measured. An increase or decrease in cell number resulted in a concomitant change in the amount of formazan formed, indicating the degree of cytotoxicity caused by the test material. Briefly, after treatments, cells were treated with 10% of MTT for 2 h followed by dissolving the formazan crystals in solvent and measuring the absorbance of solution at 570 nm. The absorbance of control cells at 6, 12 and 24 h were separately set as 100% viability and the values of treated cells were calculated as a percentage of the control.

2.15. Mucoadhesion study

2.15.1. *In vitro* wash-off test. The mucoadhesive property of the nanoparticles was evaluated by an *in vitro* adhesion test method known as the wash-off test method.²⁵ Freshly excised pieces of goat intestinal mucosa (5 × 5 cm) were mounted with the mucous side exposed on to glass slides with cotton thread. About 50 nanoparticles were spread onto each prepared glass slide and immediately thereafter the slides were hung up to a USP tablet disintegration test apparatus (Tab Machines, Mumbai). When the test apparatus was operated, the sample was subjected to slow up and down movement in the test fluid at 37 °C contained in the 1L vessel of the apparatus. Readings were taken at intervals of 30 min up to 5 h by stopping the machine and counting the number of nanoparticles still adhering to the mucosal surface. The test was performed at intestinal (pH 7.4) and simulated gastric fluid (pH 1.2) conditions.

2.15.2. *Ex vivo* mucoadhesive test. In this method, the force required to separate bio-adhesive samples from freshly excised goat intestine was determined.²⁶ Keeping the mucosal side out, the intestine was secured on to each glass vial using nylon thread. The diameter of each exposed mucosal membrane was 2 cm. The vials with the nasal tissue were kept at 37 °C for 10 min. To the exposed tissue on this vial, a constant amount of nanoparticle was applied. The height of the vial was adjusted so that the nanoparticles could adhere to the mucosal tissues of both vials. Water was added at a constant rate to the pan on the other side of the modified balance until the two vials were separated. The weight of water showed the weight required for displacement.

The adhesive force expressed as the detachment stress (dyne cm⁻²) is calculated using the following equation:

$$\text{Detachment stress (dyne cm}^{-2}\text{)} = mgA^{-1}$$

where, m is the mass (g) required to detach the membrane, g is acceleration due to gravity taken as 980 cm sec⁻² and A is the area of tissue exposed which is equal to πr^2 (r is the radius of the exposed mucosal membrane).

2.16. Statistical analysis

All the data were expressed as the mean \pm SD. Results were statistically analyzed by Student's t test for significant differences between the group mean using GraphPad software.²⁷ The significant difference between the experimental and the control

group was set at different levels as $p < 0.05$, $p < 0.01$ and $p < 0.001$

3. Results and discussion

3.1. Effect of variation of surfactant concentration on the different properties of chitosan nanoparticles

The results showing the effects of variation of surfactant concentration on different properties of chitosan nanoparticles are shown in Table 2. In the case of MMT containing chitosan nanoparticles, yield (%) remained almost unchanged irrespective of surfactant concentration. Encapsulation efficiency (%) was also found to remain the same. It was also observed that neither the surfactant nor the MMT alone produced any significant effect on the drug loading efficiency, except the yield. Surfactant alone provided a somewhat low yield which might be due to the loss during isolation. At a fixed level of MMT concentration, drug loading efficiency showed an increasing trend while particle size exhibited a decreasing trend as the concentration of the surfactant increased. The presence of surfactant could increase the interlayer distance of silicate layers of MMT. The higher the concentration of surfactant, the higher the interlayer distance to accommodate the polymer as well as the drug. This could have resulted in an increase in drug loading efficiency. As the surfactant was soluble in water, it could decrease the solubility of ionically crosslinked chitosan in water thus favoring the solid particle formation and consequently decreasing the viscosity of the dispersion phase. The lower dispersion phase viscosity facilitated the formation of smaller particles. The dispersing effect of the surfactant also favored the formation of smaller particles as the concentration of surfactant increased. Besides this, the physical interaction between the chitosan macromolecules may have been destructed due to shear resulting in the formation of a dispersing phase of lower viscosity²⁸ which favors the formation of smaller particles. Zeta potential values of the nanoparticles showed that the zeta potential increased with the decrease in particle size. The zeta potential of nanoparticles which did not contain tween 80 and isoniazid was found to be less than that of the formulations containing both tween 80 and isoniazid. The zeta potential was found to be positive for all the formulations. Nanoparticles prepared without surfactant had a lower zeta potential indicating that they would aggregate in acidic or basic medium. On the other hand, particles prepared with surfactant exhibited a higher zeta potential probably because the surfactant prevented the counter-ions from binding within chitosan. Such particles would be expected to be stable.

Isoniazid has normally three pK_a values 1.8 based on the hydrazine nitrogen, 3.5 based on the pyridine nitrogen and 10.8 based on the acidic group.²⁹ At pH 1.2, the pK_a of isoniazid is found to be around 2 due to protonation of the hydrazine nitrogen whereas at a basic pH of 7.4 it is found to be around 12. The increase in the zeta potential with the incorporation of the drug suggests that at least a part of the drug-polymer association was surface-adsorbed. Thus, a part of the drug was embedded within the chitosan matrix and the rest was adsorbed on the surface of the nanoparticles.

3.2. Fourier transmission infra-red spectroscopy (FTIR) study

In the spectrum of pure chitosan (Fig. 1a), the broad absorption band that appeared in the range 3200–3450 cm^{-1} was due to the hydrogen-bonded OH stretching and NH_2 asymmetric stretching. The characteristic peaks of amide I and amide II appeared at 1646 cm^{-1} (C=O stretching) and 1569 cm^{-1} (N-H in plane deformation coupled with C=N stretching), respectively.³⁰ The peaks exhibited in the spectrum for MMT (Fig. 1b) at 3435, 1639 and 1051–544 cm^{-1} were for –OH stretching, –OH bending and oxide bands of metals like Si, Al, Mg, etc. Fig. 1c represents the spectrum of isoniazid. The absorption peaks that appeared at 1664 and 1551 cm^{-1} were due to the amide I (C=O stretching)

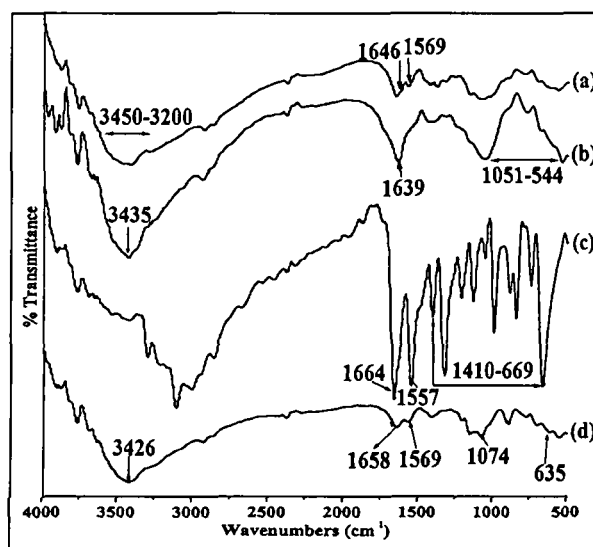


Fig. 1 FTIR spectra of (a) pure chitosan, (b) MMT, (c) isoniazid and (d) NPV

Table 2 Effect of variation of surfactant concentration on the different properties of chitosan nanoparticles^a

Sample code	Yield of nanoparticle (%)	Encapsulation efficiency (%)	Drug loading efficiency (%)	Average diameter/nm	Zeta potential/mV	Zeta potential of the same formulations without drug/mV	Zeta potential of nanoparticles after 3 h of drug release/mV
NPI	92.81 (± 0.01)	73.10 (± 0.02)	25.39 (± 0.08)	451.8 (± 15)	21.22 (± 0.03)	17.05 (± 0.01)	18.53 (± 0.04)
NP1I	91.27 (± 0.05)	72.98 (± 0.04)	25.61 (± 0.04)	—	—	—	—
NP1II	91.38 (± 0.01)	73.32 (± 0.04)	28.18 (± 0.01)	322.4 (± 12)	28.24 (± 0.1)	21.67 (± 0.07)	23.89 (± 0.01)
NP1V	91.19 (± 0.01)	73.48 (± 0.01)	29.27 (± 0.01)	305.7 (± 13)	30.01 (± 0.06)	23.12 (± 0.01)	26.33 (± 0.04)
NPV	92.52 (± 0.05)	73.41 (± 0.03)	31.63 (± 0.02)	282.2 (± 15)	36.93 (± 0.01)	30.41 (± 0.03)	33.12 (± 0.01)
NPV1	86.16 (± 0.08)	73.60 (± 0.02)	25.58 (± 0.01)	—	—	—	—

^a Each value represents average of five readings, standard deviation in parenthesis

and amide II (N–H bending of secondary amide group), respectively. Besides this, multiple peaks appeared in the range $1410\text{--}669\text{ cm}^{-1}$.²⁰

All the characteristic peaks of chitosan, MMT and isoniazid appeared and their intensities decreased in the spectrum of isoniazid loaded chitosan-MMT nanoparticles (Fig. 1d). Moreover, the intensity of the peak that appeared in the range $3450\text{--}3200\text{ cm}^{-1}$ (Fig. 1a) decreased and shifted to lower wave number. This indicated an interaction between MMT and chitosan. The decrease in hydroxyl peak intensity was reported by Maji *et al.*³¹ while studying the properties of wood polymer nanocomposites. All these indicated a better dispersion of MMT and isoniazid in the chitosan-MMT nanoparticles.

3.3. X-ray diffraction (XRD) study

Isoniazid (Fig. 2, curve 2a) shows multiple peaks at $2\theta = 12$ to 50° due to its crystalline nature. A similar type of diffractogram was reported by Fukuoka *et al.*³² Chitosan (curve 2b) shows its characteristic diffraction peak at $2\theta = 20.3^\circ$ which corresponds to the (100) plane of the orthorhombic crystal.³³ MMT exhibits the two characteristic peaks at $2\theta = 9.01^\circ$ and 26.7° which are assigned to the (001) and (002) planes (curve 2c).³⁴ The characteristic peaks for MMT and isoniazid were found to disappear in the diffractogram of MMT/chitosan nanoparticles (curve 2d). It could be said that either the full expansion of the MMT gallery occurred, which was not possible to detect by XRD, or the MMT layers became delaminated and no crystal diffraction peak appeared.³⁵ These findings suggested the occurrence of a molecular level dispersion of isoniazid in isoniazid loaded chitosan-MMT nanoparticles. The molecular level dispersion of isoniazid in the chitosan-hydroxyethyl

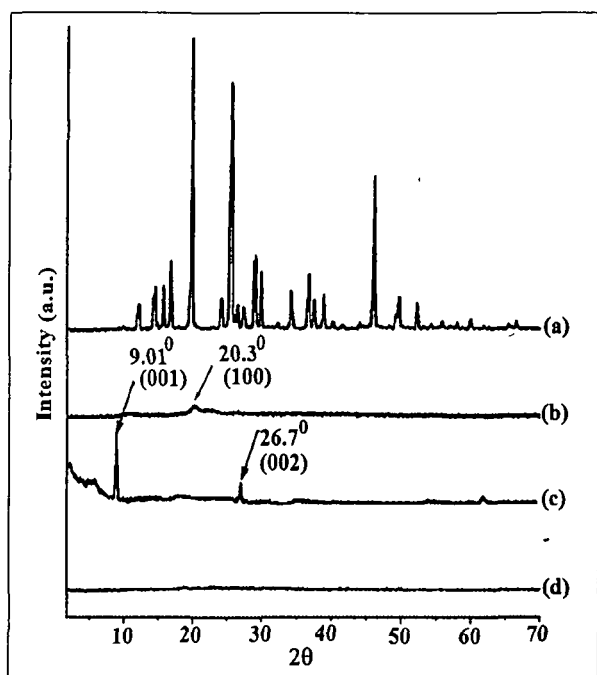


Fig. 2 XRD patterns of (a) isoniazid, (b) chitosan, (c) MMT and (d) NPV.

cellulose blended microsphere was reported by Aminabhavi *et al.*³⁶

3.4. Scanning electron microscopy (SEM) study

SEM micrographs of chitosan-MMT nanoparticles and isoniazid loaded nanoparticles are shown in Fig. 3a and 3b, respectively. The surface of the nanoparticles without isoniazid appeared less smooth and agglomerated as compared to isoniazid loaded nanoparticles. Isoniazid loaded nanoparticles had a spherical shape and a smooth surface. Selvaraj *et al.*¹¹ reported that acyclovir loaded chitosan nanoparticles had a solid dense structure with a smooth spherical shape.

3.5. Transmission electron microscopy (TEM) study

TEM micrographs of isoniazid loaded chitosan nanoparticles devoid of MMT and with MMT are shown in Fig. 3c and 3d, respectively. Fig. 3d shows the presence of platelets of MMT tactoids in which the dark lines are the intersection of MMT layers. The bright areas are polymer matrix and isoniazid. A similar observation was reported by Wang *et al.*³⁷ while studying the biopolymer/MMT structure by TEM. The results indicated that MMT was incorporated and dispersed in the chitosan matrix.

3.6. Swelling study

The effect of pH on the percentage swelling of isoniazid loaded nanoparticles at two different pH namely, 1.2 and 7.4, are shown in Fig. 4. It was observed that the swelling of isoniazid loaded chitosan-MMT nanoparticles was greater in gastric pH (1.2) than in intestinal pH (7.4). In an acidic medium, the amine groups of chitosan molecules were ionized to ammonium ions. These cationic charges acted as repulsive forces between the polymer molecules³⁸ and hence increased the swelling. In alkaline pH, the inherent hydrophobicity of chitosan nanoparticles prevented them

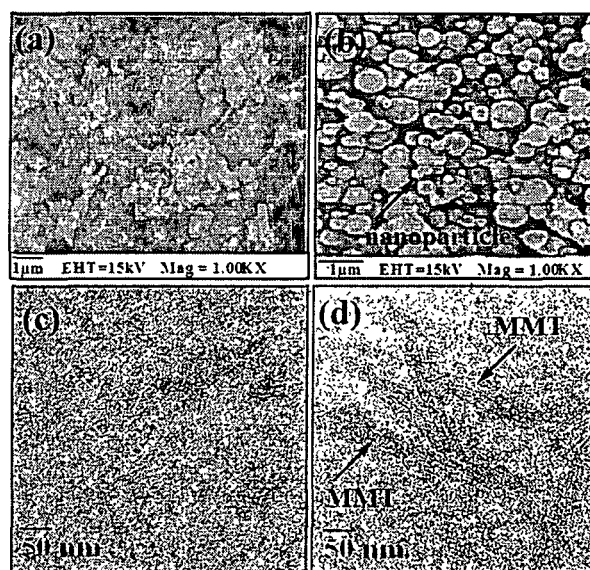


Fig. 3 SEM micrographs of (a) chitosan-MMT nanoparticles without isoniazid, (b) NPV and TEM micrographs of (c) NPVI and (d) NPV.

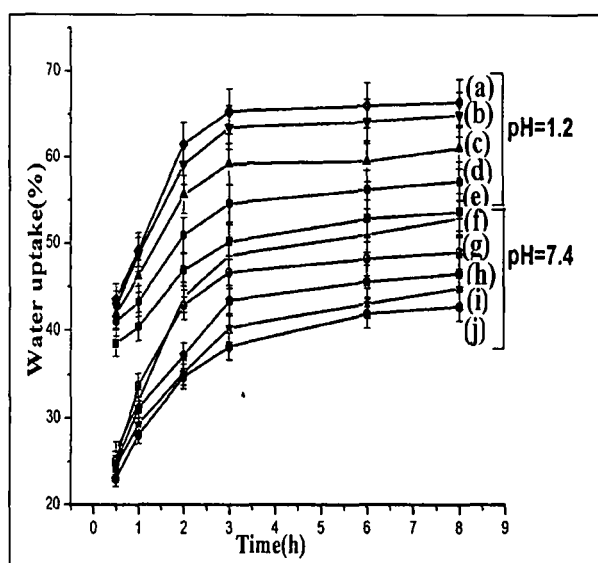


Fig 4 Percentage swelling degree at pH 1.2 of (a) NPV, (b) NPV, (c) NPV, (d) NPV and (e) NPI and at pH 7.4 of (f) NPV, (g) NPV, (h) NPV, (i) NPV and (j) NPI

from fast swelling³⁹ Furthermore, the percentage swelling was found to increase with the increase in time and decrease in particle size of the nanoparticles. The lower the particle size, the higher was the surface area. Higher surface area facilitated better contact of the nanoparticles with the solvent and thus improved swelling.

3.7. *In vitro* Release Studies

The drug release profile of the nanoparticles at two different pH, namely 1.2 and 7.4, are shown in Fig 5. The cumulative release (%) of isoniazid from chitosan-MMT nanoparticles was found to be pH-dependent. The cumulative release (%) of isoniazid decreased with the increase in the pH of the medium. The two

main factors governing the release profile of isoniazid from nanoparticles were the swelling nature of the polymer and the solubility of the drug in the medium. The difference in release profile was due to the difference in the solubilities of chitosan in gastric and intestinal pH.⁴⁰ Chitosan was more soluble in gastric pH compared to intestinal pH. The solubility of isoniazid increased at acidic pH due to its basic nature as reported in literature.⁴¹ A lower pH of the medium favoured both the swelling of the polymer and the solubility of the drug. Cumulative release (%) of isoniazid was also found to increase with the increase in time and decrease in particle size of the nanoparticles. The explanation for this observation is similar to that stated earlier.

Moreover, a burst release of about 50% drug was observed in the first 3 h of the test. The lower diffusion path due to the lower particle size along with other already stated factors played an important role in controlling the release rate. The adsorbed drug on the surface of nanoparticles might be the main factor responsible for the initial burst release. This was supported by the zeta potential value.⁸

3.8. Cytotoxicity test

The results of the MTT-assay are shown in Fig 6. It was observed that the cell viability varied between 85–90% within the studied surfactant (tween 80) concentration. This indicated that the surfactant was not highly cytotoxic to the cells (Fig 6a). Tween 80 did not exhibit any significant cytotoxicity when evaluated in CaCo-2 cells.⁴²

In our case, a slight decrease in cell viability was observed as the concentration of surfactant increased. The use of nonionic surfactants as penetration enhancers has been reported due to their non-irritating nature and low toxicity.⁴³ Addition of surfactant resulted in an increase in the dispersion of nanoparticles and enhanced their interaction with the cells leading to a decrease in cell viability. MMT showed very low cytotoxicity as is evident from Fig 6b. A similar result was also reported by Wang *et al.*³⁶ Fig 6c and 6d show the cell viability (%) of isoniazid alone and clay free isoniazid loaded nanoparticles. In

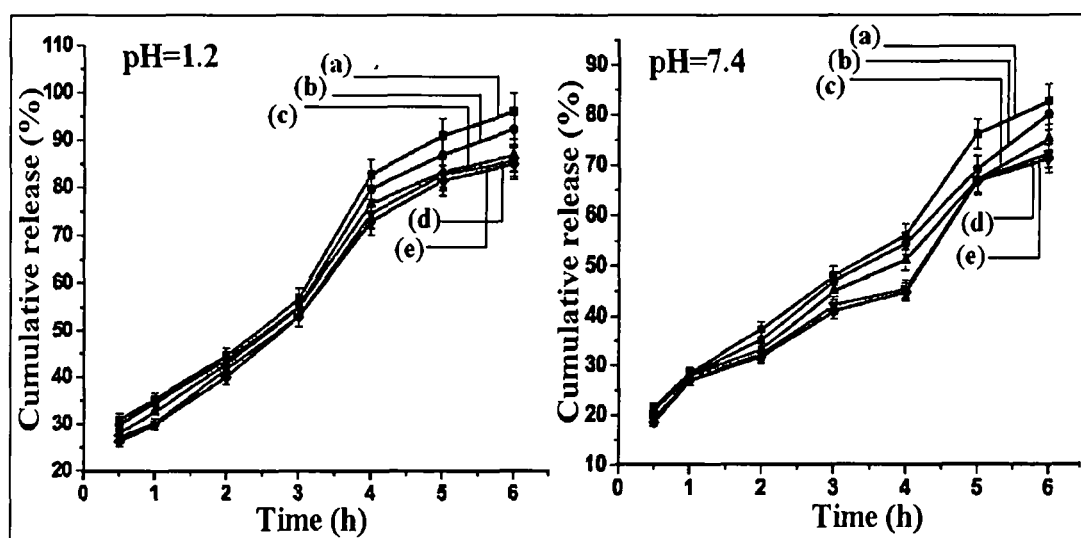


Fig 5 Cumulative percentage drug release at pH 1.2 of (a) NPV, (b) NPV, (c) NPV, (d) NPV and (e) NPI and at pH 7.4 of (a) NPV, (b) NPV, (c) NPV, (d) NPV and (e) NPI

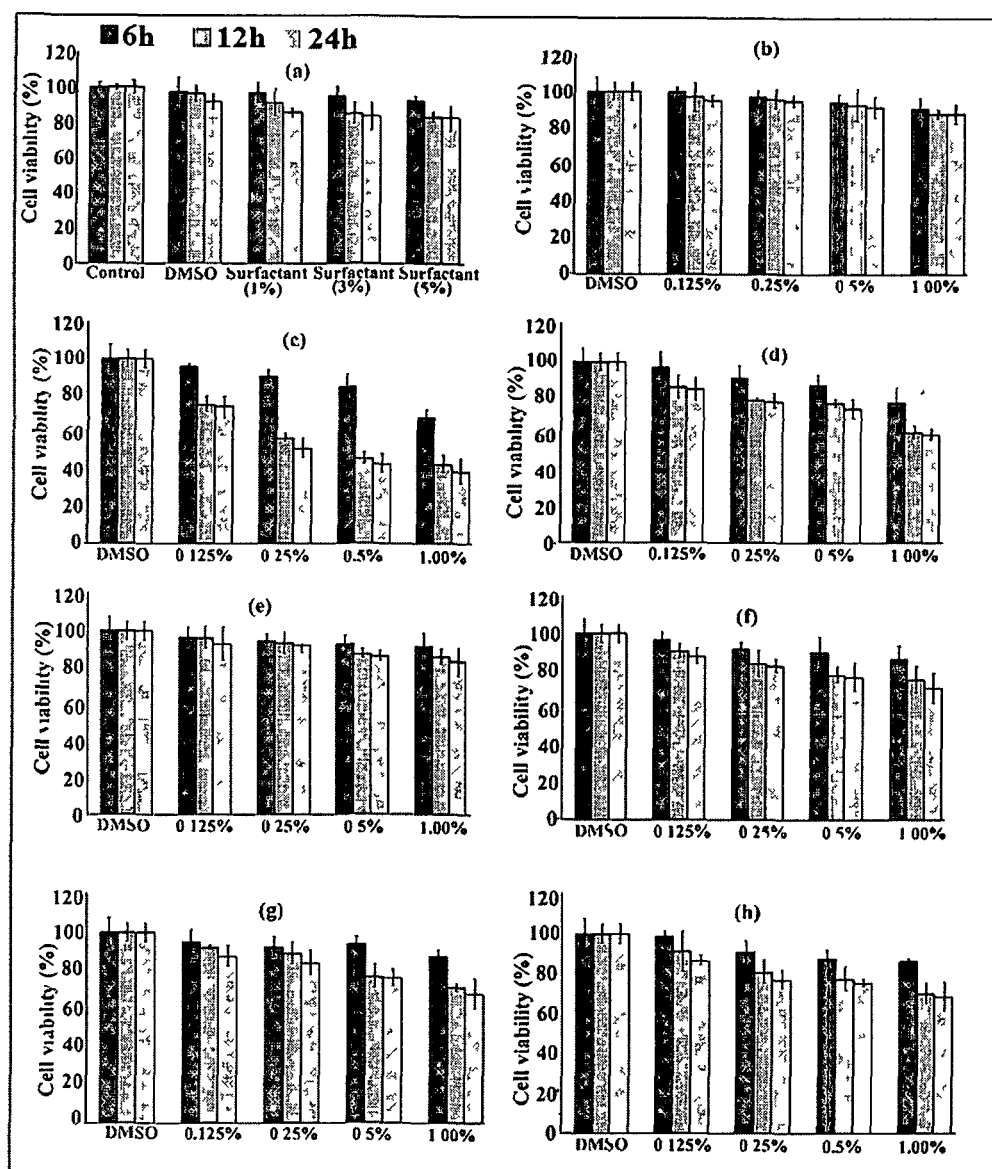


Fig 6 Cell viability study with variation of (a) surfactant, (b) clay, (c) isoniazid, (d) drug embedded nanoparticles, (e) NPI, (f) NPIII, (g) NPIV and (h) NPV at 6 h, 12 h and 24 h

both these cases, the cell viability decreased with the increase in the concentration of isoniazid. The cytotoxicity was found to be less in the case of isoniazid embedded polymeric nanoparticles compared to those of isoniazid alone. The polymer slowed down the release of isoniazid and hence decreased the interaction of the drug with the cell. It was observed further (Fig 6d and 6e) that the cell viability of nanoparticles containing clay was greater compared to clay-free nanoparticles. This might be due to the fact that the silicate layers hindered the release of drug in the cell because of its tortuous path. Fig 6(e–h) shows the results of cell viability of nanoparticles prepared under different concentrations of surfactants (0–0.25 ml). Nanoparticles prepared using surfactant exhibited higher cytotoxicity than those prepared without surfactant. The cytotoxicity of nanoparticles increased up to the use of 3% (v/w) surfactant, beyond that the value

remained almost unchanged. The nanoparticles prepared without tween 80 had large particle size compared to nanoparticles prepared with tween 80. The higher the surfactant concentration, the lower the particle size observed and the higher was the surface area. Due to the higher surface area, the contact of the nanoparticles with the cell increased and hence the cytotoxicity also increased. The increase of cytotoxicity value with time was due to more contact between the drug and the cell wall. The cell viability of the nanoparticles synthesized with and without surfactant was within the range of 70–90%.

3.9. *In vitro* wash-off test for evaluation of mucoadhesive properties

Results of the *in vitro* wash off test of chitosan-MMT nanoparticles containing isoniazid are given in Table 3. The

Table 3 Results of *in vitro* wash-off test to assess mucoadhesive properties of nanoparticles prepared^a

pH	Sampl code	No of particles taken	Reading after every 30 min									
			1	2	3	4	5	6	7	8	9	10
12	NPI	50	35.4 (± 0.5)	32.4 (± 0.5)	25.4 (± 1.0)	20.4 (± 0.5)	12.2 (± 0.7)	10.8 (± 0.7)	8.6 (± 0.5)	5.0 (± 0.6)	0	0
	NPIII	50	44 (± 0.6)	42 (± 0.9)	40 (± 1.4)	35 (± 0.6)	30 (± 0.6)	20.4 (± 0.5)	15 (± 0.6)	12.4 (± 0.5)	10.2 (± 0.7)	4.8 (± 0.4)
	NPIV	50	52.8 (± 1.3)	50 (± 0.6)	46.8 (± 1.2)	45 (± 0.6)	42.8 (± 0.7)	37.8 (± 1.0)	32 (± 0.6)	23.2 (± 0.4)	21.6 (± 0.5)	17 (± 1.3)
	NPVI	65	60 (± 0.9)	58 (± 0.6)	57 (± 0.9)	55.4 (± 0.8)	51.4 (± 0.5)	47.2 (± 0.4)	35.2 (± 0.4)	30 (± 0.6)	22.4 (± 0.8)	14 (± 1.3)
74	NPI	50	25 (± 1.4)	20.2 (± 0.7)	10.2 (± 7.4)	8 (± 0.6)	4 (± 0.6)	2.2 (± 0.4)	0	0	0	0
	NPIII	50	36 (± 0.9)	33 (± 0.9)	28.4 (± 0.5)	22.4 (± 0.5)	16 (± 0.6)	14.8 (± 0.4)	12 (± 0.6)	7.6 (± 1.0)	2.8 (± 0.4)	0
	NPIV	50	44 (± 0.9)	35 (± 0.6)	32.2 (± 0.7)	26 (± 1.1)	21 (± 0.6)	18.4 (± 1.0)	11.2 (± 0.4)	8.8 (± 0.4)	5.4 (± 0.5)	0
	NPVI	50	45.2 (± 0.7)	43.8 (± 0.7)	42 (± 0.6)	40.8 (± 0.4)	37.2 (± 1.0)	35.4 (± 0.5)	31.8 (± 0.4)	28 (± 0.6)	22.8 (± 0.4)	16.6 (± 0.5)

^a Each value represents the average of five readings, standard deviation in parenthesis**Table 4** Weight required to detach the membrane at different time intervals^a

Sample code	Mass required to detach after 5 min/g	Detachment force/dyne cm ⁻²	Mass required to detach after 10 min/g	Detachment force/dyne cm ⁻²	Mass required to detach after 15 min/g	Detachment force/dyne cm ⁻²	Mass required to detach after 20 min/g	Detachment force/dyne cm ⁻²
NPI	9.95 (± 0.05)	3103.8 (± 12.7)	16.5 (± 0.03)	5147.0 (± 2.6)	21.1 (± 0.03)	6582 (± 7.6)	21.8 (± 0.01)	6800.4 (± 2.5)
NPIII	16.5 (± 0.01)	5147.0 (± 2.6)	19.6 (± 0.05)	6124.1 (± 19.0)	21.3 (± 0.01)	6644.4 (± 2.5)	22.0 (± 0.02)	6862.8 (± 5.1)
NPIV	17.85 (± 0.05)	5568.2 (± 12.7)	20.2 (± 0.01)	6301.3 (± 2.6)	21.6 (± 0.04)	6737.9 (± 10.2)	22.2 (± 0.02)	6925.1 (± 5.1)
NPVI	18.25 (± 0.02)	5692.9 (± 5.1)	22.1 (± 0.01)	6893.9 (± 2.6)	22.5 (± 0.03)	7018.7 (± 7.6)	23.5 (± 0.01)	7330.7 (± 2.5)

^a Each value represents average of five readings, standard deviation in parenthesis

results represented in table are the average readings of five samples. The test was carried out in gastric pH (pH = 1.2) and intestinal pH (pH = 7.4). The mucoadhesion was found to be higher in gastric pH than in intestinal pH. The mucoadhesive properties were also enhanced with the decrease in the particle size of the nanoparticles.

At acidic pH, the free amino groups of chitosan nanoparticles might get protonated and became positively charged. These could strongly bind to the negatively charged mucus layer. The higher surface area of the nanoparticles was responsible for the observed enhanced mucoadhesive property exhibited by chitosan nanoparticles having a lower particle size. Sabitha *et al.*⁴⁴ reported that chitosan-alginate microcapsules showed lower mucoadhesive properties in intestinal pH compared to gastric pH.

3.10. *Ex vivo* mucoadhesive test

Table 4 shows the results of an *ex vivo* mucoadhesion test. The results are the mean value of five readings. It was observed that the detachment force increased with the decrease in particle size of the nanoparticles. The lower the particle size, the higher the surface area and hence the nanoparticles could strongly adhere to the mucosal surface. Rekha *et al.* reported that mucoadhesive properties of the succinyl chitosan particles were enhanced due to better penetration of smaller sized particles into the mucus layers.⁴⁵

Conclusion

This work demonstrated the successful preparation of isoniazid loaded chitosan-MMT nanoparticles by ionic gelation followed by chemical crosslinking. Both the swelling and release of isoniazid from the nanoparticles were found to increase with an increase in the pH of the medium and the size of the nanoparticles. The FTIR study indicated the interaction of the clay with the chitosan polymer. The exfoliation of MMT layers was examined by XRD and TEM. XRD results also showed the molecular level dispersion of isoniazid in the chitosan-MMT nanoparticles. SEM showed that the surface of the chitosan-MMT nanoparticles was less smooth compared to those of isoniazid loaded nanoparticles. Nanoparticles containing clay were less cytotoxic than clay-free nanoparticles. The lower the size of the nanoparticles, the higher the cytotoxicity. The mucoadhesivity of the nanoparticles was better in gastric pH and increased with the decrease in particle size.

Acknowledgements

University grant commission (UGC) is acknowledged for financial support.

References

- R Riva, H Ragelle, A Rieux, N Duhem, C Jero^{me} and V Preat, *Adv Polym Sci*, 2011, **244**, 19–44.
- M Z Hussein, M A Yarmo, M Z H A Rahman, Z Zainal and A A S Liang, *Malay J Analyt Sci*, 2001, **7**, 35–40.
- W Tiyaboonchai, *Naresuan University J*, 2003, **11**, 51–66.
- M Prabharan, *J Biomater Appl*, 2008, **23**, 5–32.
- Y Shirokawa, K Tsurua, S Hayakawa, A Osakaa, M A Lopes, J D Santos and M H Fernandes, *Biomaterials*, 2005, **26**, 485–493.
- J P Venter, A F Kotze, R A Velty and M Rinaudo, *Int J Pharm*, 2006, **313**, 36–42.
- E B Denkbass and R M Ottenbrite, *J Bioact Compat Polym*, 2006, **21**, 351–368.
- P S Pourshahab, K Gilani, E Moazeni, H Eslahi, M R Fazeli and H Jamalifar, *J Microencapsulation*, 2011, **28**, 605–613.
- N Ahmed, M Michelin-Jamois, H Fessi and A Elaissari, *Soft Matter*, 2012, **8**, 2554–2564.
- G V Joshi, B D Kevadiya, H A Patel, H C Bajaj and R V Jasra, *Int J Pharm*, 2009, **374**, 53–57.
- S Selvaraj, N Saravanakumar, J Karthikeyan, D D Evangeline, D Lathamary and N N Rajendran, *Der Pharmacia Lettre*, 2010, **2**, 420–431.
- A Grenha, C I Grainger, L A Dailey, B Sejo, G P Martin, C R Lopez and B Forbes, *Eur J Pharm Sci*, 2007, **31**, 73–84.
- A Mahapatro and D K Singh, *J Nanobiotechnol*, 2011, **9**, 1–11.
- Y Wu, W Yang, C Wang, J Hu and S Fu, *Int J Pharm*, 2005, **295**, 235–245.
- J P Zheng, L Luan, H Y Wang, L F Xi and K D Yao, *Appl Clay Sci*, 2007, **36**, 297–301.
- F H Lin, Y H Lee, C H Jian, J M Wong, M J Shieh and C Y Wang, *Biomaterials*, 2002, **23**, 1981–1987.
- Y Dong and S S Feng, *Biomaterials*, 2005, **26**, 6068–6076.
- K C Gupta and M N V R Kumar, *Biomaterials*, 2000, **21**, 1115–1119.
- A Tripathi, R Gupta and S A Saraf, *Int J Pharm Tech Res*, 2010, **2**, 2116–2123.
- N Devi and T K Maji, *Drug Dev Ind Pharm*, 2010, **36**, 56–63.
- N Devi and T K Maji, *AAPS PharmSciTech*, 2009, **10**, 1412–1419.
- R Cassano, S Trombino, T Ferrarelli, M V Mauro, C Giraldi, M Manconi, A M Fadda and N Picci, *Society for Biomat*, 2011, DOI 10.1002/jbm.a.33302.1-7.
- A Hussain, V Saikia and A M Ramteke, *Free Radicals and Antioxidants*, 2012, **2**, 8–11.
- F Denizot and R Lang, *J Immunol Methods*, 1986, **89**, 271–277.
- C M Lehr, J A Bowstra, J J Tukker and H E Junginger, *J Controlled Release*, 1990, **13**, 51–62.
- B R Gandhi and J R Robinson, *Ind J Pharm Sci*, 1988, **50**, 145–152.
- G J Bourke, L E Daly and J McGilvary, 3rd ed, Blackwell Scientific Publication, Oxford, 2009.
- C G da Trindade Neto, A LP Fernandes, A IB Santos, W A Moraes, M VM Navarro, T NC Dantas, M R Pereira and J LC Fonseca, *Polym Int*, 2005, **54**, 659–666.
- N F Atta, A Galal and R A Ahmed, *Int J Electrochem Sci*, 2011, **6**, 5097–5113.
- I F Amaral, P L Granja and M A Barbosa, *J Biomater Sci Polym Ed*, 2005, **16**, 1575–1593.
- B K Deka and T K Maji, *Compos Sci Technol*, 2010, **70**, 1755–1761.
- E Fukuoka, M Makita and S Yamamura, *Chem Pharm Bull*, 1993, **41**, 2166–2171.
- Z Zong, Y Kimura, M Takahashi and H Yamane, *Polymer*, 2000, **41**, 899–906.
- A Bahari, M Asgharzadeh and M Najafikhah, *Afr J Pure Appl Chem*, 2011, **5**, 429–435.
- W H Lu, G J Zho and Z H Xue, *Forestry Studies in China*, 2006, **8**, 35–40.
- S C Angadi, L S Manjeshwar and T M Aminabhavi, *Int J Biol Macromol*, 2010, **47**, 171–179.
- X Wang, Y Du and J Luo, *Nanotechnology*, 2008, **19**, 1–7.
- N V Gupta and H G Shivakumar, *Trop J Pharm Res*, 2010, **9**, 257–264.
- K C Gupta and M N Ravi Kumar, *J Mater Sci Mater Med*, 2001, **12**, 753–759.
- U Guliyeva, F Uner, S Ozsoy and R Haziroglu, *Eur J Pharm Biopharm*, 2006, **62**, 17–25.
- C Becker, J B Dressman, G L Amidam, H E Junginger, S Kopp, K K Midha, V P Shah, S Stavchansky and D M Barends, *J Pharm Sci*, 2007, **96**, 522–531.
- S M O'Sullivan, J A Woods and N M O'Brien, *Br J Nutr*, 2004, **91**, 757–764.
- N A Monteiro-Riviere, A O Inman, Y Y Wang and R J Nemanich, *Nanomed Nanotechnol Biol Med*, 2005, **1**, 293–299.
- P Sabitha, J V Ratna and K R Reddy, *International Journal of Chemical Technology*, 2010, **2**, 88–98.
- M R Rekha and C P Sharma, *Trends Biomater Artif Organs*, 2008, **21**, 107–115.

Soy flour nanoparticles for controlled drug delivery: effect of crosslinker and montmorillonite (MMT)

Cite this: DOI: 10.1039/c3nj00480e

Nibedita Banik,^a Murshid Iman,^a Anowar Hussain,^b Anand Ramteke,^b Ratan Boruah^c and Tarun K. Maji^{*a}

Soy flour (SF)–Montmorillonite (MMT) nanoparticles crosslinked with glutaraldehyde (GA) have been made and used as a carrier for isoniazid. The nanoparticles have been characterized by fourier transmission infra-red spectroscopy (FTIR), X-ray diffractometry (XRD), scanning electron microscopy (SEM) and transmission emission microscopy (TEM). The effects of MMT and glutaraldehyde on the nanoparticles have been assessed with regard to swelling, encapsulation efficiency and consequently, the release of isoniazid in different mediums. The drug release mechanism has been studied for different time periods by UV-Vis spectroscopy. Cytotoxicity testing has been performed by MTT assay analysis. The results imply that the nanoparticles can be exploited as a potential drug carrier for controlled release applications.

Received (in Montpellier, France)

7th May 2013,

Accepted 26th August 2013

DOI: 10.1039/c3nj00480e

www.rsc.org/njc

1 Introduction

In the present scenario of pharmaceutical research, polymers have been extensively used as an active agent for drug delivery. They can control the release of a drug over an extended period by forming a matrix or membrane, or by forming (nano) carriers and thus avoiding repetitive dosing.¹ Pharmaceutical developments are gradually giving more attention to delivery systems which enhance desired therapeutic objectives while lowering side effects.² Nowadays, biodegradable polymers are preferred to synthetic polymers as controlled drug delivery systems due to their low toxicity, easy availability and cell biocompatibility.³ Soy flour (SF) is one such natural biodegradable polymer which can be explored for controlled drug delivery applications. Soy flour is derived from soybean which is a renewable resource and found in nature in abundance. Soybeans are classified as oil seeds, a staple food of nutritional value and a rich source of protein. Soy flour has easy availability, good processability and is non toxic.^{4–7} The uses of soy flour as a drug delivery device have not been explored much.

Nanoparticles have evoked much interest recently for the delivery of drugs such as peptides, proteins and genes due to their ability to protect these from degradation in the gastrointestinal tract by proteolytic enzymes.^{8,9} Different bioactive agents have been successfully encapsulated within polymers and have been tested for their therapeutic activity.¹⁰ Nanoparticles can be prepared from a variety of

materials such as proteins, polysaccharides and other natural polymers. The selection of matrix materials is dependent on many factors including size of nanoparticles required, inherent properties of the drug, *e.g.*, aqueous solubility and stability, surface charge and permeability, degree of biodegradability, biocompatibility and cytotoxicity, the desired drug release profile, and antigenicity of the final product.¹¹

Montmorillonite (MMT) clay is smectite clay having two silica tetrahedral sheets layered between one alumina octahedral sheet. MMT is a clay mineral with a large specific surface area, exhibits good adsorbability, cation exchange capacity, excellent mucoadhesive properties and drug-carrying capability.¹² Due to its good physical and chemical properties, MMT has received considerable attention in recent years for drug delivery systems applications.¹³

Isoniazid is an antituberculosis drug which can be used as a model drug. Isoniazid normally has three pK_a values: 1.8 based on hydrazine nitrogen, 3.5 based on pyridine nitrogen and 10.8 based on acidic group. In pH 1.2, the pK_a of isoniazid is found to be around 2 due to protonation of hydrazine nitrogen whereas in basic pH of 7.4 it is found to be around 12.¹⁴ The main preparation processes of protein nanoparticles are the emulsification process,¹⁵ desolvation method¹⁶ and templating synthesis.¹⁷ Desolvation method is more apt for nanoparticle preparation as it eliminates the use of organic solvents, and provides removal both of the oily residues of the preparation process and of surfactants required for emulsion stabilization.¹¹ Varieties of crosslinkers are reported to be used for controlling the release behavior of drugs.^{18–20} Glutaraldehyde, a crosslinker of synthetic origin, has been used as a successful crosslinking agent in many studies to cross link biopolymers like SF, starch *etc.*²¹

But, to the best of our knowledge, there is no report for synthesizing drug loaded SF–MMT nanoparticles by using this

^a Department of Chemical Sciences, Tezpur University, Assam, 784028, India.
E-mail: tkn@tezu.ernet.in; Fax: +91 3712 267005; Tel: +91 3712 267007 ext. 5053

^b Department of Molecular Biology and Biotechnology, Tezpur University, Assam, 784028, India

^c Department of Physics, Tezpur University, Assam, 784028, India

Paper

method. In this paper, efforts have been made to prepare isoniazid loaded SF-MMT nanoparticles by desolvation method followed by crosslinking chemically with glutaraldehyde (GA). This report aims at the study of the effect of clay and glutaraldehyde on various properties of soy flour nanoparticles employing desolvation method and use of the synthesized nanoparticles to study the controlled release of isoniazid.

2 Experimental

2.1 Materials

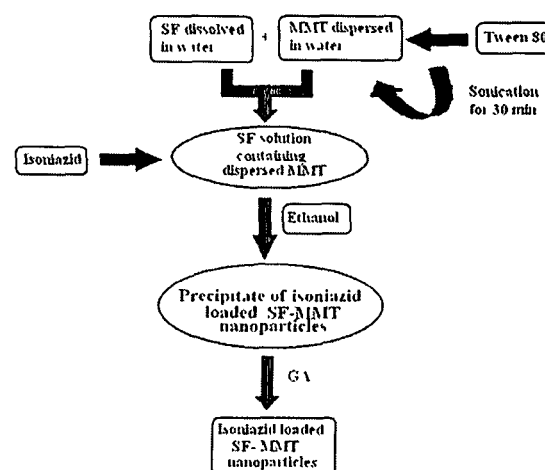
Soy flour (SF) was purchased from Raja Soya, Tezpur (Assam, India) and its molecular weight is found to be around 59 000 from gel permeation chromatography analysis using Waters Model No. 2414 using HSP gel™ AQ 3.0, 6.0 × 150 mm column with water as the mobile phase. Montmorillonite K-10, isoniazid, histopaque 1077 and (3-[4,5-dimethylthiazol-2-yl]-2,5-diphenyl tetrazolium bromide) (MTT) were obtained from Sigma Aldrich, Germany. Tween 80, ethanol, and glutaraldehyde (25% w/v) were purchased from Merck, India. RPMI 1640 and fetal bovine serum (FBS) were procured from HiMedia Laboratories (Mumbai, India). The rest of the chemicals were of analytical grade and used directly.

2.2 Method

Preparation of isoniazid-loaded SF nanoparticles. Nanoparticles were prepared with SF following a desolvation method with modifications.²² 0.5 g of SF was dissolved in 50 mL deionized water and stirred for 1 h at room temperature in a beaker by varying the percentage of MMT *viz.* 0, 1, 3, 5% (dry weight of SF) was swelled in 50 mL of water along with 0.005 mL Tween 80 (surfactant) for 24 h. It was then stirred vigorously by a mechanical stirrer for 48 h and sonicated for 30 min. This dispersed MMT solution was added to 50 mL of 1% (w/v) SF solution. This was followed by the addition of isoniazid (0.01 g) to the beaker under stirring. SF-MMT nanoparticles form on addition of ethanol (50 mL) dropwise into the dispersion. Ethanol acts as a desolvating agent. After 1 h, the temperature of the system was brought down to 5–10 °C to harden the nanoparticles. GA was added as a cross-linker and the temperature was increased to 45 °C. Thereafter, rotary evaporation was applied using a Buchi Rotavapor RII at 30 °C (BUCHI Labor-technik AG, Flawil, Switzerland) to remove ethanol, which was then replaced with the same volume of deionized water. The nanoparticles were separated by centrifuging the solution for 30 min. The product was washed several times with water and dried. The dried nanoparticles were kept in an ampule, stored in a refrigerator and redispersed in deionised water for further use. Scheme 1 depicts the preparation process of isoniazid-loaded SF-MMT nanoparticles. A series of 7 samples was prepared using the formulation by varying the concentration of MMT and GA as shown in Table 1.

2.3 Calculation of process yield

Process yield was calculated using the following equation as described in the literature.²³



Scheme 1 Flowchart showing the main steps in the preparation of isoniazid-loaded SF-MMT nanoparticles

$$\text{Process yield (\%)} = \frac{[(\text{Weight of nanoparticles} \times 100)]}{[\text{Weight of (drug + clay + polymer)}]}$$

2.4 Calibration curve of isoniazid

A calibration curve is essential to estimate the release rate of drug from nanoparticles in the suitable solvent medium. A calibration curve was drawn as per the procedure.²⁴

A known concentration of isoniazid (in double distilled water) was scanned in the range 200–400 nm by using a UV-Vis spectrophotometer (UV-2001 Hitachi, Tokyo, Japan). A sharp peak at 262 nm was noticed for isoniazid having concentration in the range of 0.001–0.01 g per 100 mL. The absorbance values at 262 nm obtained with respective concentration were recorded and plotted. From this calibration curve, the unknown concentration of isoniazid was obtained from the absorbance value.

2.5 Calculation of drug loading efficiency and encapsulation efficiency of the nanoparticles

The drug loading efficiency of nanoparticles with different formulations was determined by ultracentrifugation of samples at room temperature for 30 min. The amount of free isoniazid was determined by noting the absorbance value of the supernatant liquid at 262 nm using a UV-Vis spectrophotometer. The encapsulation efficiency (EE) of the nanoparticles was calculated using the following equations:²⁵

$$\begin{aligned} \text{Encapsulation efficiency (EE) (\%)} \\ = \frac{(\text{Total amount of drug} - \text{Free amount of drug})}{\text{Weight of dry nanoparticles}} \times 100 \end{aligned}$$

2.6 Fourier transmission infra-red spectroscopy (FTIR) study

To study the interaction between SF, GA, MMT and isoniazid *etc.* we had performed FTIR analysis. FTIR spectra of nanoparticles were taken in a Nicolet (model Impact-410, USA)

Table 1 Effect of variation of MMT and GA concentration on the different properties of SF nanoparticles^a

Sample code	SF % w/v (amount in g in 50 mL water)	MMT % w/w w.r.t SF (amount in g in 50 mL water)	Yield (%)	Encapsulation efficiency (%)	Average diameter (nm)	Zeta potential (mV)
SF/M0/GA50	1 (0.5)	0 (0.00)	90.54 (±0.05)	60.93 (±0.02)	642.2 (±12)	-41.32 (±0.03)
SF/M1/GA50	1 (0.5)	1 (0.005)	90.82 (±0.01)	57.41 (±0.04)	641.7 (±15)	-40.13 (±0.08)
SF/M3/GA50	1 (0.5)	3 (0.015)	91.26 (±0.03)	54.53 (±0.04)	647.4 (±12)	-42.29 (±0.3)
SF/M5/GA50	1 (0.5)	5 (0.025)	91.12 (±0.05)	52.12 (±0.01)	632.9 (±10)	-39.16 (±0.04)
SF/M5/GA10	1 (0.5)	1 (0.025)	91.13 (±0.01)	53.62 (±0.03)	648.2 (±10)	-43.88 (±0.03)
SF/M5/GA30	1 (0.5)	1 (0.025)	91.66 (±0.03)	52.91 (±0.01)	638.1 (±12)	-40.25 (±0.01)
SF/M5/GA70	1 (0.5)	1 (0.025)	90.81 (±0.01)	50.69 (±0.04)	629.6 (±14)	-34.72 (±0.01)

^a Each value represents the average of five readings, standard deviation in parenthesis.

spectrophotometer. The nanoparticles were ground to powder, mixed with KBr and compressed under vacuum and then the spectra were recorded in the range of 4000–400 cm^{-1} .

2.7 Particle size determination

Particle sizes of the prepared nanoparticles were determined using a dynamic light scattering (DLS) analyzer (model DLS—Nano ZS, Zetasizer, Nanoseries, Malvern Instruments). The particle size measurements were performed in distilled water using a quartz cell. Each analysis was performed at 25 °C with a detection angle of 90°. Measurements of the nanoparticle suspension were done triplicate for a single batch of nanoparticles and the results were the average of three measurements.

2.8 Pore size analysis

The BET surface areas were determined by N_2 adsorption using a Quantachrome instrument (Model: NOVA 1000e). All the BET values in this study were measured with a precision of $\pm 5\%$. The pore size and pore volume were determined following the Barrett-Joyner-Halenda (BJH) method in the same instrument at a relative pressure of about $0.05 < P/P_0 < 0.9$ using the Barrett-Joyner-Halenda (BJH) equation. Prior to analysis, samples were dried overnight in an oven at 373 K and degassed in a high vacuum for 12 h at 373 K to remove any residual moisture and other volatiles.

2.9 X-Ray diffraction (XRD) study

The degree of intercalation and distribution of isoniazid in SF-MMT nanoparticles were examined by X-ray diffractometry. It was carried out in a Rigaku X-ray diffractometer (Miniflex, UK) using $\text{CuK}\alpha$ ($\lambda = 0.154 \text{ nm}$) radiation at a scanning rate of 1° min^{-1} with an angle ranging from 2 to 70° of 2θ .

2.10 Scanning electron microscopy (SEM) study

The samples were mounted on a brass holder and sputtered with platinum. The surface morphologies of SF-MMT nanoparticles loaded with isoniazid were studied by using a scanning electron microscope (JEOL JSM - 6390LV) at an accelerated voltage of 15 kV.

2.11 Transmission emission microscopy (TEM) study

The dispersion of the silicate layers of clay in SF nanoparticles was examined by using a transmission electron microscope (JEOL JEM-2100) at an accelerated voltage of 200 kV.

2.12 Water uptake studies

Water uptake studies were performed in both phosphate buffer (pH 7.4) and 0.1 N HCl solution (pH 1.2) according to the procedure described in the literature.²⁶

Nanoparticles (0.1 g) were taken in a pouch made of nylon cloth. The empty pouch was first conditioned by immersing it in either 0.1 N HCl (pH 1.2) or phosphate buffer (pH 7.4) for different time periods (1–8 h). The pouch containing the nanoparticles was immersed in a similar way in either 0.1 N HCl (pH 1.2) or phosphate buffer (pH 7.4) for similar time periods. The weights of wet nanoparticles after a definite time period were determined by deducting the respective conditioned weight of the empty nylon pouch from this. Water uptake (%) was determined by measuring the change in the weight of the nanoparticles. The percentage of water uptake for each sample determined at time 't' was calculated using the following equation.

$$\text{Water uptake (\%)} = [(w_2 - w_1)/w_1] \times 100$$

where w_1 is the initial weight of nanoparticles before swelling and w_2 is the final weight of nanoparticles after swelling for a predetermined time 't'.

The experiments were performed five times and are represented as a mean value.

2.13 In vitro drug release studies

To study the release profile of the isoniazid loaded SF-MMT nanoparticles, dried drug loaded samples were immersed in a solution of different pH values, namely 1.2 and 7.4, and stirred continuously. At a scheduled time interval, 5 mL solution was withdrawn, filtered and assayed spectrophotometrically at 262 nm using a UV-Vis spectrophotometer for the determination of the cumulative amount of drug release upto a time t. Each determination was carried out five times. To maintain a constant volume, 5 mL of the solution having the same pH was returned to the container.²⁷

2.14 Isolation of lymphocytes, culture and treatment

Chicken blood was collected from a local butcher shop. It was diluted in the ratio of 1:1 with phosphate buffer saline (PBS) and layered 6 mL into 6 mL histopaque (1.077 g mL^{-1}). The isolation of lymphocytes and study of cell viability were done as per the procedure stated in the literature.²⁸ Lymphocytes were

isolated from the sample after centrifugation for 30 min at 400 g, washed with PBS and finally with serum free media separately through centrifugation for 10 min at 250 g. Cell pellets were then suspended in PBS and cell viability was checked by Trypan blue exclusion method using a haemocytometer. Cell viability of more than 90% was used for subsequent study.

Aliquots of 200 μ L of isolated cells were cultured in RPMI supplemented with 10% heat inactivated fetal bovine serum (FBS). Initially cells were maintained for 4 h in RPMI without FBS at 37 °C in 5% CO₂ incubator. Cells were then treated as per the experimental requirements and kept in the presence of FBS for 6, 12 and 24 h, respectively.

2.15 Cytotoxicity experiments

Cytotoxicity assay was performed by measuring the viability of cells according to the method as illustrated by Denizot and Lang.²⁹ The key component (3-[4,5-dimethylthiazol-2-yl]-2,5-diphenyl tetrazolium bromide) (MTT) is yellowish in color and mitochondrial dehydrogenase of viable cells cleave the tetrazolium ring, yielding purple insoluble formazan crystals which were dissolved in suitable solvent. The resulting purple solution was spectrophotometrically measured. An increase or decrease in cell number resulted in a concomitant change in the amount of formazan formed, indicating the degree of cytotoxicity caused by the test material. Briefly, after treatments, cells were treated with 10% of MTT for 2 h followed by dissolving the formazan crystals in solvent and measuring the absorbance of solution at 570 nm. The absorbances of control cells at 6, 12 and 24 h were separately set at 100% viability and the values of treated cells were calculated as a percentage of the control.

2.16 Statistical analysis

All the data were expressed as means \pm SD (standard deviation). Results were statistically analyzed by Student's *t*-test for significant differences between group means using GraphPad software.³⁰ The significant difference between the experimental and the control group was set at different levels as $p < 0.05$, $p < 0.01$ and $p < 0.001$.

3 Results and discussion

3.1 Effect of variation of MMT and GA concentration on the different properties of SF-MMT nanoparticles

The results showing the effect of the variation of MMT and GA concentration on the different properties of SF nanoparticles are shown in Table 1. Encapsulation efficiency of MMT-free crosslinked nanoparticles exhibited a higher value compared to that of MMT-containing crosslinked nanoparticles. The encapsulation efficiency was found to decrease with the increase in MMT content in the nanoparticles. This could be attributed to the presence of the silicate layers of MMT which interacted with the -OH groups to the -NH₂ group of SF and the -CHO groups of GA resulting in lengthening of the polymer chains. The silicate layers of MMT restricted the movement of the intercalated polymer chains freely. As a result, the formation of a

porous structure might take place during the dehydration stage. This in turn would produce many fine channels from the interior to the surface of the particles. Thus, part of the drug might get diffused from the particles to the external medium resulting in the decrease of both encapsulation and drug loading efficiency.^{31,32} The hindrance offered by the MMT layers was absent in MMT-free crosslinked nanoparticles. Hence, it showed high encapsulation and drug loading efficiency.

Similarly, at a fixed MMT content, the encapsulation efficiency of nanoparticles was found to decrease with the increase in the glutaraldehyde (GA) concentration. GA, a crosslinker, might further restrict the free motion of the intercalated polymer chains and thus facilitate the formation of a porous structure. The drug could migrate from the interior of the nanoparticles to the outer surface or preparing medium through the channels.

The average diameter of the nanoparticles was obtained in the range 629–648 nm. The variation in MMT concentration did not affect the particle size. However, the average diameter showed a decreasing trend on increasing the GA concentration. The amino groups present in soy flour interacted with the hydroxyl groups of MMT and GA. With the increase in the concentration of GA, the availability of free amino groups on nanoparticles reduces due to which the nanoparticles became more compact and hence the diameter would be less.

Zeta potential values of the nanoparticles were found in the range -35 to -44 mV indicating good stability of the nanoparticles. The variation of MMT did not show any significant effect on the zeta potential. However, the zeta potential values increased as the GA concentration increased from 10 to 70%. The increase in the zeta potential indicated that the stability of the nanoparticles increased with the increase in the concentration of GA and they would not aggregate in acidic or basic medium.³³

3.2 Fourier transmission infra-red spectroscopy (FTIR) study

In the spectrum of pure soy flour (SF) (Fig. 1a), the broad absorption band appeared at around 3450 cm⁻¹ due to the hydrogen-bonded OH stretching and NH₂ asymmetric stretching vibrations. The SF characteristic peaks of amide I, amide II and amide III appeared at 1648 cm⁻¹ (C=O stretching), 1548 cm⁻¹ (N-H bending) and 1240 cm⁻¹ (C-N stretching) respectively.³⁴ It is known that polypeptides and proteins of mainly α -helical structure exhibit absorption bands near 1648 cm⁻¹ (amide I) and 1548 cm⁻¹ (amide II). The amide III band in the spectrum is due to the presence of glutamic acid in soy flour.²¹ The peaks exhibited in the spectrum for MMT (Fig. 1b) at 3435, 1639 and 1163–460 cm⁻¹ were for -OH stretching, -OH bending and oxide bands of metals like Si, Al, Mg, *etc.* Fig. 1c represents the spectrum of isoniazid. The absorption peaks at 1664 and 1557 cm⁻¹ were due to the amide I (C=O stretching) and amide II (N-H bending of secondary amide group), respectively. Besides this, multiple peaks appeared in the range 1410–669 cm⁻¹.²⁶

All the characteristic peaks of SF, MMT and isoniazid appeared and their intensities decreased in the spectrum of isoniazid loaded SF-MMT nanoparticles (Fig. 1d). The intensity of the peak of soy flour appearing in the range 3450–3200 cm⁻¹

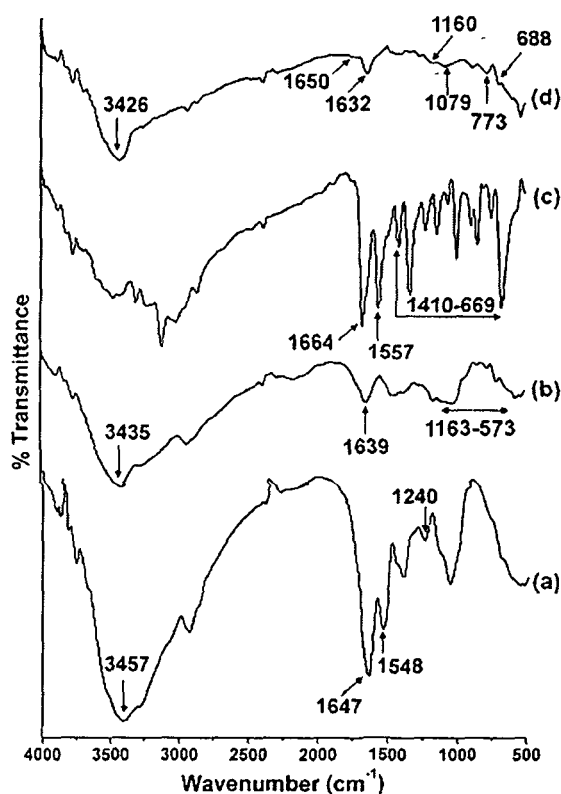
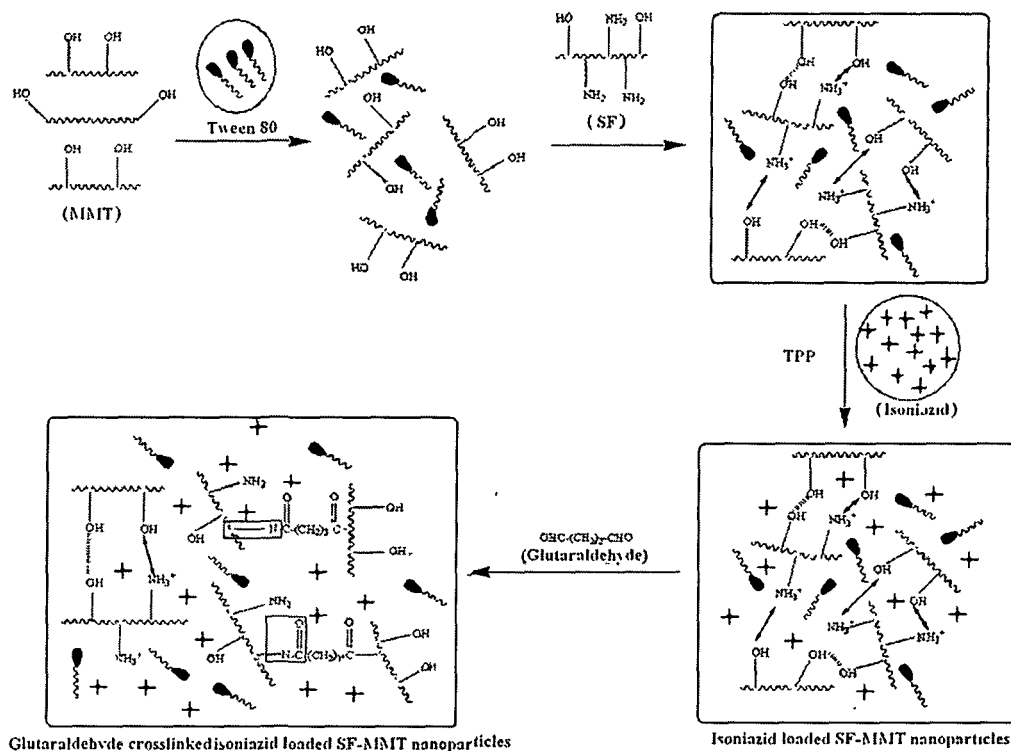


Fig. 1 FTIR spectra of (a) pure SF, (b) MMT, (c) isoniazid and (d) SF/M5/GA50

(Fig. 1a) was decreased and shifted to a lower wave number in drug loaded SF-MMT nanoparticles (Fig. 1d) and the NH_2 group of SF and MMT. This indicated an interaction between the hydroxyl group and the NH_2 group of MMT and SF. The decrease in hydroxyl peak intensity was reported by Maji *et al.*³⁵ while studying the properties of wood polymer nanocomposites. In the FTIR spectra of GA crosslinked SF-MMT nanoparticles, two common bands appear at 1650 and 1160 cm^{-1} . The presence of these two peaks, corresponding to $-\text{N}-\text{C}=\text{O}$ and C-N stretching vibrations, respectively, indicates the interaction of the aldehydic ($-\text{CHO}$) group of GA with the $-\text{OH}$ and $-\text{NH}_2$ groups present in SF, respectively. A plausible mechanism for the formation of $-\text{N}-\text{C}=\text{O}$ and C-N linkages is presented schematically in Scheme 2.

3.3 Pore size analysis

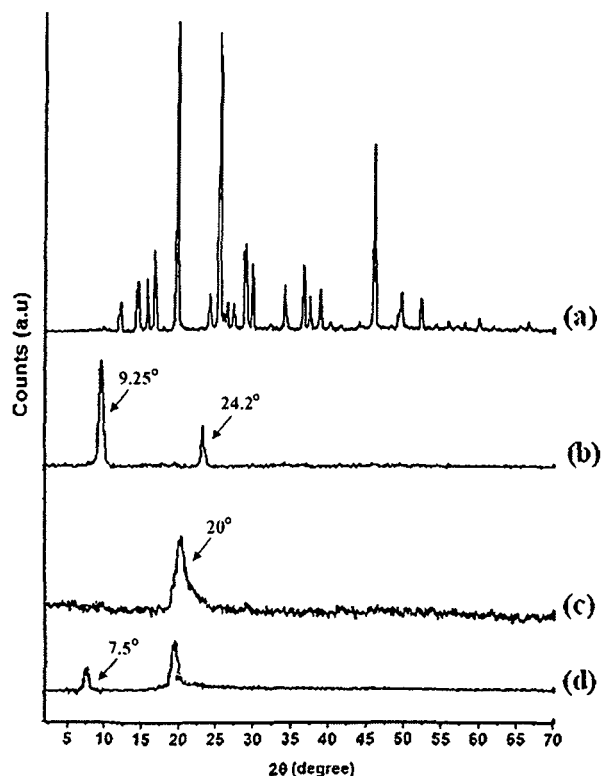
The surface area studied using N_2 adsorption-desorption isotherms at very low relative pressures (P/P_0) exhibited high adsorption of N_2 , confirming the presence of porous structures in the nanoparticles. From Table 2 it is observed that the pore size of the crosslinked SF nanoparticles (SF/M0/GA50) is higher than the crosslinked SF-MMT nanoparticles (SF/M0/GA50). With the inclusion of MMT in the SF matrix, the surface area also increases. These observations can be attributed to the fact that when MMT is incorporated in the SF matrix, it blocks some of the pores of SF and consequently a decrease in the porosity is observed and also the surface area also increases.



Scheme 2 Plausible mechanism for the interaction of GA with SF in isoniazid-loaded SF-MMT nanoparticles

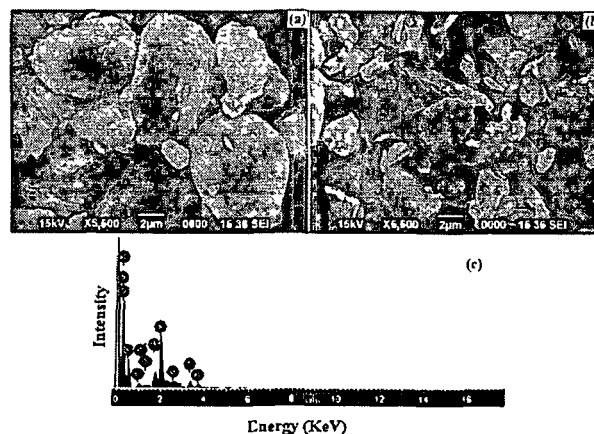
Table 2 Effect of variation of MMT on the porosity and surface area of SF–MMT nanoparticles loaded with isoniazid

Sample codes	Pore size (m g^{-1})	Surface area ($\text{m}^2 \text{g}^{-1}$)
SF/M0/GA50	0.538 ± 0.001	351.5 ± 5
SF/M5/GA50	0.351 ± 0.003	362.8 ± 2

**Fig. 2** XRD patterns of (a) isoniazid, (b) MMT, (c) SF and (d) SF/M5/GA50

3.4 X-Ray diffraction (XRD) study

The crystallinity and MMT incorporation into the SF nanoparticles was studied by XRD analysis. Fig. 2(a–d) represents the XRD diffraction pattern of isoniazid, MMT, pure SF and isoniazid-loaded SF nanoparticles. Curve 2 (a) showed multiple peaks at $2\theta = 12$ to 50° which was due to the crystalline nature of isoniazid.³⁶ MMT exhibits two characteristic peaks at $2\theta = 9.25$ and 24.2° which are assigned to the (001) plane (curve 2b).²¹ Soy flour (curve 2c) shows its characteristic diffraction peak at

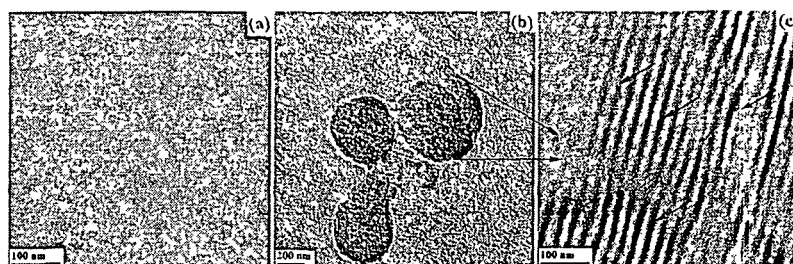
**Fig. 3** SEM micrographs of (a) SF/M0/GA50, (b) SF/M5/GA50 and (c) EDX of SF/M5/GA50

around $2\theta = 20^\circ$.³⁴ The peak of isoniazid was found to disappear in the diffractogram of MMT/SF nanoparticles (curve 2d). Crystalline peaks of isoniazid disappear because it is well dispersed in the SF–MMT matrix due to vigorous mixing. However, after the incorporation of MMT the intensity of the peak at $2\theta = 20^\circ$ decreased and shifted to lower 2θ value. Furthermore, a new peak corresponding to MMT with decreased intensity appeared at around $2\theta = 7.5^\circ$. This indicated that the MMT layers were partially exfoliated and dispersed into the nanocomposite. The subordination of intensity of the peak at $2\theta = 9.25^\circ$ to $2\theta = 7.5^\circ$ indicated the collapse of the layered structure of MMT when incorporated into the nanoparticles.^{34,37}

3.5 Scanning electron microscopy (SEM) study

SEM analysis was performed to study the surface morphology of SF nanoparticles and SF–MMT nanoparticles. Fig. 3a and b represent the SEM micrographs of SF nanoparticles and SF–MMT nanoparticles, respectively. The surface of SF nanoparticles (Fig. 3a) appeared smooth. However, on addition of MMT into SF nanoparticles the surface appeared rough (Fig. 3b). This might be due to the good interaction of SF with MMT particles. Due to this interaction, SF–MMT nanoparticles look more agglomerated than the nanoparticles which do not contain MMT.³⁸

Further work was done through energy dispersive X-ray (EDX) analysis of clay-loaded nanoparticles as shown in Fig. 3c. Elements such as Al, Na and Si, which are mainly from

**Fig. 4** TEM micrographs of crosslinked SF nanoparticles (a) without MMT within the 100 nm range, (b) and (c) with MMT at the 200 and 100 nm scale, respectively

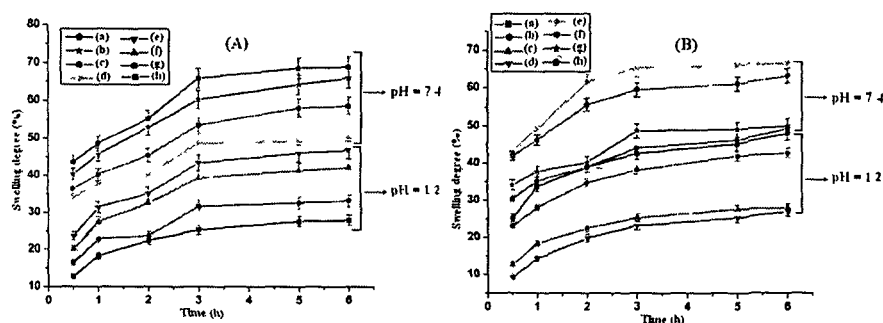


Fig. 5 Percentage swelling degree at pH 7.4 and 1.2 (A) ((a) SF/M0/GA50, (b) SF/M1/GA50, (c) SF/M3/GA50, (d) SF/M5/GA50, (e) SF/M0/GA50, (f) SF/M1/GA50, (g) SF/M3/GA50, (h) SF/M5/GA50) and (B) ((a) SF/M5/GA10, (b) SF/M5/GA30, (c) SF/M5/GA50, (d) SF/M5/GA70, (e) SF/M5/GA10, (f) SF/M5/GA30, (g) SF/M5/GA50, (h) SF/M5/GA70)

the silicate nanoclay, were detected indicating that the MMT had been successfully incorporated into the nanoparticles.³⁹

3.6 Transmission electron microscopy (TEM) study

TEM micrographs of isoniazid-loaded SF nanoparticles devoid of MMT, and with MMT at 200 and 100 nm scales are shown in Fig. 4a–c, respectively. Fig. 4c shows the presence of platelets of MMT tactoids in which the dark lines were the intersection of MMT layers which were absent in Fig. 4a. The bright areas were for the SF matrix and isoniazid. A similar observation was reported by Choi *et al.* while studying the anionic MTM (cloisite Na⁺) and PVA

composite structure by TEM.⁴⁰ The results indicated that MMT was incorporated and dispersed in the SF matrix.

3.7 Swelling study

The effect of pH on the percentage swelling of isoniazid-loaded nanoparticles at two different pH values, namely 1.2 and 7.4, are shown in Fig. 5(A and B). It was observed that the swelling of isoniazid-loaded SF–MMT nanoparticles was more in intestinal pH (7.4) than in gastric pH (1.2). Under acidic pH values, most of the carboxylate anions of SF become protonated. The main anion–anion repulsive forces were diminished and

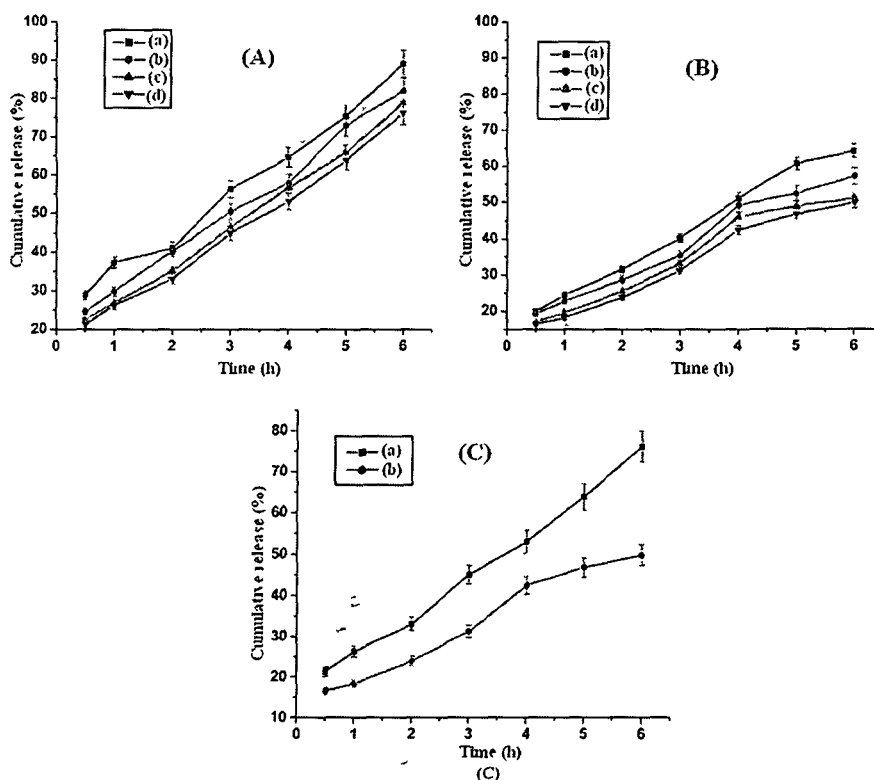


Fig. 6 Effect of variation of concentration of MMT on the percentage cumulative release of isoniazid from SF–MMT–isoniazid nanoparticles at (A) pH 7.4 ((a) SF/M0/GA50, (b) SF/M1/GA50, (c) SF/M3/GA50, (d) SF/M5/GA50), (B) pH 1.2 ((a) SF/M0/GA50, (b) SF/M1/GA50, (c) SF/M3/GA50, (d) SF/M5/GA50) and (C) represents the comparison of percentage cumulative release of SF/M5/GA50 at (a) pH 7.4 and (b) pH 1.2

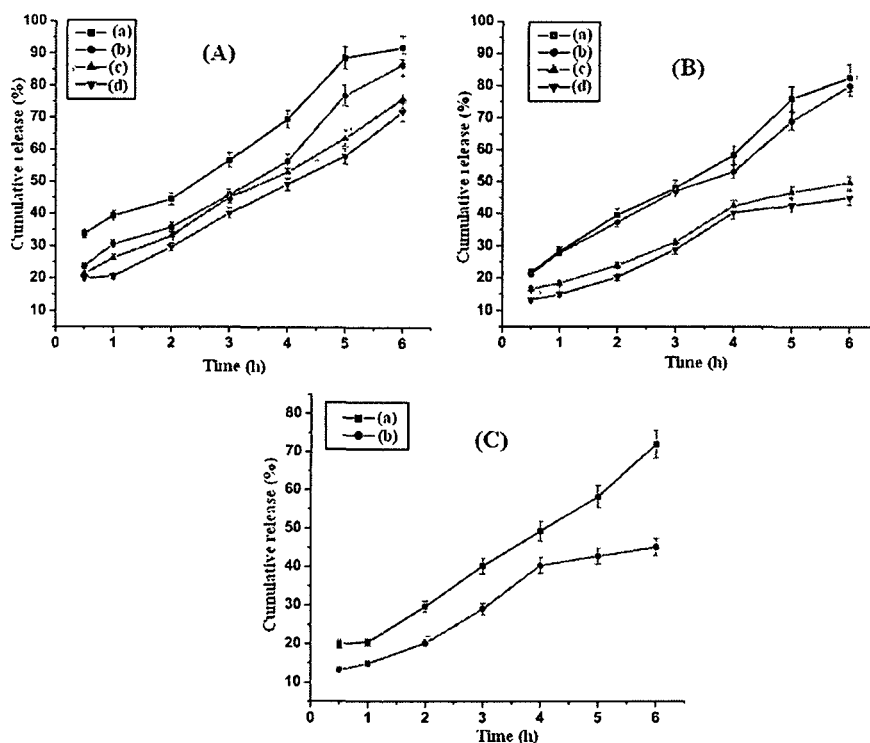


Fig. 7 Effect of variation of concentration of GA on the percentage cumulative release of isoniazid from SF-MMT-isoniazid nanoparticles at (A) pH 7.4 ((a) SF/M5/GA10, (b) SF/M5/GA30, (c) SF/M5/GA50, (d) SF/M5/GA70), (B) pH 1.2 ((a) SF/M5/GA10, (b) SF/M5/GA30, (c) SF/M5/GA50, (d) SF/M5/GA70) and (C) represents the comparison of percentage cumulative release of SF/M5/GA70 at (a) pH 7.4 and (b) pH 1.2

accordingly a decrease in swelling values was observed. At alkaline pH values, some carboxylate groups were ionized and the electrostatic repulsion between COO⁻ groups caused an augmentation of the swelling degree.⁴¹ Furthermore, the percentage swelling degree was found to increase with the increase in time.

With the increase in the concentration of MMT, the percentage swelling degree decreased. The water absorption is decreased by the presence of dispersed phase of MMT into the SF matrix of the nanoparticles. The MMT particles act as a barrier for water molecules which results in the decrease of water transmission through the crosslinked SF-MMT nanoparticles. MMT may elongate the path of water particles in the nanoparticles.³² Similarly, nanoparticles containing a higher concentration of GA swelled less due to higher cross-linking densities and less availability of the polar groups.⁴² With the incorporation of GA, the surface of the nanoparticles became hardened which leads to lesser penetration of water molecules into it. This is reflected in the lowering of % swelling of the GA-crosslinked nanoparticles. Hence, by varying the content of GA, the swelling properties of the nanoparticles can be tailored.

3.8 *In vitro* release studies

The drug release profile of the nanoparticles at two different pH values, namely 1.2 and 7.4, for 6 hours are shown in Fig. 6(A-C) and

7(A-C). The cumulative release (%) of isoniazid from SF-MMT nanoparticles was found to be pH dependent. Fig. 6(C) and 7(C) showed that for the nanoparticles with the same formulation, the release was more in the intestinal pH than in the gastric pH. In alkaline medium, the breaking of hydrogen bonding between the SF and isoniazid facilitated the release of the drug and thus enhanced the cumulative release.⁴³ Moreover, the high degree of swelling in intestinal pH facilitates the solvent access to the drug incorporated in the polymeric matrix, increasing contact with it and consequently allowing greater release.

From Fig. 6(A and B) it is clearly observed that the cumulative release (%) of isoniazid decreases with an increase in MMT content and time. This is because as the concentration of the MMT particles in the nanoparticles increases, the percentage swelling degree of the nanoparticles decreases. Consequently, the solvent particles cannot properly reach the isoniazid molecules encapsulated in the nanoparticles to facilitate their release. As the time interval increases, the swelling increases and more and more solvent particles reach the drug molecule and hence aid the release of isoniazid from the nanoparticles. Fig. 7(A and B) showed that the cumulative release (%) of isoniazid decreases with an increase in the concentration of GA. This is due to the increase in cross-linking density of the nanoparticles with the increase in GA concentration. As more crosslinked nanoparticles are formed, the solvent access to the isoniazid molecule encapsulated in

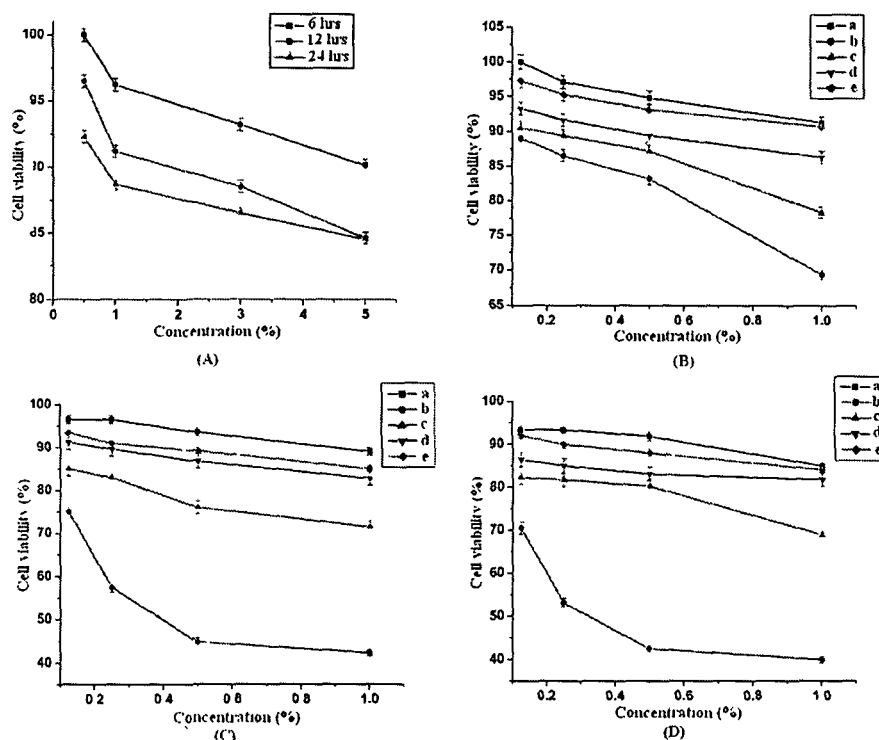


Fig. 8 Cell viability study (A) with variation of MMT at 6, 12 and 24 h, (B) comparison of cell viability at 6 h for (a) SF, (b) isoniazid, (c) SF/M0/GA50, (d) SF/M1/GA50 and (e) SF/M5/GA50, (C) comparison of cell viability at 12 h for (a) SF, (b) isoniazid, (c) SF/M0/GA50, (d) SF/M1/GA50 and (e) SF/M5/GA50 at 6, 12, and 24 h, and (D) comparison of cell viability at 24 h for (a) SF, (b) isoniazid, (c) SF/M0/GA50, (d) SF/M1/GA50 and (e) SF/M5/GA50

the SF-MMT nanoparticles to bring it out of the nanoparticles decreases and hence the cumulative release of isoniazid decreases.

3.9 Cytotoxicity test

The results of the MTT-assay are shown in Fig. 8. Fig. 8(A) depicts the cell viability of MMT at different time intervals (6, 12 and 24 h) and different concentrations (0.5, 1, 3 and 5%). It was observed that the cell viability varied between 84–100% within the studied MMT concentration. This indicated that MMT was not cytotoxic to the cells. The cell viability decreased with the increase in the concentration of the nanoparticles and time interval.

Fig. 8B–D showed the effect of concentration of SF, isoniazid, SF/M0/GA50, SF/M1/GA50 and SF/M5/GA50 on cell viability at 6, 12 and 24 h, respectively. SF showed very low cytotoxicity as is evident from Fig. 8B(a), C(a) and D(a). Fig. 8B(b)–D(b) shows the cell viability (%) of isoniazid alone which shows that isoniazid is highly cytotoxic. The cell viability at 24 h for 1% isoniazid is only 40%. The cytotoxicity was found to be less for isoniazid loaded SF-MMT nanoparticles compared to those of isoniazid alone. The SF-MMT slowed down the release of isoniazid and hence decreased the interaction of drug with the cell. It was observed further (Fig. 8B(c–e), C(c–e) and D(c–e)) that the cell viability of clay-containing nanoparticles was more compared to clay-free nanoparticles. This might be due to the

fact that the silicate layers of clay hindered the release of drug in the cell because of its tortuous path.

4 Conclusion

This work demonstrated the successful preparation of isoniazid-loaded SF-MMT nanoparticles by desolvation method followed by chemical crosslinking. Both the swelling and release of isoniazid from the nanoparticles were found to enhance with the decrease in the clay and GA content. The percentage swelling degree and cumulative release increased in alkaline pH compared to acidic pH. FTIR study indicated the interaction of MMT with SF polymer. The exfoliation of MMT layers was examined by XRD and TEM. XRD results also showed the molecular level dispersion of isoniazid in the SF-MMT nanoparticles. SEM study showed that the surface of the SF-MMT nanoparticles was less smooth compared to SF nanoparticles. Nanoparticles containing MMT were less cytotoxic than clay-free nanoparticles.

References

- 1 R. Riva, H. Ragelle, A. Rieux, N. Duhem, C. Jérôme and V. Pr at, *Adv. Polym. Sci.*, 2011, **244**, 19–44.
- 2 S. L. Patwekar and M. K. Baramade, *Int. J. Pharm. Pharm. Sci.*, 2012, **4**, 757–763.
- 3 M. Z. Hussein, M. A. Yarmo, M. Z. H. A. Rahman, Z. Zainal and A. A. S. Liang, *Malaysian J. Anal. Sci.*, 2001, **7**, 35–40.

- 4 C. S Venter, *Journal of Family Ecology and Consumer Sciences*, 1999, 27, 24–33
- 5 E F Fabiyi, *Pak. J Nutr*, 2006, 5, 453–457
- 6 M A Porter and A M Jones, *J Am Oil Chem Soc*, 2003, 80, 557–562.
- 7 L Xiang, C. Tang, J. Cao, C. Wang, K. Wang, Q. Zhang and Q Fu, *Chin J Polym Sci*, 2009, 27, 843–849
- 8 J Tan, Y Wang, X. Yip, F. Glynn, R. K Shepherd and F Caruso, *Adv Mater*, 2012, 24, 3362–3366.
- 9 X Zhang, M Oulad-Abdelghani, A N. Zelkin, Y. Wang, Y Haikel, D Mainard, J C Voegel, F. Caruso and N Benkirane-Jessel, *Biomaterials*, 2010, 31, 1699–1706
- 10 N Ahmed, M Michelin-Jamois, H. Fessi and A. Elaissari, *Soft Matter*, 2012, 8, 2554–2564.
- 11 M Jahanshahi and Z. Babaei, *Afr J Biotechnol*, 2008, 7, 4926–4934
- 12 X Wang, Y Du and J Luo, *Nanotechnology*, 2008, 19, 1–7.
- 13 G V Joshi, B D Kevadiya, H A Patel, H C. Bajaj and R V Jasra, *Int J Pharm*, 2009, 374, 53–57
- 14 N F Atta, A Galal and R A. Ahmed, *Int J Electrochem Sci*, 2011, 6, 5097–5113
- 15 Z Gao, A J Shukla, J R Johnson and W R Crowley, *Pharm Res*, 1995, 12, 857–863.
- 16 C J Coester, K Langer, H Van Briesen and J. Kreuter, *J Microencapsulation*, 2000, 17, 187–193
- 17 Y Wang and F Caruso, *Adv Mater*, 2006, 18, 795–800
- 18 Y Wu, W Yang, C Wang, J Hu and S Fu, *Int J Pharm*, 2005, 295, 235–245
- 19 J P Zheng, L Luan, H Y Wang, L. F. Xi and K. D. Yao, *Appl Clay Sci*, 2007, 36, 297–301.
- 20 F H Lin, Y H Lee, C. H. Jian, J. M. Wong, M. J. Shieh and C Y Wang, *Biomaterials*, 2002, 23, 1981–1987.
- 21 M Iman, K K Bania and T K. Maji, *Ind Eng Chem Res*, 2013, 52, 6969–6983
- 22 Z Teng, Y Luo and Q J Wang, *J Agric Food Chem*, 2012, 60, 2712–2720
- 23 K C Gupta and M N V. R. Kumar, *Biomaterials*, 2000, 21, 1115–1119
- 24 N Devi and T. K. Maji, *AAPS PharmSciTech*, 2009, 10, 1412–1419.
- 25 S Selvaraj, N Saravanakumar, J. Karthukeyan, D. D. Evangeline, D. Lathamary and N N. Rajendran, *Pharm. Lett.*, 2010, 2, 420–431.
- 26 N Devi and T. K. Maji, *Drug Dev. Ind Pharm.*, 2010, 36, 56–63
- 27 R. Cassano, S. Trombino, T. Ferrarelli, M. V. Mauro, C. Giraldi, M. Manconi, A M. Fadda and N Picci, *J Biomed Mater Res, Part A*, 2012, 100A, 536–7
- 28 A. Hussain, V. Saikia and A M. Ramteke, *Free Radicals Antioxid*, 2012, 2, 8–11
- 29 F. Denizot and R. Lang, *J Immunol Methods*, 1986, 89, 271–277.
- 30 G. J. Bourke, L. E. Daly and J McGilvary, *Interpretation and Uses of Medical Statistics*, Blackwell Scientific Publication, Oxford, 3rd edn, 1985.
- 31 J. Zheng, J Shan, Z. Fan and K. Yao, *J Wuhan Univ Technol, Mater. Sci Ed*, 2011, 26, 628–633.
- 32 S Hua, H Yang and A Wang, *Drug Dev Ind Pharm*, 2010, 36, 1106–1114
- 33 N. Banik, A. Hussain, A. Ramteke, H. K. Sharma and T. K. Maji, *RSC Adv*, 2012, 2, 10519–10528.
- 34 M. Iman and T K Maji, *J Appl Polym Sci*, 2013, 127, 3987–3996.
- 35 B K. Deka and T. K Maji, *Compos Sci Technol*, 2010, 70, 1755–1761.
- 36 E. Fukuoka, M. Makita and S. Yamamura, *Chem Pharm Bull*, 1993, 41, 2166–2171
- 37 X. Huang and A N Netravali, *Biomacromolecules*, 2006, 7, 2783–2789.
- 38 Y Dong and S Feng, *Biomaterials*, 2005, 26, 6068–6076
- 39 X. Cai, B. Riedl, S. Y. Zhang and H Wan, *Composites, Part A*, 2008, 39, 727–737.
- 40 J. H. Choi, Y. W Park, T. H. Park, E. H. Song, H. J Lee, H. Kim, S J. Shin, V L C. Fai and B. Ju, *Langmuir*, 2012, 28, 6826–6831
- 41 A. Pourjavadi, M. Kurdtabar, G. R. Mahdavinia and H. Hosseinzadeh, *Polym Bull*, 2006, 57, 813–824.
- 42 M Iman and T. K. Maji, *Carbohydr Polym.*, 2012, 89, 290–297.
- 43 A. Sasmal, P. Nayak, R. Nanda, P. L Nayak, S. Sasma, Y. Chang, S. C Kang and J. Yoon, *International Journal of Plastics Technology*, 2009, 13, 8–21.

Carboxymethyl chitosan-montmorillonite nanoparticles for controlled delivery of isoniazid: evaluation of the effect of the glutaraldehyde and montmorillonite

Nibedita Banik^a, Anand Ramteke^b and Tarun K. Maji^{a*}

Chitosan, a natural biopolymer, is used for drug delivery application. But its potential application is limited by its low solubility in aqueous media. The present study was designed to prepare carboxymethyl chitosan (CMC), a water soluble derivative of chitosan, and evaluate the prospective of crosslinked CMC-Montmorillonite (MMT) nanoparticles for controlled delivery of isoniazid. The nanoparticles were characterized by Fourier Transmission Infrared Spectroscopy (FTIR), Nuclear Magnetic Resonance (NMR), X-ray diffraction (XRD), scanning electron microscopy (SEM), and Transmission emission microscopy (TEM). The effects of MMT and glutaraldehyde on nanoparticles were assessed with regard to encapsulation efficiency, percentage swelling degree, and cumulative release. Percentage swelling degree and cumulative release were studied in pH medium 1.2 and 7.4 for 6 h. The cumulative release was studied by UV-visible spectrophotometer. Cell viability study was performed by MTT assay analysis. FTIR and NMR study indicated the successful preparation of CMC. FTIR study confirmed the interaction of MMT with CMC. The exfoliation of MMT layers and molecular level dispersion of isoniazid in CMC was examined by XRD and TEM. SEM study showed that the surface of the CMC-MMT nanoparticles was smooth compared with those of CMC nanoparticles. Swelling and release of isoniazid from the nanoparticles increased with the decrease in the MMT and glutaraldehyde content. The percentage swelling degree and cumulative release was more in pH 1.2. Cell viability study revealed that CMC was not cytotoxic, and the nanoparticles containing MMT was less cytotoxic than those of MMT free nanoparticles. CMC-MMT nanoparticles can be exploited as potential drug carrier for controlled release applications. Copyright © 2014 John Wiley & Sons, Ltd.

Keywords: carboxymethyl chitosan, montmorillonite, glutaraldehyde, ionic gelation, drug delivery

INTRODUCTION

In the current scenario of pharmaceutical industry, polymers are extensively used as an active agent for drug delivery. They can control the release of a drug over an extended period by forming matrix or membrane, thereby evading the chances of repetitive dosing. They can also be used as structure (nano)carriers to deliver drugs.^[1] Among the polymeric materials, natural biodegradable polymers can be used for diverse applications in various biomedical fields owing to their properties as low toxicity, easy availability, and cell biocompatibility.^[2,3]

Chitosan is one such biopolymer that is widely used in the medical field to design controlled drug delivery systems. Chitosan, a cationic polymer ubiquitous modified natural polymer obtained from partial deacetylation of biopolymer chitin, which is present in crustacean shells of crabs, lobsters, insects, and other lower plants.^[3,4] Chitosan is a mucoadhesive polycation polymer at acidic pH and is non-toxic.^[5-7] Chitosan also has fungicidal effect, wound healing properties, and ability to cut down cholesterol level.^[8]

Although chitosan has a number of advantages, but its potential application is limited by its low solubility in aqueous media. It is insoluble in aqueous solutions above pH 7 and soluble in dilute acids due to the protonation of its free amino groups.^[9] To overcome the problem of solubility, several water soluble derivatives of chitosan have been synthesized, which act over a wide range of pH. Few of

these are carboxymethyl chitosan (CMC) and N-trimethyl chitosan chloride.^[10] CMC is a key derivative of chitosan and has exceptional chemical, physical, and biological properties such as low toxicity, biocompatibility, good antimicrobial activity, film-forming ability, and capacity to interact with different substances and solubility in wide range of pH. It is used in medical and pharmaceutical areas, mainly for the controlled release of drug.^[11-13]

Nanoparticles have generated much interest recently for the delivery of agents such as peptides, proteins, and genes due to their ability to protect these from degradation in the gastrointestinal tract by proteolytic enzymes.^[14,15] Different bioactive agents have been successfully encapsulated within polymers and have been tested for their therapeutic activity.^[16] Nanoparticles can be prepared from a variety of materials such as proteins, polysaccharides, and other natural polymers.

* Correspondence to: Tarun K. Maji, Department of Chemical Sciences, Tezpur University, Assam, 784028 India
E-mail: tkm@tezu.ernet.in

^a N. Banik, T. K. Maji
Department of Chemical Sciences, Tezpur University, Assam 784028, India

^b A. Ramteke
Department of Molecular Biology and Biotechnology, Tezpur University, Assam 784028, India

Montmorillonite (MMT) clay is smectite clay having silica tetrahedral sheets layered between alumina octahedral sheets. MMT has large specific surface area, exhibits good adsorbability, cation exchange capacity, excellent mucoadhesive properties, and drug-carrying capability. Because of their good physical and chemical properties, MMT has received considerable attention in the recent years for drug delivery systems applications.^[17,18]

Isoniazid is an antituberculosis drug and can be used as a model drug.

Carboxymethyl chitosan nanoparticles are prepared chiefly by ionic gelation process. Extensive research has been carried out to synthesize carboxymethyl chitosan nanoparticles loaded with drug by ionic gelation process.^[19,20] This can either be chemically crosslinked with glutaraldehyde (GA) and genipin or physically crosslinked with sodium tripolyphosphate, calcium chloride, and so on. Varieties of crosslinkers are reported to be used for controlling the release behavior of drugs. The nanoparticles prepared by physical crosslinking swell faster in release medium compared with those of chemically crosslinked nanoparticles. Therefore, a synergistic approach by using both physical and chemical crosslinking seems to be more viable to control the release behavior of drug. Similar approach has been reported by Maji *et al.*^[21] There is hardly any report for synthesizing drug loaded carboxymethyl chitosan-MMT nanoparticles by using ionic gelation method. In this paper, efforts are made to prepare isoniazid loaded carboxymethylchitosan-MMT nanoparticles by ionic gelation method followed by crosslinking chemically with GA. This paper aims at the study of the effect of clay and GA on various properties of nanoparticles.

MATERIALS AND METHODS

Materials

Low molecular weight chitosan, MMT K-10, Isoniazid, Histopaque 1077, and (3-[4,5-dimethylthiazol-2-yl]-2,5-diphenyl tetrazolium bromide) (MTT) were obtained from Sigma Aldrich, Germany. Tween 80 and calcium chloride (CaCl₂) were purchased from Merck, India. GA was procured from Loba Chemi Pvt Ltd, Mumbai, India. RPMI 1640 and fetal bovine serum (FBS) were procured from HiMedia Laboratories (Mumbai, India). The rest of the chemicals were of analytical grade and used as such received.

Synthesis of carboxymethyl chitosan

Carboxymethyl chitosan derivatives were prepared as described in the literature.^[22] Chitosan (1 g) was swollen in 100 mL of water for 24 h. To this, monochloroacetic acid (4 gm) was added, and mixture was vigorously stirred until all chitosan was dissolved in water to give a homogenous solution. After that, the pH of the solution was adjusted to 8.0 by slow addition of 5% NaHCO₃ with continuous stirring. The reaction medium became opaque due to precipitation of chitosan caused by the rise of pH but reverted to homogenous solution on heating at 90 °C. After heating at 90 °C for 6 h, the solution cooled to ambient temperature and the pH was adjusted to 6.0 by using 1% HCl solution. The precipitate was then filtered off and the product was washed and brought to neutral pH with 90% ethanol solution. It was then dissolved in dilute sodium hydroxide solution to get the neutral sodium-salt of carboxymethyl chitosan, which was separated by being lyophilized.

Determination of degree of substitution

The degree of substitution of CMC was calculated by using potentiometric titration.^[23] 0.25 g CMC was dissolved in 50 mL distilled water. The pH was adjusted to below 2.0 by adding HCl. The CMC solution was then titrated with 0.1 M aqueous NaOH solution. The degree of substitution (DS) was calculated by using the equation given in the succeeding text.

$$DS = (161 \times A) / (m_{CMC} - 58 \times A)$$

And, $A = V_{NaOH} \times C_{NaOH}$

Where V_{NaOH} and C_{NaOH} are the volume and molarity of aqueous NaOH solution, respectively, m_{CMC} is the mass of CMC (g), and 161 and 58 are the respective molecular weights of glucosamine (chitosan skeleton unit) and a carboxymethyl group.

Preparation of Isoniazid loaded CMC-MMT nanoparticles

Isoniazid loaded CMC-MMT nanoparticles were prepared by ionic crosslinking of CMC with CaCl₂ and employing the process as reported by Tavakol *et al.* with modifications.^[20] 1% (w/v) CMC solution was prepared in water at 45 °C and stirred for 1 h at room temperature in a beaker. Varying percentage of MMT (1–5% w/w of CMC) was swelled in 50 mL of water along with 0.005 mL Tween 80 (surfactant) for 24 h. It was then stirred vigorously by mechanical stirrer for 48 h and sonicated for 30 min. This dispersed MMT solution was added to 50 mL of 1% (w/v) CMC solution. This was followed by addition of isoniazid (0.01 g) to the beaker under stirring condition. 1 wt% of CaCl₂ solution was added slowly to the beaker until complete precipitation of CMC-MMT nanoparticles occurred. After 1 h, the temperature of the system was brought down to 5–10 °C to harden the nanoparticles. GA (10–70% v/w w.r.t. CMC) was added as a cross-linker and the temperature was increased to 45 °C. The reaction was contained for 30 min. The precipitate was then separated by centrifuge and freeze dried. The dried nanoparticles were kept in ampule, stored in refrigerator, and redispersed in deionised water for further use. Scheme 1 depicts the preparation process of isoniazid loaded CMC-MMT nanoparticles. CMC nanoparticles containing 0%, 1%, 3%, 5% MMT and 50% GA was designated as CMC/M0/GA50, CMC/M1/GA50, CMC/M3/GA50, CMC/M5/GA50, and having 5% MMT and 10%, 30%, 70% GA were designated as CMC/M5/GA10, CMC/M5/GA30, and CMC/M5/GA70 respectively. Five batches of the same formulations were prepared.

Calculation of process yield

Process yield was calculated using the following equation as described in the literature.^[21]

$$\text{Process Yield (\%)} = \frac{[(\text{Weight of nanoparticles} \times 100)]}{[\text{Weight of (drug + clay + polymer)}]}$$

Calibration curve of isoniazid

A calibration curve is essential to estimate the release rate of drug from nanoparticles in the suitable solvent medium. Calibration curve was drawn as per the literature.^[24]

A known concentration of isoniazid (in double distilled water) was scanned in the range 200–400 nm by using UV-Visible spectrophotometer (UV-2001 Hitachi, Tokyo, Japan). A sharp peak at 262 nm was noticed for isoniazid having concentration in the range of 0.001–0.01 g/100 mL. The absorbance values at 262 nm

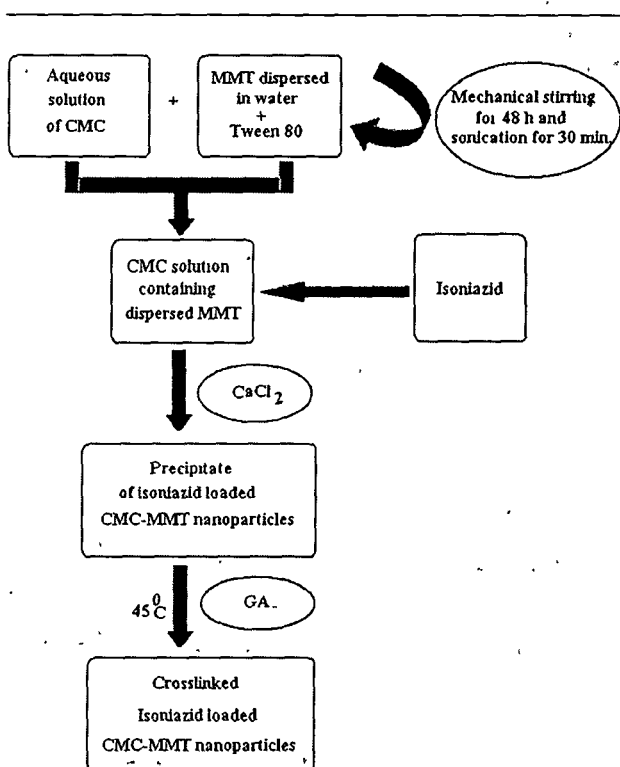
obtained with respective concentration were recorded and plotted. From this calibration curve, the unknown concentration of isoniazid was obtained by knowing the absorbance value. Figure 1 showed the calibration curve of isoniazid in the concentration range 0.001–0.0 g/100 mL, which were validated by least square regression method. Coefficient of correlation (R^2) was found to be 0.9997, which showed good linear relationship of isoniazid. The cumulative release can be calculated from the calibration curve by determining the amount of drug released. The maximum amount of drug was taken 0.01 g. But on the formation of the nanoparticles, the whole amount of drug was not encapsu-

lated in the nanoparticles. The amount of encapsulated drug and its release can be calculated from the calibration curve.

Calculation of encapsulation efficiency of the nanoparticles

The encapsulation efficiency (EE) of nanoparticles with different formulations was determined by ultracentrifugation of samples at room temperature for 30 min. The amount of free isoniazid was determined by noting the absorbance value of the supernatant liquid at 262 nm using UV-Visible spectrophotometer. The EE of the nanoparticles was calculated using the following equations.^[25]

$$\text{Encapsulation efficiency (EE) (\%)} = \frac{(\text{Total amount of drug} - \text{Free amount of drug})}{\text{Weight of dry nanoparticles}} \times 100$$



Scheme 1. Flowchart showing the main steps in the preparation of crosslinked isoniazid loaded CMC-MMT nanoparticles.

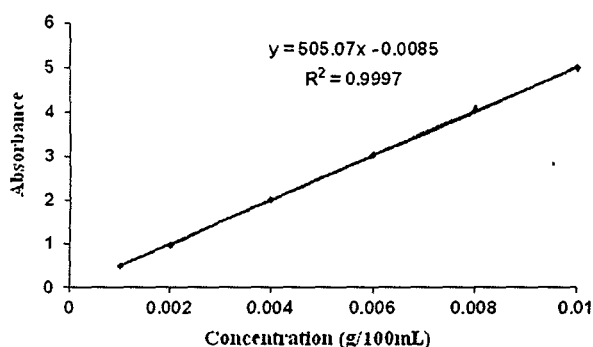


Figure 1. Calibration curve of Isoniazid. This figure is available in colour online at wileyonlinelibrary.com/journal/pat

Nuclear Magnetic Resonance study

Nuclear Magnetic Resonance (NMR) spectra of CMC were recorded with 400 MHz FTNMR (JEOL, Japan) spectrometer by using D₂O as solvent and tetramethyl silane (TMS) as the internal standard.

Fourier Transmission Infrared Spectroscopy study

Fourier Transmission Infrared Spectroscopy (FTIR) spectra of chitosan, CMC, isoniazid, and isoniazid loaded CMC-MMT nanoparticles were taken in Nicolet (model Impact-410, USA) spectrophotometer. The nanoparticles were grounded to powder, mixed with KBr, and compressed under vacuum, and then the spectra were recorded in the range of 4000–400 cm⁻¹.

Particle size determination

Particle size of the prepared nanoparticles were determined by dynamic light scattering (DLS) analyzer (model DLS—Nano ZS, Zetasizer, Nanoseries, Malvern Instruments). The particle size measurements were performed in distilled water using a quartz cell. Each analysis was performed at 25 °C with a detection angle of 90°. Measurements on nanoparticle suspension were carried out triplicate for a single batch of nanoparticles and results were the average of three measurements.

X-ray diffraction study

The degree of intercalation and distribution of isoniazid in CMC-MMT nanoparticles were examined by X-ray diffractometry. It was carried out in a Rigaku X-ray diffractometer (Miniflux, UK) using CuK α (λ =0.154 nm) radiation at a scanning rate of 1°/min with an angle ranging from 2° to 70° of 2 θ .

Scanning electron microscopy study

The samples were mounted on a brass holder, sputtered with platinum. The surface morphologies of CMC-MMT nanoparticles loaded with isoniazid were studied by using Scanning Electron Microscope (JEOL JSM – 6390LV) at an accelerated voltage of 15 kV.

Transmission emission microscopy study

The dispersion of the silicate layers of MMT in nanoparticles was examined by using Transmission Electron Microscope (JEOL JEM-2100) at an accelerated voltage of 200 kV.

Water uptake studies

Water uptake studies were performed in both phosphate buffer (pH 7.4) and 0.1 N HCl solution (pH 1.2) according to the procedure described in the literature^[24]

Nanoparticles (0.1 g) were taken in a pouch made of nylon cloth. The empty pouch was first conditioned by immersing it in either 0.1 N HCl (pH 1.2) or phosphate buffer (pH 7.4) for different time periods (1–8 h). The pouch containing the nanoparticles was immersed in a similar way in either 0.1 N HCl (pH 1.2) or phosphate buffer (pH 7.4) for the similar time periods. The weights of wet nanoparticles after a definite period were determined by deducting the respective conditioned weight of the empty nylon pouch from this. Water uptake (%) was determined by measuring the change in the weight of the nanoparticles. The percentage of water uptake for each sample determined at time, t , was calculated using the following equation

$$\text{Water uptake (\%)} = \frac{(w_2 - w_1)}{w_1} \times 100$$

Where, w_1 is initial weight of nanoparticles before swelling and w_2 is the final weight of nanoparticles after swelling for a predetermined time, t

The experiments were performed five times and represented as a mean value

In vitro drug release studies

To study the release profile of the isoniazid loaded CMC-MMT nanoparticles, dried drug loaded samples were immersed in a solution of different pH namely 1.2, 6.8, and 7.4 and stirred continuously. At scheduled time interval, 5 mL solution was withdrawn, filtered, and assayed spectrophotometrically at 262 nm by using UV-Visible spectrophotometer for the determination of cumulative amount of drug release up to a time t . Each determination was carried out five times. To maintain a constant volume, 5 mL of the solution having same pH was returned to the container^[26]

Isolation of lymphocytes, culture, and treatment

Human blood was collected from suitable donor. It was diluted in the ratio of 1 : 1 with phosphate buffer saline (PBS) and layered 6 mL into 6 mL histopaque (1.077 g/mL). The isolation of lymphocytes and study of cell viability were carried out as per the procedure stated in the literature^[27]. Lymphocytes were isolated from the sample after centrifugation for 30 min at 400 g, washed with PBS, and finally with serum-free media separately through centrifugation for 10 min at 250 g. Cell pellets were then suspended in PBS, and cell viability was checked by Trypan blue exclusion method using haemocytometer. Cell viability more than 90% was used for subsequent study.

Aliquots of 200 μ L of isolated cells were cultured in Roswell Park Memorial Institute medium (RPMI) supplemented with 10% heat inactivated FBS. Initially cells were maintained for 4 h in RPMI without FBS at 37 °C in 5% CO₂ incubator. Cells were then treated with as per experimental requirements and maintained in presence of FBS for 6, 12, and 24 h.

Cytotoxicity experiments

Cytotoxicity assay was performed by measuring the viability of cells according to the method as illustrated by Denizot and Lang^[28]. The key component (3-[4, 5-dimethylthiazol-2-yl]-2, 5-diphenyl tetrazolium bromide) (MTT) is yellowish in color and mitochondrial

dehydrogenase of viable cells cleave the tetrazolium ring, yielding purple insoluble formazan crystals, which were dissolved in suitable solvent. The resulting purple solution was spectrophotometrically measured. An increase or decrease in cell number resulted in a concomitant change in the amount of formazan formed, indicating the degree of cytotoxicity caused by the test material. Briefly, after treatments, cells were treated with 10% of MTT for 2 h followed by dissolving the formazan crystals in solvent and measuring the absorbance of solution at 570 nm. The absorbance of control cells at 6, 12, and 24 h were separately set as 100% viability and the values of treated cells were calculated as the percentage of control.

Statistical analysis

All the data were expressed as means \pm SD (standard deviation). Results were statistically analyzed by student's t -test for significant difference between group mean using GRAPHPAD Prism version 6.01 (GraphPad Software Inc, California, USA)^[29]. The significant difference between the experimental and the control group was set at different levels as $p < 0.05$, $p < 0.01$, and $p < 0.001$.

RESULTS AND DISCUSSION

Nuclear Magnetic Resonance study

The ¹H NMR spectrum for CMC in D₂O is shown in Fig. 2. The basic assignment of the chitosan resonance is that 'a' is the resonance of H-1D (4.72 ppm), 'b' is H-1A (4.65 ppm), 'h' is the resonance of three acetyl-protons (2.0 ppm), 'e' is H3-6 protons (3.6–3.7 ppm), 'g' is H-2D proton resonance (3.1 ppm). The data of NMR of chitosan is taken from literature. In the region between 4.05 and 4.55 ppm, the resonances are the protons of 3-substituted and 6-substituted carboxymethyl (–O–CH₂COOD) of CMC, 'd' is the resonance of three protons from H-6' (2 protons) and H-3' (1 proton), 'c' is the resonance of 1 proton from H-3. The resonance signal of the protons from N–CH₂COOD group can be found at $\delta = 3.25$ ppm. The result indicated that the amino groups were partly carboxymethylated along with the hydroxyl groups^[30,31]

Fourier Transmission Infrared Spectroscopy study

The FTIR spectra of chitosan, CMC, MMT, Isoniazid, and isoniazid loaded CMC-MMT nanoparticles are shown in Fig. 3. The basic absorption bands of chitosan (curve a) appeared at 3442 cm⁻¹ (OH stretching and NH stretching, overlapped), 2939 cm⁻¹

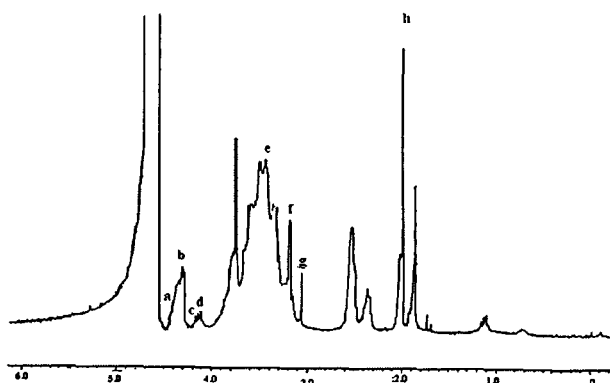


Figure 2 The NMR spectra of CMC

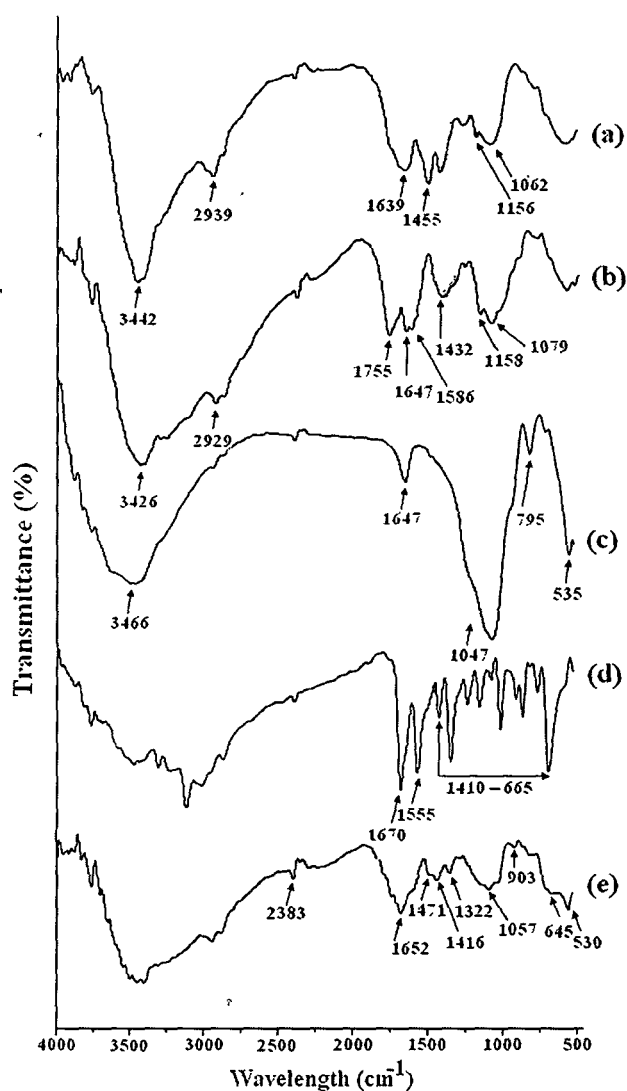


Figure 3 The FTIR spectra of (a) Chitosan, (b) CMC; (c) MMT; (d) Isoniazid; and (e) CMC/M5/GA50.

(CH stretching). The characteristics peaks of amide I and amide II appeared at 1639 cm^{-1} (C=O stretching) and 1455 cm^{-1} (N-H in plane deformation coupled with $\text{C}\equiv\text{N}$ stretching), respectively. The other peaks appeared at 1156 cm^{-1} (bridge -O- stretching), and 1062 cm^{-1} (-CO stretching) were also shown.^[32]

Curve b shows the IR spectrum of the sodium salt of CMC, where the strong peaks were found to appear at 1586 cm^{-1} and 1432 cm^{-1} corresponded to the respective asymmetric and symmetric stretching vibrations of COO^- group, 1755 cm^{-1} (for carboxylic acids, -COOH) and 1647 cm^{-1} (for deforming NH_2 vibration). The C-O absorption peak of the secondary hydroxyl group became stronger and shifted to 1079 cm^{-1} . The broad peak in CMC at $3400\text{--}3200\text{ cm}^{-1}$ was due to both O-H and N-H stretching vibrations and the peak at 2929 cm^{-1} was due to the C-H stretching vibrations.^[33] From the IR spectra, we concluded that the carboxymethyl group was successfully attached to the chitosan backbone.

Curve c represents the spectra of MMT. The peaks exhibited in the spectrum for MMT at 3435 , 1639 , and $1051\text{--}544\text{ cm}^{-1}$ were for -OH stretching, -OH bending, and oxide bands of metals

such as Si, Al, and Mg. Curve d represents the spectrum of isoniazid. The absorption peaks appeared at 1664 and 1551 cm^{-1} were due to the amide I (C=O stretching) and amide II (N-H bending of secondary amide group), respectively. Besides this, multiple peaks appeared in the range $1410\text{--}669\text{ cm}^{-1}$ ^[26]

All the characteristic peaks of CMC, MMT, and isoniazid appeared, and their intensities decreased in the spectrum of isoniazid loaded chitosan-MMT nanoparticles (curve e). In isoniazid loaded CMC-MMT nanoparticles, no absorption band was found in the region of 1755 cm^{-1} . But a new peak at 1322 cm^{-1} was observed. This peak along with peak at 1652 cm^{-1} can be credited to the stretching vibrations of calcium crosslinked carboxyl groups of CMC^[34]

Moreover, the intensity of the peak appeared at 3426 cm^{-1} for curve (b) decreased and shifted to lower wave number side isoniazid loaded CMC-MMT nanoparticles (curve e). This indicated an interaction between the hydroxyl groups of MMT and CMC. The decrease in hydroxyl peak intensity was reported by Maji *et al.*^[35] while studying the properties of wood polymer nanocomposites. All these indicated a better dispersion of MMT and isoniazid in the chitosan-MMT nanoparticles.

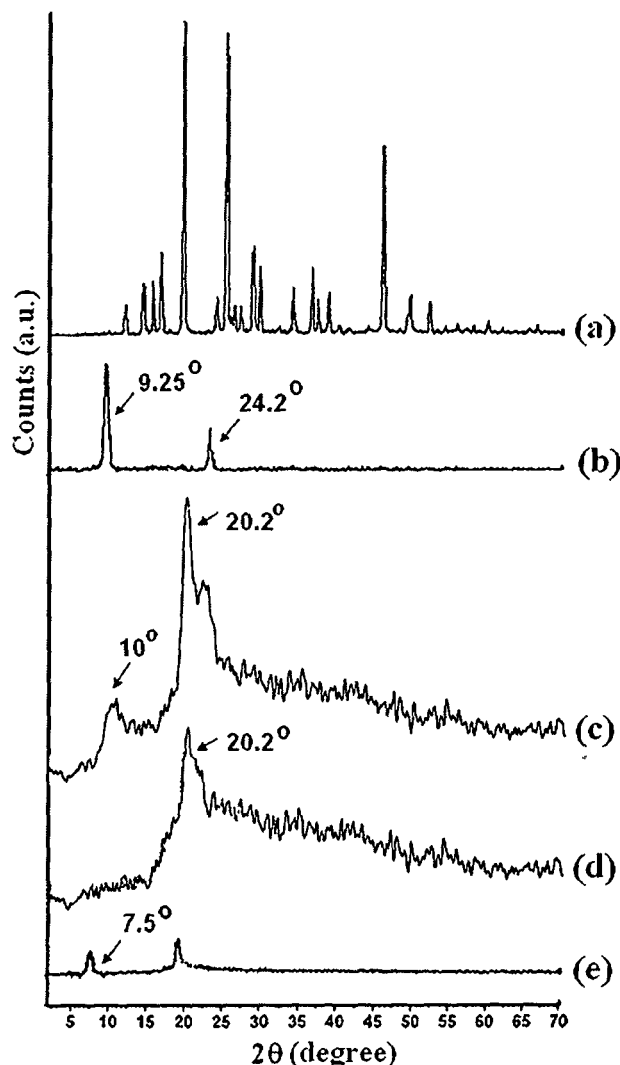


Figure 4. The XRD patterns of (a) Isoniazid; (b) MMT; (c) chitosan; (d) CMC; and (e) CMC/M5/GA50.

X-ray diffraction study

The carboxymethylation of chitosan was also confirmed by XRD study. The XRD diffractograms of the Chitosan, CMC, MMT, isoniazid, and isoniazid loaded CMC-MMT nanoparticles are shown in Fig. 4. Chitosan showed two distinct crystalline peaks at $2\theta = 10^\circ$ and 20.2° due to (020) and (100) plane, respectively (Fig. 4c).^[21,32] Conversely, in the case of CMC, the peak at 10° disappeared, and the intensity of the peak at $2\theta = 20^\circ$ diminished (Fig. 4d). The reason for the desertion and weakening of the peaks might due to the demolition of the intermolecular hydrogen bonds and the crystalline regions of chitosan, which signify the formation of CMC by the process of the carboxymethylation of chitosan.^[32]

Isoniazid (curve 4a) shows multiple peaks at $2\theta = 12^\circ$ to 50° due to its crystalline nature. Similar type of diffractogram was reported by Maji *et al.*^[21] MMT exhibits the two characteristic peaks at $2\theta = 9.25^\circ$ and 24.2° , which are assigned for (001) and (002) plane (Fig. 4b).^[26] The characteristic peaks for isoniazid were found to disappear in the diffractogram of MMT-CMC nanoparticles (curve 4e). The intensity of both the characteristic peaks for MMT was found to decrease. Further, the peak corresponding to $2\theta = 9.25^\circ$ was found to shift to the lower wavelength side of $2\theta = 7.5^\circ$, indicating the greater intercalation of the CMC matrix with the MMT layers due to an increase in inter-layer spacing. These findings suggested an increase in gallery spacing of MMT due to intercalation^[36] and occurrence of a

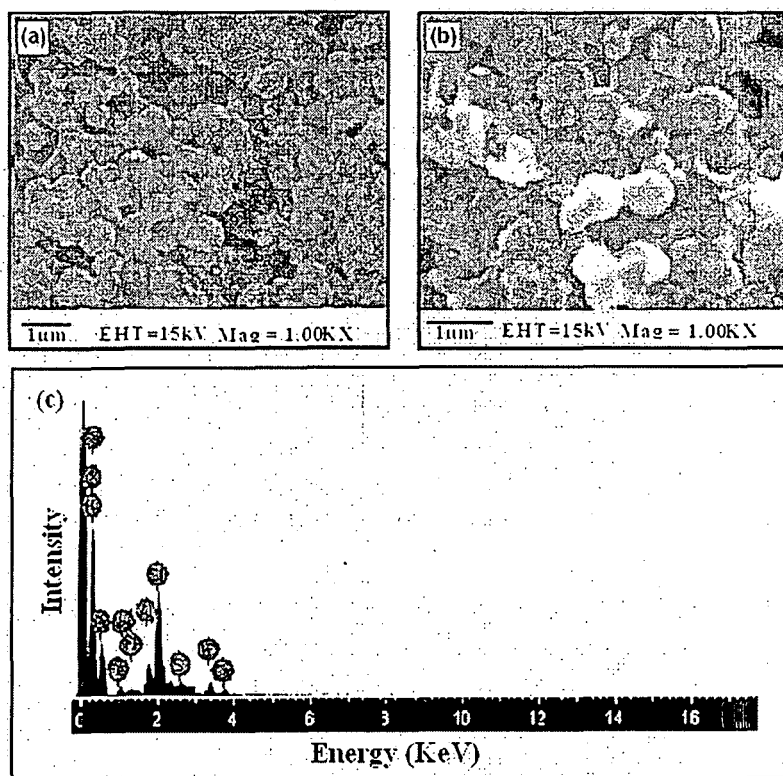


Figure 5. The SEM micrographs of (a) CMC /M0/GA50; (b) CMC/M5/GA50; and (c) EDX of CMC/M5/GA50.

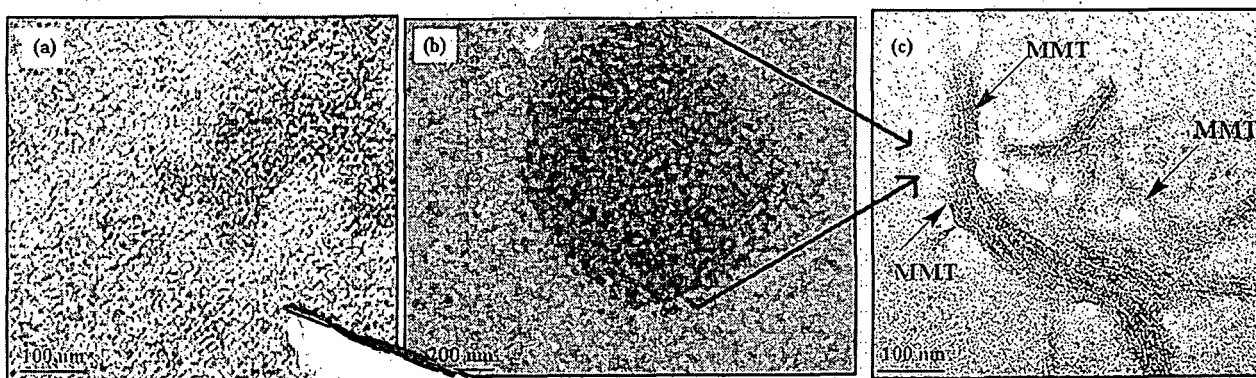


Figure 6. The TEM micrographs of CMC nanoparticles (a) without MMT range; (b) MMT containing CMC nanoparticles at 200 nm scale; and (c) with MMT at 100 nm scale, respectively.

molecular level dispersion of isoniazid in isoniazid loaded CMC-MMT nanoparticles.

Scanning electron microscopy study

Scanning electron microscopy (SEM) analysis was performed to study the surface morphology of CMC nanoparticles and CMC-MMT nanoparticles loaded with isoniazid. Figure 5a and 5b represents the SEM micrographs of CMC nanoparticles and CMC-MMT nanoparticles, respectively. The surface of CMC nanoparticles (Fig. 5a) appeared rough and slightly agglomerated. However, in addition of MMT into CMC nanoparticles, the roughness as well as the agglomeration decreased (Fig. 5b). MMT acted as a physical crosslinking agents, which enhanced the dimensional stability and hence the smoothness.^[37]

Further work was carried out through energy dispersive X-ray analysis of clay loaded nanoparticles as shown in Fig. 4c. Elements such as Al, Na, and Si, which are mainly from the silicate MMT, were detected demonstrating the effective incorporation of MMT into the nanoparticles.^[38]

Transmission electron microscopy study

Transmission electron microscopy (TEM) micrographs of isoniazid loaded carboxymethyl chitosan nanoparticles devoid of MMT and with MMT are shown in Fig. 6a and 6c, respectively. Figure 6b showed the overall shape of the nanoparticles. Figure 6c showed the presence of platelets of MMT tactoids in which the dark lines were the intersection of MMT layers. The bright areas were for polymer matrix and isoniazid. Similar observation was reported by Wang *et al.*^[18] while studying the biopolymer/MMT structure by TEM. The results indicated that MMT was incorporated and dispersed in the CMC matrix.

Effect of variation of MMT and GA concentration on the different properties of isoniazid loaded CMC-MMT nanoparticles

The results showing the effect of variation of MMT and GA concentration on different properties of CMC nanoparticles are shown in Table 1. The EE of MMT free crosslinked nanoparticles was found to be higher compared with that of MMT containing crosslinked nanoparticles. The EE decreased with the increase in MMT content in the nanoparticles. This could be attributed to the presence of the silicate layers of MMT. The -OH groups of MMT could interact with the residual -NH₂ group of CMC and -CHO groups of GA resulting in extension of the polymer chains. The silicate layers of MMT also hindered the movement of the intercalated polymer chains freely and might assist the formation of fine channels from inner to outer surface of the nanoparticles during drying process. The more the encapsulation of MMT, the higher is the chance formation of fine channels. Thus, part of the drug might get diffused from the particles to the external medium resulting in the decrease of EE. Similar results were reported by Maji *et al.*^[26] The interference offered by the MMT layers was absent in MMT free crosslinked nanoparticles. Hence, it showed higher EE.

Similarly, at a fixed MMT content, the EE of nanoparticles was found to further decrease with the increase in the GA concentration. GA might further restrict the free motion of the intercalated polymer chains and thus assist the formation of porous structure.

The average diameter of the nanoparticles was obtained in the range 541–570 nm. Sarmento *et al.* reported that similar

Table 1. Effect of variation of Montmorillonite and GA concentration on the different properties of CMC nanoparticles

Sample code	(CMC) % w/v (amount in g in 50 ml water)	MMT % w/w w.r.t CMC (amount in g in 50 mL water)	GA% v/w w.r.t. CMC (amount in mL)	Yield of nanoparticle (%)	Encapsulation efficiency (%)	Average diameter (nm)	Zeta potential (mV)
CMC/M0/GA50	1 (0.5)	0 (0.00)	0.25	92.76(±0.01)	68.12(±0.04)	543.7 (±11)	47.21(±0.02)
CMC/M1/GA50	1 (0.5)	1 (0.005)	0.25	92.09(±0.04)	64.38(±0.01)	546.3(±11)	44.08(±0.07)
CMC/M3/GA50	1 (0.5)	3 (0.015)	0.25	92.32 (±0.01)	62.11(±0.01)	544.1(±8)	42.92(±0.3)
CMC/M5/GA50	1 (0.5)	5 (0.025)	0.25	91.98(±0.03)	60.31(±0.03)	548.9(±10)	37.63(±0.02)
CMC/M5/GA10	1 (0.5)	1 (0.025)	0.05	91.62(±0.03)	61.77 (±0.02)	570.2(±11)	35.35(±0.01)
CMC/M5/GA30	1 (0.5)	1 (0.025)	0.15	91.20(±0.01)	61.03(±0.01)	564.7(±14)	35.94(±0.01)
CMC/M5/GA70	1 (0.5)	1 (0.025)	0.35	91.93(±0.02)	59.46 (±0.01)	541.1(±13)	37.83(±0.03)

*each value represents average of five readings, standard deviation in parenthesis.

type of particle size range can be effective for the oral delivery of insulin in alginate/chitosan nanoparticles.^[39] The variation in MMT concentration did not significantly affect the particle size. However, the average diameter showed a decreasing trend on increasing the GA concentration. The residual amino groups present in CMC interacted with the hydroxyl group of MMT and GA. With the increase in the concentration of GA, the availability of free amino groups on nanoparticles reduces due to which the nanoparticles became more compact and hence the diameter would be less.

Zeta potential values of the nanoparticles were found in the range 39 to 47 mV, indicating good stability of the nanoparticles. The calculation of the DS of the synthesized CMC showed that DS was 0.8219. The DS value showed that all the amino groups were not replaced by carboxymethyl groups. The surface of the nanoparticles was positively charged due to the presence of residual amino groups. With the incorporation of MMT in CMC matrix, the surface charge decreases. The reduction in surface charge might be due to the increased electrostatic interaction between the protonated amino groups of CMC and hydroxyl groups of MMT.^[34]

However, the zeta potential values increased as the GA concentration increased from 10% to 70%. The GA molecules did not allow the opposite charges to come too close and thus preventing the nanoparticles from aggregation. The increase in the zeta potential indicated that the stability of the nanoparticles increased with the increase in the concentration of GA and they would not aggregate in acidic or basic medium.^[26] All the zeta potential values were in the stable zone, indicating that the synthesized nanoparticles are highly stable.

Swelling study

The effect of pH on the percentage swelling of isoniazid loaded nanoparticles at two different pH namely, 1.2 and 7.4, are shown in Fig. 7. It was observed that the swelling of isoniazid loaded carboxymethyl chitosan-MMT nanoparticles was more in gastric pH (1.2) than in intestinal pH (7.4). At lower pH, the free amine groups become protonated and generated a repulsive force between the adjacent positively charged polymer chains, causing the swelling of the polymer and consequently diffusion of more amount of drug out of the polymer matrix.^[40,41] In alkaline pH, protonation was prevented, and hence swelling decreased.

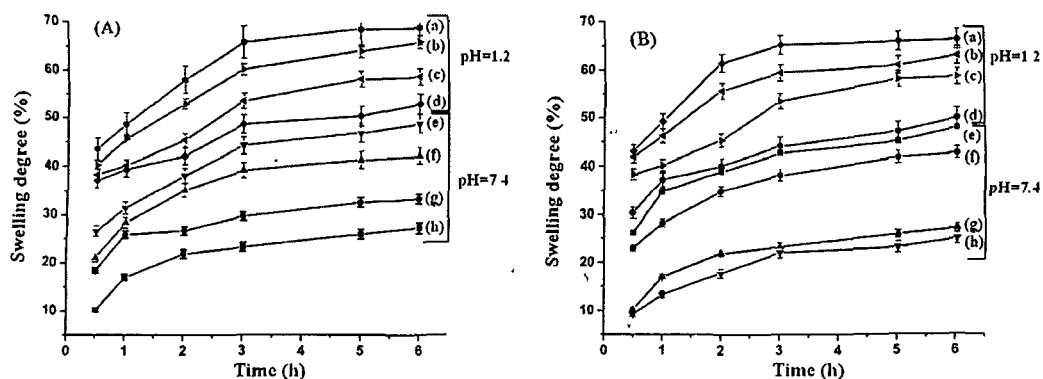


Figure 7. Percentage swelling degree at pH 1.2 and 7.4: (A) ((a)CMC/M0/GA50, (b) CMC /M1/GA50, (c) CMC /M3/GA50, (d) CMC /M5/GA50, (e) CMC /M0/GA50, (f) CMC /M1/GA50, (g) CMC /M3/GA50, (h) CMC /M5/GA50); and (B) ((a) CMC M5/GA10, (b) CMC /M5/GA30, (c) CMC /M5/GA50, (d) CMC /M5/GA70, (e) CMC /M5/GA10, (f) CMC /M5/GA30, (g) CMC /M5/GA50, (h) CMC /M5/GA70).

Figure 7(A) showed that with the increase in the concentration of MMT, the percentage swelling degree decreased. Water absorption decreased by the presence of dispersed phase of MMT into the CMC matrix of the nanoparticles. MMT particles acted as a barricade for water molecules and decreased the water transmission through the crosslinked CMC-MMT nanoparticles. Similarly, nanoparticles containing higher concentration of GA (Fig. 7B) swelled less due to higher crosslinking densities and less availability of the polar groups.^[26]

Furthermore, the percentage swelling degree was found to increase with the increase in time. With the increase in the period, higher amount of the solvents can penetrate into the CMC matrix, resulting in the increase in the percentage swelling degree.

In vitro release studies

The drug release profile of isoniazid from the nanoparticles at three different pH namely 1.2, 6.8, and 7.4 are shown in Fig. 8. The cumulative release (%) of isoniazid from CMC-MMT nanoparticles was found to be pH dependent. The cumulative release (%) of isoniazid decreased with the increase in the pH of the medium. The major factors controlling the release profile of isoniazid from nanoparticles were swelling nature of the polymer and solubility of the drug in the medium. The difference in release profile was due to the difference in the swelling of CMC in gastric and intestinal pH. CMC was swelled more in gastric pH compared with intestinal pH medium. The faster drug release rate in lower pH medium was due to the wobbly nanoparticles structure, caused by the protonation of residual amino groups of CMC in lower pH.^[40] The solubility of isoniazid increased at acidic pH due to its basic nature as reported in literature.^[42] Lower pH of the medium favored both the swelling of the polymer and solubility of the drug. The release profile of isoniazid from the nanoparticles at pH 6.8 and 7.4 is almost similar and Mariappan *et al.* and Kakemi *et al.* showed in a study in rats that the drug is poorly permeable in the stomach, and that its main absorption site is located in the intestine. Lower permeability in the stomach can be explained on the basis of isoniazid protonation in the acidic medium due to its weak base properties.^[43] The problem of permeability can be solved on preparation of the nanoparticles.

It was also observed that the cumulative release (%) of isoniazid decreased with the increase in MMT content (Fig. 8A, B, and C) and

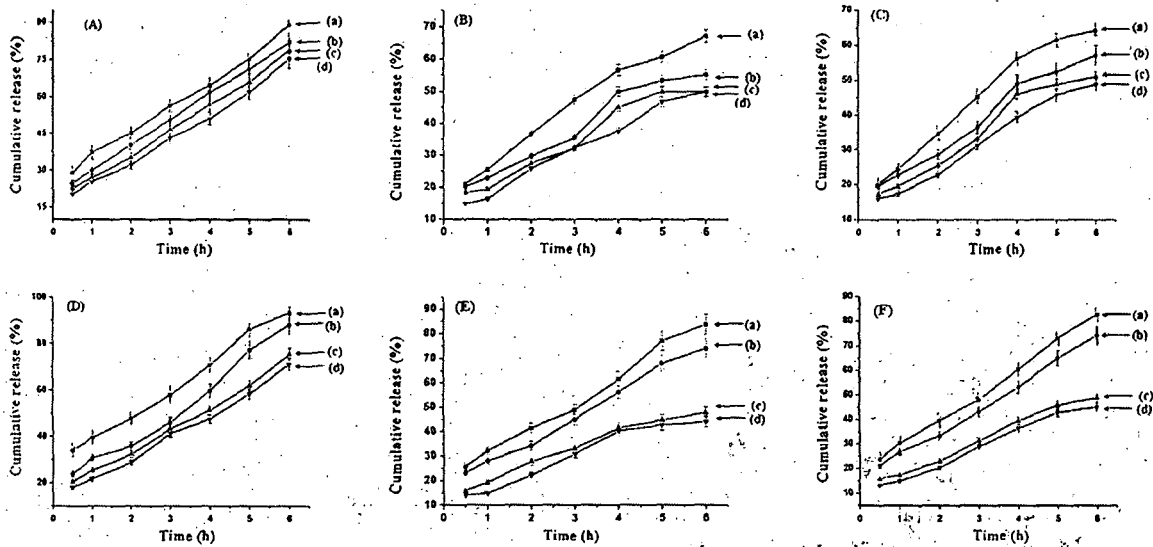


Figure 8. Cumulative release at (A) with variation of MMT at pH = 1.2 ((a) CMC/M0/GA50, (b) CMC/M1/GA50, (c) CMC/M3/GA50, (d) CMC/M5/GA50); (B) with variation of MMT at pH = 6.8 ((a) CMC/M0/GA50, (b) CMC/M1/GA50, (c) CMC/M3/GA50, (d) CMC/M5/GA50); and (C) with variation of MMT at pH = 1.2 ((a) CMC/M5/GA10, (b) CMC/M5/GA30, (c) CMC/M5/GA50, (d) CMC/M5/GA70); (D) with variation of MMT at pH = 7.4 ((a) CMC/M0/GA50, (b) CMC/M1/GA50, (c) CMC/M3/GA50, (d) CMC/M5/GA50); (E) with variation of GA at pH = 6.8 ((a) CMC/M5/GA10, (b) CMC/M5/GA30, (c) CMC/M5/GA50, (d) CMC/M5/GA70); and (F) with variation of GA at pH = 7.4 ((a) CMC/M5/GA10, (b) CMC/M5/GA30, (c) CMC/M5/GA50, (d) CMC/M5/GA70).

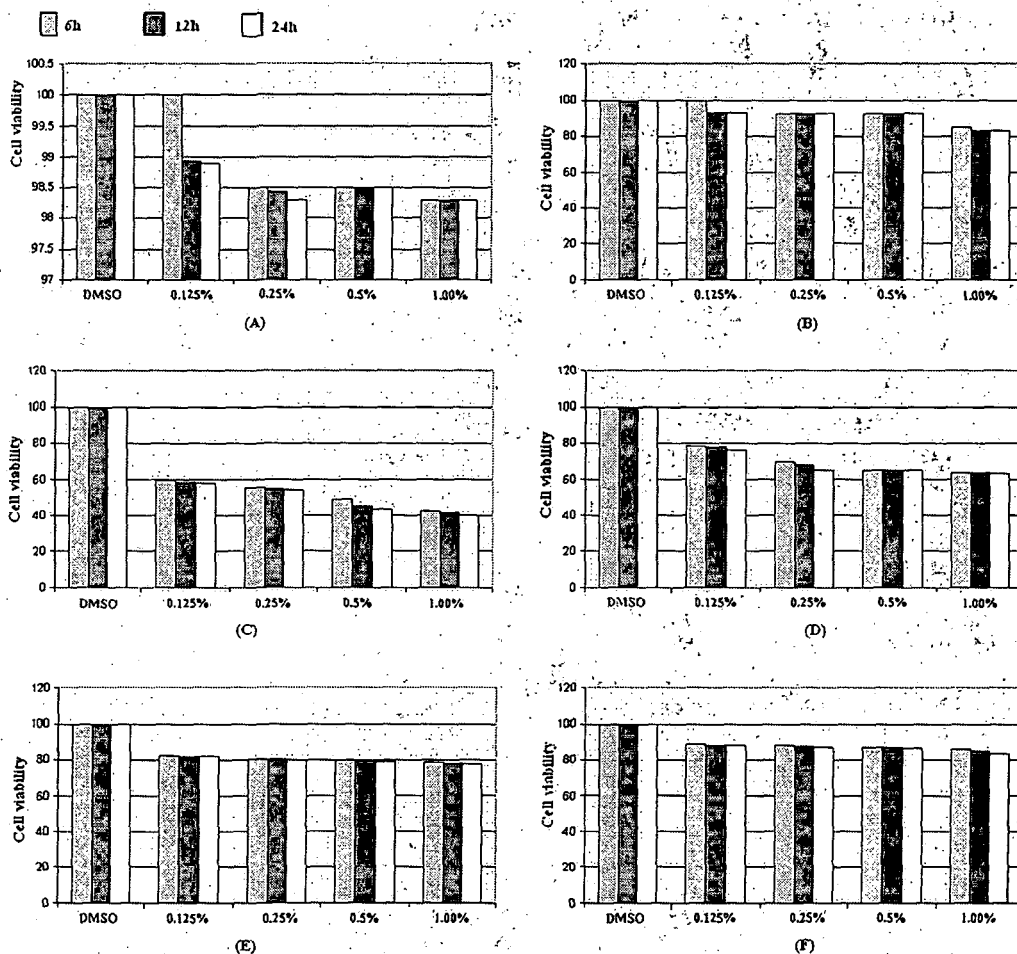


Figure 9. Cell viability study with variation of (a) CMC; (b) MMT; (c) Isoniazid; and (d) CMC/M0/GA50; (e) CMC/M1/GA50; (f) CMC/M5/GA50 at 6, 12, and 24 h. This figure is available in colour online at wileyonlinelibrary.com/journal/pat

increased with the increase in the time. The percentage swelling of the nanoparticles decreased with the increase in the concentration of MMT. Therefore, in order to facilitate the release of isoniazid, the solvent particles could not diffuse properly to interact with the isoniazid molecules encapsulated in the nanoparticles. With the increase in time, the percentage degree of swelling increased, and more and more solvent molecules could reach the drug molecule, and hence helped to release the isoniazid from the nanoparticles.

It was also seen that the cumulative release (%) of isoniazid decreased with the increase in the concentration of GA (Fig 8D, E and F). This was due to the increase in crosslinking density of the nanoparticles. The more the crosslinking, the less the accessibility of solvent to penetrate into the CMC-MMT nanoparticles, and thus a decrease in cumulative release (%) were observed.

Cytotoxicity test

The effect of varying MMT concentration (0–5%) and time (6, 12, and 24 h) on cell viability is shown in Fig 9. Figure 9(a) showed that CMC was non toxic. It had high cell viability of around 98–25%. It was also observed that the cell viability varied between 82–100% within the studied MMT concentration (Fig 8b). This indicated that the MMT was not cytotoxic to the cells. The cell viability decreased with the increase in the concentration of the nanoparticles and time interval.

Isoniazid was found to be highly cytotoxic. The cell viability for 1% isoniazid at 24 h is only 40% (Fig 9c). The cytotoxicity was found to be less for isoniazid loaded CMC-MMT nanoparticles compared with those of isoniazid alone. The MMT containing CMC nanoparticles hindered the release of isoniazid due to its tortuous path and hence reduced the interaction of drug with the cell. It was observed further (Fig 9(d–f)) that the cell viability of MMT containing nanoparticles was more compared with MMT free nanoparticles. This might be due to the fact that the silicate layers of clay stalled the release of drug in the cell because of its meandering path.

CONCLUSION

This work demonstrated the successful preparation of CMC and isoniazid loaded CMC-MMT nanoparticles by ionic gelation, followed by chemical crosslinking. FTIR and NMR study indicated the successful preparation of CMC. FTIR study also confirmed the interaction of MMT with CMC polymer. The exfoliation of MMT layers was examined by XRD and TEM. XRD results also showed the molecular level dispersion of isoniazid in the CMC-MMT nanoparticles. SEM study showed that the surface of the CMC-MMT nanoparticles was smoother compared with those of CMC nanoparticles. Both the swelling and release of isoniazid from the nanoparticles were found to enhance with the decrease in the MMT and GA content. The percentage swelling degree and cumulative release increased in gastric pH compared with intestinal pH. Cytotoxicity study revealed that the synthesized CMC was not cytotoxic and the nanoparticles containing MMT was less cytotoxic than those of MMT free nanoparticles.

Acknowledgement

Council for Scientific and Industrial research is acknowledged for the financial support.

REFERENCES

- [1] R Riva, H Ragelle, A Rieux, N Duhem, C Jérôme, V Preat, *Adv Polym Sci* **2011**, *244*, 19
- [2] M Z Hussein, M A Yarmo, M Z H A Rahman, Z Zainal, A A S Liang, *Malay J Anal Sci* **2001**, *7*, 35
- [3] S Racovita, S Vasiliu, M Popa, C Luca, *Rev Roum Chim* **2009**, *54*, 709
- [4] V L Goncalves, M C M Larenjeira, V T Favere, *Polim Cienc Technol* **2005**, *15*, 6
- [5] M Prabharan, *J Biomater Appl* **2008**, *23*, 5
- [6] Y Shirosakia, K Tsurua, S Hayakawaa, A Osakaa, M A Lopes, J D Santos, M H Fernandes, *Biomaterials* **2005**, *26*, 485
- [7] J P Venter, A F Kotze, R A Vely, *Int J Pharm* **2006**, *313*, 36
- [8] E B Denkbass, R M Ottenbrite, *J Bioact Compat Polym* **2006**, *21*, 351
- [9] J Kumirska, M X Weinhold, J Thoming, P Stepnowski, *Polymers* **2011**, *3*, 1875
- [10] A B Sieval, M Thanou, A F Kotze, J C Verhoef, J Brussee, H E Junginger, *Carbohydr Polym* **1998**, *36*, 157
- [11] Y Di, G Long, H Zhang, Q Li, *J Eng Fibers Fabr* **2012**, *6*, 39
- [12] H T Pang, X G Chen, H J Park, D S Cha, J F Kennedy, *Carbohydr Polym* **2007**, *69*, 419
- [13] S S Vaghani, M M Patel, C S Satish, K M Patel, N P Jivani, *Bull Mater Sci* **2012**, *35*, 1133
- [14] X Zhang, M Oulad Abdelghani, Y Wang, Y Haikel, D Mainard, J C Voegel, F Caruso, N Benkirane-Jessel, *Biomaterials* **2010**, *31*, 1699
- [15] J Tan, Y Wang, X Yip, F Glynn, R K Shepherd, F Caruso, *Adv Mater* **2012**, *24*, 3362
- [16] N Ahmed, M Michelin-Jamois, H Fessi, A Elaissari, *Soft Mater* **2012**, *8*, 2554
- [17] G V Joshi, B D Kevadiya, H A Patel, H C Bajaj, R V Jasra, *Int J Pharm* **2009**, *374*, 53
- [18] X Wang, Y Du, J Luo, *Nanotechnology* **2008**, *19*, 1
- [19] J Ji, S Hao, W Liu, J Zhang, D Wu, Y Xu, *Polym Bull* **2011**, *67*, 1201
- [20] M Tavakol, E Vasheghani Farahani, S Hashemi Najafabadi, *Prog Biomater* **2013**, *2*, 1
- [21] N Banik, A Hussain, A Ramteke, H K Sharma, T K Maji, *RSC Adv* **2012**, *2*, 10519
- [22] N T An, D T Thien, N T Dong, P L Dung, *Carbohydr Polym* **2009**, *75*, 489
- [23] H C Ge, D K Luo, *Carbohydr Res* **2005**, *340*, 1351
- [24] N Devi, T K Maji, *Drug Dev Ind Pharm* **2010**, *36*, 56
- [25] S Selvaraj, N Saravanakumar, J Karthikeyan, D D Evangeline, D Lathamary, N N Rajendran, *Der Pharm Lett* **2010**, *2*, 420
- [26] N Banik, M Iman, A Hussain, A Ramteke, R Boruah, T K Maji, *New J Chem* **2013**, *37*, 3981
- [27] A Hussain, V Saikia, A Ramteke, *Free Radical Antioxidants* **2012**, *2*, 9
- [28] F Denizot, R Lang, *J Immunol Methods* **1986**, *89*, 271
- [29] G J Bourke, L E Daly, J McGilvary, *Interpretation and uses of medical statistics* (4th ed.) Blackwell Scientific Publication, Oxford, **1991**
- [30] V K Mourya, N N Inamdar, A Tiwari, *Adv Mater Lett* **2010**, *1*, 11
- [31] R A Lusiana, D Siswanta, Mudasar, T Hayashita, *Int J Chem Eng Appl* **2013**, *4*, 229
- [32] P Mukhopadhyay, K Sarkar, S Soam, P P Kundu, *J Appl Polym Sci* **2013**, *129*, 835
- [33] R K Farag, R R Mohamed, *Molecules* **2013**, *18*, 190
- [34] A Anitha, S Maya, N Deepa, K P Chennazhi, S V Nair, R Jayakumar, *J Biomater Sci* **2012**, *23*, 1381
- [35] B K Deka, T K Maji, *Compos Sci Technol* **2010**, *70*, 1755
- [36] M Iman, T K Maji, *J Appl Polym Sci* **2013**, *127*, 3987
- [37] J Zheng, J Shan, Z Fan, K Yao, *J Wuhan Univ Technol Mater Sci Ed* **2011**, *26*, 628
- [38] X Cai, B Riedl, S Y Zhang, H Wan, *Composites Part A* **2008**, *39*, 727
- [39] B Sarmiento, A Ribeiro, F Veiga, P Sampaio, R Neufeld, D Ferreira, *Pharm Res* **2007**, *24*, 2198
- [40] S K Sahu, S K Mallick, S Santra, T K Maiti, S K Ghosh, P Pramanik, *J Mater Sci Mater Med* **2010**, *21*, 1587
- [41] A Anitha, S Maya, N Deepa, K P Chennazhi, S V Nair, R Jayakumar, *Carbohydr Polym* **2011**, *83*, 452
- [42] C Bceker, J B Dressman, G L Amidam, H E Junginger, S Kopp, K K Midha, V P Shah, S Stavchansky, D M Barends, *J Pharm Sci* **2007**, *96*, 522
- [43] T T Mariappan, S Singh, *Int J Tuberc Lung Dis* **2003**, *7*, 797